National Library of Canada
Bibliothèque nationale du Canada

Canadian Theses Service
Services des thèses canadiennes

Ottawa, Canada
K1A 0N4

CANADIAN THESES

THÈSES CANADIENNES

NOTICE

The quality of this microfiche is heavily dependent upon the quality of the original thesis submitted for microfilming. Every effort has been made to ensure the highest quality of reproduction possible.

If pages are missing, contact the university which granted the degree.

Some pages may have indistinct print especially if the original pages were typed with a poor typewriter ribbon or if the university sent us an inferior photocopy.

Previously copyrighted materials (journal articles, published tests, etc.) are not filmed.

Reproduction in full or in part of this film is governed by the Canadian Copyright Act, R.S.C. 1970, c. C-30. Please read the authorization forms which accompany this thesis.

AVIS

La qualité de cette microfiche dépend grandement de la qualité de la thèse soumise au microfilmage. Nous avons tout fait pour assurer une qualité supérieure de reproduction.

S'il manque des pages, veuillez communiquer avec l'université qui a conféré le grade.

La qualité d'impression de certaines pages peut laisser à désirer, surtout si les pages originales ont été dactylographiées à l'aide d'un ruban usé ou si l'université nous a fait parvenir une photocopie de qualité inférieure.

Les documents qui font déjà l'objet d'un droit d'auteur (articles de revue, examens publiés, etc.) ne sont pas microfilmés.

La reproduction, même partielle, de ce microfilm est soumise à la Loi canadienne sur le droit d'auteur, SRC 1970, c. C-30. Veuillez prendre connaissance des formules d'autorisation qui accompagnent cette thèse.

THIS DISSERTATION
HAS BEEN MICROFILMED
EXACTLY AS RECEIVED

LA THÈSE A ÉTÉ
MICROFILMÉE TELLE QUE
NOUS L'AVONS REÇUE

NL 339 (r. 86/01)

Canada

National Library of Canada | Bibliothèque nationale du Canada

Ottawa, Canada
K1A 0N4

62

TC –

0-315-22928-4

CANADIAN THESES ON MICROFICHE SERVICE – SERVICE DES THÈSES CANADIENNES SUR MICROFICHE

PERMISION TO MICROFILM – AUTORISATION DE MICROFILMER

• Please print or type – Écrire en lettres moulées ou dactylographier

AUTHOR – AUTEUR

Full Name of Author – Nom complet de l'auteur

MOHAMED REFAAT SHEHATA

Date of Birth – Date de naissance	Canadian Citizen – Citoyen canadien
Sept. 8, 1954	☐ Yes / Oui ☒ No / Non
Country of Birth – Lieu de naissance	**Permanent Address – Résidence fixe**
EGYPT	TATOUN, EL-FAYOUM EGYPT

THESIS – THÈSE

Title of Thesis – Titre de la thèse

INFRARED AND STRUCTURAL STUDIES OF AMMONIA MONOHYDRATE AND AMMONIA DIHYDRATE

Degree for which thesis was presented Grade pour lequel cette thèse fut présentée	Year this degree conferred Année d'obtention de ce grade
Ph.D.	1985
University – Université	**Name of Supervisor – Nom du directeur de thèse**
ALBERTA	J. E. BERTIE

AUTHORIZATION – AUTORISATION

Permission is hereby granted to the NATIONAL LIBRARY OF CANADA to **microfilm** this thesis and to **lend** or **sell copies of the film.**

The author reserves other publication rights, and neither the thesis nor extensive extracts from it may be printed or otherwise reproduced without the author's written permission.

L'autorisation est, par la présente, accordée à la BIBLIOTHÈQUE NATIONALE DU CANADA de **microfilmer** cette thèse et de **prêter** ou de **vendre des exemplaires du film.**

L'auteur se réserve les autres droits de publication; ni la thèse ni de longs extraits de celle-ci ne doivent être imprimés ou autrement reproduits sans l'autorisation écrite de l'auteur.

ATTACH FORM TO THESIS – VEUILLEZ JOINDRE CE FORMULAIRE À LA THÈSE

Signature	Date
M.R. Shehata	14 May, 1985

NL-91 (r. 84/03)

Canada

THE UNIVERSITY OF ALBERTA

INFRARED AND STRUCTURAL STUDIES OF AMMONIA MONOHYDRATE AND AMMONIA DIHYDRATE

by

MOHAMED REFAAT SHEHATA

A THESIS

SUBMITTED TO THE FACULTY OF GRADUATE STUDIES AND RESEARCH

IN PARTIAL FULFILMENT OF THE REQUIREMENTS FOR THE DEGREE

OF DOCTOR OF PHILOSOPHY

DEPARTMENT OF CHEMISTRY

EDMONTON, ALBERTA

FALL 1985

THE UNIVERSITY OF ALBERTA

RELEASE FORM

NAME OF AUTHOR MOHAMED REFAAT SHEHATA

TITLE OF THESIS INFRARED AND STRUCTURAL STUDIES OF AMMONIA MONOHYDRATE AND AMMONIA DIHYDRATE

DEGREE FOR WHICH THESIS WAS PRESENTED Ph.D.

YEAR THIS DEGREE GRANTED 1985

Permission is hereby granted to THE UNIVERSITY OF ALBERTA LIBRARY to reproduce single copies of this thesis and to lend or sell such copies for private, scholarly or scientific research purposes only.

The author reserves other publication rights, and neither the thesis nor extensive extracts from it may be printed or otherwise reproduced without the author's written permission.

(Signed) M. R. Shehata

PERMANENT ADDRESS:

Tatoun, El-Fayoum
Egypt

DATED May 2nd 1985

THE UNIVERSITY OF ALBERTA

FACULTY OF GRADUATE STUDIES AND RESEARCH

The undersigned certify that they have read, and recommend to the Faculty of Graduate Studies and Research, for acceptance, a thesis entitled INFRARED AND STRUCTURAL STUDIES OF AMMONIA MONOHYDRATE AND AMMONIA DIHYDRATE submitted by MOHAMED REFAAT SHEHATA in partial fulfilment of the requirements for the degree of DOCTOR OF PHILOSOPHY

Supervisor

External Examiner

DATE

May 2nd 1985

TO MY FAMILY

ABSTRACT

The dihydrate of ammonia has been isolated for the first time. Its x-ray powder diffraction pattern can be indexed on a cubic unit cell with a = 7.118 Å, with a 95% confidence limit of 0.015 Å at ~105K, and four formula units per unit cell. The infrared spectrum suggests O-H...O distances of ~2.76 Å, short O-H...N distances of 2.74 ± 0.02 Å, and N-H...O distances of ~3.2 Å or longer. The presence of two sharp bands for the isolated O-H...O or O-D...O and a third for the O-H...N or O-D...N stretching vibrations suggests the existence of two types of water molecules in ammonia dihydrate. The infrared spectrum shows no indication of more than one type of ammonia in ammonia dihydrate. A structure which agrees with these spectroscopic findings and fits these bond lengths well, neglecting the hydrogen atoms, has been found in $P2_13$ cubic space group. In this structure two sets of oxygen and one set of nitrogen atoms occupy the special positions of multiplicity four, of site group C_3. The fractional coordinates for O_I, O_{II} and N atoms are x = 0.7111, 0.1410 and 0.3635, respectively. The observed and calculated diffraction intensities, neglecting the hydrogen atoms, compare very well and support the above structure for the heavy atoms.

The infrared spectra also show a triplet for isolated

NH or ND stretching frequencies, which means that the site symmetry of the ammonia molecules is C_1 and not C_3 as suggested by $P2_13$. Thus, the crystal structure of ammonia dihydrate is probably the orthorhombic $P2_12_12_1$. That the crystal cannot be cubic is also seen from consideration of apparent site symmetries of water molecules under the cubic structures. The spectral assignment of infrared features of $NH_3 \cdot 2H_2O$, $ND_3 \cdot 2D_2O$ and their isotopomers at 100K are reported.

The infrared spectra of $NH_3 \cdot H_2O$, $ND_3 \cdot D_2O$ and their partially deuterated or hydrogenated isotopomers at 100K are reported. The mid-infrared spectrum of $NH_3 \cdot H_2O$ is slightly modified from that obtained by Morrison. The ammonia and water molecules, except for the hydrogen atoms in the "O-H...O-H" chains, in the $P2_12_12_1$, D_2^4, crystal have a D_{2h} pseudo-symmetry. No evidence of the possible disorder of the hydrogen atoms is observed. Oriented gas model calculations gave the approximate relative intensities of the unit cell components of the molecular vibrations. Three unit cell components are observed for ν_3 and probably ν_4 of ammonia instead of the six predicted under D_2, three components are calculated to have near zero intensity and only three components are expected under D_{2h}. The symmetric deformation of ammonia, ν_2, yields two unit cell modes with significant intensity,

separated by 37 cm^{-1} for NH_3 and 23 cm^{-1} for ND_3. The intramolecular coupling in the water molecules is negligible because $\nu_{O-H...N}(HOD)$ is ~430 cm^{-1} below $\nu_{O-H...O}(HOD)$. So, the two strong $\nu_{OH}(H_2O)$ and the four strong $\nu_{OD}(D_2O)$ absorptions are due to intermolecular coupling. The bending mode of water, ν_2, is tentatively assigned at 1696, 1467 and 1243 cm^{-1} for H_2O, HOD and D_2O, respectively. The lattice vibrations are assigned to rotational or translational motions.

ACKNOWLEDGEMENTS

I would like to extend my sincere gratitude to Dr. John E. Bertie for his guidance and patience throughout the course of my studies and in the preparation of this thesis.

I would also like to thank Dr. Martin Cowie for his helpful discussions in the x-ray work. Particular thanks to the staff of the electronics, machine and glass shops of the Chemistry Department for their excellent workmanship.

I am very grateful to the academic staff of this department especially those who were involved in my course work.

Special thanks to my family for their encouragement through the years.

Financial support by the University of Alberta is gratefully acknowledged.

TABLE OF CONTENTS

CHAPTER		PAGE
1.	INTRODUCTION	1
	1.1 General Introduction	1
	1.2 Ammonia-Water Equilibrium Phase Diagram	2
	1.3 Review of Spectroscopic and Structural Studies of the Hydrates of Ammonia	10
	1.4 Objectives	31
2.	EXPERIMENTAL TECHNIQUES	34
	2.1 Introduction	34
	2.2 Chemicals	34
	2.3 Preparation of Ammonia Monohydrate and Deuterated Ammonia Monodeuterate	35
	2.4 Preparation of Ammonia Dihydrate	40
	2.5 Sample Recovery and Grinding	41
	2.6 Characterization of the Hydrates	43
	2.7 Preparation of Low Temperature Infrared Mulls	45
	2.8 Infrared Instrumentation	48
3.	EXPERIMENTAL RESULTS	55
	3.1 Introduction	55
	3.2 Characterization of Ammonia Monohydrate Samples	56
	3.3 X-Ray Data of Ammonia Dihydrate	60
	3.4 Infrared Spectra of the Mulling Agents	63

CHAPTER PAGE

3.5 Infrared Spectra of Ammonia Monohydrate..... 74

3.6 Infrared Spectra of Deuterated Ammonia Monodeuterate..... 86

3.7 Infrared Spectra of Ammonia Dihydrate..... 86

3.8 Infrared Spectra of $NH_3 \cdot 2H_2O$, x% D..... 101

3.9 Infrared Spectra of $ND_3 \cdot 2D_2O$, x% H..... 111

4. DISCUSSION OF INFRARED SPECTRUM OF AMMONIA MONOHYDRATE..... 129

4.1 General..... 129

4.2 Calculations of the Relative Infrared Intensities of N-H Stretching Modes..... 132

4.3 The N-H and N-D Stretching Vibrations..... 136

4.4 A Useful D_{2h} Pseudo-Symmetry..... 148

4.5 Water Stretching Vibrations..... 151

4.6 The Intramolecular Angle Deformation Vibrations..... 164

4.7 Lattice Vibrations..... 171

4.8 Other Features in the Spectrum of Ammonia Monohydrate..... 173

5. AMMONIA DIHYDRATE: STRUCTURE AND SPECTRAL ASSIGNMENTS..... 174

5.1 Indexing of the Powder X-Ray Diffraction Pattern of Ammonia Dihydrate..... 174

5.2 The Crystal Structure of Ammonia Dihydrate... 178

CHAPTER PAGE

5.3 The NH and ND Stretching Vibrations..... 187

5.4 Water Stretching Vibrations..... 191

5.5 Intramolecular Angle Deformation Vibrations.. 200

5.6 Lattice Vibrations..... 204

6. CONCLUSION..... 208

*****

REFERENCES 211

APPENDIX I 219

APPENDIX II 225

APPENDIX III 233

APPENDIX IV 246

APPENDIX V 249

LIST OF TABLES

TABLE	DESCRIPTION	PAGE
1.1	The important points in NH_3-H_2O phase diagram.....	4
2.1	Volumes used for sample preparations.....	38
3.1	X-ray powder diffraction pattern of ammonia monohydrate at ~105K.....	57
3.2	X-ray powder diffraction pattern of ammonia dihydrate at ~105K.....	61
3.3	Infrared spectral features of liquid propane at 100K.....	69
3.4	Infrared spectral features of liquid propylene at 100K.....	71
3.5	Infrared spectral features of liquid Freon-13 at 100K.....	73
3.6	Infrared spectral features of ammonia monohydrate at 100K.....	83
3.7	Infrared spectral features of deuterated ammonia monodeuterate at 100K.....	93
3.8	Infrared spectral features of ammonia dihydrate at 100K and 150K.....	102
3.9	Infrared spectral features of partially deuterated ammonia dihydrate at 100K.....	109

TABLE	DESCRIPTION	PAGE
3.10	Infrared spectral features of deuterated ammonia dideuterate containing <1 and 5 mole% H at 100K.....	125
4.1	Correlation table for ammonia monohydrate...	131
4.2	Calculation of the dipole moment derivatives for the stretching vibrations of ammonia in ammonia monohydrate.....	137
4.3	Molecular constants used in normal coordinate calculations.....	144
4.4	Normal coordinate calculations of ammonia monohydrate stretching frequencies.....	145
4.5	Correlation table for ammonia molecules in ammonia monohydrate.....	150
4.6	O-H stretching frequencies of ammonia monohydrate.....	153
4.7	O-D stretching frequencies of deuterated ammonia monodeuterate.....	154
4.8	Relative intensities of O-H...N vibrations in $NH_3 \cdot H_2O$.....	156
4.9	Relative intensities of O-H...O stretching vibrations in $NH_3 \cdot H_2O$.....	163
4.10	Infrared spectral assignments of $NH_3 \cdot H_2O$ and $ND_3 \cdot D_2O$.....	165

TABLE	DESCRIPTION	PAGE
4.11	Relative intensities of ν_2 bending vibrations of water.....	170
5.1	The observed differences between the squares of the reciprocal interplanar distances.....	176
5.2	Indexing of the x-ray powder diffraction lines of ammonia dihydrate in a primitive cubic unit cell.....	177
5.3	Estimation of R(O...O) and R(O...N) distances in ammonia dihydrate at ~100K.....	181
5.4	Correlation table for ammonia molecules in ammonia dihydrate.....	188
5.5	Normal coordinate calculations of ammonia dihydrate stretching frequencies of NH_3 and ND_3.....	190
5.6	Infrared spectral assignments of $NH_3 \cdot 2H_2O$ and $ND_3 \cdot 2D_2O$.....	192
5.7	O-H stretching frequencies of ammonia dihydrate.....	197
5.8	O-D stretching frequencies of deuterated ammonia dideuterate.....	198

LIST OF FIGURES

FIGURE	DESCRIPTION	PAGE
1.1	Ammonia-water equilibrium phase diagram.....	5
1.2	NH_3-H_2O phase diagram in the region of ammonia dihydrate.	9
1.3	Structure of $2NH_3 \cdot H_2O$ above 90K.....	14
2.1	Glassware used for sample preparations.....	37
2.2	The low-temperature infrared cell.....	46
3.1	Microdensitometer trace of a CuK_α photograph of $NH_3 \cdot H_2O$ at 105K.....	59
3.2	Microdensitometer trace of a CuK_α photograph of $NH_3 \cdot H_2O$ at 105K.....	64
3.3	Infrared spectra of liquid propane, propylene and Freon-13 at 100K and 1 cm^{-1} resolution (6000-4000 cm^{-1}).....	65
3.4	Infrared spectrum of liquid propane at 100K and 1 cm^{-1} resolution (4000-200 cm^{-1}).....	66
3.5	Infrared spectrum of liquid propylene at 100K and 1 cm^{-1} resolution (4000-200 cm^{-1})..	67
3.6	Infrared spectrum of liquid Freon-13 at 100K and 1 cm^{-1} resolution. (4000-400 cm^{-1}).....	68
3.7	Infrared spectra of $NH_3 \cdot H_2O$ at 100K and 1 cm^{-1} resolution (5300-3300 cm^{-1}).....	75

FIGURE	DESCRIPTION	PAGE
3.8	Infrared spectra of $NH_3 \cdot H_2O$ at 100K and 1 cm^{-1} resolution (4000-400 cm^{-1}).....	76
3.9	Infrared spectrum of $NH_3 \cdot H_2O$ at 100K and 1 cm^{-1} resolution (3500-2750 cm^{-1}).....	77
3.10	Absorption by the antisymmetric N-H stretching modes of $NH_3 \cdot H_2O$ at 100K and 1 cm^{-1} resolution (3450-3350 cm^{-1}).....	78
3.11	Infrared spectra of $NH_3 \cdot H_2O$ at 100K and 1 cm^{-1} resolution (2250-1350 cm^{-1}).....	79
3.12	Infrared spectrum of $NH_3 \cdot H_2O$ at 100K and 1 cm^{-1} resolution	80
3.13	Infrared absorbance spectrum of $NH_3 \cdot H_2O$ at 100K and 1 cm^{-1} resolution, $\nu_R(H_2O)$.....	81
3.14	Infrared absorbance spectrum of $NH_3 \cdot H_2O$ at 100K and 1 cm^{-1} resolution (500-200 cm^{-1})...	82
3.15	Infrared spectra of $ND_3 \cdot D_2O$, <1% H at 100K and 1 cm^{-1} resolution (3950-2550 cm^{-1}).....	87
3.16	Infrared spectra of $ND_3 \cdot D_2O$, <1% H at 100K and 1 cm^{-1} resolution (4000-400 cm^{-1}).....	88
3.17	Infrared spectrum of $ND_3 \cdot D_2O$, <1% H at 100K and 1 cm^{-1} resolution (2600-2000 cm^{-1}).....	89
3.18	Absorption by the antisymmetric N-D stretching modes of $ND_3 \cdot D_2O$, <1% H at 100K and 1 cm^{-1} resolution (2250-2510 cm^{-1}).....	90

FIGURE	DESCRIPTION	PAGE
3.19	Infrared spectra of $ND_3 \cdot D_2O$ containing <1% H at 100K and 1 cm^{-1} resolution (2000-1000 cm^{-1}).....	91
3.20	Infrared spectrum of $ND_3 \cdot D_2O$, <1% H at 100K and 1 cm^{-1} resolution (1000-450 cm^{-1}).....	92
3.21	Infrared spectra of $NH_3 \cdot 2H_2O$ at 100K and 1 cm^{-1} resolution (5200-3350 cm^{-1}).....	95
3.22	Infrared absorbance spectra of $NH_3 \cdot 2H_2O$ at 100K and 1 cm^{-1} resolution (4000-200 cm^{-1})..	96
3.23	Absorption by the antisymmetric N-H stretching modes of $NH_3 \cdot 2H_2O$ at 100K and 1 cm^{-1} resolution (3420-3375 cm^{-1}).....	97
3.24	Infrared spectra of $NH_3 \cdot 2H_2O$ at 100K and 1 cm^{-1} resolution (2500-1200 cm^{-1}).....	98
3.25	Infrared absorpance spectra of $NH_3 \cdot 2H_2O$ at 1 cm^{-1} resolution and 100K (curve E) and 150K (curve F) (1200-600 cm^{-1}).....	99
3.26	Infrared absorbance spectrum of $NH_3 \cdot 2H_2O$ at 150K and 1 cm^{-1} resolution (4000-200 cm^{-1})..	100
3.27	The infrared absorbance spectra of the N-D and O-D stretching region of $NH_3 \cdot 2H_2O$ neat and containing NH_2D and HOD at 100K and 1 cm^{-1} resolution (2600-1800 cm^{-1}).....	104

FIGURE	DESCRIPTION	PAGE
3.28	Infrared absorbance spectra of isotopically impure $NH_3 \cdot 2H_2O$ (1800-1500 cm^{-1}) and $ND_3 \cdot 2D_2O$ (1350-1050 cm^{-1}) at 100K and 1 cm^{-1} resolution.....	105
3.29	Infrared absorbance spectra of $NH_3 \cdot 2H_2O$ at 100K and 1 cm^{-1} resolution, neat and containing deuterium impurity (1200-600 cm^{-1}).....	106
3.30	Infrared absorbance spectra of $NH_3 \cdot 2H_2O$ at 100K and 1 cm^{-1} resolution, neat and containing deuterium impurity (1200-600 cm^{-1}).....	107
3.31	Absorption by isolated ND_2H and HOD (3400-3200 cm^{-1}) and isolated NH_2D and HOD (2550-2350 cm^{-1}) in ammonia dihydrate...	108
3.32	Infrared absorbance spectra of $ND_3 \cdot 2D_2O$, <1% H at 100K and 1 cm^{-1} resolution (4000-200 cm^{-1}).....	112
3.33	Infrared absorbance spectra of $ND_3 \cdot 2D_2O$ containing 5% H at 100K and 1 cm^{-1} resolution (4000-2000 cm^{-1}).....	113
3.34	Infrared absorbance spectra of $ND_3 \cdot 2D_2O$ containing <1 and 5% H at 100K and 1 cm^{-1} resolution (3600-2600 cm^{-1}).....	114

FIGURE	DESCRIPTION	PAGE
3.35	N-H and O-H stretching absorbance bands of NHD_2 and HOD isolated in $ND_3 \cdot 2D_2O$ at 100K and 1 cm^{-1} resolution (3600-2600 cm^{-1}).....	115
3.36	O-D stretching absorbance bands of $ND_3 \cdot 2D_2O$, <1% H at 100K and 1 cm^{-1} resolution (2500-2000 cm^{-1}).....	116
3.37	O-D stretching absorbance bands of $ND_3 \cdot 2D_2O$ mulled in propylene at 100K (2500-2000 cm^{-1}).....	117
3.38	O-D stretching absorbance bands of $ND_3 \cdot 2D_2O$ mulled in Freon-13 at 100K (2500-2000 cm^{-1}).....	118
3.39	O-D stretching absorbance bands of $ND_3 \cdot 2D_2O$, 5% H mulled in propane at 100K (2500-2000 cm^{-1}).....	119
3.40	O-D stretching absorbance bands of $ND_3 \cdot 2D_2O$, 5% H mulled in propylene at 100K (2500-2000 cm^{-1}).....	120
3.41	O-D stretching absorbance bands of $ND_3 \cdot 2D_2O$, 5% H mulled in Freon-13 at 100K and 1 cm^{-1} resolution (2500-2000 cm^{-1}).....	121
3.42	Infrared absorbance spectra of $ND_3 \cdot 2D_2O$, containing <1 and 5% H (1900-1100 cm^{-1}).....	122

FIGURE	DESCRIPTION	PAGE
3.43	Infrared absorbance spectra of $ND_3 \cdot 2D_2O$ containing <1 and 5% H (1100-400 cm^{-1}).....	123
3.44	Infrared absorbance spectra of $ND_3 \cdot 2D_2O$ containing <1% H.....	124
4.1	The structure of $NH_3 \cdot H_2O$ projected on the 100 plane.....	134
4.2	The structure of $NH_3 \cdot H_2O$ projected on the 100 plane. The changes in the dipole moments during the B_1 unit cell group vibration based on ν_{3a}.....	135
4.3	The structure of $NH_3 \cdot H_2O$ projected on the 100 plane. The changes in the molecular dipole moments during the B_1 unit cell group vibration based on ν_{3b}.....	138
4.4	The structure of $NH_3 \cdot H_2O$ projected on the 100 plane. The changes in the molecular dipole moments during the B_3 unit cell group vibration based on ν_{3b}.....	139
4.5	The structure of $NH_3 \cdot H_2O$ projected on the 100 plane. The changes in the molecular dipole moments during the B_3 unit cell group vibration based on ν_1.....	140
4.6	The structure of $NH_3 \cdot H_2O$ projected on the 100 plane. The changes in the molecular	

FIGURE	DESCRIPTION	PAGE
	dipole moments during the B_1 unit cell group vibration based on ν_1.....	141
4.7	Ammonia monohydrate, only the chains of O-H...O are shown. The dipole moment change per unit cell, for the A unit cell O-H...O stretching vibration.....	157
4.8	Ammonia monohydrate, only the chains of O-H...O are shown. The dipole moment change per unit cell for the B_3 unit cell O-H...O stretching vibration.....	158
4.9	Ammonia monohydrate, only the chains of O-H...O are shown. The dipole moment change per unit cell for the B_2 unit cell O-H...O stretching vibration.....	159
4.10	Ammonia monohydrate, only the chains of O-H...O are shown. The dipole moment change per unit cell for the B_1 unit cell O-H...O stretching vibration.....	160
5.1	The structure of $NH_3 \cdot 2H_2O$ at 100K.....	183
5.2	The geometry around the atoms O_I, O_{II} and N in the ammonia dihydrate structure.....	184

CHAPTER 1

INTRODUCTION

1.1 General Introduction

There are three hydrates of ammonia: ammonia hemihydrate[1] ($2NH_3 \cdot H_2O$), ammonia monohydrate[1] ($NH_3 \cdot H_2O$) and, most recently, ammonia dihydrate[2,3] ($NH_3 \cdot 2H_2O$). The crystal structure of the first two hydrates have been reported[4,5] (Section 1.3).

These compounds are ideal for studying hydrogen bonds of types O-H...O, O-H...N and N-H...O. Infrared spectra of ammonia hemihydrate and ammonia monohydrate and some of their isotopomers have been recently studied[6-13] (Section 1.3).

In this thesis, the ammonia dihydrate has been separated for the first time and its powder x-ray diffraction pattern is recorded.[14] The crystal structure of ammonia dihydrate is deduced from its powder x-ray diffraction pattern and its infrared spectrum. Also, the infrared spectra of ammonia monohydrate and ammonia dihydrate and their isotopic derivatives at 100K are presented and assigned in the region ~5000 to 200 cm^{-1}. Objectives of this work appear in Section 1.4.

Section 1.2 contains a review of the solid-liquid equilibrium diagram of the ammonia-water system and Section 1.3 contains the thermodynamic properties[15] of $2NH_3 \cdot H_2O$ and $NH_3 \cdot H_2O$ and a review of spectroscopic and structural studies of the hydrates of ammonia.

1.2 Ammonia-Water Equilibrium Phase Diagram

The study of the ammonia-water system to construct the equilibrium phase diagram and to seek any stable compounds has been undertaken by many authors.[1-3,16-22] Three solid hydrates were found: ammonia hemihydrate (65.41 wt% NH_3), ammonia monohydrate (48.59 wt% NH_3) and, more recently, ammonia dihydrate (32.10 wt% NH_3).

The first temperature-composition phase diagram was constructed by F. Rupert[16,17] in 1909. The diagram shows two maxima corresponding to ammonia hemihydrate ($2NH_3 \cdot H_2O$) and monohydrate ($NH_3 \cdot H_2O$). After Rupert, several authors[1,18-22] confirmed the existence of both hemihydrate and monohydrate.

The melting point of the hemihydrate and the monohydrate were both found by all authors to be around -79°C, if we take into account that Mironov's[22] temperatures are systematically 2° higher than those of other authors. The melting point of the hemihydrate was found[1-3,15-21] to be ~0.2-0.4° higher than that of the

monohydrate (except by Mironov[22] who found a higher value for the monohydrate, by 0.4°, than for the hemihydrate). The important points in the phase diagram are listed in Table 1.1. Results by other authors that are not listed in this table can be found in M. Morrison's thesis[23] (table 1.1, p. 4). The results of Baume and Tykociner[20] and of Elliott[21] were incorrectly reported by Morrison; the values given in Table 1.1 were taken from the original papers.

Postma's[1] results were used to construct the ammonia-water phase diagram shown in Figure 1.1, because his melting and eutectic points have been confirmed by Hildenbrand and Giauque[15]. F. Freidrichs,[24] in 1923, disputed the existence of the discrete solid compounds, $NH_3 \cdot H_2O$ and $2NH_3 \cdot H_2O$, and suggested that a continuous series of solid solutions (mixed crystals) was formed. In 1924, Elliott[21] found that visual observation gave no indication of the formation of mixed crystals. In 1953, Hildenbrand and Giauque[15] showed that both ammonia hemihydrate and ammonia monohydrate crystallize as pure compounds, even in their eutectic regions, to within 0.02 and 0.05 mole % respectively. In 1955, Mironov[22] excluded the existence of a continuous series of mixed crystals for concentrations higher than 32.7 wt% NH_3, by eutectic crystallization and by obtaining enough data to construct

Table 1.1 The important points in NH_3-H_2O phase diagram.

	Baume & Tykociner[20,a]		Elliott[21,b]		Postma[1]		Hildenbrand & Giauque[15]		Rollet & Vuillard[2]	
	Wt% NH_3	T°C	Wt% NH_3	T°C	Wt% NH_3	T°C	Wt% NH_3	T°C	Wt% NH_3	T°C
ice-$NH_3 \cdot 2H_2O$ transition	--	--	--	--	--	--	--	--	32.9	-98.0
$NH_3 \cdot 2H_2O$-$NH_3 \cdot H_2O$ eutectic	--	--	--	--	--	--	--	--	35.3	-98.8
ice-$NH_3 \cdot H_2O$ metastable eutectic	32.0	-102.6	--	--	33.4	-100.3	--	--	33.9	-103.3
$NH_3 \cdot H_2O$, m.p.	48.7	-79.6	48.6	-79.1	48.7	-79.0	48.6	-79.01	48.57	-79.0
$NH_3 \cdot H_2O$-$2NH_3 \cdot H_2O$ eutectic	57.5	-87.5	55.9	-88.4	57.12	-86.0	--	-85.9	--	-86.5
$2NH_3 \cdot H_2O$, m.p.	64.8	-79.3	65.4	-78.8	65.4	-78.8	65.4	-78.84	--	--
$2NH_3 \cdot H_2O$-NH_3 eutectic	78.7	-95.0	80.0	-92.59	80.53	-92.5	--	-92	--	--

[a]Measured from the author's figure with an estimated precision of ±0.2 wt% or ±0.2°.
[b]Measured by replotting Elliott's values with an estimated precision of ±0.2 wt% or ±0.2°. -92.59 is the author's value.

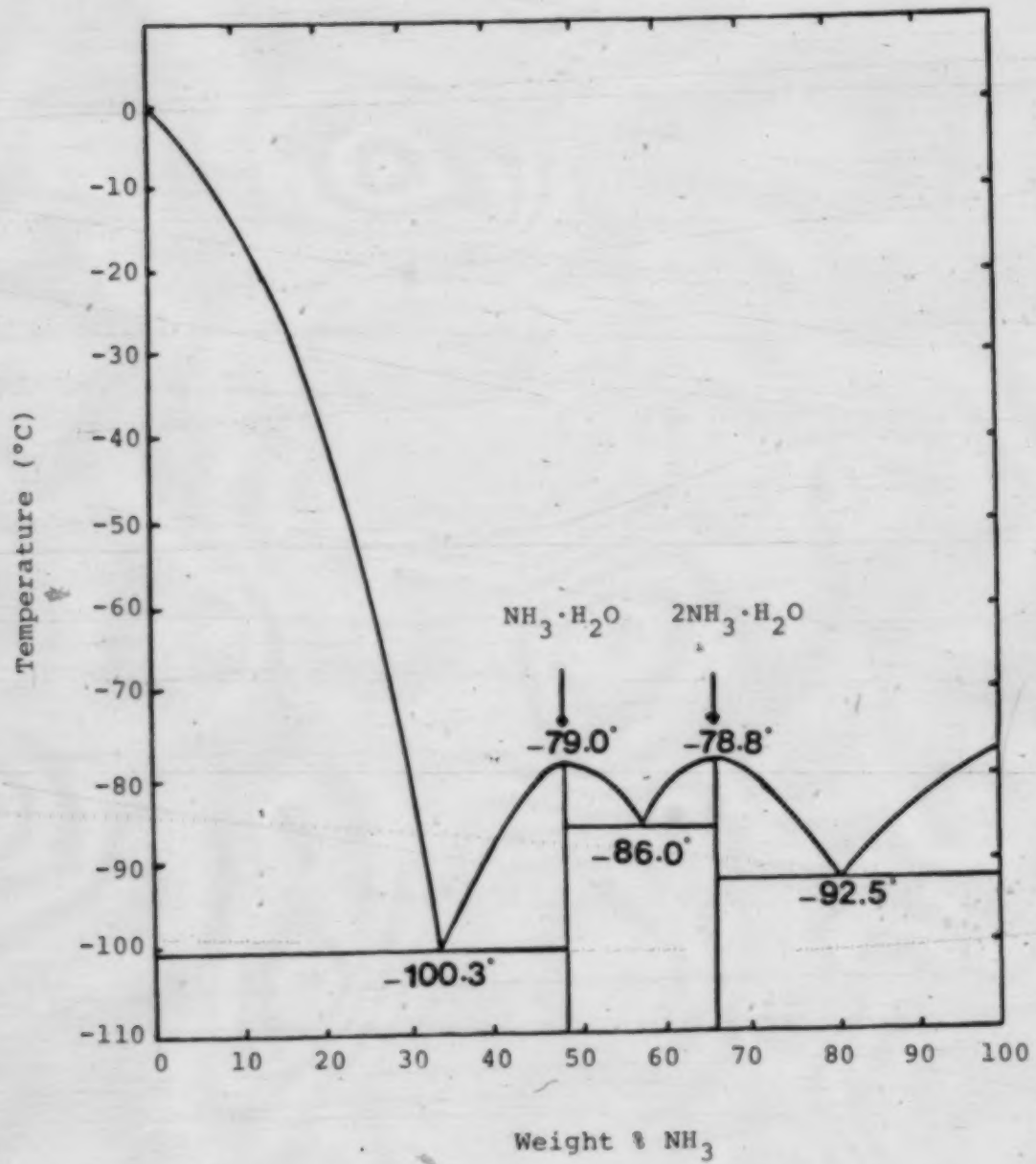

Figure 1.1 Ammonia-water equilibrium phase diagram. After Postma (Ref. 1) with compositions converted from mole % NH_3 to weight % NH_3.

the monohydrate-ice solidus curve at -101.3°C (or -103.3°C, if corrected for his systematic 2° error).

Mironov suggested that the primary crystallization for the composition with 50.1 wt% NH_3 at -99°C might correspond to the hemihydrate on the metastable continuation of its liquidus curve. So he predicted the possibility that a special investigation could reveal the metastable portion of the hemihydrate liquidus which would intersect with the extrapolated ice branch to form a metastable eutectic (ice-$2NH_3 \cdot H_2O$) at ~-127°C between 35-40 wt% NH_3.

Almost all workers[1,16-22] had indicated a problem with supercooling and very high viscosity of solutions with compositions between 28 and 34 wt% NH_3. This hindered the crystallization, and determination of the ice-$NH_3 \cdot H_2O$ eutectic was not an easy task. Most of the authors[1,16-21] tried to locate this eutectic by extrapolation of the liquidus branches. They reported eutectic temperatures from below -120° to -100.3°C. Postma[1] introduced seed crystals, prepared from the solution under investigation, to enhance the crystallization. In regions of very intense supercooling Postma determined the solidus and liquidus by heating the crystals and observing the temperature at which the last crystals disappeared. For solutions with composition

between 0 and 32.7 wt% NH_3, Postma could not determine the temperature of eutectic crystallization.

In 1956 Rollet and Vuillard[2,3] obtained evidence of a new compound, $NH_3 \cdot 2H_2O$ or ammonia dihydrate, which decomposes before melting. They solidified their samples by cooling them in liquid nitrogen and studied by thermal analysis the changes that occurred as the solids were slowly warmed. They found that samples of over 42 weight percent ammonia always crystallized on cooling while those with less than 42 weight percent ammonia formed a glass on cooling. On warming, the glass transition occurred at -145°C for all compositions up to 40 weight percent of ammonia. On further warming three transitions were seen, at -115°C, -103.3°C and -98.00 or -98.8°C depending on the composition. Rollet and Vuillard attributed the transition at -115°C to the crystallization of ice and monohydrate from the very viscous liquid that exists above the glass transition. They found that when the mass, first vitrified, was reheated slowly, then kept at -100°C for several hours, then recooled, the thermal analysis (on heating) no longer showed the event at -103.3°C. So, they attributed the -103.3°C transition to the metastable eutectic between ice and monohydrate. The existence of the transition at -98.0 or -98.8°C, which occurs everytime the sample is warmed so is not due to metastable species,

must indicate that the solution which is formed at the -103.3°C eutectic recrystallizes to form a new compound. From the variation with composition (bottom of Figure 1.2) of the length of the plateau on the temperature-time graphs, they determined the new compound to be the dihydrate. The transition at -98.0°C exists for ammonia concentrations up to 32.9 weight percent (transition point B in Figure 1.2) with maximum duration at 32.2 weight percent (point A in Figure 1.2), which corresponds to ammonia dihydrate (32.10 wt% NH_3). The transition at -98.8°C appears for ammonia concentrations between 32.2 to 35.3 weight percent with maximum duration at 35.3 weight percent corresponding to dihydrate-monohydrate eutectic point (eutectic point D in Figure 1.2).

In 1973 Van Kasteren[25] unaware of Rollet and Vuillard's work, studied two mixtures of ammonia and water with 4.46 and 26.81 mole% NH_3, i.e. 4.23 and 25.72 wt% NH_3, as coolants which have a phase transition at low temperatures. He concluded that there are two eutectic mixtures with melting points of -102.0° and -96.8°C and the thermal history determined which type would dominate. Upon heating the mixture that melted at -102.0°C, it recrystallized between -102° and -97°C and finally melted at -96.8°C.

The phase diagram between 25 and 50 weight percent of

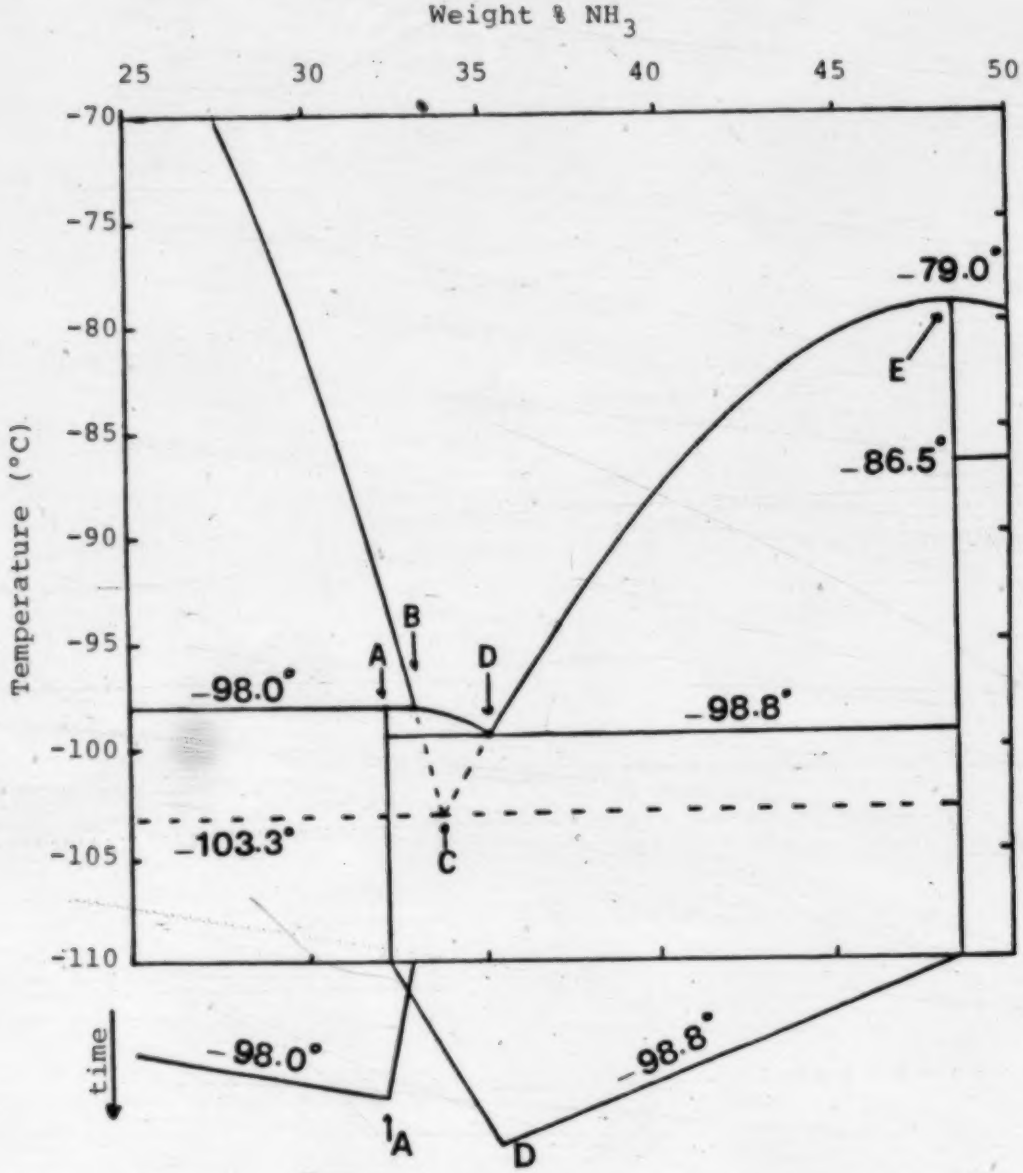

Figure 1.2 NH_3-H_2O phase diagram in the region of ammonia dihydrate. After Rollet and Vuillard (Ref. 2,3). (A) 32.2 wt% NH_3, $NH_3 \cdot 2H_2O$ melting point at -98.0 or -98.8°C; (B) 32.9 wt% NH_3, ice-dihydrate transition at -98.0°C; (C) 33.9 wt% NH_3, ice-monohydrate metastable eutectic at -103.3°C; (D) 35.3 wt% NH_3, dihydrate-monohydrate eutectic at -98.8°C; (E) 48.57 wt% NH_3, $NH_3 \cdot H_2O$ melting point at -79.0°C

ammonia according to Rollet and Vuillard is shown in Figure 1.2, and with Figure 1.1, represents the current state of knowledge.

1.3 Review of Spectroscopic and Structural Studies of the Hydrates of Ammonia

Several infrared spectra of ammonia hemihydrate and monohydrate and of their isotopically-substituted forms have been reported.[6-13,26] The crystal structure of ammonia hemihydrate[4] and ammonia monohydrate[5] have also been reported. No spectroscopic or structural studies of the dihydrate of ammonia have been reported prior to this work.

In 1953 Hildenbrand and Giauque[15] in a study of some thermodynamic properties of ammonia hemihydrate and monohydrate concluded, according to what is mentioned in Section 1.2, that these two compounds must crystallize in very pure form at their normal melting points. They calculated the heat of fusion of the hemihydrate and the monohydrate to be 2352 and 1568 Cal $mole^{-1}$ at their respective melting points, -78.84 and -79.01°C. The entropies of hemihydrate and monohydrate were found to be 15.42 and 7.89 Cal $deg^{-1}mole^{-1}$, respectively, at 100K, the temperature at which the spectra in this thesis were obtained. Hildenbrand and Giauque[15] found two sharp

maxima in the heat-capacity curve of ammonia hemihydrate in the region near 52K, which were attributed to the angular motions in more than one crystal plane and possibly to the presence of two structurally different ammonium groups. No transitions were seen in the case of monohydrate. They concluded that both of the above hydrates approach zero entropy at the absolute zero of temperature within 0.1 Cal $deg^{-1}mole^{-1}$ and thus all hydrogen bonds and other structural details must be essentially ordered in the crystalline states of these substances below 50K.

It should be noted that ammonia hemihydrate and ammonia monohydrate were considered by Hildenbrand and Giauque to be ammonium oxide $(NH_4)_2O$ and ammonium hydroxide NH_4OH, respectively.

In 1953 Waldron and Hornig[26] reported mid-infrared spectra of what they claimed to be ammonia hemihydrate and monohydrate at -195°C. They prepared their samples by condensing ammonia and water vapour onto a NaCl or KBr plate at liquid nitrogen temperature and it seems unlikely that they could have obtained the correct phases. The structure of the ammonia hydrates were not known at this time, so they reported several conclusions concerning them. The possibility of the ionic structure was excluded due to the absence of the bending vibration of NH_4^+ at

about 1400 cm^{-1} from their spectra. Their spectra closely paralleled those of crystalline ammonia and ice, with some differences. The absence of the strong ice band at ~812 cm^{-1} was attributed to the replacement of one of the O-H...O bonds by a weaker O-H...N bond. They noted the shift in the symmetric bending vibration of ammonia, which occurs at ~1060 cm^{-1} in the pure crystal, to 1102 cm^{-1} in their monohydrate and to 1020 and 1091 cm^{-1} in the hemihydrate. They assumed that the doubling in the hemihydrate indicates that the two ammonia molecules occupy different sites in the hemihydrate. The absorption near 1625 cm^{-1} was attributed to the bending vibration of H_2O with the probability that some of it was caused by the doubly-degenerate bending vibration of ammonia. The peak at 2950 cm^{-1}, which appeared in the spectrum of both hydrates, was assigned to N-H...O bonds. So they suggested that only one of the ammonia molecules in ammonia hemihydrate is involved in this sort of bonding. The hemihydrate peak at 3140 cm^{-1} was attributed to possibly a weaker N-H...O bond from the second ammonia molecule. The peaks at 3220 and 3365 cm^{-1} could not be assigned in detail and were attributed to hydrogen bonded O-H and N-H vibrations.

In 1953 Siemons and Templeton[4] studied the crystal structure of ammonia hemihydrate by means of single-

crystal x-ray diffraction. They found that it crystallizes in the orthorhombic system with space group[27] Pnma, and the unit-cell axes a = c = 8.41 ± 0.03 Å and b = 5.33 ± 0.02 Å at -95 ± 10°C. They calculated the density of the solid to be 0.916 gcm^{-3} at -95°C if they assumed four molecules per unit-cell. This was acceptable compared to their rough value of a little more than 0.8 gcm^{-3} measured for the liquid around its melting point. They concluded that each molecule occupies a site of symmetry m, i.e. C_s site symmetry. The coordinates of equivalent positions are: $(x, 0.25, z)$; $(\bar{x}, 0.75, \bar{z})$; $(0.5-x, 0.75, 0.5+z)$; $(0.5-x, 0.25, 0.5-z)$.

The structure of the hemihydrate, Figure 1.3, consists of a three-dimensional network of alternating nitrogen and oxygen atoms, connected by hydrogen bonds of types N_I-H...O and O-H...N_I. One-half of the ammonia molecules (designated N_IH_3) take part in this network. The other half (designated $N_{II}H_3$) are attached to this network by a single hydrogen bond of the type O-H...N_{II}. The hydrogen atoms of $N_{II}H_3$ are not hydrogen bonded, so $N_{II}H_3$ molecules are free to rotate about the O-H...N_{II} hydrogen bond. This free rotation was suggested by the electron density maps, which indicated more violent thermal motion at N_{II} than at N_I, and by the transition in the heat-capacity curve observed by Hildenbrand and Giauque[15]

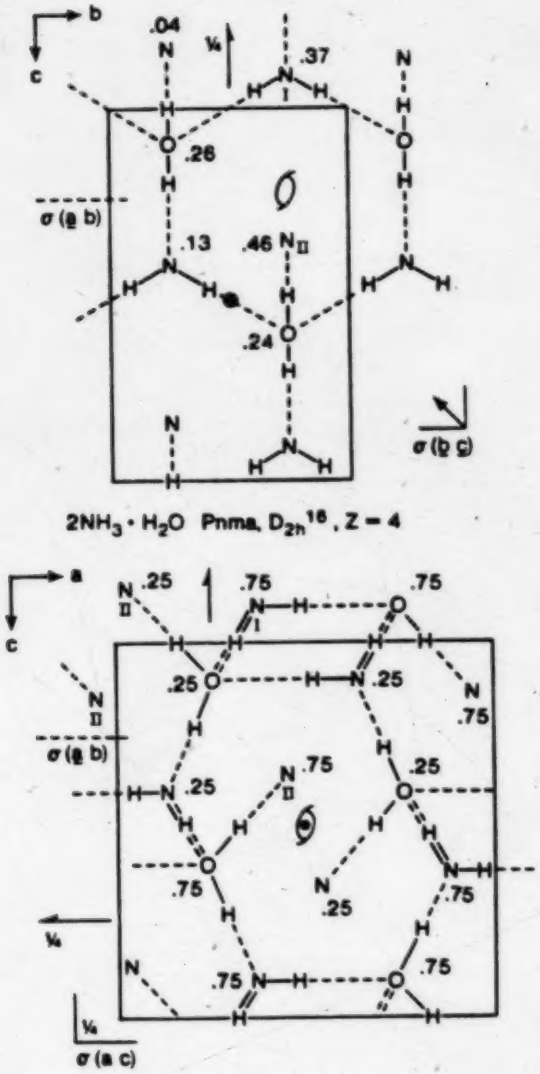

Figure 1.3 Structure of $2NH_3 \cdot H_2O$ above 90K, after Ref. 13. The hydrogen atoms of $N_{II}H_3$ are not shown, for clarity. The double full or dashed lines in the ac projection represent bonds to two atoms separated by one unit cell along b.

at 52K.

The interatomic distances were found to be smaller than 3.25 Å for oxygen and nitrogen atoms connected by hydrogen bonds, and larger than 3.6 Å for atoms not connected by hydrogen bonds. The O...N distances O-H...N_I and O-H...N_{II} were found to be 2.84 Å and 2.85 Å, respectively. The two electron pairs of each oxygen atom form three hydrogen bonds of the type N_I-H...O with N_I...O distances of 3.13, 3.22 and 3.22 Å. Thus each oxygen atom is five coordinated. The arrangement of the bonds at N_I was found to be nearly tetrahedral, with angles from 107° to 112°. The angle between the O-H...N bonds at the water molecules is 116°.

The locations of the hydrogen atoms were fixed by those of the heavy atoms, and comply with the Pnma symmetry of the heavy atoms. The same symmetry was assumed for the average positions of the hydrogens of N_{II}.

The presence of two non-equivalent ammonia molecules in the structure of ammonia hemihydrate was confirmed in 1971 by S. Eletr and C.T. O'Konski.[28] In their study of ^{14}N nuclear quadrupole resonance of ammonia hemihydrate, four absorption frequencies were observed. The frequencies were unambiguously paired by their Zeeman behaviour and each pair was assigned to one type of

ammonia molecule. The temperature dependence of these frequencies was reported from 77 to 190K. The temperature dependence curve for one pair was much steeper than that for the other pair and was assigned to $N_{II}H_3$ type molecules. This interpretation is in accord with the heat-capacity anomaly observed by Hildenbrand and Giauque[15] near 52K and with the assumption made by Siemons and Templeton[4], that the $N_{II}H_3$ molecules rotate about the hydrogen bond. Eletr and O'Konski also concluded that neither N_I nor N_{II} can be NH_4^+, because that ion would have a nearly zero quadrupole coupling constant, because of its essentially tetrahedral symmetry.

In 1959 Olovsson and Templeton[5] determined by means of single-crystal x-ray diffraction that the crystal system of ammonia monohydrate at -95 and -160°C is orthorhombic with space group[27] $P2_12_12_1$. If they assumed four molecules in the unit-cell, which had the dimensions $a = 4.51 \pm 0.01$, $b = 5.587 \pm 0.003$ and $c = 9.700 \pm 0.005$ Å at -160°C, they calculated the density of the solid to be 0.952 gcm^{-3}. This was an acceptable value compared with the approximate density of the liquid, 0.89 gcm^{-3}, at -68°C determined by Hildenbrand and Giauque,[15] that of ice, 0.92 gcm^{-3}, that of ammonia hemihydrate, 0.917 gcm^{-3} at -95°C, and that of ammonia[29], 0.857 gcm^{-3} at -196°C. The atoms are on C_1 sites.

The structure was found to consist of planar chains of water molecules that are connected by hydrogen bonds of O...O distance 2.76 Å at -160°C. The chains are oriented along the a axis and lie approximately in the z = 0 and z = 1/2 planes. They are cross-linked by the ammonia molecules into a three-dimensional network by short bonds, 2.775 Å, of the type O-H...N and long bonds, 3.21, 3.26 and 3.29 Å, of the type N-H...O. The oxygen atom contributes one-third of an electron pair to each of three N-H...O bonds and one electron pair to each O-H...O bond. So, the oxygen atoms are six-coordinated and the nitrogen atoms are four-coordinated. The rotation about the three-fold axis of ammonia is believed to be quite restricted. The structure of $NH_3 \cdot H_2O$ projected on the 100 plane is drawn, after Ref. 5, in Figure 4.1 and the one projected on the 001 plane is drawn in Figure 4.7 (only "O-H...O-H" chains are shown for clarity).

The positions of the hydrogen atoms as stated above were fixed by those of the heavy atoms. However, the positions of the hydrogen atoms of the water molecules in the water chains were uncertain. Choice of one position fixes the hydrogen positions for the rest of the water molecules in the same chain. Olovsson and Templeton concluded that if the space-group symmetry, of $P2_12_12_1$, does not apply exactly to the hydrogen atoms, or if there

is disorder, the sense of the chains may be different in different parts of the crystal.

In 1980, Bertie and Morrison[6] published mid-infrared spectra, 4000 to 400 cm^{-1}, of ammonia hemihydrate and ammonia monohydrate at 95K. They prepared infrared samples by a low-temperature mulling technique developed in 1964 by Bertie and Whalley.[30] Bertie and Morrison's spectra were quite different from those reported earlier by Waldron and Hornig.[26] However, the samples used by Bertie and Morrison were characterized by their x-ray powder diffraction patterns, and their cell parameters at ~100K were found to agree very well with the published data.[4,5] Hornig's samples were not so characterized and there is no doubt that Bertie and Morrison's spectra are the correct ones.

The assignment of the bands in ammonia monohydrate[6] was based on site effects only, and intermolecular coupling was neglected. Bertie and Morrison[6] suggested that the three N-H...O bonds of length 3.21, 3.26 and 3.29 Å are very weak hydrogen bonds, being over 0.3 Å longer than the 2.9 Å sum of the van der Waals radii of nitrogen and oxygen atoms. The three N-H...O bonds were considered to be roughly equivalent[18] to N-H...N bonds of length 3.31, 3.36 and 3.39 Å or to O-H...O bonds of length 3.11, 3.16 and 3.19 Å. Thus, the N-H stretching frequencies of

these three bonds were considered to be very similar, by analogy with the case of O-H...O bonds.[31-35] Each ammonia molecule was, thus, suggested to exhibit a pattern of N-H stretching frequencies similar to that of a molecule with C_3 symmetry, and therefore similar to those in solid ammonia. Thus, the intense doublet in the spectrum of ammonia monohydrate at 3402/3387 cm^{-1} was assigned to the two components under the site group of the antisymmetric N-H stretching vibration ν_3 and ν_3'. The much weaker features at 3330, 3305, 3287 and 3270 cm^{-1} were assigned to $\nu_1(NH_3)$ in Fermi resonance with $2\nu_4(NH_3)$. Bertie and Morrison[6] found from the correlation[32-37] between the O-H stretching frequency and O...O distance that the O-H frequency is near 3250 cm^{-1} for an O...O distance of 2.76 Å and near 3000 cm^{-1} for an O...O distance of 2.675 Å. They assumed that the correlation is good to ~ ± 100 cm^{-1}. So, the peak at 3190 cm^{-1} was assigned to the O-H...O bond of length 2.76 Å and that at 2910 cm^{-1} was assigned to the O-H...N bond of length 2.775 Å, which is equivalent to an O...O bond of length 2.675 Å. The three sharp bands at 1664, 1650 and 1625 cm^{-1} were assigned to $\nu_4(NH_3)$ and the two sharp bands at 1133 and 1095 cm^{-1} were assigned to $\nu_2(NH_3)$; even though there are only two components of ν_4 and only one of ν_2 under the site group. The peak at 1540 cm^{-1} was assigned to $\nu_2(H_2O)$.

All features below 1000 cm^{-1} were assigned to rotational vibrations of the water and/or ammonia molecules.

The assignment for ammonia hemihydrate was made by Bertie and Morrison[6] according to the site group, and the intermolecular coupling was ignored. The doublet at 3397/3374 cm^{-1} was assigned to ν_3^1 and ν_3^2 of both types of ammonia molecules. Neither the symmetric N-H stretching vibration nor $2\nu_4(NH_3)$ were detected above the broad absorption from 3200 to 3350 cm^{-1}. The broad peaks at 3125 and 2975 cm^{-1} were assigned to the O-H stretching vibrations in the O-H...N bonds of length 2.85 and 2.83 Å, respectively. The 150 cm^{-1} separation of the peaks was attributed to site splitting. It is too large for it to result from intramolecular coupling alone, and the intermolecular coupling is expected to be small because each water molecule is surrounded by ammonia molecules, whose stretching frequencies are quite different from those of the water molecules. The difference of 0.02 Å between the O-H...N bonds of the two types of ammonia given by x-ray work[4] is too small for the corresponding O-H stretching vibrations to be separated by 150 cm^{-1}, and a difference of ~0.04 Å was suggested.[4] The three bands at 1625, 1590 and 1555 cm^{-1} were assigned to an overlapping of $\nu_2(H_2O)$ and $\nu_4(NH_3)$. The three sharp bands at 1156, 1092, and 1083 cm^{-1} were assigned to $\nu_2(NH_3)$ despite

the 70 cm^{-1} separation between the extreme features. Bertie and Morrison suggested that the 1156 cm^{-1} feature is an overtone or a combination band. All features below 1000 cm^{-1} were assigned to rotational vibrations of the water and/or ammonia molecules.

By analogy with the ices,[30,38,39] Bertie and Morrison suggested that the sharp features in the absorption by the rotational lattice vibrations of the monohydrate are an indication that the structure is ordered, and noted that a more definitive indication of disorder[39,40] can be obtained from the absorption by the translational lattice vibrations in the far-infrared.

In 1981, Sill, Fink and Ferraro[8] obtained a spectrum of an ammonia-water mixture prepared by depositing a thin film from a mixture of gaseous ammonia and water and annealing this film at a temperature of 162K. The film was then recooled to 96K and the spectrum was recorded. The spectrum that they obtained was that reported earlier by Staats and Morgan[41] to be due to the cubic phase of ammonia. Other workers had disagreed[42,43] with Staats and Morgan's spectrum of ammonia, so Sill et al. resolved the argument by showing that Staats and Morgan's spectrum was not of a pure phase of ammonia, but is instead of an ammonia-water mixture. The nature of the sample of Sill et al. is not clear. Sill et al. initially claimed, by

comparing the integrated absorptions of the hydrate with those of solid ammonia and ice, that the spectrum represented mostly the hemihydrate. But the spectrum was found to have several similarities to Bertie and Morrison's[6] spectrum of the monohydrate, samples of which were characterized by their x-ray diffraction patterns. There are some differences between their spectrum and Bertie and Morrison's monohydrate spectrum. The relative intensities are not quite the same in the two spectra, and two additional weak features were observed in Sill et al.'s spectrum at 1231 and 825 cm^{-1}. Sill et al. did not observe the shoulder at 3287 cm^{-1} nor the weak feature at 2142 cm^{-1} that were seen by Bertie and Morrison.

In 1981, Bertie and Morrison[7] published mid-infrared spectra of fully and partially deuterated samples of ammonia hemihydrate and ^{15}N-substituted samples of ammonia monohydrate and hemihydrate. The shifts of the frequencies upon ^{15}N-substitution of ammonia monohydrate confirmed the previous general assignments by Bertie and Morrison,[6] and revealed a third component of $\nu_3(NH_3)$ of $^{15}NH_3 \cdot H_2O$ at 3384 cm^{-1} which corresponds to a questionable shoulder at 3392 cm^{-1} in the spectrum of $^{14}NH_3 \cdot H_2O$. It was suggested that the basic source of the doublet is site splitting and the extra feature at 3392 cm^{-1} is separated from that at 3387 cm^{-1} by Davydov splitting. The ^{15}N isotope shifts

calculated for rotational vibrations of ammonia under C_{3v} symmetry are too small to detect for bands as broad as those observed.

The absorption by the stretching vibrations of N-H and O-H bonds was found to be more diffuse than that by N-D and O-D bonds in ammonia hemihydrate, which indicates that the former is more affected by anharmonicity. The band assigned to $\nu_4(ND_3)$ and $\nu_2(D_2O)$ is much sharper than the equivalent band in $2NH_3 \cdot H_2O$ and has a different shape. This was attributed to a substantial reduction in the width of the absorption by $\nu_2(H_2O)$ on deuteration, which is known to occur for ice.[44] Further, the O-D stretching band in $2ND_3 \cdot D_2O$ at 2355 cm^{-1} was found to be split, with a sharp dip at 2333 cm^{-1} and a second maximum at 2326 cm^{-1}, while the corresponding O-H stretching band at 3125 cm^{-1} is not split.[6] The symmetric stretching vibration of type I ND_3 molecules and the first overtones of the anti-symmetric ND_3 deformation and D_2O deformation vibrations are all expected to absorb near 2340 cm^{-1} and, thus, could be the cause of the splitting. Another possible source of this splitting was suggested to be an Evans hole arising from Fermi resonance between the overtone, $2\nu_2(D_2O)$ or $2\nu_4(ND_3)$, and the broad $\nu_{OD}(D_2O)$ band. It was confirmed later by J.E. Bertie and J.P. Devlin[12] that the hole in the spectrum of $2ND_3 \cdot D_2O$ is an Evans hole and it

arises from intermolecular interaction between ν_{OD} of D_2O and ν_1 of ND_3.

The strong doublet of $2ND_3 \cdot D_2O$ at 2530/2502 cm^{-1} was found to be split by 28 cm^{-1} which is larger than the 23 cm^{-1} split of the corresponding doublet of $2NH_3 \cdot H_2O$ at 3397/3374 cm^{-1}. A larger splitting for the deuterated species is usually caused by kinetic, or G matrix coupling and occurs for solid and gaseous water[45] and ammonia.[46] So, if there were just one type of ammonia molecule in the crystal the larger splitting for ND_3 would indicate that the splitting was due to intramolecular coupling, not to intermolecular effects. Another possible source of the splitting is the two components of ν_3 under C_s site symmetry. But this last possibility was proven to be incorrect, and the splitting was shown to be due to the two types of ammonia molecules in ammonia hemihydrate, i.e. due to multiple-site splitting. So, the larger splitting in $2ND_3 \cdot D_2O$ was attributed to different kinetic coupling in the two types of ammonia molecule.

The two sharp lines at 2445 and 2432 cm^{-1} in the spectrum of 5% D in $2NH_3 \cdot H_2O$ were assigned[7] to the stronger hydrogen bonded N_I-D, of $N_I \ldots O$ bond lengths of 3.24 and 3.11 Å respectively, i.e. ν_{N_I-D} of $N_I H_2 D$ molecules of C_1 and C_s symmetry, respectively. The four lines at 2501/2490/2473/2461 cm^{-1} were assigned to type II

ammonia molecules, $\nu_{N_{II}-D}(N_{II}H_2D)$, under the assumption that the molecule can have either of the two inequivalent orientations that preserve the plane of symmetry. In solid ammonia,[46] $\nu_{N-D}(NH_2D)$ is at 2447 cm^{-1}, ~60 cm^{-1} below $\nu_3(ND_3)$, and $\nu_{N-H}(ND_2H)$ is at 3329 cm^{-1}, ~44 cm^{-1} below $\nu_3(NH_3)$. By analogy, the separations between the peaks at 2530 and 2502 cm^{-1} in $2ND_3 \cdot D_2O$, and the average frequencies of $\nu_{N_{II}-D}(N_{II}H_2D)$ at 2501/2490/2473/2461 cm^{-1} and of $\nu_{N_I-D}(N_IH_2D)$ at 2445/2432 cm^{-1} were found to be 49 and 64 cm^{-1}, respectively.

This assignment of $N_{II}H_2D$ was found to be incorrect by Bertie and Devlin[13] who showed that $N_{II}H_2D$ yields only 2473 cm^{-1}. The 2461 cm^{-1} feature was observed by them[13] at 2456 cm^{-1}, but it was not present in all samples. Further, Bertie and Devlin showed the bands at 2490 and 2501 cm^{-1} to be due to N-D stretching modes of $N_{II}D_2H$ of C_1 and C_s symmetries, which were calculated[7] to be at 2500 and 2506 cm^{-1}, respectively.

Similarly, the separations between the peaks at 3397 and 3374 cm^{-1} in $2NH_3 \cdot H_2O$, and the unresolved peak of $\nu_{N_{II}-H}(N_{II}D_2H)$ at 3355 cm^{-1} and the average frequency of $\nu_{N_I-H}(N_ID_2H)$ at 3322/3308 cm^{-1} were found[7] to be 42 and 59 cm^{-1}, respectively. It was, thus, concluded that the 2502 cm^{-1} peak in the spectrum of $2ND_3 \cdot D_2O$ is due to $\nu_3(N_ID_3)$ and the 2530 cm^{-1} is due to $\nu_3(N_{II}D_3)$. Similarly, the

3397 and 3374 cm^{-1} peaks in $2NH_3 \cdot H_2O$ are due to $\nu_3(N_{II}D_3)$ and $\nu_3(N_ID_3)$, respectively. This assignment was supported by theoretical calculations, in which the diagonal N-H stretching force constants that were calculated from the isolated N_I-D stretching frequencies at 2432 and 2445 cm^{-1} were used to calculate the splitting of ν_3 of an NH_3 molecule of C_s symmetry. The calculated splittings of the two components of $\nu_3(NH_3)$ and $\nu_3(ND_3)$ under C_s symmetry, ν_3' and ν_3'', were found[7] to be 11 and 9 cm^{-1}, respectively. No reasonable value of the interaction force constant was found to predict the observed 23 and 28 cm^{-1} splitting of the doublet in $2NH_3 \cdot H_2O$ and $2ND_3 \cdot D_2O$, respectively, so it was concluded[7] that the splitting cannot be due to the loss of degeneracy of the ammonia molecules and must, therefore, be due to the two types of ammonia molecules.

The symmetric deformation vibrations $\nu_2(NH_3)$ were found[7] to absorb at 1156/1092/1083 cm^{-1} and the corresponding $\nu_2(ND_3)$ at 884/848/838 cm^{-1}. The higher frequency splitting was found to be 36 cm^{-1} in $2ND_3 \cdot D_2O$ compared with 64 cm^{-1} in $2NH_3 \cdot H_2O$. This greater reduction on deuteration than the $\sqrt{2}$ expected, led Bertie and Morrison[7] to suggest that the bands at 884 and 1156 cm^{-1} may not be due to a component of ν_2 but may arise from an overtone or combination transition whose intensity is

enhanced by Fermi resonance with ν_2. This suggestion was supported by a shift of only 2 cm^{-1} of the peak at 1156 cm^{-1} upon ^{15}N-substitution of $2NH_3 \cdot H_2O$, compared with the 5 cm^{-1} shift calculated for ν_2. But, a detailed frequency calculation[7] has shown that the two bands observed for $\nu_2(NH_2D)$ at 1056 and 1021 cm^{-1}, and the two bands observed for $\nu_2(ND_2H)$ at 962 and 936 cm^{-1} are most likely due to multiple-site splitting. It was concluded that the lower frequency component of each doublet, at 1021 cm^{-1} for NH_2D and 936 cm^{-1} for ND_2H, arises from the type II ammonia molecule that also absorbs near 843 cm^{-1} in $N_{II}D_3$ and 1088 cm^{-1} in $N_{II}H_3$. The higher-frequency component of each doublet, at 1056 cm^{-1} in NH_2D and 962 cm^{-1} for ND_2H, arises from the type I ammonia molecule which also absorbs at 1156 and 884 cm^{-1} in N_IH_3 and N_ID_3. The 1156 and 884 cm^{-1} bands were thought to be pushed to high frequency by a Fermi resonance. It was suggested that this Fermi resonance interaction is also active in $NH_3 \cdot H_2O$, to cause the 40 cm^{-1} split of the bands due to $\nu_2(NH_3)$, since this split cannot be due to site splitting.

It was found[7] that the two lower frequency peaks of $2NH_3 \cdot H_2O$ at 1092 and 1083 cm^{-1} broadened and merged as the concentration of deuterium isotopic impurity increased, and a similar but less pronounced effect was seen for the 848 and 838 cm^{-1} peaks of $2ND_3 \cdot D_2O$. It was, therefore,

concluded[7] that these peaks are split by intermolecular coupling into the infrared-active B_{1u} and B_{3u} vibrations under the unit cell group which is isomorphous with D_{2h}. However, Bertie and Devlin[13] recently observed four features for the coupled ν_2 modes at 15K, which are expected under the C_i unit cell group. The difference in the splitting between the observed coupled and uncoupled frequencies is attributed[13] to intermolecular coupling between the two types of ammonia molecules.

T. Huston, I.C. Hisatsune and J. Heicklen[10] have obtained spectra of presumably amorphous and crystalline ammonia monohydrate and hemihydrate at 83K. Their spectra differ from those obtained by Bertie et al.[6,7,13] except in some major peaks. The samples used by Bertie and Morrison[6,7] were characterized by their x-ray powder diffraction patterns, and their cell parameters at ~100K were found to agree very well with the published data.[4,5] However, the samples used by T. Huston, I.C. Hisatsune and J. Heicklen[10] were not so characterized and there is no doubt that Bertie and Morrison's spectra are the correct ones.

C. Thornton, M.S. Khatkale and J.P. Devlin[9] studied the isotopically decoupled vibrational spectra and proton exchange rates for crystalline NH_3, and amorphous films of NH_3+D_2O and ND_3+H_2O. In crystalline ammonia, they[9] showed

that proton/deuteron migration away from the exchange centers is impossible at temperatures up to 150K. In amorphous films of NH_3+D_2O and ND_3+H_2O they concluded that proton/deuteron transfer does not occur below 125K but is rapid at T > 135K. Bertie and Devlin[11] found that there is no significant proton/deuteron exchange in pure ammonia hemihydrate at T ≈ 140K. This was attributed to the presence of ion-pair defect (NH_4^+, OH^-) which are lacking in mobility in the structure of ammonia hemihydrate. The mobilization of the NH_4^+ ion defects was induced by either ammonia or water doping of the hemihydrate. However the water subsystem invariably remained blocked to proton transfer despite the induced proton transfer within the ammonia subsystem and only less than 5% of the water molecules experienced isotopic exchange after several hours at 135K. The fact that ammonia hemihydrate crystallizes from a 2:1 ammonia-water amorphous solid at 120K, made it possible to prepare samples of $2ND_3 \cdot H_2O$ or $2NH_3 \cdot D_2O$ with very little or no isotopic exchange.[11] Bertie and Devlin[11] also found that water-rich samples crystallized in the 125-130K range with complete isotopic scrambling within the ammonia subsystem of the hemihydrate. Thus, it was not possible[11] to form crystals of $ND_3 \cdot H_2O$ or $NH_3 \cdot D_2O$ in films condensed at low temperatures without isotopic scrambling.

Bertie and Devlin[13] studied the infrared spectra of crystalline films of $2NH_3 \cdot D_2O$, $2ND_3 \cdot H_2O$, $2NH_3 \cdot H_2O$ and $2ND_3 \cdot D_2O$, both pure and containing ND_3, NH_3, NH_2D, ND_2H, H_2O, D_2O and HOD as impurities, at temperatures between ~130 and 15K. They observed a quartet due to ν_3 of type II ammonia of isolated or of intermolecularly coupled ones in ammonia hemihydrate at 15K. This quartet exhibited slight shifts of frequencies and relative intensities on dilution or change of water isotope, which indicate that the intermolecular coupling is significant and that the coupled quartet is in fact due to coupled modes of the unit cell and are not just the site group components. Bertie and Devlin[13] also reported the existence of two nonequivalent sets of type II ammonia molecules below 52K, each of which is free to reorient above the transition, which explains the source of the two lambda transitions at 51.6 and 53.3K that are indicated by the specific heat.[15] They[13] reported a change of the unit cell group for type II ammonia from D_{2h} to C_i at the transition near 52K. This was inferred from the observation of six N-D stretching bands of isolated $N_{II}H_2D$. From the rearrangement of intensity of the N-D stretching bands of $N_{II}H_2D$ between 35 and 15K, Bertie and Devlin[13] calculated the energy difference between preferred and unpreferred orientations to be ~23 cm^{-1}, i.e., 270 $Jmol^{-1}$.

In the case of type I ammonia, Bertie and Devlin[13] observed a triplet, expected under D_{2h}, for the coupled $\nu_3(N_I D_3)$ at 15K instead of the quartet expected under C_i. This indicates that the D_{2h} selection rules for type I ammonia are retained at 15K.

Bertie and Devlin[13] identified the bands due to ν_4 of ammonia in ammonia hemihydrate for the first time. The disappearance of the site splitting of $\nu_4(NH_3)$ for each kind of ammonia in the pure crystals and the appearance of a doublet that depends on isotopic composition for each of the coupled $\nu_2(H_2O)$ bands lead to the conclusion that intermolecular coupling is significant for ammonia and water molecules and the allowed unit cell group modes all contribute to the observed bands.[13]

1.4 Objectives

The main objective of this thesis is instigated by Rollet and Vuillard's[2,3] discovery of the existence of ammonia dihydrate from differential thermal analysis measurements. The first successful isolation of crystalline ammonia dihydrate is achieved in this work (Section 2.4).

The purpose of further study of ammonia dihydrate is to obtain information about its crystal structure, to obtain its infrared spectrum and to make the spectral

assignments, i.e. determine the molecular motions that cause the spectral features. So, the x-ray powder diffraction pattern of ammonia dihydrate was recorded (Sections 2.6, 3.3) and the infrared spectra of ammonia dihydrate and its isotopomers were recorded at 100K between the frequencies of ~5000 and 200 cm^{-1} (Sections 3.7, 3.8 and 3.9).

The infrared spectra of $2NH_3 \cdot H_2O$, and its isotopomers and those of $NH_3 \cdot H_2O$ and $^{15}NH_3 \cdot H_2O$ for samples that were authenticated by powder x-ray diffraction, have been reported in the spectral region 4000 to 400 cm^{-1} and the general assignments have been made.[6,7] Also, most recently, infrared spectra of condensed films of $2NH_3 \cdot H_2O$, $2ND_3 \cdot D_2O$, $2NH_3 \cdot D_2O$ and $2ND_3 \cdot H_2O$ have been reported[13] between the temperatures 100 and 15K in the spectral region 4000 to 400 cm^{-1}. However, it has not been found possible[9,11] to form crystals of $ND_3 \cdot H_2O$ or $NH_3 \cdot D_2O$ in films condensed at low temperatures. So, the second objective of this thesis is to obtain and interpret infrared spectra of authentic samples of deuterated-ammonia monodeuterate between the frequencies of ~5000 and 400 cm^{-1} (Section 3.6). A detailed interpretation of the spectra of $NH_3 \cdot H_2O$ and $ND_3 \cdot D_2O$ will give information on the probable disorder of the positions of its hydrogen atoms that were postulated from the single crystal x-ray

study. Further, the infrared studies of ammonia monohydrate and ammonia dihydrate, and the infrared data already obtained for the hemihydrate will provide extensive information on the intermolecular interactions and their effect on molecular vibrations in ammonia-water systems.

An overall objective to this thesis is to study and expand the understanding of the behaviour of the hydrogen bonds in the hydrates of ammonia.

CHAPTER 2

EXPERIMENTAL TECHNIQUES

2.1 Introduction

This chapter deals with the experimental techniques used in sample preparation and identification and mid-infrared spectroscopy of ammonia monohydrate, fully deuterated ammonia monohydrate and ammonia dihydrate and its isotopic forms.

The ammonia monohydrate was prepared according to the technique described by Bertie and Morrison.[6,7] The technique for the preparation of ammonia dihydrate was developed based on the facts in the literature.[2,3]

Powder x-ray diffraction methods at low temperature were used to identify all the compounds under investigation in this work. A low temperature mulling technique, developed initially by Bertie and Whalley,[30] was followed, with slight changes, to prepare the infrared samples and assemble the low temperature infrared cell.

2.2 Chemicals

Anhydrous ammonia (99.99 mole%) from Matheson of

Canada Ltd., was used as supplied. No impurities in the ammonia were detected by x-ray powder diffraction. The powdered solid ammonia was prepared by condensing the ammonia gas into a small stainless steel mortar sitting in the liquid nitrogen can which is described in Section 2.5. The solid ammonia was ground under liquid nitrogen and the x-ray photograph was recorded using the methods described in Section 2.6.

Ammonia-d_3 (99.0 atom% D), from Merck Sharp & Dohme Canada Ltd., was used as supplied.

Deuterium oxide, obtained from spectral services in this department, was checked for isotopic purity by comparing the proton magnetic resonance spectra of the residual H in the D_2O, and of solutions made by dissolving 5 mole% of H_2O in D_2O and 10 mole% of H_2O in D_2O. The relative integrated intensities of the proton signals of the three solutions were compared and showed the purity of the D_2O to be at least 99 atom% D.

Commercial propane (99.98%), propylene (99.99%) and chlorotrifluoromethane (90.00%), supplied by Matheson of Canada Ltd., were used as received.

2.3 Preparation of Ammonia Monohydrate and Deuterated Ammonia Monodeuterate

The method of preparation was that described by

Bertie and Morrison.[6,7]

The apparatus used for sample preparation is depicted in Figure 2.1. The volume of the tube C was calibrated by adding to it the weights of distilled water which correspond to 1 mL, 2 mL and 3 mL of water at room temperature. The density of water[47] is 0.99823 g cm^{-3} at 20°C. The volumes of water and ammonia used in the preparations are listed in Table 2.1. They were calculated from the above density of water and an ammonia density[48] of 0.7253 g cm^{-3} at -70°C.

Both the sample apparatus B and the calibrated tube C in Figure 2.1 were cleaned, dried and connected to the vacuum line. A 1 mL syringe was used to transfer the specified amounts of triply distilled water or deuterium oxide (Table 2.1) into the small test tube A in Figure 2.1. This tube was connected to the vacuum line and the water was degassed by three freeze-pump-thaw cycles before it was distilled to the pre-evacuated sample apparatus B (Figure 2.1). If D_2O was used the entire vacuum line was exposed to D_2O vapour overnight, to deuterate its surface, and thoroughly re-evacuated before use. The ammonia was condensed into tube C which was cooled in a methanol/liquid nitrogen bath at ~-90°C. The temperature of the bath was allowed to warm up to -70°C, where the volume of ammonia was adjusted to that required. The

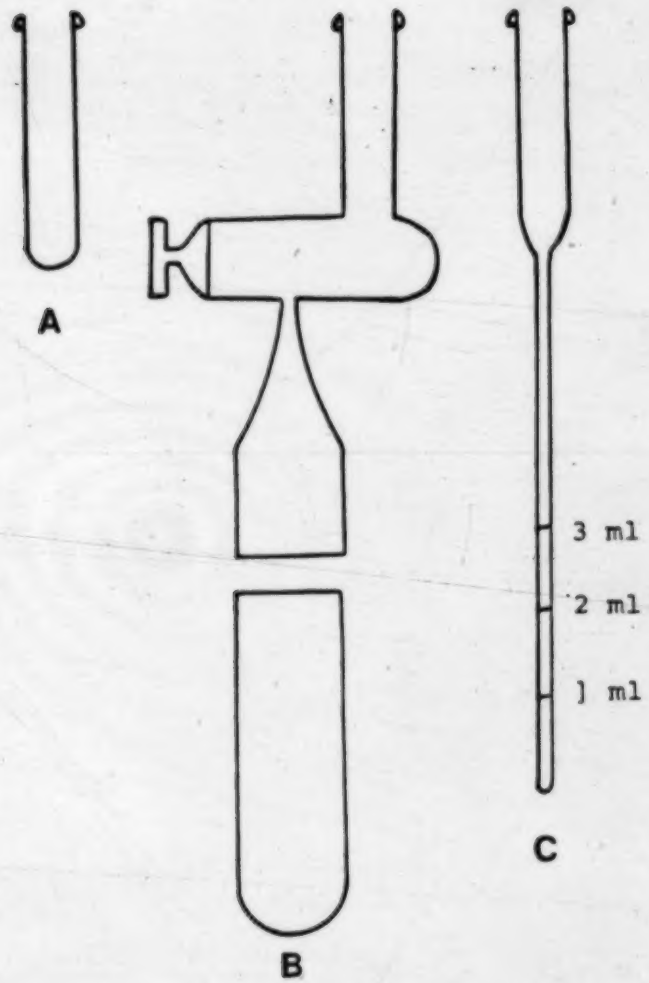

Figure 2.1 Glassware used for sample preparations: (A) small test tube; (B) sample apparatus; (C) long graduated tube.

Table 2.1 Volumes used for sample preparations.

Sample	Volume of NH_3 (mL)	Volume of H_2O (mL)	Volume of D_2O (mL)	Mole ratio NH_3:H_2O[b]	Impurities[c]
$NH_3 \cdot H_2O$(1)	3.00	2.31	-	1:1.00	None
$NH_3 \cdot H_2O$(2),(3)	3.00	2.31	-	1:1.00	$2NH_3 \cdot H_2O$
$NH_3 \cdot H_2O$(4)	3.00	2.37	-	1:1.03	None
$ND_3 \cdot D_2O$(1),(2)	1.00[a]	-	0.77	1:1.00	None
$NH_3 \cdot 2H_2O$(1),(2)	2.00	3.07	-	1:2.00	ice, $NH_3 \cdot H_2O$
$NH_3 \cdot 2H_2O$(3)-(5)	2.00	3.17	-	1:2.06	ice, $NH_3 \cdot H_2O$
$NH_3 \cdot 2H_2O$(6)	2.00	3.07	-	1:2.00	None
$NH_3 \cdot 2H_2O$(7)	1.00	1.54	-	1:2.00	ice, $NH_3 \cdot H_2O$
$NH_3 \cdot 2H_2O$(8)-(9)	1.00	1.54	-	1:2.00	None
$NH_3 \cdot 2H_2O$, 2% D	1.00	1.48	0.06	1:2.00	None
$NH_3 \cdot 2H_2O$, 5% D	1.00	1.40	0.14	1:2.00	None
$NH_3 \cdot 2H_2O$, 10% D	1.00	1.27	0.27	1:2.00	None
$ND_3 \cdot 2D_2O$(1)-(4)	1.00[a]	-	1.54	1:2.00	None
$ND_3 \cdot 2D_2O$, 5% H	1.00[a]	0.13	1.41	1:2.00	None

[a] The volume of ND_3 (mL).

[b] The mole ratio of ammonia (NH_3 + ND_3) to water (H_2O + D_2O).

[c] The impurities were identified by both x-ray diffraction photographs and infrared spectra. Only the pure samples were used to produce the spectra in this thesis.

ammonia was then distilled into sample apparatus B. The stopcock was closed and apparatus B was disconnected from the vacuum line.

Apparatus B contained two layers, one of ice and one of ammonia, at this stage. To mix them, they were swirled, keeping the temperature below -35°C. The lower, ice, layer started to dissolve in the upper, ammonia, layer as the upper layer melted. After complete dissolution of the ice in the liquid ammonia, the sample was vitrified by immersion in liquid nitrogen. The sample apparatus B was then transferred to a methanol/liquid nitrogen slush at -98°C and the temperature of the bath was allowed to rise very slowly to ~-79°C, the melting point of ammonia monohydrate. Complete crystallization was achieved by controlling the temperature of the bath for about one hour slightly below -79°C. Two-thirds of the sample was then allowed to melt by slightly raising the bath temperature. The temperature of the bath was then lowered very slowly by gradual addition of small amounts of liquid nitrogen to slightly below -79°C. The temperature was kept constant between -80°C and -85°C for about one to two hours until complete crystallization of ammonia monohydrate was attained. The sample apparatus was then lowered into liquid nitrogen dewar.

2.4 Preparation of Ammonia Dihydrate

The apparatus and the method used to measure the required volumes (Table 2.1) of ammonia and triply distilled water were the same as in the case of ammonia monohydrate. A homogeneous solution of ice and liquid ammonia was again made by swirling the sample apparatus B below -35°C. The sample apparatus B was immersed in liquid nitrogen until the solution was vitrified, and was then lowered into an FTS Multi-Cool System (which was previously calibrated with copper and iron constantan thermocouples to have ±1°C accuracy) at ~-120°C, where 1-chlorobutane liquid was used. The bath temperature was raised slowly (~1 h) to -101 ± 1°C, where it was kept constant for ~1 h. The solution was again vitrified and the temperature was raised slowly (~1 h) from ~-120°C to ~-100°C. The bath temperature was cycled between ~-100 and -94°C about six times in 1 h, and was then held constant at ~-98.5 ± 1°C for ~4 h before the sample was cooled to liquid nitrogen temperature. The temperature cycling appears to be necessary for successful crystallization.

The x-ray powder diffraction photographs showed that a new crystalline phase (ammonia dihydrate) had been obtained at this stage, but also showed impurities of ice and ammonia monohydrate. Ice and ammonia monohydrate can

also be identified in the IR spectra of impure sample compared to that of the pure one. The pure samples were obtained by slowly melting about half of the sample at ~-93°C, the other half served as seed crystals. The bath temperature was then reduced to -98.5 ± 1°C where it was held constant for ~ 4 h. This melting and recrystallizing process was repeated, allowing only about one quarter of the sample to melt. The sample was cooled to liquid nitrogen temperature and no impurities were detectable in its x-ray powder diffraction pattern. If the stoichiometry of the sample was not quite correct, ice or the monohydrate, but no other species, was detected as an impurity in the dihydrate. Ice and the monohydrate impurities can also be identified in the infrared of the impure samples compared to the pure one.

2.5 Sample Recovery and Grinding

After the sample was prepared and cooled to 77K further handling was done in an uninsulated cylindrical metal can (cold can) into which liquid nitrogen was poured. The can was connected to a metal side arm, which was designed to contain the outer jacket of the infrared cell, and contained a brass metal block, with wells of different sizes in its top surface, which provided a working area. Plexiglass covers were used over the cold

can to prevent atmospheric condensation inside the can.

A heat gun was used to warm the stopcock and the ground glass joint of the sample apparatus B (Figure 2.1) to room temperature, while the lower part, containing the sample, was kept in liquid nitrogen. Apparatus B then was filled with dry nitrogen gas by lowering it into the cold can and opening its stopcock. The lower tube containing the sample was rapidly separated, inside the cold can, from the stopcock and the joint and was placed inside an appropriate well in the brass block. A long-handled chisel and a long-handled spike were used to scrape the solid sample. All tools were cooled to liquid nitrogen temperature before they touched the sample. The scraped sample was transferred with a long spatula into a small glass bottle, which was full of liquid nitrogen and sat in one of the wells in the brass block. The cap was screwed onto the small bottle, with the help of long-handled tweezers, and the bottle was placed inside a larger glass bottle which was full of liquid nitrogen. The cover of the larger bottle was connected to a wire, and was screwed onto the larger bottle. The larger bottle was then suspended by the wire inside a five-liter dewar full of liquid nitrogen.

A SPEX grinding tube, containing an impactor, was placed upright in a special holder on the brass block

inside the cold can. A small amount of the sample to be ground was transferred to the grinding tube from the storage bottle by means of a precooled spatula. The grinding tube was closed and transferred, in liquid nitrogen, to the SPEX freezer mill which contained liquid nitrogen. The sample was ground for about 150 periods of 4 seconds each, which were separated by 20 seconds for heat dissipation. The grinding tube was then returned, in liquid nitrogen, to the cold can where its cover was removed and the ground sample was transferred to a screw-top bottle which, when full, was put inside a second screw-top bottle and stored under liquid nitrogen.

2.6 Characterization of the Hydrates

All the samples were characterized by their x-ray powder diffraction patterns. The x-ray beam was generated by an Enraf Nonius diffractis 601 generator. Copper and molybdenum tubes, with nickel and zirconium filters respectively, were used to produce radiation of mean wavelength of 1.5418 Å for CuK_α and 0.7107 Å for MoK_α. A Jarrell-Ash precession camera was operated as a flat-plate powder camera.

The sample to be examined was packed, with a fine glass rod, inside a 0.5 mm glass capillary tube, which sat in a hole in a small brass block inside the cold can. The

capillary was fixed to a Teflon holder by means of an oil drop, which would freeze to the glass capillary, and a screw in the side of the holder. The capillary was transferred with the holder under liquid nitrogen to the x-ray camera. The sample was cooled with a stream of cold nitrogen gas produced by electrical heating of liquid nitrogen in a fifty liter dewar. The cold stream was surrounded by a warm stream of nitrogen gas to prevent atmospheric ice condensation on the outside of the capillary. The rates of flow of warm and cold streams were controlled by variac settings of 80 V and 100 V respectively. The temperature was measured with a thermocouple (an iron-constantan #36 gauge and/or a copper-constantan #40 gauge) placed inside a 0.5 mm sealed capillary tube, to be -165 ± 5°C.

The usual exposure time was about eight hours. The sample was continually rotated in place to account for reflections from all possible orientations and to obtain smoother lines. A flat-plate powder diffraction pattern consists of a set of concentric circles, and each circle results from x-ray diffraction by particular crystal planes. The inner and outer diameters of the concentric circles on the film were measured to ±0.05 mm with a device (Charles Supper Co. Inc.) for measuring powder photographs on a light box, where the square-shaped film

was taped in place.

The film measurements were input to a computer program "POWDER",[49] which utilizes the Bragg equation ($\lambda = 2d \sin\theta$) to calculate the interplanar spacing, called the d-spacings, and the diffraction angles 2θ, where λ is the wavelength of the x-ray radiation. The crystal-to-film distance was calibrated to be 59.8 mm with ice Ih[50] which gives cell parameters of a = 4.498, c = 7.329 ± 0.006 Å at -165 ± 5°C. The Miller indices, the 2θ values, and the estimated unit cell parameters were input to a program DREFINE,[51] which refines the unit cell parameters by a least-squares fit of $\sin^2\theta$ values.

A microdensitometer (Joyce, Loebl and Co. Ltd., Model MK III C) was used to obtain the relative intensities of the diffraction circles.

2.7 Preparation of Low-Temperature Infrared Mulls

A low-temperature mulling technique, developed initially by Bertie and Whalley,[30] was followed with some modifications.

A cross-section of the low-temperature infrared cell is shown in Figure 2.2. The mulls were prepared in the cold can (Section 2.5). The inner part of the cell was placed upright on the brass block inside the cold can and connected to a vacuum line by a rubber tube. Plexiglass

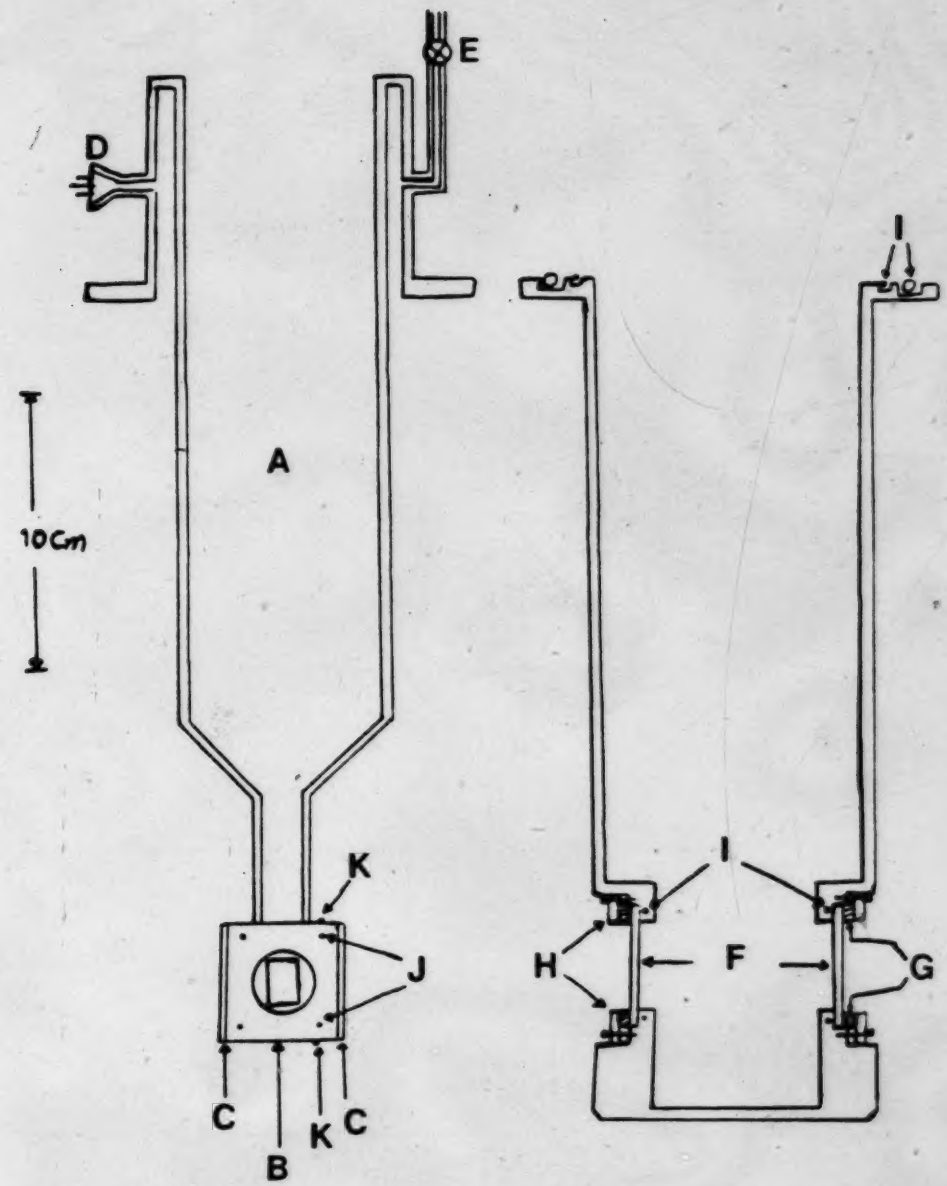

Figure 2.2 The low temperature infrared cell: (A) liquid nitrogen reservoir; (B) sample holder; (C) heaters; (D) electrical connection (E) vacuum valve; (F) CsI windows; (G) Teflon ring; (H) metal retaining ring; (I) O-rings; (J) 4 screws to press the faceplate against the sample holder; (K) thermocouple holes.

covers were fitted on the top of the can and below the flange of the inner part of the cell. A heating tape, to prevent ice condensation on the cell, was wrapped around the cell between the plexiglass and the flange.

One full spatula of the ground sample was transferred into a shallow stainless-steel mortar and was mixed for about five minutes by a stainless-steel pestle, with a few drops of mulling agent that were directly condensed into the mortar. The resulting mull was then transferred, on a long spatula, onto a cold cesium iodide window, which sat on a metal holder inside the cold can. A second precooled window was placed over the first one and the windows were rubbed against each other to achieve a uniform mull.

The two windows containing the mull were put into the sample holder of the cell, B in Figure 2.2, and were pressed against it with a spring and a faceplate. The faceplate was then screwed to the sample holder with a long screwdriver which passed through a hole in the side of the cold can. The heating tape was then removed and the outer part of the cell, which was purged with dry nitrogen gas, was put inside the side arm of the can. The inner part of the cell was rapidly put inside the outer part, and the vacuum valve was opened promptly to evacuate the cell through the pre-evacuated rubber tube. At the same time liquid nitrogen was quickly poured into the

inner jacket (A) of the cell. The cell was evacuated to $\sim 10^{-2}$ torr and was then connected to the vacuum line by glass fittings instead of the rubber tube and was evacuated for at least one hour at $\sim 10^{-3}$ torr before it was removed from the vacuum line and put into the sample compartment of the spectrometer.

The temperature of the sample was monitored by two copper-constantan thermocouples, which were fitted at the top and the bottom of the sample holder (Figure 2.2). The temperature of the sample was controlled to 100 ± 5K by two heaters C in Figure 2.2. In this temperature range all the mulling agents used; propane (m.p. = 83K), propylene (m.p. = 88K) and chlorotrifluoromethane (m.p. = 92K) are liquids.

2.8 Infrared Instrumentation

The infrared spectra were recorded with a Nicolet 7199 or Bruker IFS-113V Fourier transform infrared spectrophotometer[52-57] at 1 cm^{-1} resolution and a sample temperature of 100K. The Nicolet instrument is based on the Michelson interferometer, which is controlled by a Nicolet 1180 computer. The Bruker instrument is based on Genzel's modification of Michelson's interferometer and is controlled by an Aspect 2000 computer.

The varying signal at the detector is an

interferogram, which is the intensity as a function of optical path difference between the two arms of the interferometer. The frequency of a signal from the detector, f, is related to the vacuum wavenumber, ν, of the infrared radiation through the optical retardation velocity, v, i.e. the speed at which the optical path difference between the two beams changes, by the relationship $f = v\nu$.

The wavenumber range of interest to this work was primarily 4000 - 400 cm^{-1}. Accordingly, the beamsplitter of germanium on potassium bromide substrate was used in the Nicolet 7199 instrument, with a globar source, aperture of 6.35 mm diameter, a mercury cadmium telluride, HgCdTe, detector operating at 77K, and a mirror velocity of 0.783 cm s^{-1} which optimizes the signal-to-noise ratio in this range with this detector. At a mirror velocity of 0.783 cm s^{-1}, 400 cm^{-1} and 4000 cm^{-1} correspond to the electronic frequencies 626 Hz and 6.26 KHz. Thus, the 3dB points of the high-and-low pass electronic filters of the Nicolet 7199 spectrometer were set to 100 Hz and 10 KHz as a compromise between reducing electronic noise and not attenuating the signal.

The Nicolet interferograms were digitized at optical path-difference intervals of the helium-neon laser wavelength, 0.632991 μm, which means that infrared

radiation at all wavenumbers up to $(2 \times 0.632991\ \mu m)^{-1}$, i.e. 7899.0 cm^{-1} was correctly represented in the resultant spectrum. In fact no radiation above 7899.0 cm^{-1} is detected with the optical components and detector used, so the spectra were subject to no error due to the presence of radiation out of the 0 - 7899.0 cm^{-1}, correctly sampled, range.

In the Bruker instrument a globar source with aperture of 10 mm diameter, and deuterated triglycine sulphate, DTGS, detector operating at room temperature were used.

Three infrared regions were investigated with the Bruker instrument: 6000 - 1200 cm^{-1}, 4000 - 400 cm^{-1}, and 700 - 200 cm^{-1}. These regions are those covered by the silicon on calcium fluoride, germanium on potassium bromide, and 3 μ mylar, beam splitters, respectively. The optical velocities were set to 0.559, 0.665 and 0.396 cm s^{-1} for these three regions, respectively. These velocities were judged to give the best compromise between collection time and signal-to-noise ratio.

The low-and-high pass electronic filters of the Bruker spectrometer were set to cut on at: 12,500 and 17 Hz, for the 6000 - 1200 cm^{-1} (3354.0 - 670.8 Hz) and 4000 - 400 cm^{-1} (2660.0 - 266.0 Hz) ranges, and to 550 and 17 Hz, for the 700 - 200 cm^{-1} (277.2 - 79.2 Hz) range.

The Bruker interferograms of the regions 6000 - 1200 cm^{-1} and 4000 - 400 cm^{-1} were digitized at intervals of the laser wavelength, which means that infrared radiation of wavenumber from 0 to 7899.0 cm^{-1} was correctly sampled. The Bruker interferograms of the region 700 - 200 cm^{-1} were digitized once every four wavelengths of the laser, which means that infrared radiation of wavenumbers from 0 to 1974.7 cm^{-1} was correctly sampled.

The white light interferogram is used to trigger the electronics in both instruments to start data collection at the same optical retardation for each interferogram. There are three gain controls on the Nicolet, GAN, the base gain which was set to give a peak-to-peak signal near zero path difference of about 5 to 10 V, SGL, the factor by which the base gain is raised for the first 1024 points, which was set to one, and SGH, the factor by which the gain is multiplied above the 1024th point, which was set to 8. The Nicolet 1180 computer normalizes the averaged interferogram to unit gain. The gain of the amplifier was constant in the Bruker instrument throughout the interferogram, and was automatically set by the Aspect 2000 computer to yield a maximum signal (at zero optical retardation) that was greater than half of, but less than, the signal which saturates the analog-to-digital converter, ADC. Keeping the signal high reduces the

digitization noise.[57]

For the reported spectra, 500 interferograms were averaged to reduce the noise to an insignificant level. The averaging was done under Nicolet's medium correlation or Bruker's high correlation, to ensure that the zero path positions coincided on all interferograms included in the average. If satisfactory correlation was not obtained for an interferogram, it was not included in the average. The averaged interferogram was multiplied by the Happ-Genzel apodization function[52] to improve the instrument line shape by reducing the spectral side lobes, or pods, which result from the finite distance travelled by the moving mirror. The apodized interferogram was zero filled[56] once before it was Fourier transformed to yield a single beam spectrum, which is the intensity of infrared radiation which reaches the detector, $I(\nu)$, as a function of the wavenumber, ν.

The single-beam sample spectrum $I_S(\nu)$, was obtained with the sample in place and the single-beam background spectrum, $I_B(\nu)$, was obtained by the same procedure but without the sample cell. The ratio of the sample spectrum to the background spectrum gave the transmittance spectrum, $I_S(\nu)/I_B(\nu)$, or, multiplied by 100, the percent transmission spectrum, which was converted to the absorbance spectrum, $\log_{10}(I_B(\nu)/I_S(\nu))$. On the Nicolet

instrument the digital spectra were plotted via a "FIT" routine, which removes the discontinuities in the slope of the spectrum without changing the data points. No such routine was used by the Bruker instrument.

The phase correction of the Fourier transforms was done by the multiplicative method.[56,58] The full description of the Nicolet and Bruker operating parameters used in this work are given in Appendix I.

The low-temperature infrared cell was sealed into the sample compartments of the spectrometers by O-rings and plexiglass or brass fittings. The Nicolet compartment was purged by dry nitrogen gas for about half an hour, and the Bruker compartment was evacuated for about ten minutes, before it was opened to the rest of the spectrometer. For each mull, two independent collections were always taken under the same conditions to check the reproducibility of weak features.

Both the absorbance spectrum of the empty cell, which had very weak features from the CsI windows, and the absorbance spectrum of the mulling agent were subtracted from the absorbance spectrum of the sample to obtain the resultant spectrum of the hydrate. Occasionally, lines due to gaseous carbon dioxide and water vapor also had to be subtracted. On both instruments, the subtraction routine subtracts a fraction of a reference spectrum from

the sample spectrum. Each time a subtraction was to be done, several test subtractions were done in which the reference spectrum was multiplied by different factors. The optimum fraction of the reference spectrum was chosen and the final subtraction was executed with the help of an interactive subtraction program. The spectra were stored on a removable disk for future retrieval.

Both Nicolet and Bruker interferometers were frequency-calibrated by measuring the spectra of water vapor and carbon dioxide at 0.06 cm^{-1} resolution, and were found to agree with the accepted frequencies[59] to at least 0.1 cm^{-1}.

CHAPTER 3

EXPERIMENTAL RESULTS

3.1 Introduction

The experimental results of the current work are described in this Chapter. All samples were characterized by their x-ray powder diffraction patterns at ~105K, and the diffraction data are summarized in Sections 3.2 and 3.3.

The infrared spectra of the mulling agents, propane, propylene and Freon-13, at 100K are described in Section 3.4. The infrared spectra of ammonia monohydrate and its deuterated form at 100K are described in Sections 3.5 and 3.6, respectively, and that of ammonia dihydrate and its isotopic forms are described in Sections 3.7 to 3.9.

The spectra of ammonia monohydrate and its deuterated form were obtained with the Nicolet 7199 FTIR spectrometer, unless otherwise stated. The spectra of ammonia dihydrate and its isotopic forms were recorded with the Bruker IFS-113V spectrometer. All spectra were plotted without smoothing, and have not been redrawn.

In this thesis, $NH_3 \cdot 2H_2O$ containing x mole percent of D and $ND_3 \cdot 2D_2O$ containing x mole percent of H will be

referred to for brevity as $NH_3 \cdot 2H_2O$, x% D and $ND_3 \cdot 2D_2O$, x% H, respectively.

3.2 Characterization of Ammonia Monohydrate Samples

All samples of ammonia monohydrate and deuterated ammonia monohydrate were identified by their x-ray powder diffraction patterns[5,6] at 105 ± 5K. The only impurities observed were ammonia hemihydrate[4,6] and ice[50] (Table 2.1). The impurities were also identified in the infrared spectra by comparing the spectra of samples with different amounts of impurity to those of the pure ones.

The x-ray data of ammonia monohydrate are summarized in Table 3.1 and are the averages of at least six measurements. The diffraction pattern is indexed, as shown in Table 3.1, on the orthorhombic space group,[5] $P2_12_12_1(D_2^4)$. The lattice parameters at 105 ± 5K were found to be a = 4.51 Å, b = 5.59 Å and c = 9.69 Å all with 95% confidence limit of 0.01 Å, which agree very well with those reported in the literature[5] (a = 4.51 ± 0.01, b = 5.587 ± 0.003 and c = 9.700 ± 0.005 Å at ~110K).

The observed relative intensities of the diffraction lines listed in Table 3.1 were measured as peak heights and as areas of peaks on a microdensitometer trace of CuK_α photographs, one of which is shown in Figure 3.1. The two lines at 2θ values of 31.3 and 31.9 were resolved in some

Table 3.1 X-ray powder diffraction pattern of ammonia monohydrate at ~105K.

Index[a]	d_{obs}[b]	d_{calc}[c]	$2\theta_{obs}$[b]	$2\theta_{calc}$[c]	I_{obs}[d]	I_{calc}[e]	
002	4.87(1)	4.845	18.21(5)	18.309	40	28	40
011		4.844		18.313		12	
101		4.086		21.75		0.43	
012	3.68(2)	3.66	24.21(7)	24.30	11	10	
110	3.52(1)	3.51	25.31(6)	25.38	34	40	
102	3.31(1)	3.300	26.94	27.02	100	21	100
111		3.299		27.03		79	
112	2.86(2)	2.84	31.3(1)	31.48	47	46	
013	2.80(1)	2.797	31.9(1)	31.99	70	53	61
020		2.796		32.00		8	
021		2.687		33.34		1.6	
103		2.625		34.15		~0	
004	2.425(6)	2.423	37.08(9)	37.108	9	2.7	11
022		2.422		37.116		8	
113		2.377		37.855		1.1	1.3
120		2.376		37.861		0.2	
121	2.310(2)	2.308	39.00(4)	39.03	26	38	
200	2.253(3)	2.253	40.02(7)	40.02	13	N.S.F.	
014		2.223		40.58		0.14	
201		2.194		41.14		0.23	
104	2.136(1)	2.134	42.32(3)	42.357	16	10	22
122		2.133		42.364		12	
023		2.114		42.77		0.84	
210		2.089		43.30		0.02	
202	2.043(2)	2.043	44.34(2)	44.341	<5	3.0	4.3
211		2.042		44.343		1.3	
114	1.996(2)	1.994	45.45(5)	45.49	~6	11	
212	1.916(5)	1.919	47.5(1)	47.37	<5	0.7	6.4
123		1.914		47.50		5.7	
203		1.848		49.31		~0	
015	1.830(3)	1.831	49.8(1)	49.789	<5	0.5	7.4
024		1.831		49.789		1.2	
031		1.831		49.801		5.7	

(Continued)

Table 3.1 (Continued)

Footnotes for Table 3.1

[a] Indexed on an orthorhombic space group $P2_12_12_1$, (D_2^4).

[b] CuK_α radiation, $\lambda = 1.5418$ Å. The numbers in parentheses are 95% confidence limits in the last digit.

[c] Calculated using a = 4.51, b = 5.59, c = 9.69 all ± 0.01 Å.

[d] Measured as peak height and as area of peaks on a microdensitometer trace of CuK_α photographs. Estimated accuracy ± 20%.

[e] Calculated from the calculated 2θ and the observed structure factors [Ref. 5] using the flat-plate powder equation [Ref. 40]. N.S.F. means that no structure factor was reported.

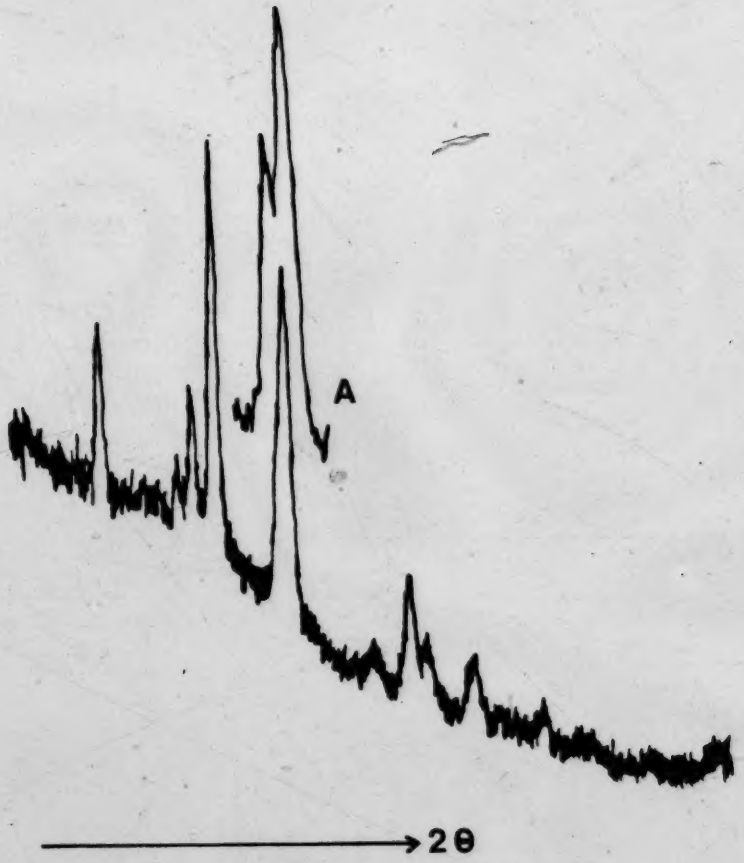

Figure 3.1 Microdensitometer trace of a CuK_α photograph of $NH_3 \cdot H_2O$ at 105K. Curve A is expanded to show the resolution of two lines in some of CuK_α photographs.

CuK_α photographs and are shown in Figure 3.1, curve A. These relative intensities compare well with those calculated according to the flat-plate powder equation:[40,60]

$$I \alpha [(1 + \cos^2 2\theta)/(\sin^2\theta \cos\theta)]\cos 2\theta \, pF^2 \ldots (3.2.1)$$

where p is the multiplicity factor,[27] which takes into account the number of reflections from a single crystal that are superimposed to form a powder line, and F is the observed structure factor obtained from Olovsson and Templeton.[5]

3.3 X-Ray Data of Ammonia Dihydrate

The powder x-ray diffraction pattern of ammonia dihydrate at 105 ± 5K is given in Table 3.2. The data are the average of at least nine measurements of CuK_α and MoK_α photographs.

The diffraction pattern is indexed, as shown in Table 3.2, on the cubic unit cell,[27] $P2_13(T^4)$, a = 7.118 Å with a 95% confidence limit of 0.015 Å.

The observed relative intensities, listed in Table 3.2, were measured as peak heights and as areas of peaks on a microdensitometer trace of CuK_α photographs, one of

Table 3.2 X-ray powder diffraction pattern of ammonia dihydrate at ~105K.

Index[a]	d_{obs}[b]	d_{calc}[c]	$2\theta_{obs}$[b]	$2\theta_{calc}$[c]	I_{obs}[d]	I_{calc}[e]
100		7.118		12.44		0
110	5.04(1)	5.03	17.59(5)	17.62	22	23
111	4.11(1)	4.11	21.60(6)	21.62	10	0.7
200	3.563(8)	3.559	25.00(6)	25.02	55	68
210	3.187(7)	3.183	28.01(7)	28.03	65	7
120						72 } 79
211	2.907(4)	2.906	30.76(6)	30.77	100	100
220	2.519(4)	2.517	35.66(5)	35.68	15	19
300		2.373		37.92		0
221						5 } 5
310	2.252(4)	2.251	40.07(5)	40.06	25	0.5
130						11 } 12
311	2.146(2)	2.146	42.12(5)	42.10	15	40
222	2.056(6)	2.055	44.05(9)	44.07	3	4
320	1.972(2)	1.974	46.02(6)	45.97	7	13
230						1 } 14
321	1.902(3)	1.902	47.84(4)	47.81	30	9
312						32 } 41
400		1.779		51.34		3
410						2
401		1.726		53.04		0.1 } 3
322						1
411	1.679(2)	1.678	54.66(8)	54.71	<10	1.7
330						0.6 } 2
331		1.633		56.34		0.2
420		1.592		57.94		0.2
421	1.552(3)	1.553	59.57(8)	59.51	<10	0.7
412						7 } 8
332		1.518		61.06		1.4
422	1.46(1)	1.453	64.0(1)	64.09	<10	0.7
430						0.5
403		1.424		65.57		0 } 0.5
500						0

(Continued)

Table 3.2 (Continued)

Index[a]	d_{obs}[b]	d_{calc}[c]	$2\theta_{obs}$[b]	$2\theta_{calc}$[c]	I_{obs}[d]	I_{calc}[e]	
510	1.396(8)	1.396	67.04(8)	67.04	<10	~0	~3
501						1	
431						1.6	
413						~0	
511		1.370		68.49		2.6	~3
333						0.2	
432	1.32(1)	1.322	71.7(3)	71.36	<10	3.2	4
423						0.2	
520						0.6	
502						0.1	

[a] Indexed on a cubic space group $P2_13$, (T^4).

[b] The numbers in parentheses are 95% confidence limits in the last digit. CuK_α radiation, λ = 1.5418 Å, was used except for the bottom five observed lines which were obtained from MoK_α radiation, λ = 0.7107 Å. The 2θ values from the MoK_α photographs were recalculated to get the corresponding 2θ values of CuK_α radiation.

[c] Calculated using a = 7.118 ± 0.015 Å (95% confidence limit) and λ = 1.5418 (CuK_α).

[d] Calculated from atomic scattering factors for oxygen and nitrogen [Ref. 61], the isotopic thermal parameters B_t = 1.42 for oxygen and 1.54 for nitrogen [Ref. 5], and the flat-plate powder equation 3.1.

[e] Measured as peak heights and as areas of peaks on a microdensitometer trace of CuK_α photographs, except for the bottom five observed lines which were estimated from MoK_α photographs. Estimated accuracy ±20%.

which is shown in Figure 3.2. The diffraction intensities expected on a flat-plate powder photograph were calculated using equation (3.2.1) and support the above structure for the heavy atoms. The structure factors were calculated from the atomic scattering factors[61] for oxygen and nitrogen atoms and the isotropic thermal parameters, B_t = 1.42 for oxygen and 1.57 for nitrogen, which were found for ammonia monohydrate.[5] The hydrogen atoms were neglected in the calculation.

The calculation of the relative intensities and the computer program used are described in Appendix III.

3.4 Infrared Spectra of the Mulling Agents

The infrared spectra of liquid propane, propylene and chlorotrifluoromethane (Freon-13) at 100K and 1 cm^{-1} resolution are shown in Figures 3.3 to 3.6. The spectra were recorded with the Bruker instrument. The frequencies of the spectral features are listed in Tables 3.3 to 3.5. The mulling agents were mulled with CsI powder in order to have spectra with strong absorption, which match the absorption by the mulling agents in the spectra of the mulled ammonia hydrates. The optimum fractions of the mulling agents' spectra which were used in the final subtraction were chosen as described in Section 2.8.

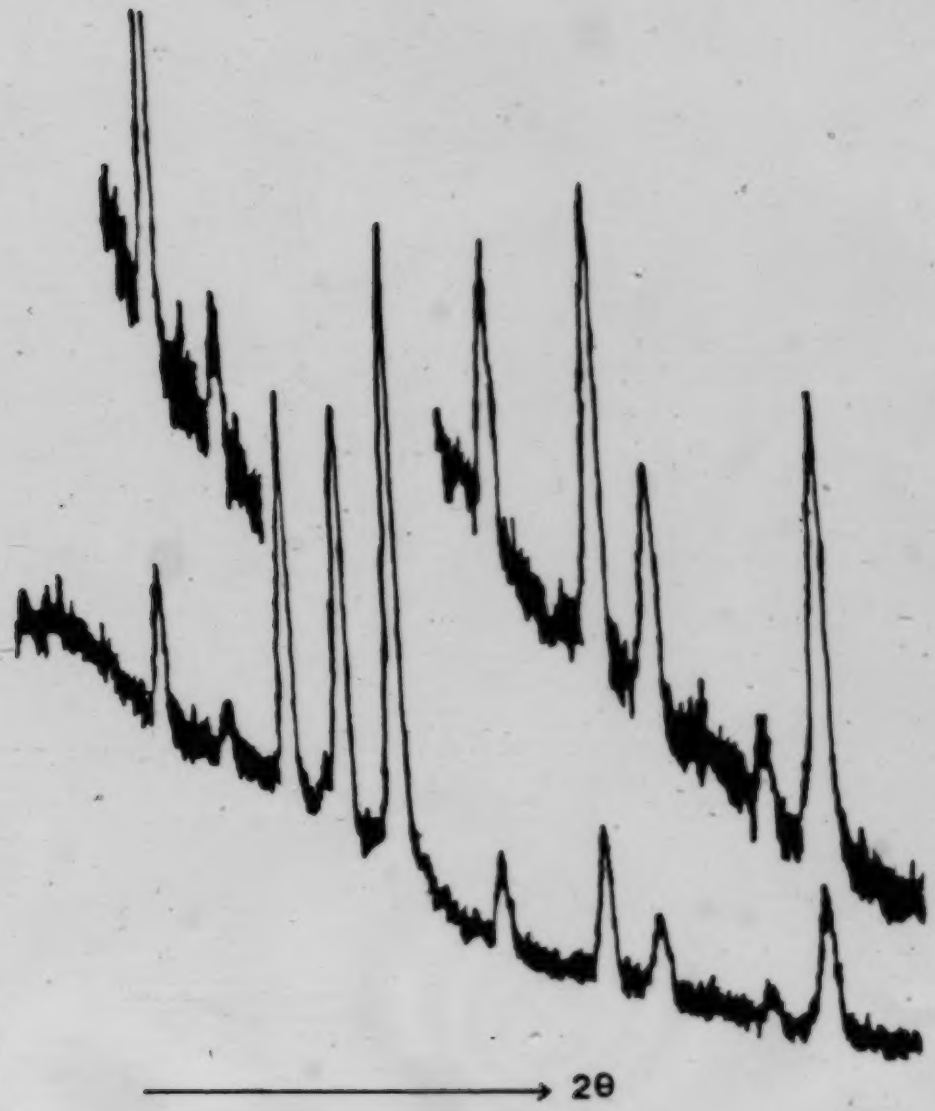

Figure 3.2 Microdensitometer trace of a CuK_α photograph of $NH_3 \cdot 2H_2O$ at 105K.

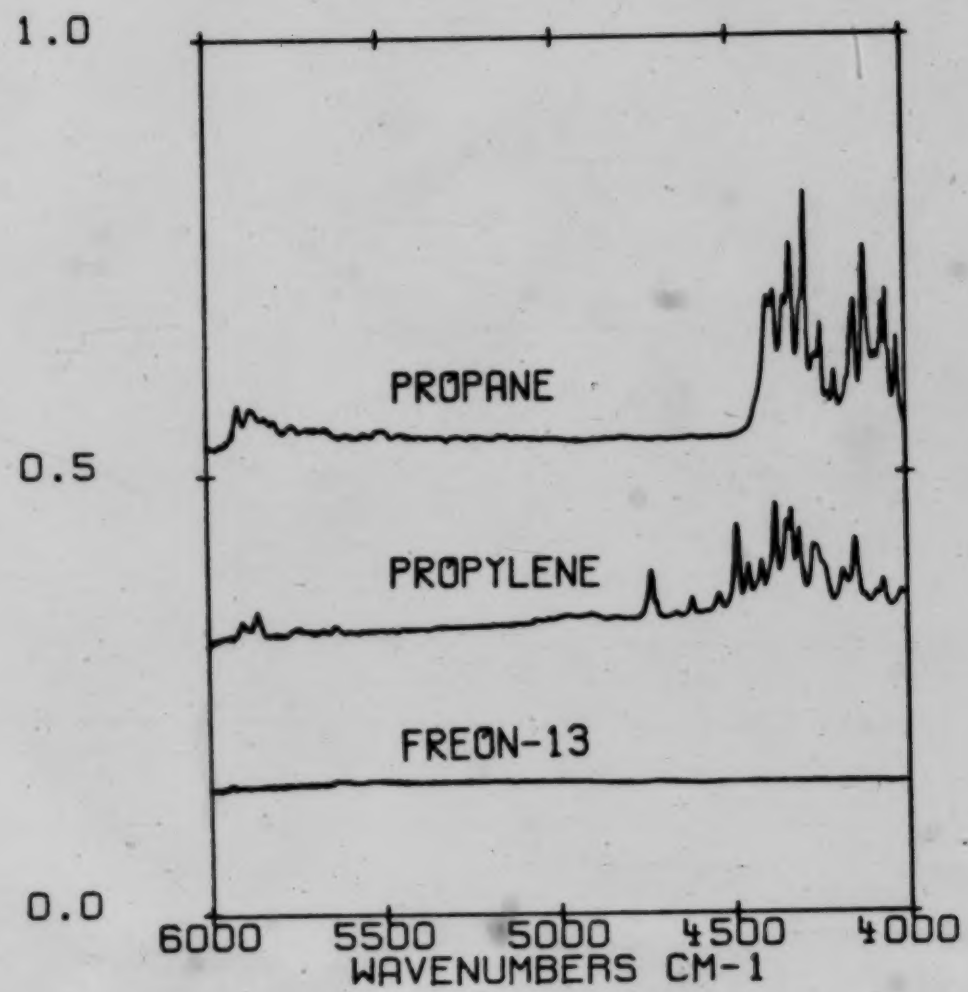

Figure 3.3 Infrared absorbance spectra of liquid propane, propylene and Freon-13 at 100K and 1 cm^{-1} resolution.

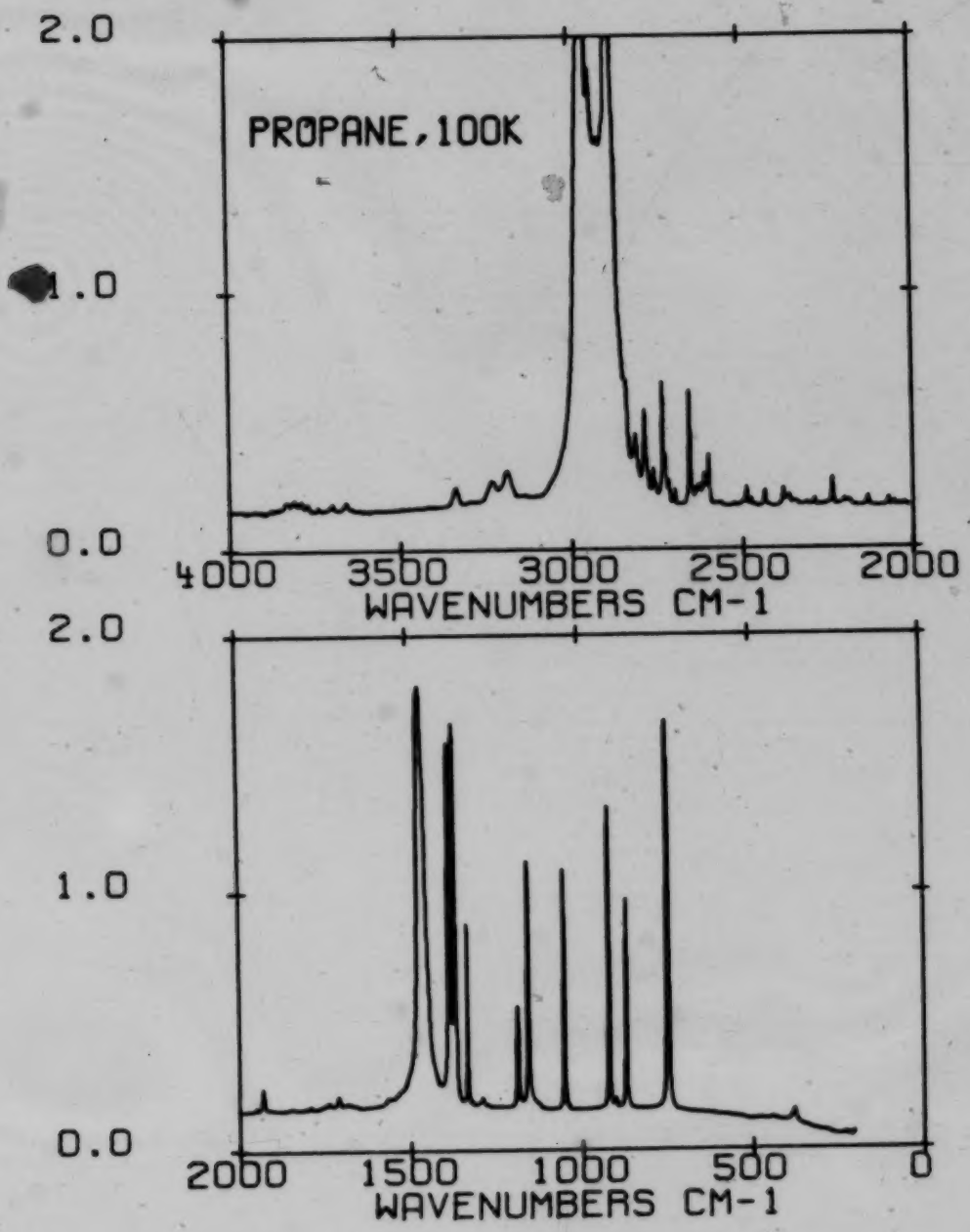

Figure 3.4 Infrared absorbance spectrum of liquid propane at 100K and 1 cm^{-1} resolution.

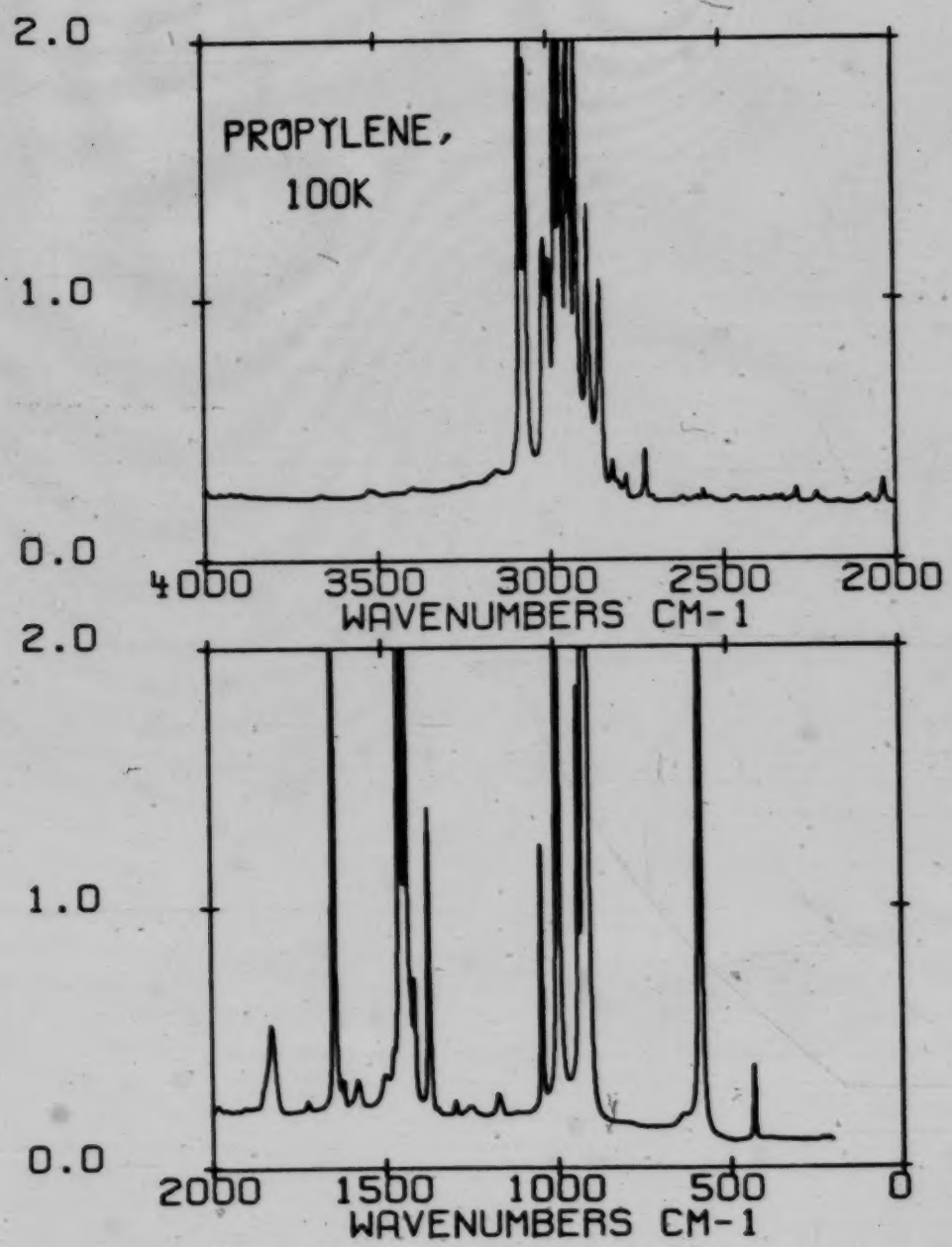

Figure 3.5 Infrared absorbance spectrum of liquid propylene at 100K and 1 cm^{-1} resolution.

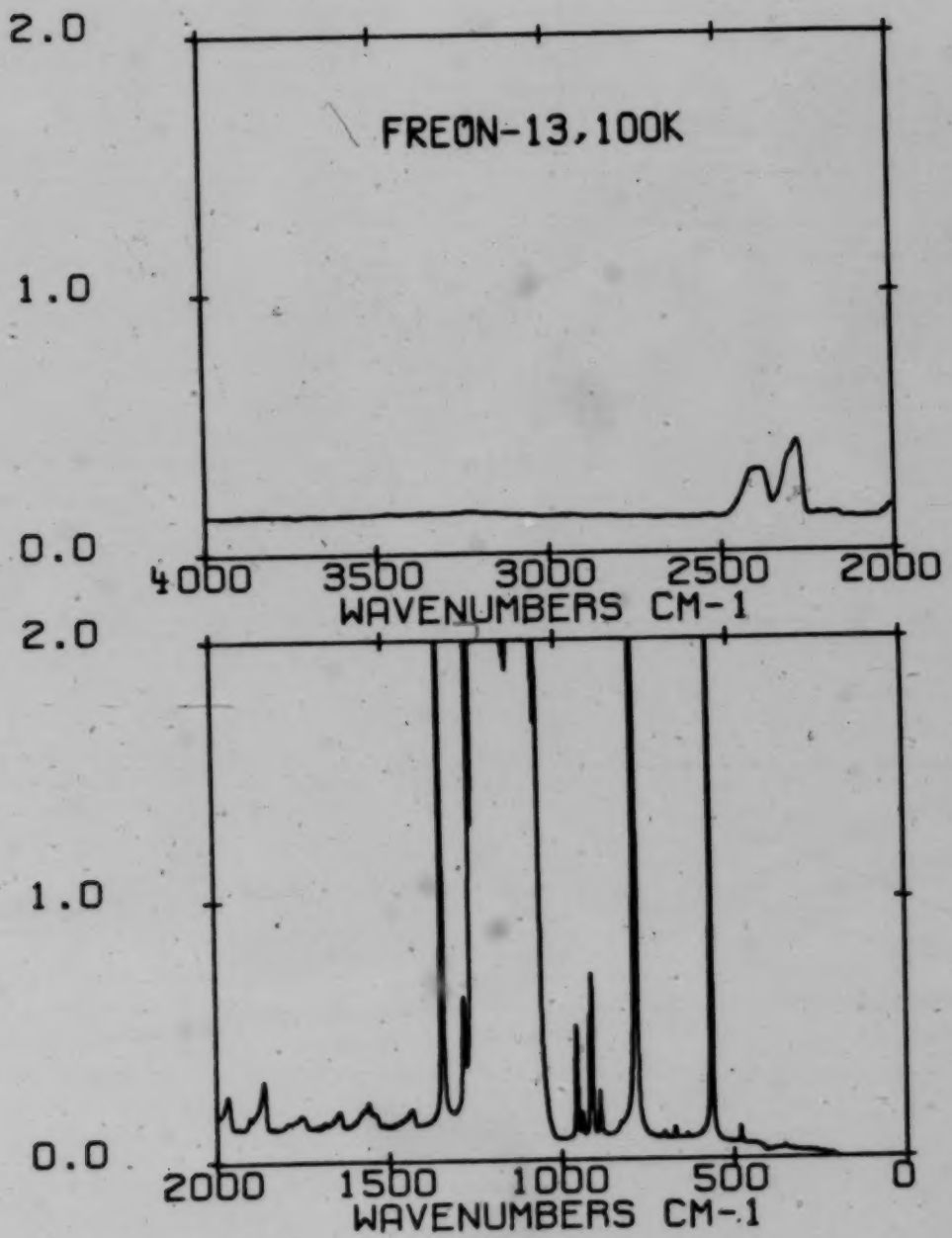

Figure 3.6 Infrared absorbance spectrum of liquid Freon-13 at 100K and 1 cm^{-1} resolution.

Table 3.3 Infrared spectral features of liquid propane at 100K.

ν/cm^{-1}[a]	Intensity[b]	ν/cm^{-1}[a]	Intensity[b]	ν/cm^{-1}[a]	Intensity[b]
5908(1)	vw	~2880(10)	vvs*	~1949	vvw
~5870	vw	~2851	sh	1929(1)	vw
4391(2)	w	2838(3)	m	~1842	vvw
4373(2)	w	2811(2)	w	~1788	vvw
4342(2)	w	~2801	sh	~1736	vvw
4324(1)	w	2784(2)	w	1707(2)	vw
~4296	sh	2759(2)	vw	~1677	vvw
4283(1)	w	~2751	sh	1561(2)	vw
~4257	vw	2731(2)	m	~1525	sh
4239(2)	w	2723(1)	w	1470(1)	vs
~4218	vvw	2713(2)	vw	1466(1)	vs
4201(2)	vw	2695(2)	vw	1464(1)	vs
~4170	vvw	2652(1)	m	~1456	sh
~4153	sh	~2626	vw	~1428	sh
4143(2)	w	2610(2)	w	1384(1)	vs
4114(1)	w	2597(2)	w	1369(1)	vs
4065(1)	w	2486(1)	w	~1360	sh
4053(1)	w	2473(2)	vw	1332(1)	s
4045(2)	vw	2431(1)	vw	~1289	vvw
4023(2)	w	2378(1)	vw	1186(1)	m
~3830	vvw	2360(2)	vw	1155(1)	s
~3808	vvw	~2340	vvw	~1130	sh
~3786	vvw	~2307	vvw	1051(1)	s
~3768	vvw	2286(3)	vw	919(1)	s
~3738	vvw	2234(2)	vw	~ 900	vvw
~3696	vvw	~2199	vvw	869(1)	s
~3655	vvw	~2189	vvw	747(1)	vs
3336(3)	w	~2182	vvw	~ 439	vvw
3229(4)	w	2131(2)	vw	375	vw
3186(4)	w	~2070	vvw		
~2955(12)	vvs*	~2054	vvw		
2933(1)	vs	~2036	vvw		
2910(3)	vs	~2031	vvw		
~2896	sh				

(Continued)

Table 3.3 (Continued)

[a]The numbers in parentheses are the 95% confidence limits in the last digit.

[b]vvs, vs, s, m, w, vw, vvw and sh mean: very very strong, very strong, strong, medium, weak, very weak, very very weak and shoulder, respectively. The (*) means that the absorption is very very strong above the scale and the mid-point is reported.

Table 3.4 Infrared spectral features of liquid propylene at 100K.

ν/cm^{-1}[a]	Intensity[b]	ν/cm^{-1}[a]	Intensity[b]	ν/cm^{-1}[a]	Intensity[b]
5897(2)	vw	~3224	vvw	~2160	vvw
5854(2)	vw	3150(3)	vw	~2080	vvw
4725(1)	w	~3098	sh	2033(2)	vw
~4709	sh	3079(3)	vvs*	~1981	vvw
~4650	vvw	3065(1)	vs	~1900	vvw
4607(2)	vw	2978(4)	vvs*	~1850	sh
4528(2)	vw	2964(2)	vvs*	1827(2)	m
4480(1)	w	2940(4)	vvs*	1723(2)	vw
4448(2)	vw	2918(3)	vvs*	1646(3)	vvs*
4409(2)	vw	3016(1)	s	1623(2)	w
4370(1)	w	3-12(1)	s	1617(2)	w
4338(2)	w	2998(1)	s	1577(3)	w
4324(1)	w	2886(1)	s	1496(3)	w
4301(1)	w	2852(1)	s	1473(2)	w
4263(1)	w	2817(2)	vw	~1452(5)	vvs*
~4228	sh	~2803	vvw	~1436(2)	vvs*
4177(2)	vw	2779(2)	vw	~1423	sh
~4166	sh	2723(1)	w	1413(2)	m
4143(1)	w	~2702	vvw	1371(1)	s
~4109	vvw	~2573	vvw	1346(3)	vw
~4079	vvw	2555(2)	vw	1295(2)	w
4062(2)	vw	~2533	vvw	1249(3)	w
~4011	vvw	~2462	vvw	1170(2)	w
3994(3)	vw	~2410	vvw	1043(1)	s
~3952	vvw	~2382	vvw	~ 994(5)	vvs*
~3920	vvw	~2369	vvw	934(1)	vs
~3892	vvw	~2345	vvw	~ 912(10)	vvs*
~3660	vvw	~2327	vvw	~ 792	vvw
3523(3)	vw	~23-2	vvw	~ 633	sh
~3509	vvw	2286(2)	vvw	~583(3)	vvs*
~3405	vvw	2227	vw	429(1)	m
3394(3)	vw	~2111	vvw		

(Continued)

Table 3.4 (Continued)

[a]The numbers in parentheses are the 95% confidence limits in the last digit.

[b]vvs, vs, s, m, w, vw, vvw and sh mean: very very strong, very strong, strong, medium, weak, very weak, very very weak and shoulder, respectively. The (*) means that the absorption is very very strong above the scale and the mid-point is reported.

Table 3.5 Infrared spectral features of liquid Freon-13 at 100K.

ν/cm^{-1}[a]	Intensity[b]	ν/cm^{-1}[a]	Intensity[b]	ν/cm^{-1}[a]	Intensity[b]
~2415	w,br	~1640	vw	914(1)	m
~2306	sh	~1570	sh	908(1)	m
2278(3)	w	1555(2)	vw	886(1)	w
~2221	vvw	~1536	vw	~881	sh
~2170	vvw	~1454	sh	825(1)	vw
~2029	vvw	1429(2)	vw	~815	sh
~2006	sh	1341(2)	vvs*	780(4)	vvs*
1965(2)	w	1279(1)	m	775(1)	vs
~1902	vw	1556(2)	vvs*	697(1)	vw
~1889	sh	~1196(50)	vvs*	666(2)	vw
1860(2)	w	~1103(35)	vvs*	630(1)	vw
~1786	sh	1060(2)	vvs*	560(1)	vvs*
~1750	vw	953(1)	m	478(1)	vw
~1683	vvw	938(1)	vw	~348	vvw

[a] The numbers in parentheses are the 95% confidence limits in the last digit.

[b] vvs, vs, s, m, w, vw, vvw and sh mean: very very strong, very strong, strong, medium, weak, very weak, very very weak and shoulder, respectively. The (*) means that the absorption is very very strong above the scale and the mid-point is reported.

3.5 Infrared Spectra of Ammonia Monohydrate

The infrared spectra of ammonia monohydrate at 100K and 1 cm^{-1} resolution are shown in Figures 3.7 to 3.14. The frequencies of the spectral features are listed in Table 3.6. The frequencies reported by Bertie and Morrison[6] are included in Table 3.6 for comparison.

The spectral features and their wavenumbers agree with those reported by Morrison[3] except in the following cases. A triplet has been recorded at 3403.2/3392.1/ 3387.3 cm^{-1} (Figure 3.10), to replace the previous 3402/3387 cm^{-1} doublet. The spectrum has been generally improved, causing a change in the details of the features near 3300 cm^{-1} and in the shape and frequency of the OH stretching band at 2887 cm^{-1} (Figures 3.8 and 3.9). Two extra shoulders have been recorded at ~3235 and ~1594 cm^{-1} (Figures 3.9 and 3.11). A weak band has also been recorded at 1402 cm^{-1} (Figure 3.11). The detailed shape of the top of the 900 cm^{-1} band has been changed (Figure 3.13). A sharp band at 420.4 cm^{-1} has also been recorded (Figure 3.8).

The relative intensities of the very weak features in the regions 5000 - 4600 cm^{-1}, 4450 - 3520 cm^{-1} and 2100 - 1950 cm^{-1} vary slightly from one mull to the other.

The absorption by the mulling agents has been correctly subtracted from the spectra presented as

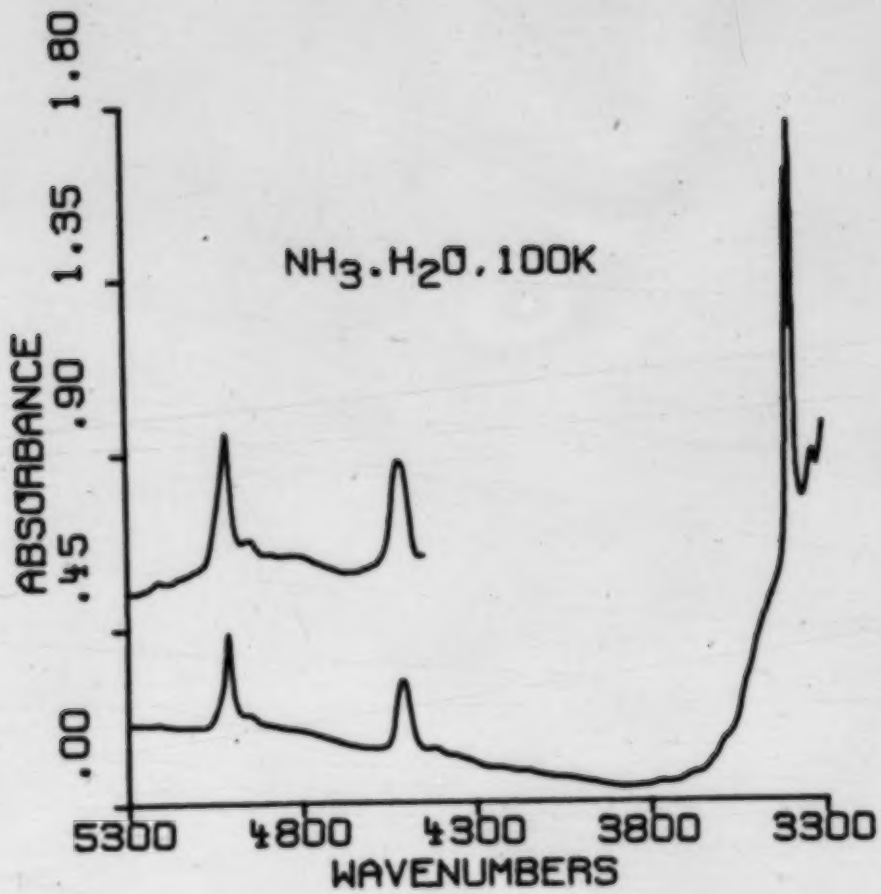

Figure 3.7 Infrared spectra of $NH_3 \cdot H_2O$ at 100K and 1 cm^{-1} resolution. From mulls in Freon-13 and propane (above).

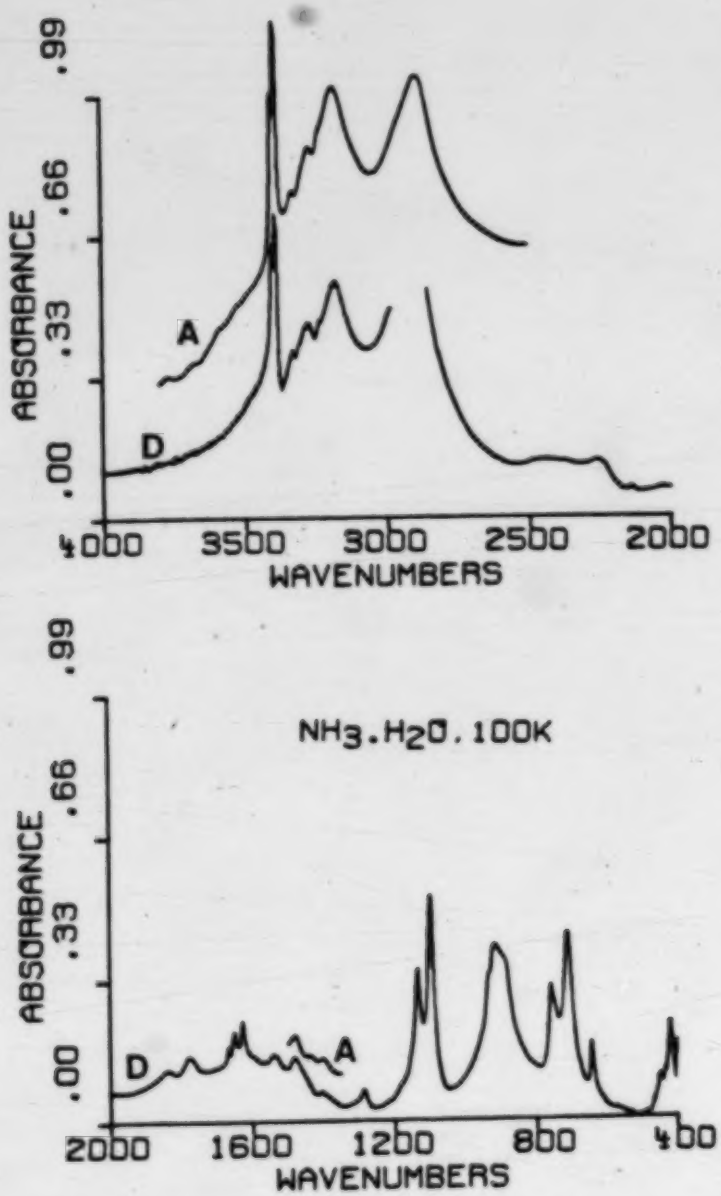

Figure 3.8 Infrared spectra of $NH_3 \cdot H_2O$ at 100K and 1 cm^{-1} resolution. Curves A and D are from mulls in Freon-13 and propane, respectively.

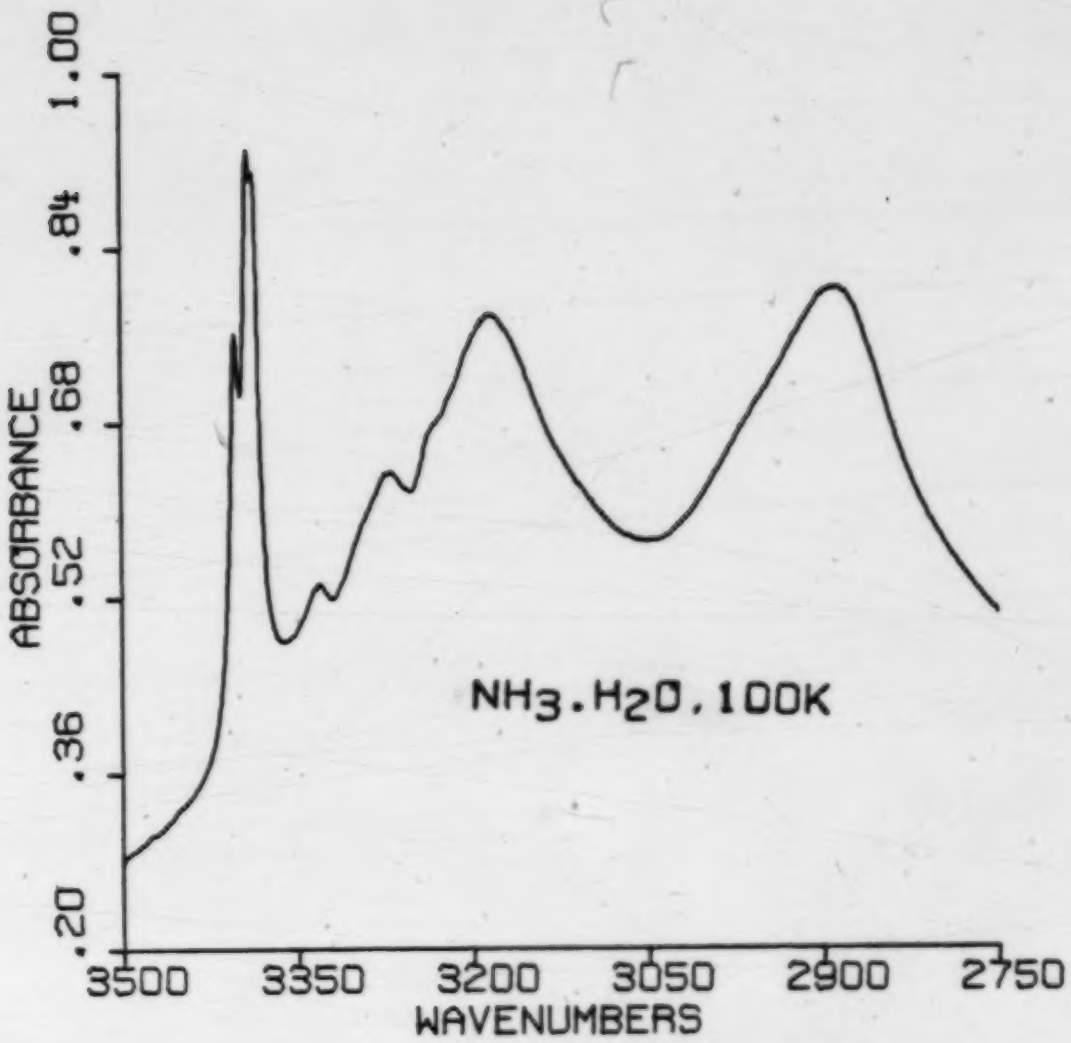

Figure 3.9 Infrared spectrum of $NH_3 \cdot H_2O$ at 100K and 1 cm^{-1} resolution. From a mull in Freon-13.

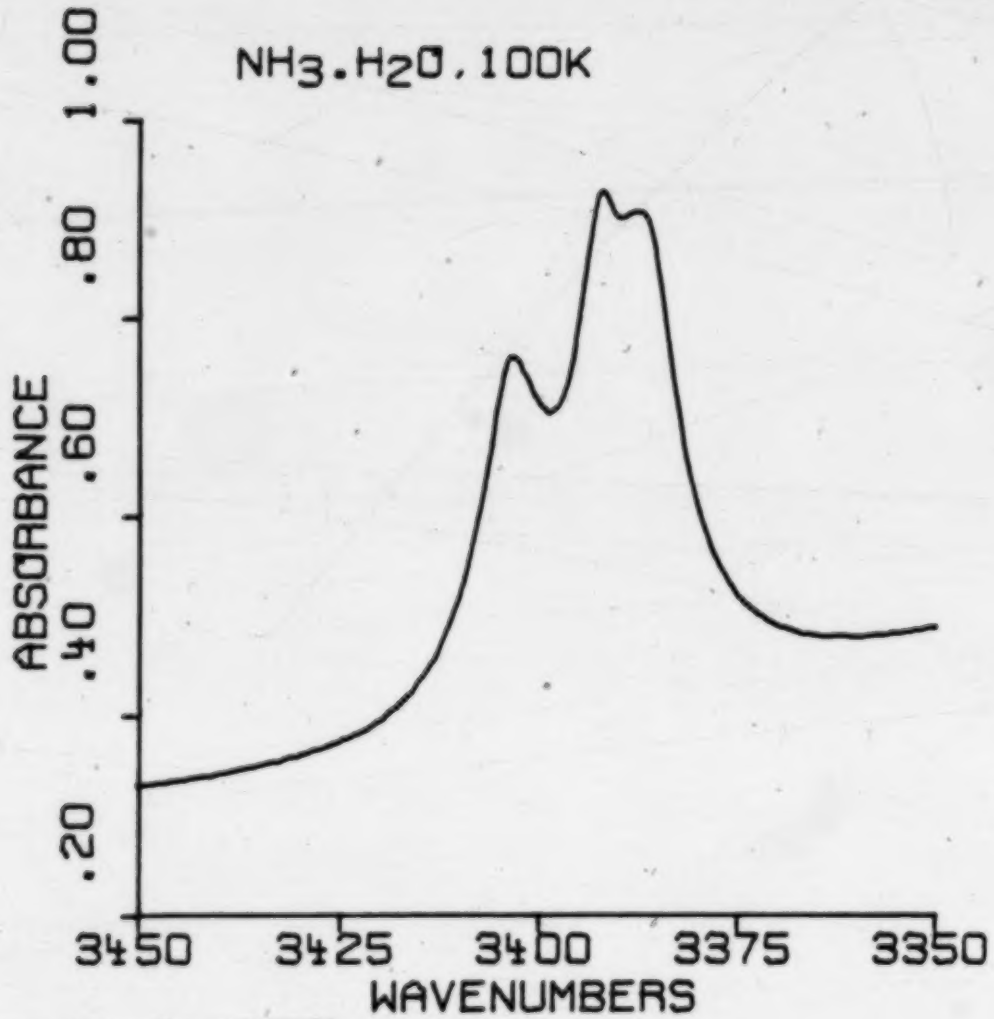

Figure 3.10 Absorption by the antisymmetric N-H stretching modes of $NH_3 \cdot H_2O$ at 100K and 1 cm^{-1} resolution. From a mull in Freon-13.

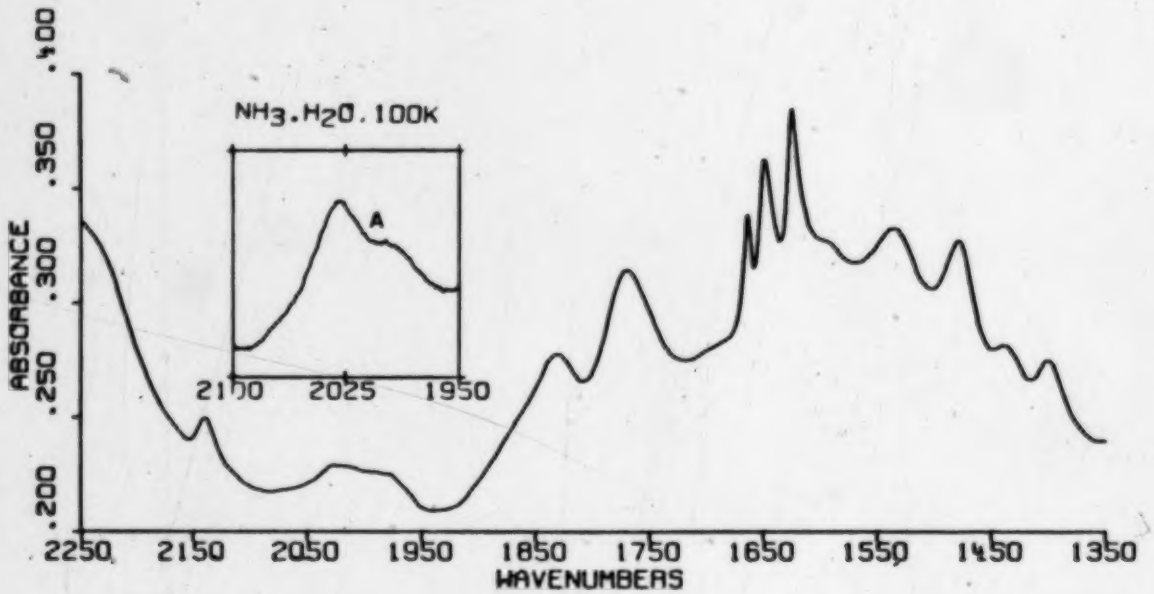

Figure 3.11 Infrared spectra of $NH_3 \cdot H_2O$ at 100K and 1 cm^{-1} resolution. From mulls in Freon-13 (below) and propane (curve A), expanded.

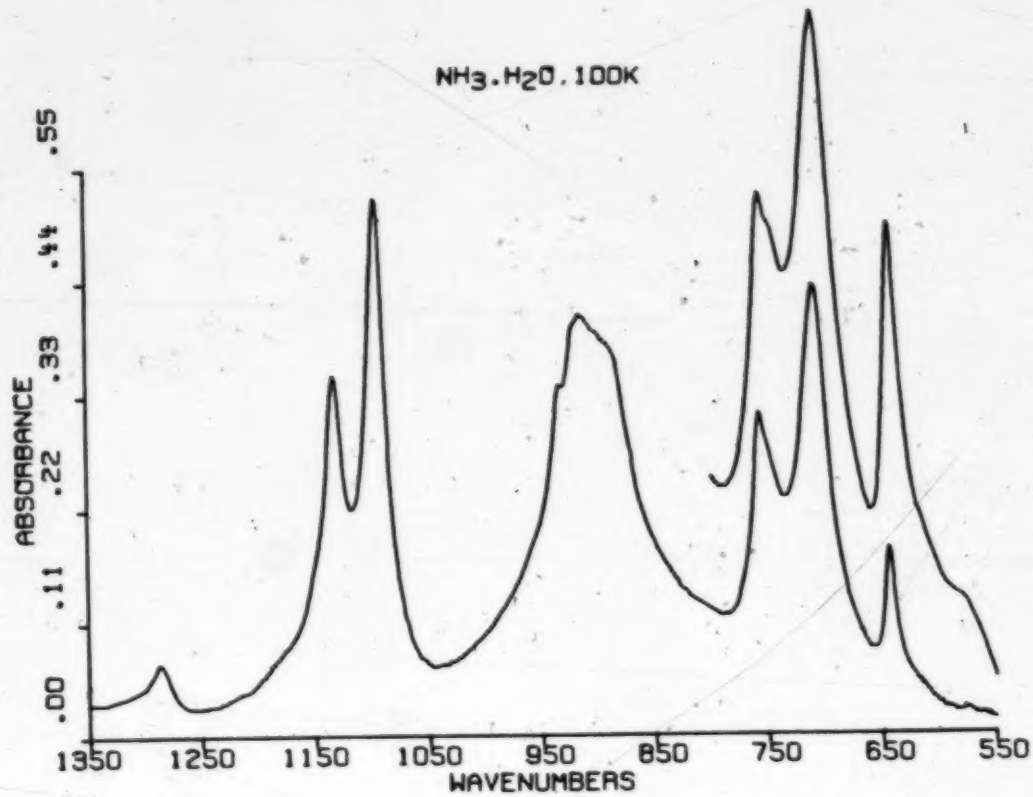

Figure 3.12 Infrared spectrum of $NH_3 \cdot H_2O$ at 100K and 1 cm^{-1} resolution. From mulls in propane except above ~600 cm^{-1} in the top curve was plotted from a mull in propylene. The top curve was offset for clarity.

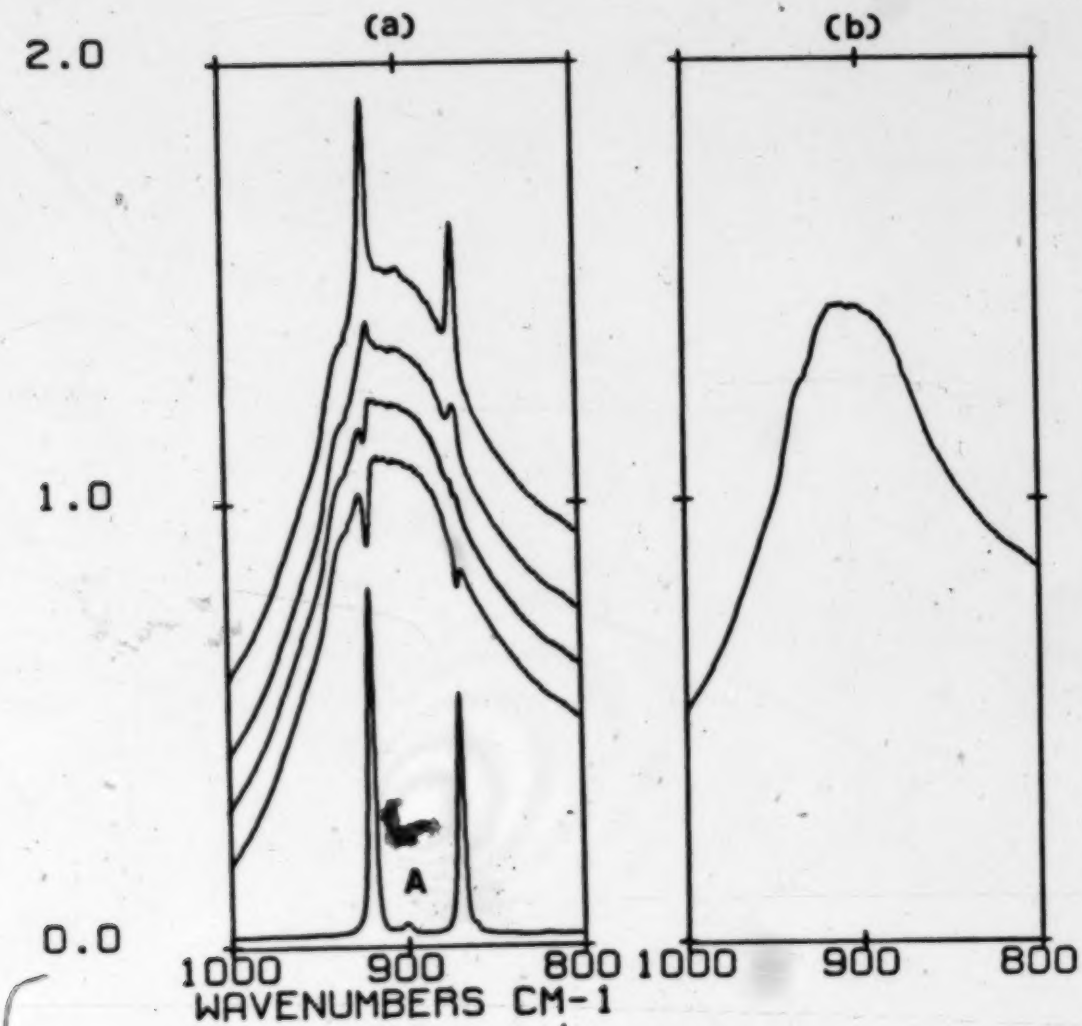

Figure 3.13 Infrared absorbance spectrum of $NH_3 \cdot H_2O$ at 100K and 1 cm^{-1} resolution, $\nu_R(H_2O)$. (a) Detailed subtraction of propane (curve A) from a spectrum of $NH_3 \cdot H_2O$ in propane. (b) The resultant spectrum after subtraction and straight line generation.

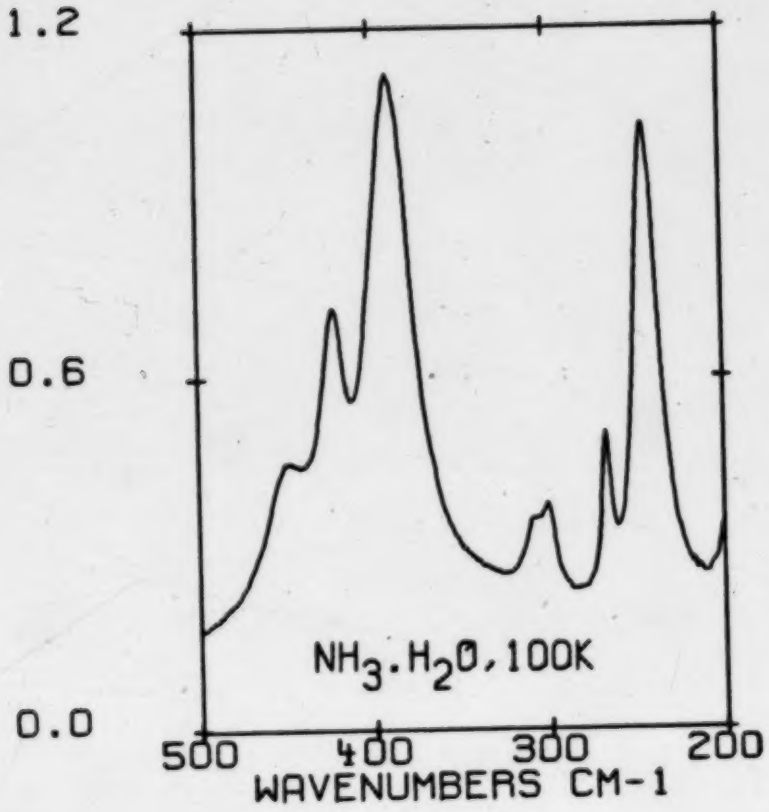

Figure 3.14 Infrared absorbance spectrum of $NH_3 \cdot H_2O$ at 100K and 1 cm^{-1} resolution. From a mull in propane.

Table 3.6 Infrared spectral features of ammonia monohydrate at 100K.

This Work		Bertie & Morrison[6]	
ν/cm^{-1}[a]	Intensity[b]	ν/cm^{-1}[c]	Assignment[d]
~5210	vw		
5015(1)	w		$(\nu_3+\nu_4)NH_3$
~4953	sh		
~4800	w,br		
4515(4)	w		$(\nu_3+\nu_2)NH_3$
~4417	vw,br		
~4366			
~4320			
~4240			
~4150			
~3771			
~3689			
~3590			
~3531			
3403.2(5)	vs	3402(2)	$\nu_3(NH_3)$
3392.1(5)	vs	--	
3387.3(5)	vs	3387(2)	
3332(2)	s	3330(3)	$\nu_1(NH_3)$; $2\nu_4(NH_3)$;
~3294	sh	3305(2)	$2\nu_2(H_2O)$?
--		3287(2)	
3275(3)	s	3270(5)	$\nu_{O-H...O}(H_2O)$
3235	sh	--	$\nu_1(NH_3)$; $2\nu_4(NH_3)$?
3182(2)	vs	3190(10)	$\nu_{O-H...O}(H_2O)$
~2950	sh,br	--	
2887(10)	vs	2910(10)	$\nu_{O-H...N}$
~2432	w,br	2500-2250	
2260(3)	w		
2140.8(5)	vw	2142(2)	
2028(4)	vw	~2025	
1994(5)	vw		
1834(3)	w	1833(5)	
1773(3)	w	1770(5)	
~1696	sh	~1700	$\nu_2(H_2O)$

(Continued)

Table 3.6 (Continued)

This Work		Bertie & Morrison[6]	Assignment[d]
ν/cm^{-1}[a]	Intensity[b]	ν/cm^{-1}[c]	
1665.5(5)	m	1664(1)	$\nu_4(NH_3)$
1650.1(5)	m	1650(2)	
1627.0(5)	m	1625(2)	
~1594	sh	--	
1537(2)	w	1540(5)	
1480(2)	w	1483(5)	
1439(4)	w	1440(5)	
1402(2)	w	--	
1287.1(5)	w	1287(2)	
1133.4(5)	s	1133(2)	$\nu_2(NH_3)$
1095.9(5)	vs	1095(2)	
~ 932	sh	--	$\nu_R(H_2O)$
914(2)	s	908(3)	
		895(2)	
~ 894	sh	884(2),	
757.6(5)	s	757(2)	
~ 750	sh	~ 747	
709.9(5)	s	708(2)	
644.2(5)	m	641(2)	
~ 579	sh	--	
448(3)	mw	448(2)	$\nu_R(NH_3)$
421(1)	m		
389(2)	ms	< 400	
308(3)	w		$\nu_R(NH_3)$; ν_T ?
300(2)	w		
266.6(5)	mw		ν_T
243(2)	ms		

[a] The numbers in parentheses are the 95% confidence limits in the last digit.

[b] vs, s, ms, m, mw, w, vw, sh and br, mean: very strong, strong, medium strong, medium, medium weak, weak, very weak, shoulder and broad, respectively.

[c] The estimated accuracies of the frequencies in brackets as given in Ref. 6.

[d] The complete assignments are presented later in Table 4.11.

described in Section 2.8. The regions where one mulling agent absorbs strongly were plotted from spectra of samples whose mulling agents show weak or no absorption in those regions. A gap was left in curve D Figure 3.8, in place of strong propane absorption around 2900 cm^{-1} and curve A Figure 3.8, shows the spectrum of a mull in Freon-13 in this region. A straight line was drawn in place of propane absorption at ~1450 cm^{-1} in curve D Figure 3.8 and curve A is the spectrum of a mull in Freon-13. The region 2100 - 1950 cm^{-1} is shown from a mull in propane, curve A in Figure 3.11 (using the Bruker instrument) because of uncertainty caused by Freon-13 absorption in the main spectrum. A straight line was also drawn in place of uncertainty from a propane mull at ~750 cm^{-1} in Figure 3.12 and this region of the spectrum of a mull in propylene is shown. The shoulder at ~579 cm^{-1} was found to vary in intensity. The region 1000 - 800 cm^{-1} in Figure 3.13 was plotted from a mull in propane (recorded on the Bruker instrument) and shows the subtraction of different fractions of the propane spectrum in Figure 3.13(a). The band shape resulting from propane subtraction and straight line generation to remove small residual features is shown in Figure 3.13(b); it is identical to that obtained from mulls in Freon-13.

The infrared spectrum in Figure 3.14 was recorded

with the Bruker IFS-113V spectrometer down to 200 cm^{-1} from a mull in propane. Below 200 cm^{-1} CsI windows absorb very strongly.

3.6 Infrared Spectra of Deuterated Ammonia Monodeuterate

The infrared spectra of deuterated ammonia monodeuterate, $ND_3 \cdot D_2O$, < 1% H, at 100K and 1 cm^{-1} resolution are shown in Figures 3.15 - 3.20. The frequencies of the spectral features are shown in Table 3.7. In Figure 3.15 the sample used to obtain curve C had slightly more hydrogen impurity than that in the sample used to obtain curve B but still less than 1%.

Gaps were left because of absorptions by propane, in curve A of Figure 3.16 from ~3150 to ~2700 cm^{-1} and in curve A of Figure 3.19 from ~1500 to 1400 cm^{-1} and the spectra shown in these regions are of mulls in Freon-13. A straight line was drawn in curve A of Figure 3.16 from ~1500 to 1400 cm^{-1} and curve B was plotted from a spectrum of a mull in Freon-13.

3.7 Infrared Spectra of Ammonia Dihydrate

Infrared spectra of ammonia dihydrate at 100K and 1 cm^{-1} resolution are shown in Figures 3.21 - 3.25. Figure 3.26 shows the infrared spectrum of ammonia dihydrate at

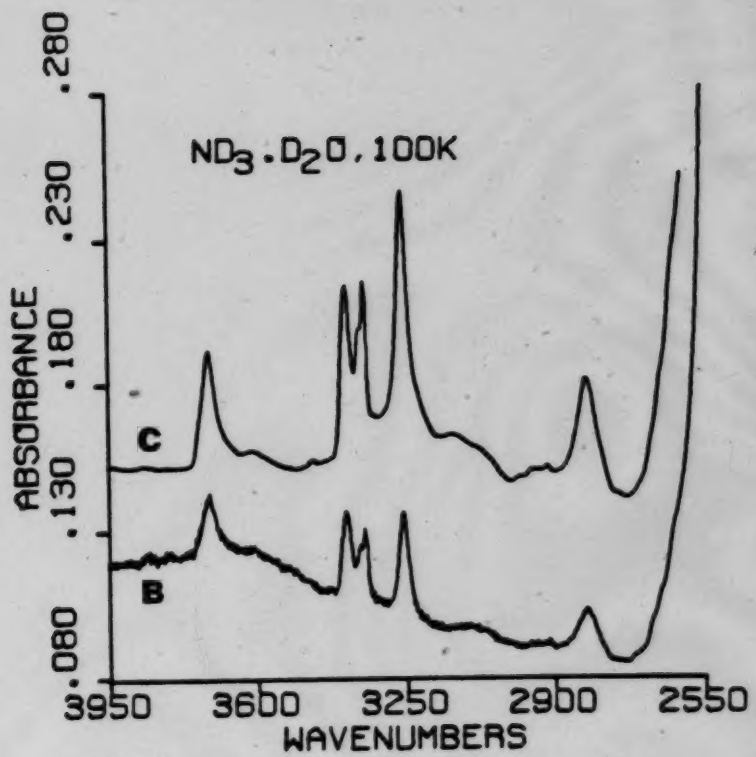

Figure 3.15 Infrared spectra of $ND_3 \cdot D_2O$, <1% H at 100K and 1 cm^{-1} resolution. The sample used to obtain curve C had more H than that in the sample used to obtain curve B. From mulls in Freon-13.

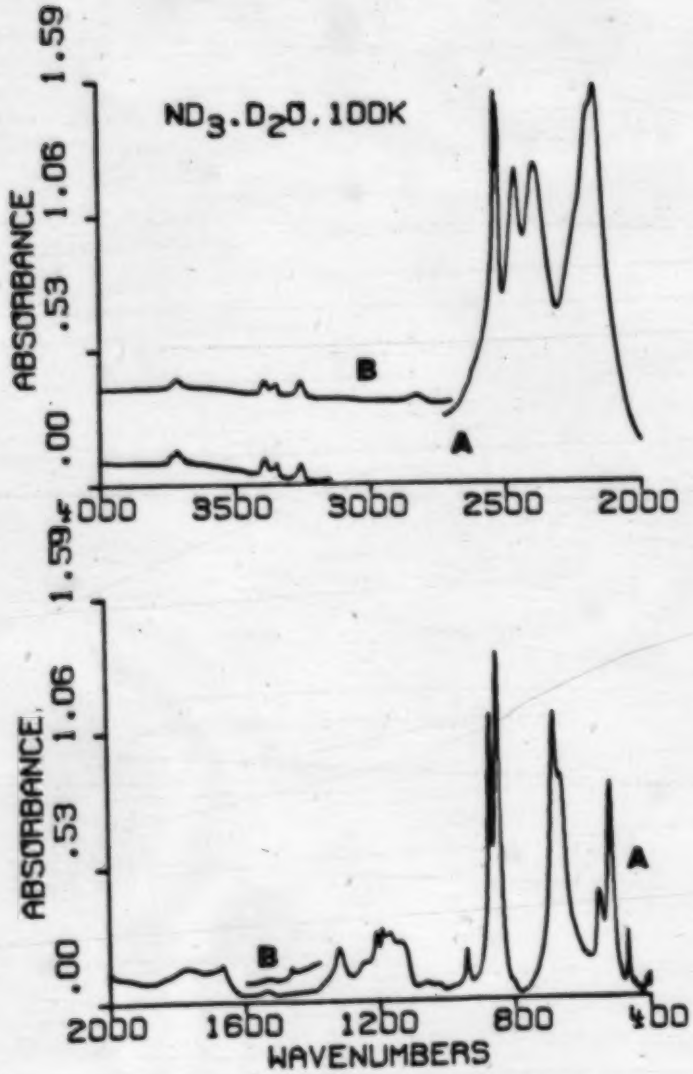

Figure 3.16 Infrared spectra of $ND_3 \cdot D_2O$, <1% H at 100K and 1 cm^{-1} resolution. Curves A and B are from mulls in propane and Freon-13, respectively.

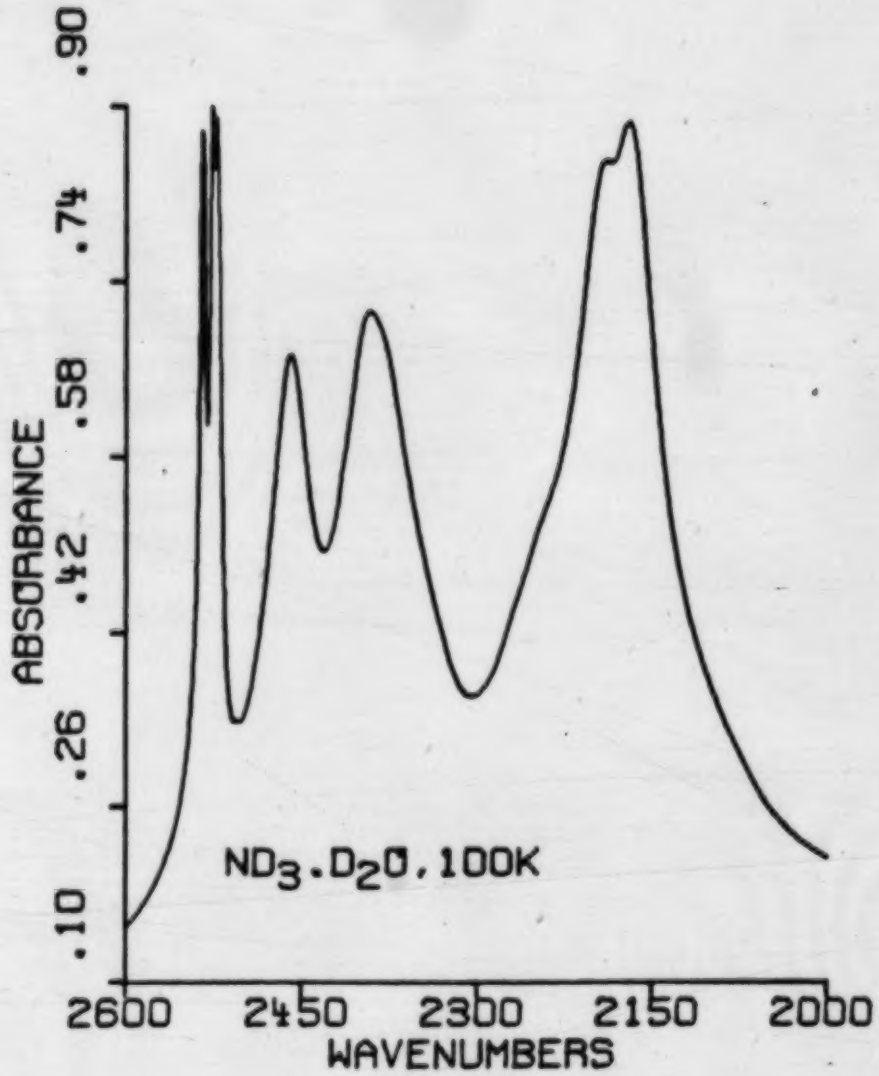

Figure 3.17 Infrared spectrum of $ND_3 \cdot D_2O$, <1% H at 100K and 1 cm^{-1} resolution. From a mull in Freon-13.

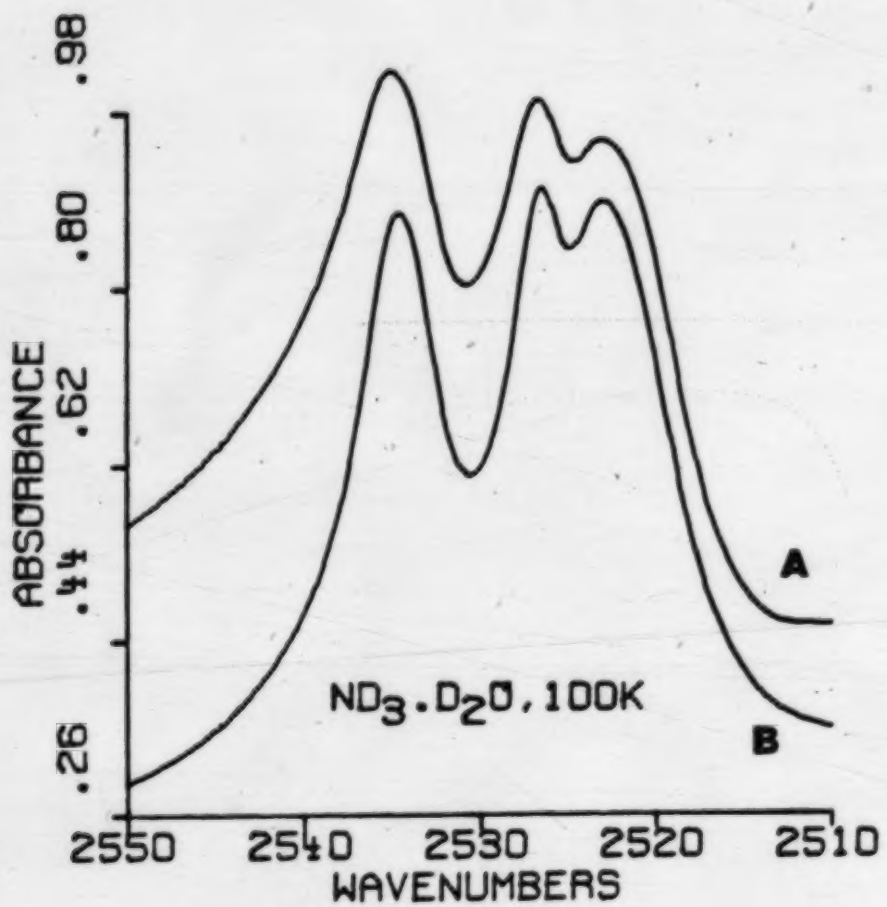

Figure 3.18 Absorption by the antisymmetric N-D stretching modes of $ND_3 \cdot D_2O$, <1% H at 100K and 1 cm^{-1} resolution. Curves A and B are from mulls in propane and Freon-13, respectively.

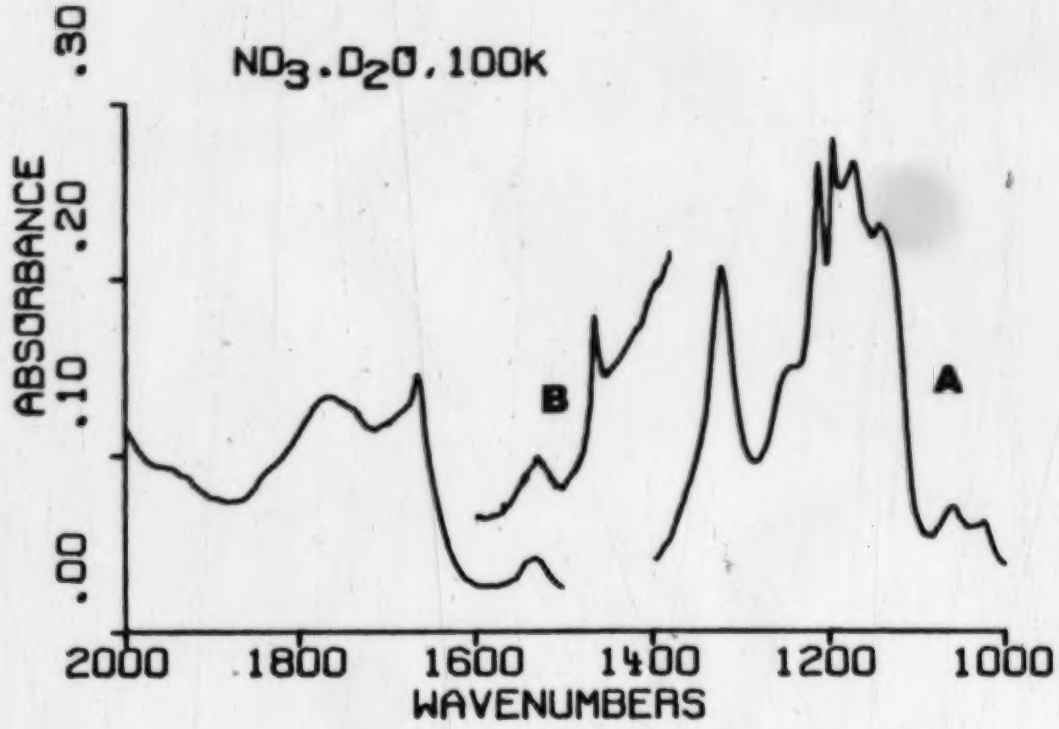

Figure 3.19 Infrared spectra of $ND_3 \cdot D_2O$ containing <1% H at 100K and 1 cm^{-1} resolution. Curves A and B are from mulls in propane and Freon-13, respectively.

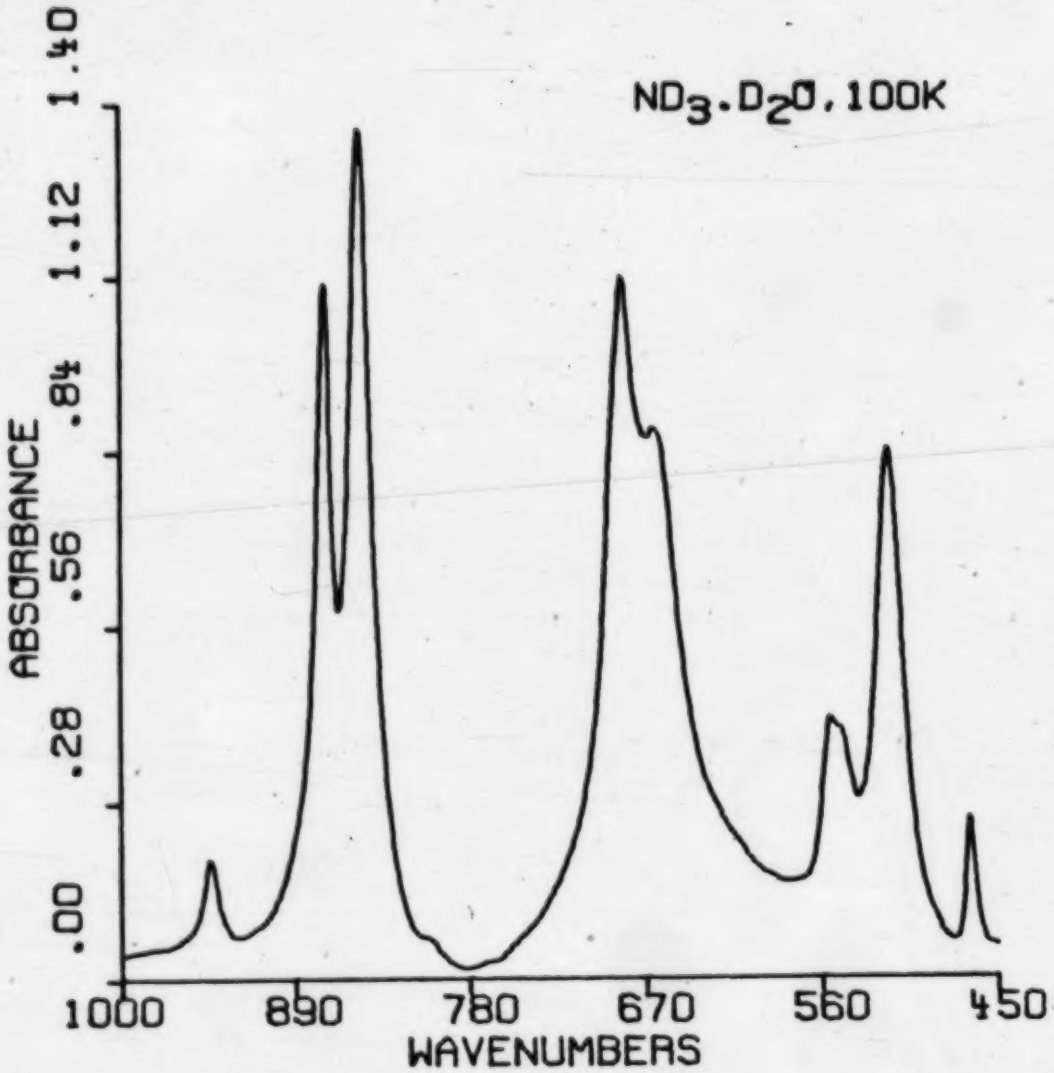

Figure 3.20 Infrared spectrum of $ND_3 \cdot D_2O$, <1% H at 100K and 1 cm^{-1} resolution. From a mull in propane.

Table 3.7 Infrared spectral features of deuterated ammonia monodeuterate at 100K.

ν/cm^{-1}[a]	Intensity[b]	Assignment[c]
3715(2)	w	$(\nu_3+\nu_4)ND_3$
~3610	sh,br	
~3471	vw	
3392(2)	w	$(\nu_3+\nu_2)ND_3$
~3362	sh	$\nu_{NH}(ND_2H)$
3349.2(5)	w	
~3345	sh	
3259(2)	w	$\nu_{O-D\ldots O}(HOD)$
~3135	vw	
~3085	vw	
~2954	vw	
~2940	vw	
~2917	vw	
2825(5)	w	$\nu_{O-D\ldots N}(HOD)$
2534.3(5)	vs	$\nu_3(ND_3)$
2526.1(5)	vs	
2522.2(6)	vs	
2459(2)	vs	$\nu_{O-D\ldots O}(H_2O)$
~2414	sh	$\nu_1(ND_3)$; $2\nu_4(ND_3)$?
2390(1)	vs	$\nu_{O-D\ldots O}(H_2O)$
~2260	sh	
2189(2)	vs	$\nu_{O-D\ldots N}$
2165(2)	vs	
~1929	sh	
~1836	sh	
1767(3)	mw,br	
~1675	sh	
1666.8(9)	mw	
1534(2)	vw	
1467(2)	w	$\nu_2(HOD)$
1319.5(9)	mw	
1243(3)	mw	$\nu_2(D_2O)$

(Continued)

Table 3.7 (Continued)

ν/cm^{-1}[a]	Intensity[b]	Assignment[c]
~1217	sh	$\nu_4(ND_3)$
1209.1(5)	mw	
1192.6(5)	mw	
1135(3)	mw	
1060(4)	vw	
1023(2)	vw	
943.4(6)	mw	
870.6(9)	vs	$\nu_2(ND_3)$
848.2(8)	vs	
~ 806	sh	ν_R(HOD) ?
682.3(6)	vs	$\nu_R(D_2O)$
661(2)	s	
554(1)	ms	
~ 548	sh	
516.3(6)	s	
466.7(5)	mw	

[a] The numbers in parentheses are the 95% confidence limits in the last digit.

[b] vs, s, ms, mw, w, vw, sh and br, mean: very strong, strong, medium strong, medium weak, weak, very weak, shoulder and broad, respectively.

[c] The complete assignments are presented later in Table 4.11.

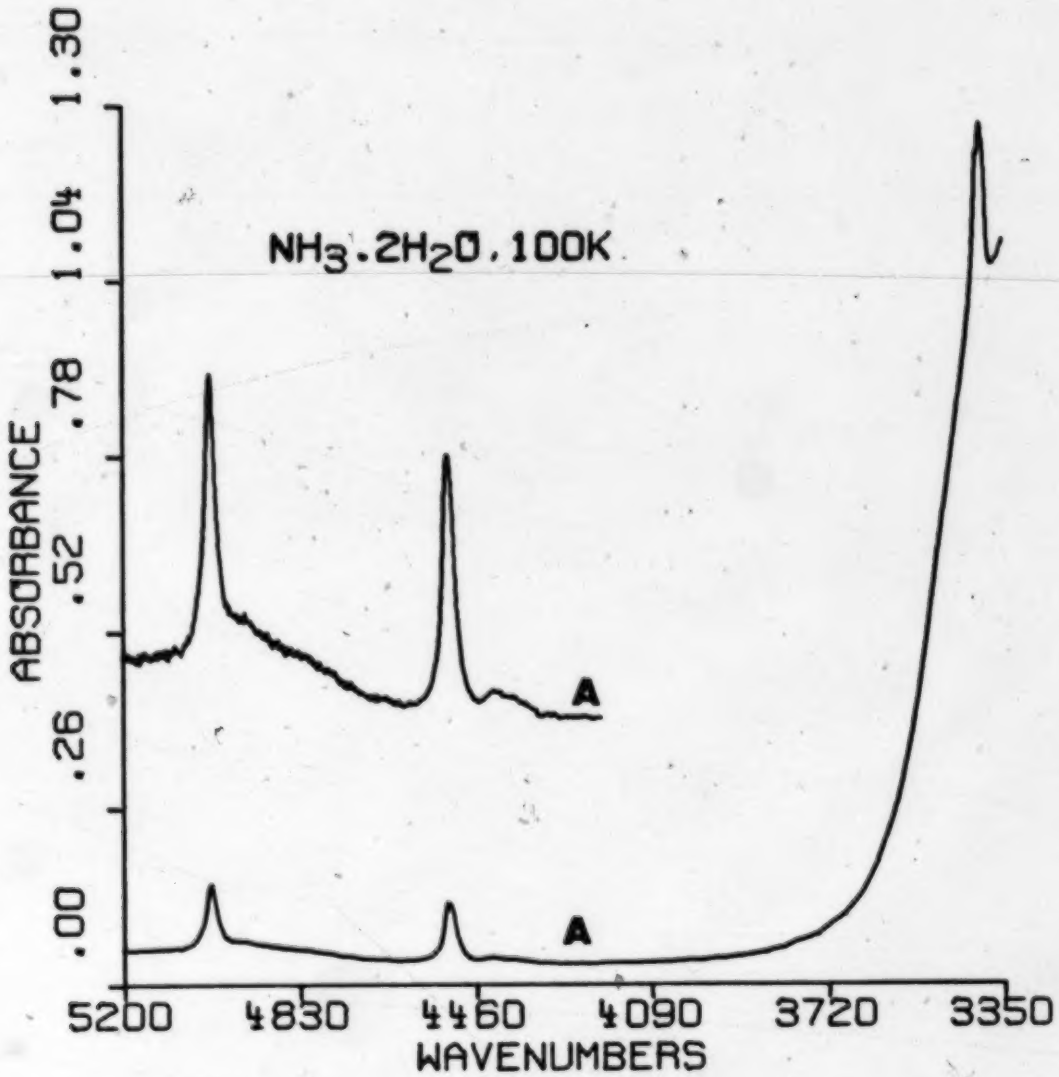

Figure 3.21 Infrared spectra of $NH_3 \cdot 2H_2O$ at 100K and 1 cm^{-1} resolution. From a mull in Freon-13.

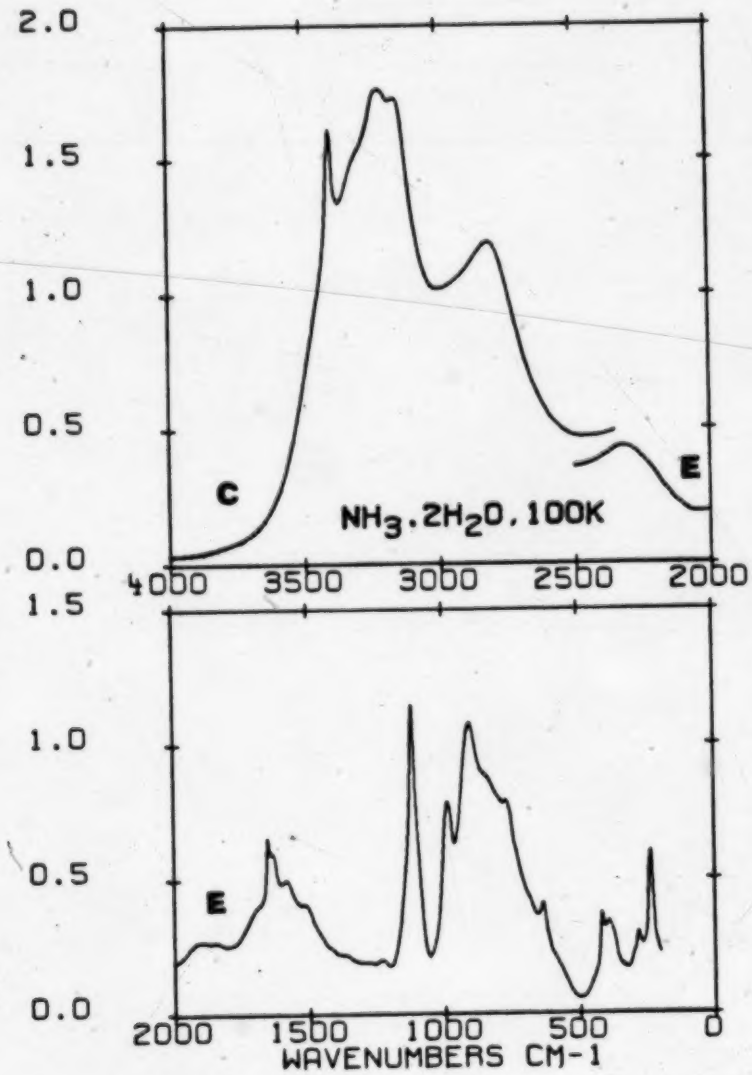

Figure 3.22 Infrared absorbance spectra of $NH_3 \cdot 2H_2O$ at 100K and 1 cm^{-1} resolution. Curves C and E are from mulls in Freon-13 and propane, respectively.

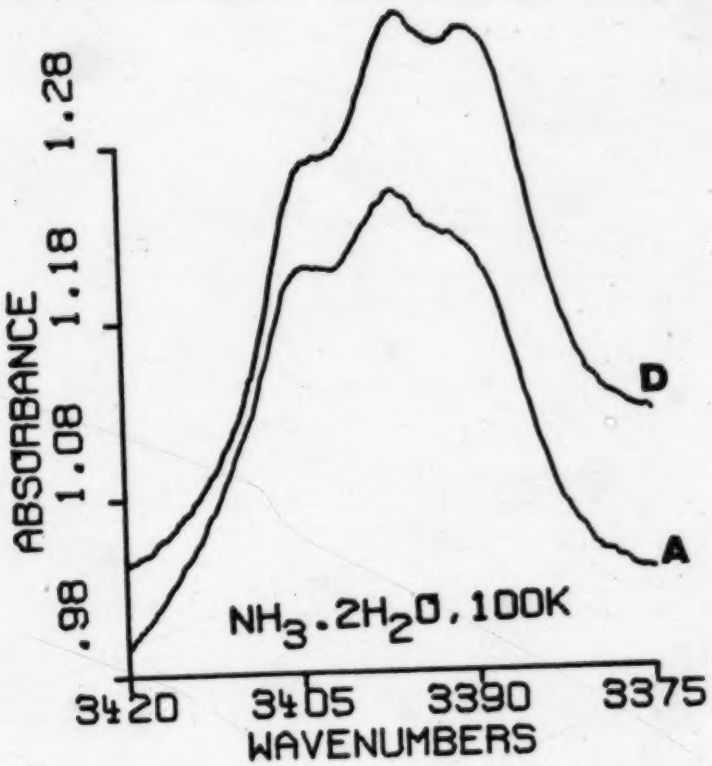

Figure 3.23 Absorption by the antisymmetric N-H stretching modes of $NH_3 \cdot 2H_2O$ at 100K and 1 cm^{-1} resolution. Curves A and D are from mulls in Freon-13 and propane, respectively.

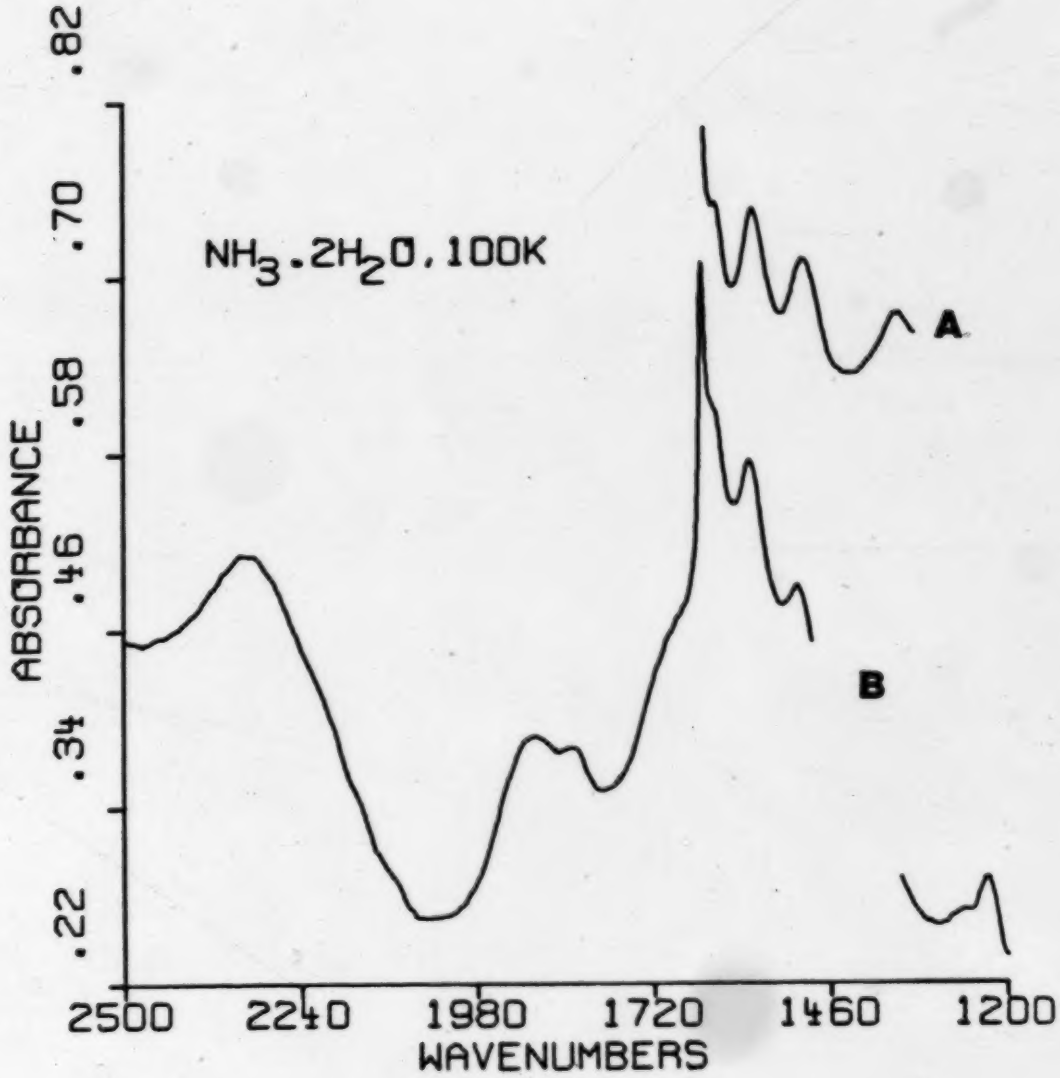

Figure 3.24 Infrared spectra of $NH_3 \cdot 2H_2O$ at 100K and 1 cm^{-1} resolution. Curves A and B are from mulls in Freon-13 and propane, respectively.

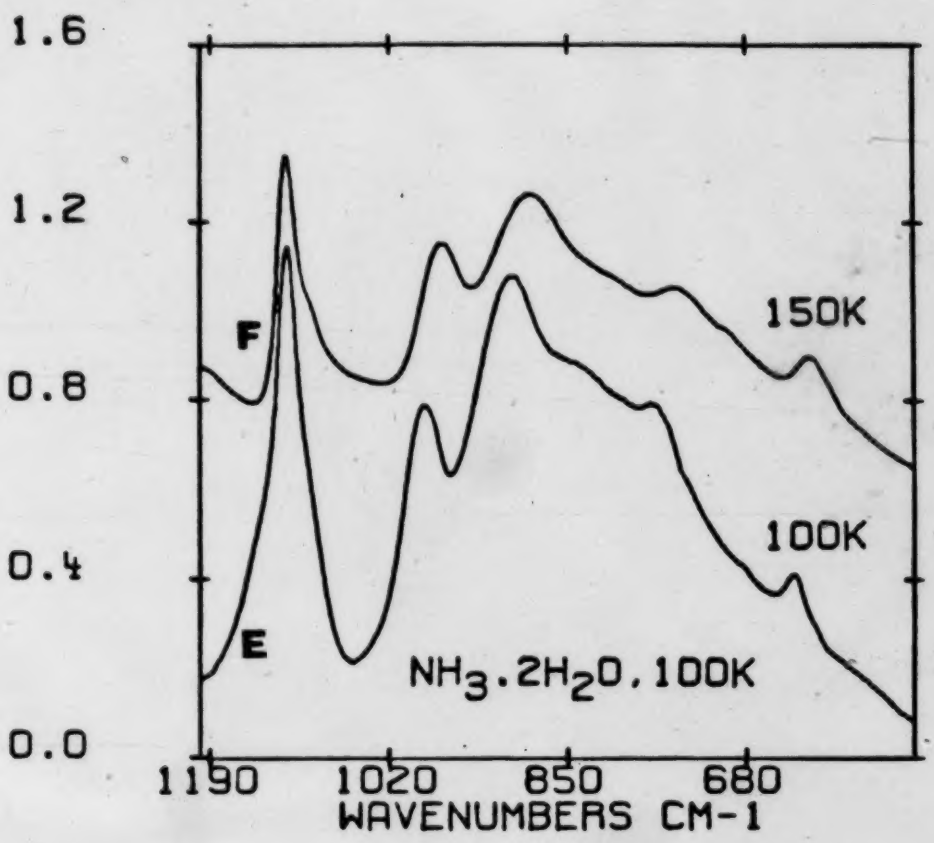

Figure 3.25 Infrared absorbance spectra of $NH_3 \cdot 2H_2O$ at 1 cm^{-1} resolution and 100K (curve E) and 150K (curve F). From mulls in propane.

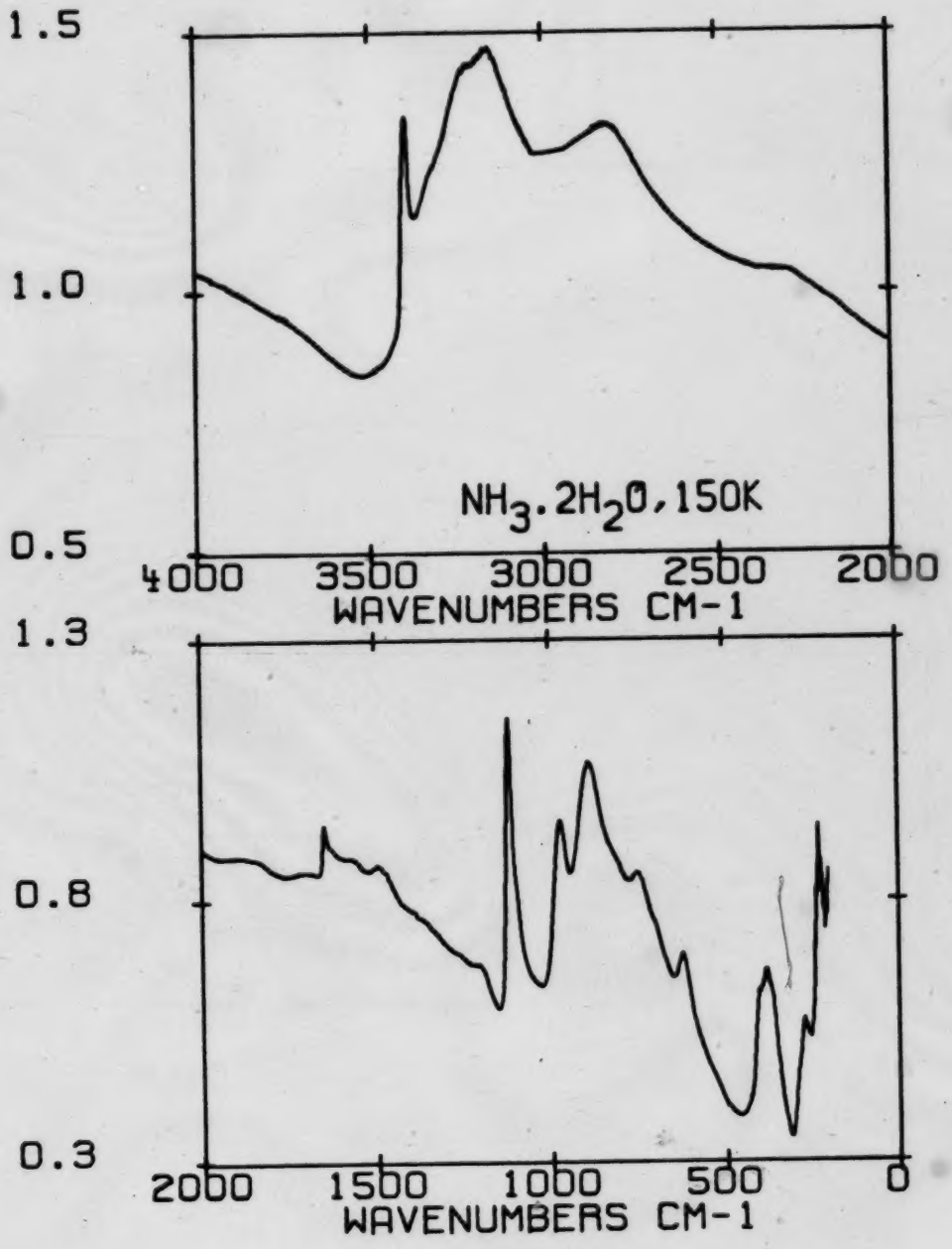

Figure 3.26 Infrared absorbance spectrum of $NH_3 \cdot 2H_2O$ at 150K and 1 cm^{-1} resolution. From a mull in propane.

~150K and 1 cm^{-1} resolution. Almost all the propane mulling agent was lost to the vacuum line at that temperature. A straight line was drawn in place of absorption by propane at ~2900 cm^{-1}. The spectrum at ~150K was only recorded once and 1-chlorobutane/liquid nitrogen slush was used in place of the liquid nitrogen in the inner jacket (A), Figure 2.2, of the low-temperature cell to maintain the temperature of ~150K. As shown in Figure 3.26 the spectrum at ~150K indicates strong scattering, especially in the high wavenumber region and is only used to support the assignments.

The frequencies of the spectral features of ammonia dihydrate at 100 and 150K are listed in Table 3.8. A gap was left in place of strong propane absorption in curve B Figure 3.24 and the corresponding region was plotted from a spectrum of a mull in Freon-13.

3.8 Infrared Spectra of $NH_3 \cdot 2H_2O$, x%D

The infrared spectra of ammonia dihydrate containing 2, 5 and 10 mole percent of deuterium at 100K and 1 cm^{-1} resolution are shown in Figures 3.27 to 3.31. The infrared frequencies of the spectral features which are different from those of pure ammonia dihydrate are listed in Table 3.9.

Curve A in Figures 3.27 and 3.28 and curve C in

Table 3.8 Infrared spectral features of ammonia dihydrate at 100K and 150K.

At 100K		At 150K	
ν/cm^{-1}[a]	Intensity[b]	ν/cm^{-1}	Assignment[c]
5019.7(8)	w	5015	$(\nu_3+\nu_4)NH_3$
~4950	vw,br		
~4830	vw,br		
4521.1(9)	w	4519	$(\nu_3+\nu_2)NH_3$
~4424	vw,br		
~4375	vw,br		
3404.0(5)	vs	3396	
3396.3(4)	vs	3393	$\nu_3(NH_3)$
3391.2(9)	vs	3391	
~3298	sh	3320	
3207(5)	vs	3224	$\nu_{O-H...O}(H_2O)$
3150(4)	vs	3156	
2803(6)	s	2809	$\nu_{O_{II}-H...N}(H_2O)$
2319(5)	w,br	2295	
~2200	sh		
~2150	sh		
~2103	sh		
1898(4)	w,br	1880	
1840(3)	w	1835	
~1697	sh	1691	$\nu_2(H_2O)$
1649.2(5)	s	1645	$\nu_4(NH_3)$
1631(2)	sh	~1615	
1577(2)	ms	1562	
1505(4)	ms	1491	
~1361	w	1354	
~1279	w	1257	
1231(2)	w	1198	
~1150	sh,br	1098 sh	
1115.9(7)	vs	1117.5	$\nu_2(NH_3)$

(Continued)

Table 3.8 (Continued)

At 100K		At 150K	
ν/cm^{-1}[a]	Intensity[b]	ν/cm^{-1}	Assignment[c]
986(2)	s	969	$\nu_R(H_2O)$
900(2)	vs	885	
~ 838	sh	~ 809	
766(3)	s	749	
684	sh	~ 700	
633(1)	ms	620	
~ 614	w,sh		
~ 560	sh,br	~	
~ 450	sh,br		$\nu_R(NH_3)$
415.7(6)	ms	402	
391(2)	ms	382	
~ 373	sh	~ 364	
297(1)	m or sh	290	ν_T
283(1)	ms	274	
~ 239	sh		
235.0(15)	s	227	

[a] The numbers in parentheses are the 95% confidence limits in the last digit.

[b] vs, ms, s, m, w, vw, sh and br mean: very strong, medium strong, strong, medium, weak, very weak, shoulder and broad, respectively.

[c] The complete assignments are listed in Table 5.8.

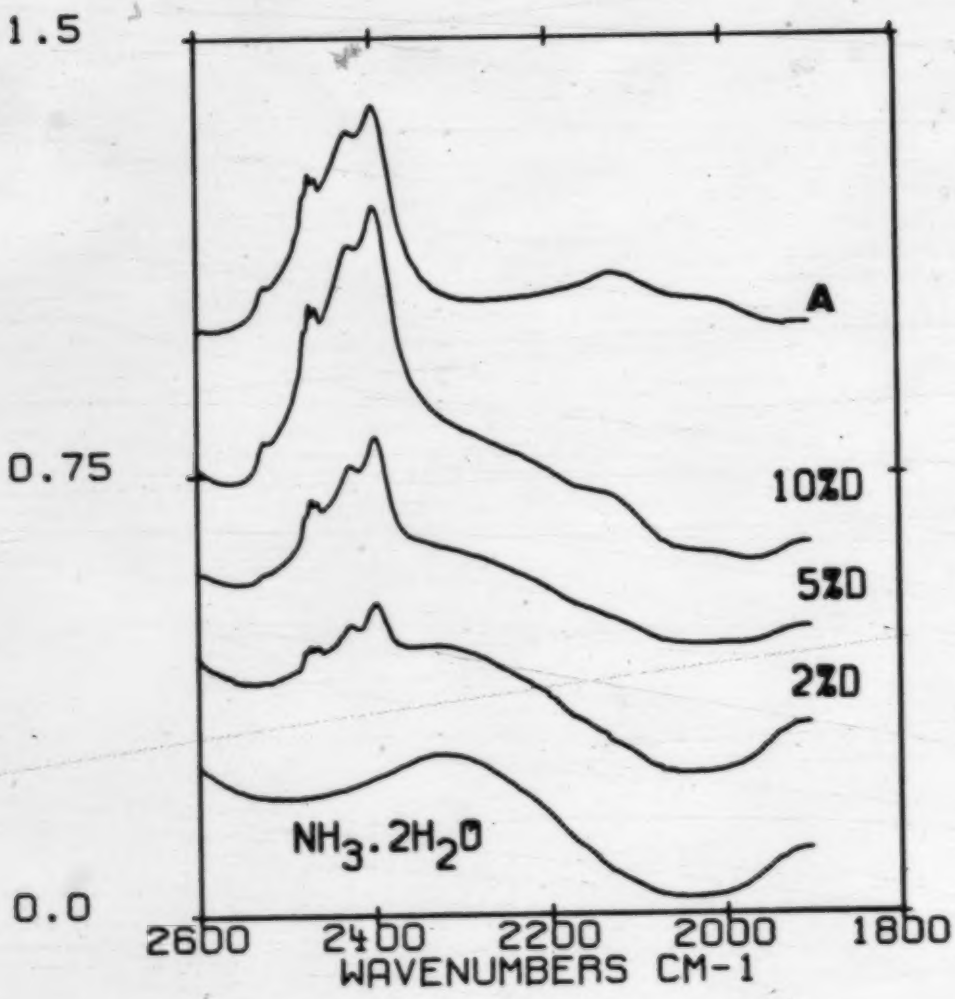

Figure 3.27 The infrared absorbance spectra of the N-D and O-D stretching region of $NH_3 \cdot 2H_2O$ neat and containing NH_2D and HOD at 100K and 1 cm^{-1} resolution. From mulls in propane. Curve A is the difference between the "10% D" and "$NH_3 \cdot 2H_2O$" curves.

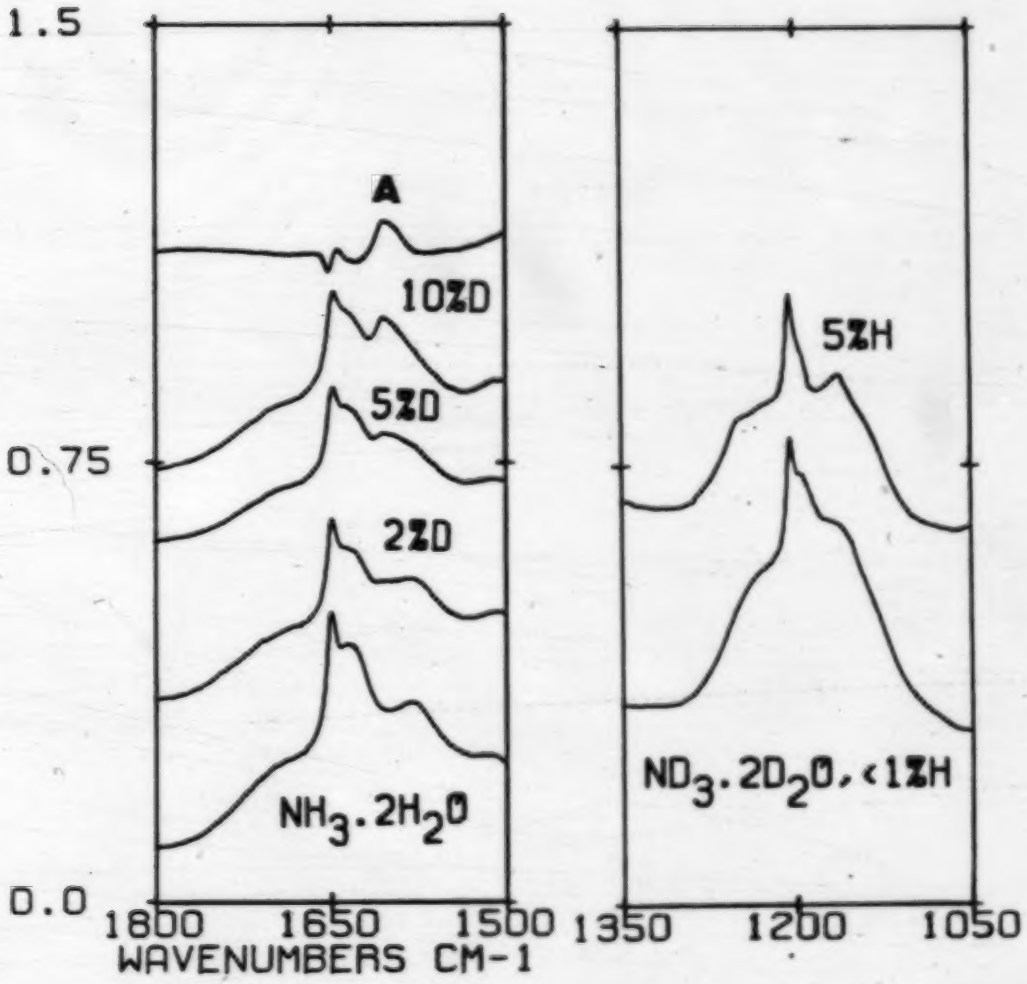

Figure 3.28 Infrared absorbance spectra of isotopically impure $NH_3 \cdot 2H_2O$ and $ND_3 \cdot 2D_2O$ at 100K and 1 cm^{-1} resolution. From mulls in propane. The absorption of the host has been subtracted from curve A.

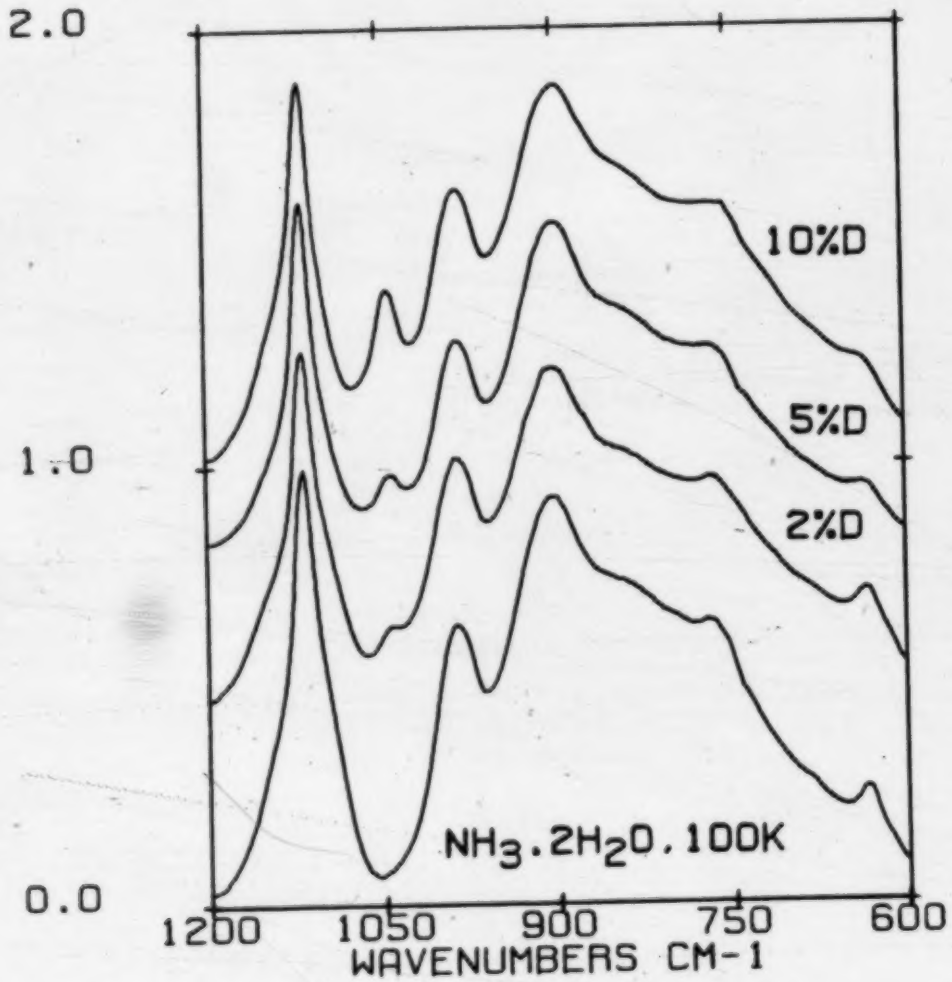

Figure 3.29 Infrared absorbance spectra of $NH_3 \cdot 2H_2O$ at 100K and 1 cm^{-1} resolution, neat and containing deuterium impurity. From mulls in propane.

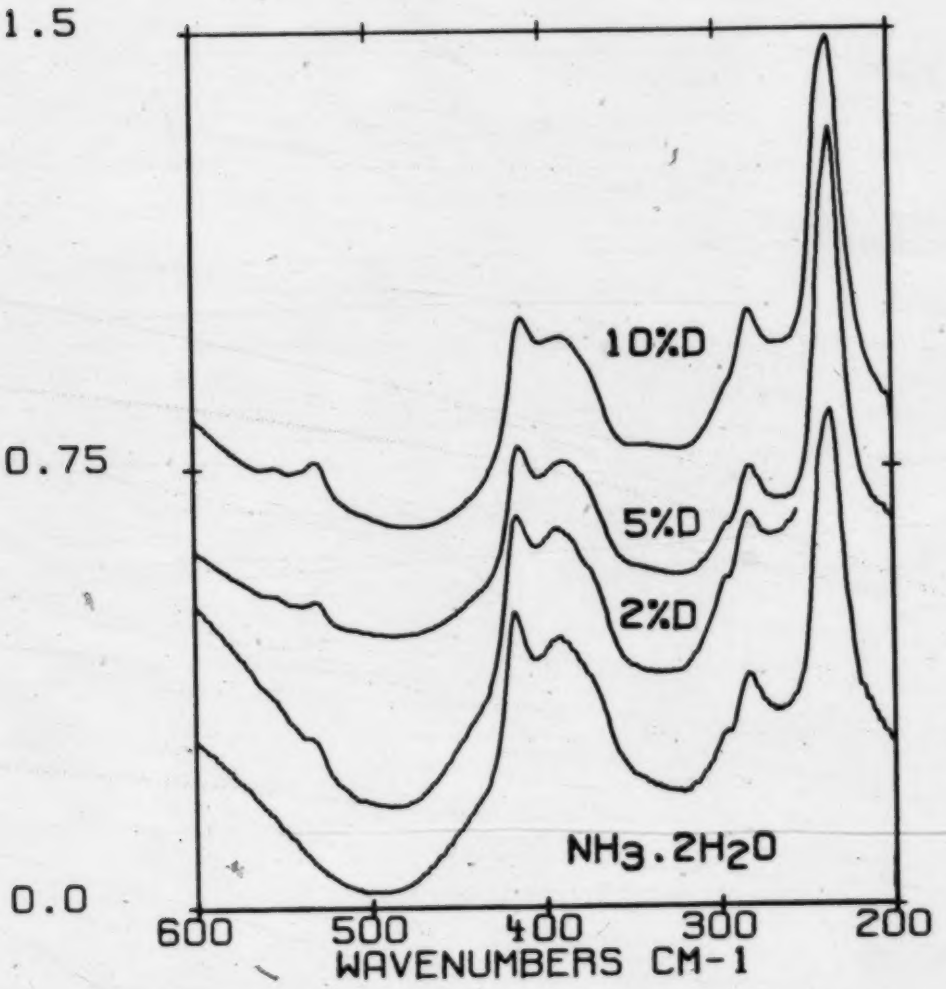

Figure 3.30 Infrared absorbance spectra of $NH_3 \cdot 2H_2O$ at 100K and 1 cm^{-1} resolution, neat and containing deuterium impurity. From mulls in propane.

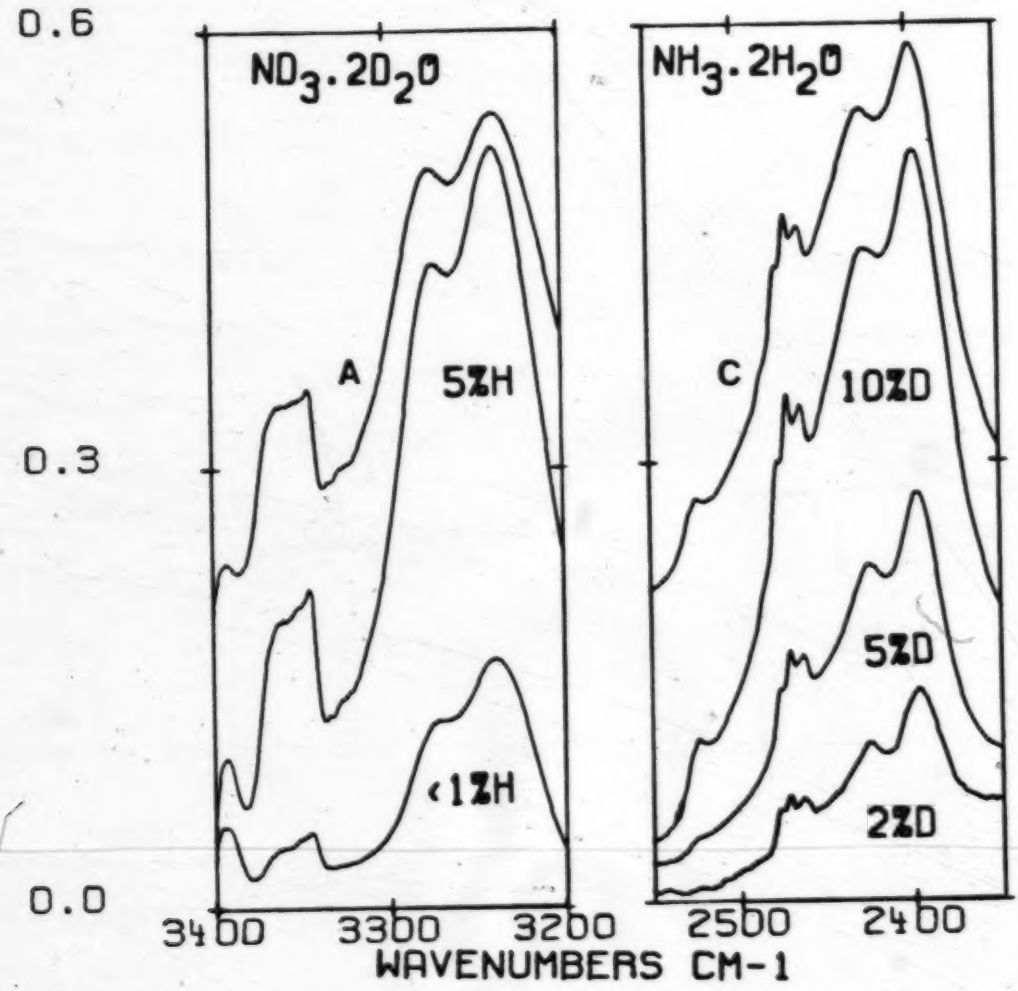

Figure 3.31 Absorption by isolated ND_2H and HOD (left) and isolated NH_2D and HOD (right) in ammonia dihydrate. The absorption by the host has been subtracted from curves A and C. From mulls in Freon-13 (left) and propane (right) at 100K and 1 cm^{-1} resolution.

Table 3.9 Infrared spectral features of partially deuterated ammonia dihydrate at 100K.[a]

Neat[b] ν/cm^{-1}		2% D[b] ν/cm^{-1}		5% D[b] ν/cm^{-1}		10% D[b] ν/cm^{-1}		Assignment
				2527(2)	vw	2527(2)	vw	$\nu_{ND}(ND_2H)$
				2523(2)	vw	2523(2)	vw	
		2475.5(5)	w	2476.2(5)	m	2476.2(5)	ms	$\nu_{ND}(NH_2D)$
		2470.3(5)	w	2470.5(5)	m	2470.5(5)	ms	
		2462.2(6)	w	2462.6(6)	m	2462.7	ms	
		2424(2)	m	2425(2)	ms	2425(2)	s	$\nu_{O_{II}-H...O_I}(HOD)$
		2395(2)	m	2396(2)	ms	2396(2)	s	$\nu_{O_I-H...O_{II}}(HOD)$
				~2126	vw,br	2128(6)	w	$\nu_{O_{II}-H...N}(HOD)$
						2122[c]		
						~2010	vw,br	
1649.2(5)	s	1649.1(6)	s	1648.4(5)	s	1646.8(8)	s	$\nu_4(NH_3)$
1577(2)	ms	1582(2)	ms	1591(2)	ms	1595(3)	ms	
						1601[c]		$\nu_4(NH_2D)$
~1279	w	~1277	vw					
1231(2)	w	1231(1)	w	1237(4)	w	1240(2)	w	
		~1040	sh	1041(3)	w	1041(4)	m	$\nu_2(NH_2D)$
~ 614	sh	~ 614	sh					
~ 560	sh,br							

(Continued)

Table 3.9 (Continued)

Neat[b]		2% D[b]		5% D[b]		10% D[b]		
ν/cm^{-1}		ν/cm^{-1}		ν/cm^{-1}		ν/cm^{-1}		Assignment
		~ 554	vw	554(2)	vw	554(2)	vw	ν_R(HOD)
		~ 542	vw	~ 542	vw	~ 541	vw,sh	
		533(2)	vw	532(2)	vw	532(2)	vw	
						~ 342	w,br	$\nu_R(NH_2D)$

[a]Only features which change with the addition of a few percent of D are included.

[b]The numbers in parentheses are the 95% confidence limits in the last digit. vs, s, ms, m, w, vw, sh and br mean: very strong, strong, medium strong, medium, weak, very weak, shoulder and broad, respectively.

[c]After subtraction of the neat compound.

Figure 3.31 are the spectra of ammonia dihydrate containing 10 mole percent of deuterium from each of which the spectrum of $NH_3 \cdot 2H_2O$ was subtracted. The subtraction at ~1648 cm^{-1} in curve A Figure 3.28 shows a slight frequency shift, from 1649.2 cm^{-1} in the neat compound to 1646.8 cm^{-1} in the compound containing 10% D.

3.9 Infrared Spectra of $ND_3 \cdot 2D_2O$, x% H

The infrared spectra of deuterated ammonia dideuterate containing <1 and 5 mole percent of H at 100K and 1 cm^{-1} resolution are shown in Figures 3.32 to 3.44. The infrared frequencies are listed in Table 3.10.

A gap was left in place of the strong propane absorption between ~3100 and ~2730 cm^{-1} in curve A, Figure 3.32 and in curve E Figure 3.33. The region was replotted in both cases, from spectra of mulls in Freon-13. A straight line was drawn in place of strong propane absorption between ~1490 and ~1430 cm^{-1} in Figure 3.32 and gaps were left in this region in Figure 3.42 and the spectrum of the region was replotted in Figure 3.42 from mulls in Freon-13.

Curves C in Figure 3.35 and A in Figure 3.31 are the differences between the spectra of $ND_3 \cdot 2D_2O$, 5% H and $ND_3 \cdot 2D_2O$, <1% H. Figures 3.36 to 3.41 show the

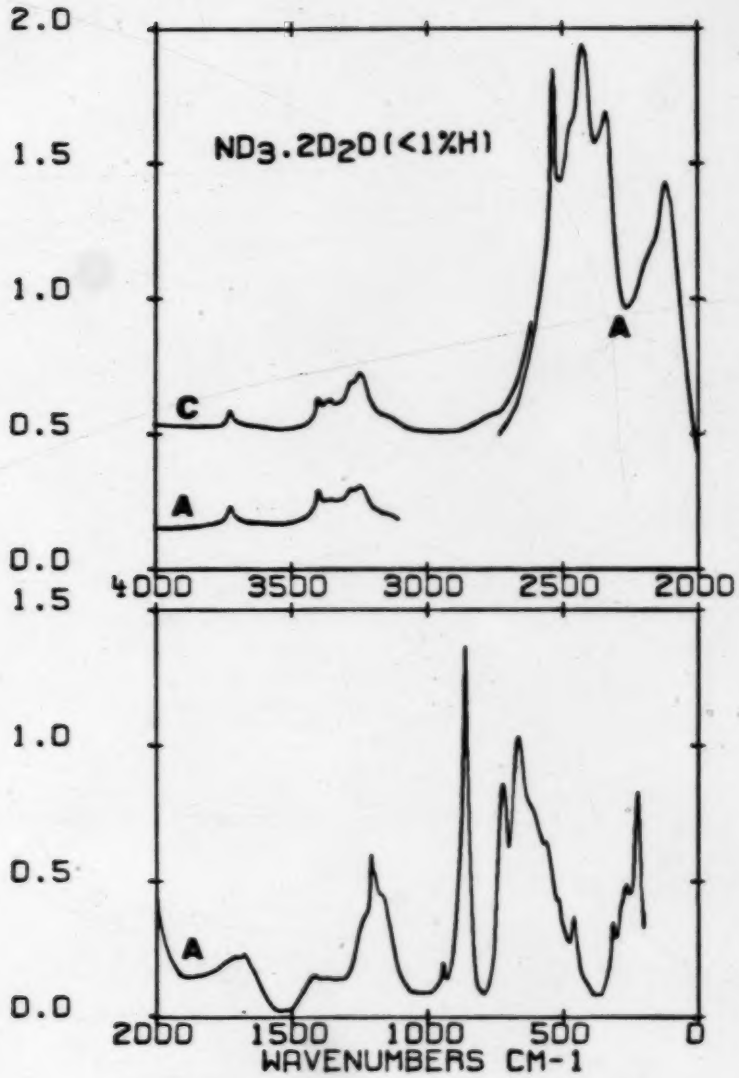

Figure 3.32 Infrared absorbance spectra of $ND_3 \cdot 2D_2O$, <1% H at 100K and 1 cm^{-1} resolution. Curves A and C are from mulls in propane and Freon-13, respectively.

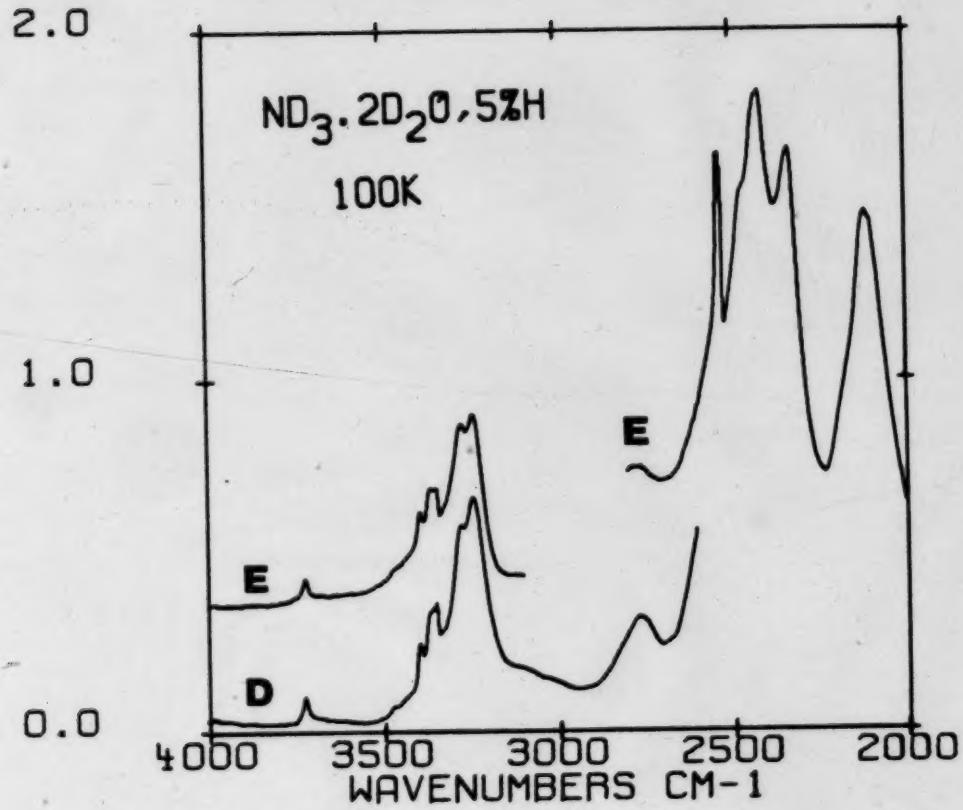

Figure 3.33 Infrared absorbance spectra of $ND_3 \cdot 2D_2O$ containing 5% H at 100K and 1 cm^{-1} resolution. Curves D and E are from mulls in Freon-13 and propane, respectively.

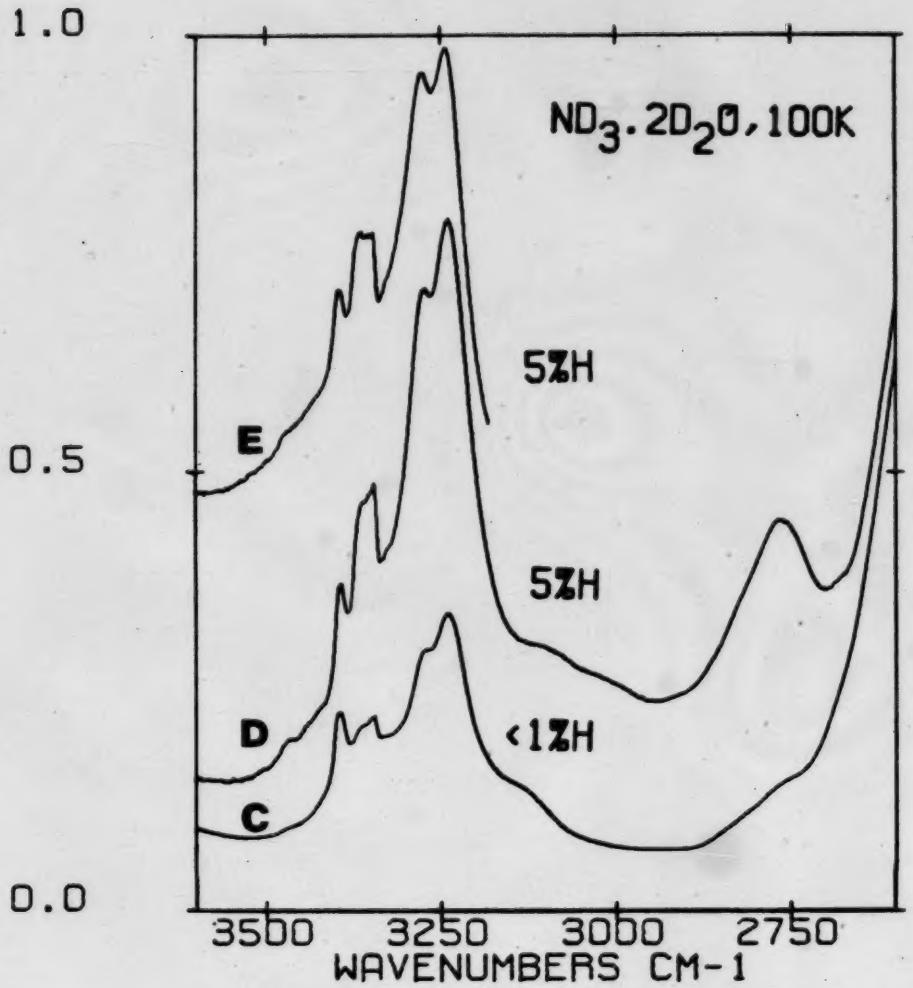

Figure 3.34 Infrared absorbance spectra of $ND_3 \cdot 2D_2O$ containing <1 and 5% H at 100K and 1 cm^{-1} resolution from mulls in propane (top) and Freon-13 (middle and bottom).

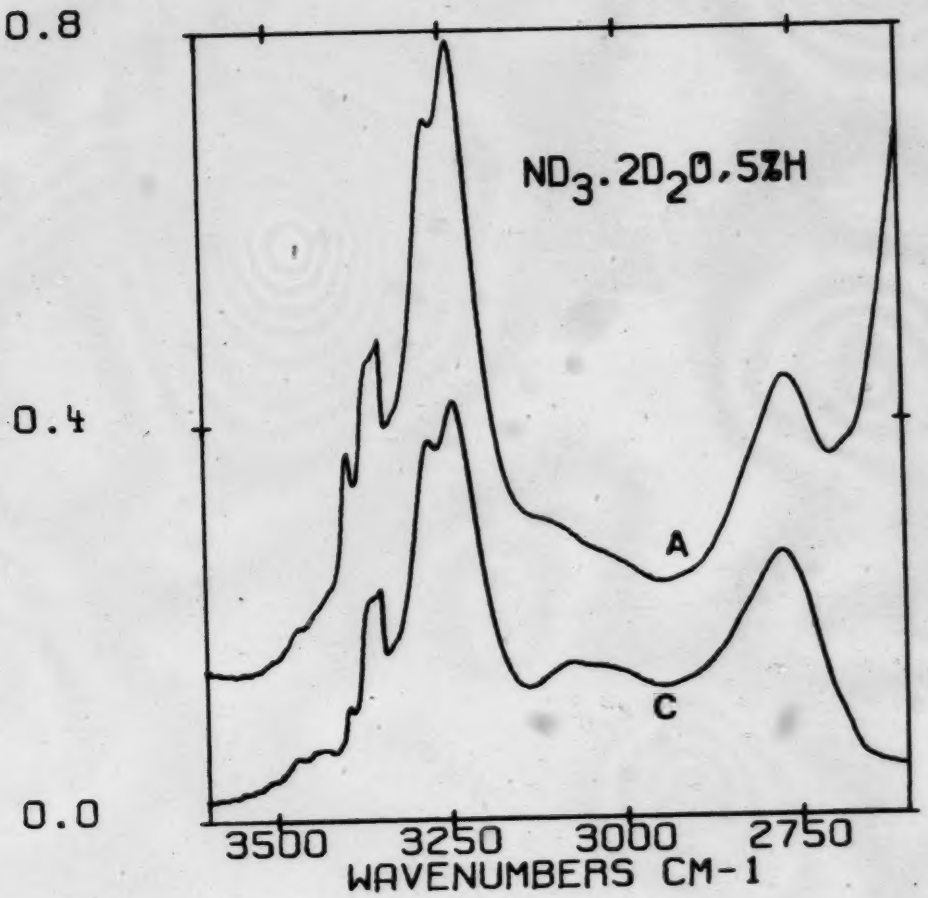

Figure 3.35 N-H and O-H stretching absorbance bands of NHD_2 and HOD isolated in $ND_3 \cdot 2D_2O$ at 100K and 1 cm^{-1} resolution. Curve A is from a mull in Freon-13. The absorption by $ND_3 \cdot 2D_2O$ (<1% H) has been subtracted from curve C.

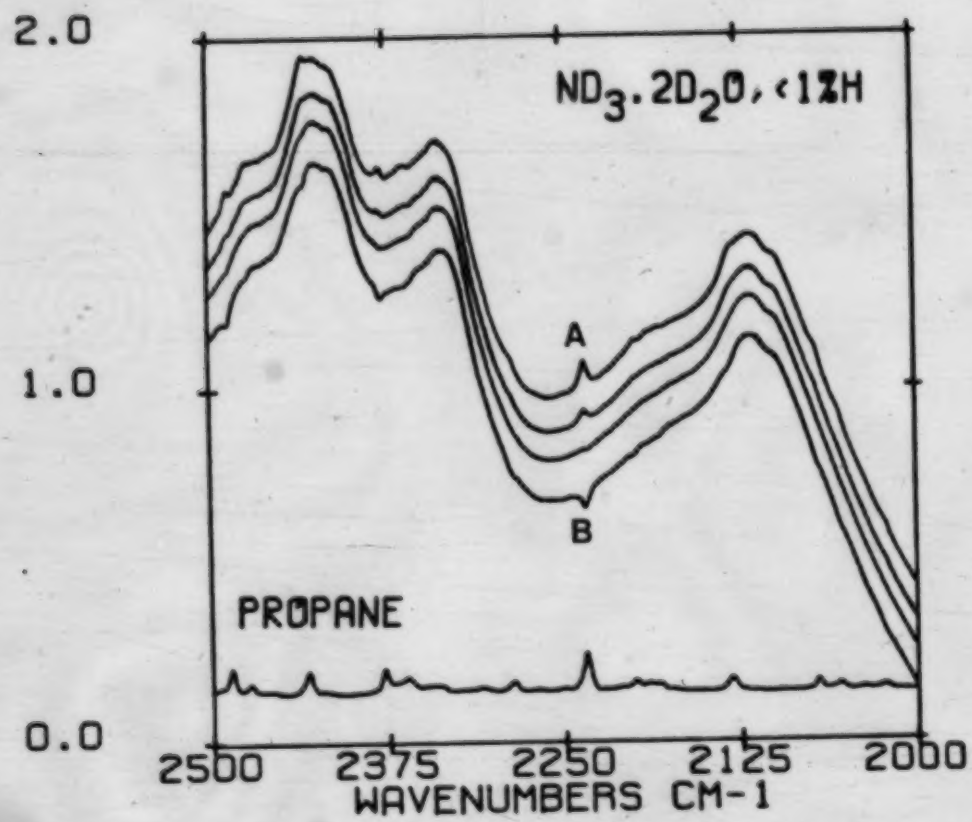

Figure 3.36 O-D stretching absorbance bands of $ND_3 \cdot 2D_2O$, <1% H at 100K and 1 cm^{-1} resolution. The figure shows step-by-step subtraction of propane absorption. Curve A without subtraction and curve B with over subtraction of propane absorption.

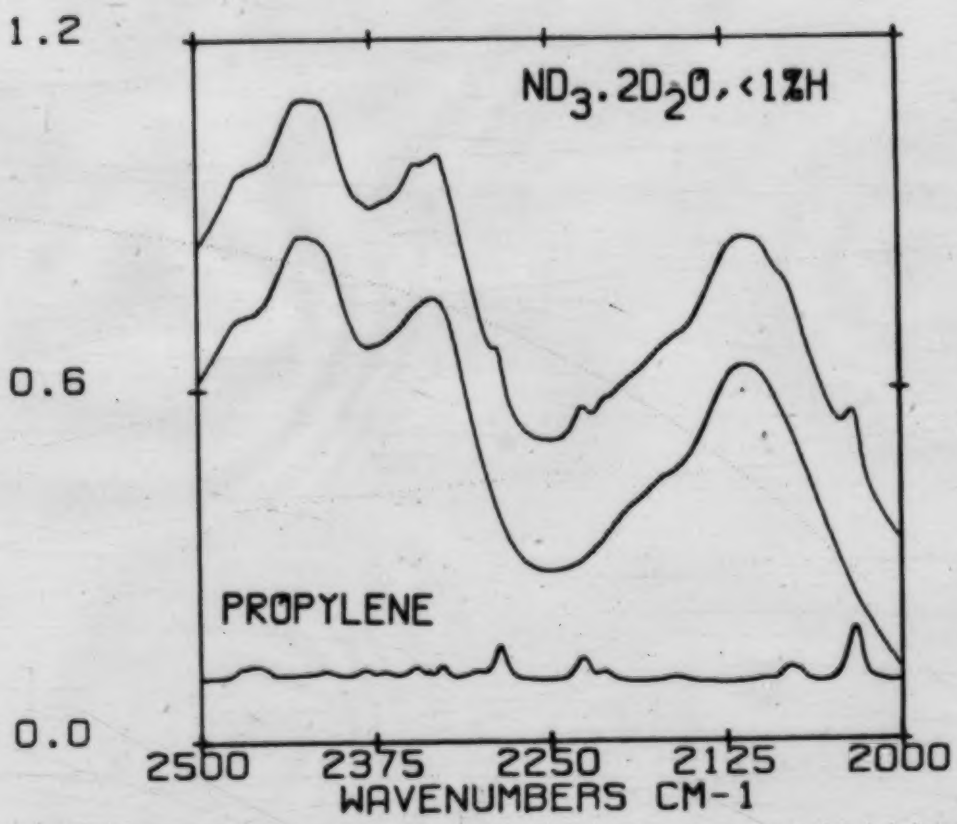

Figure 3.37 O-D stretching absorbance bands of $ND_3 \cdot 2D_2O$ mulled in propylene at 100K. The absorption by propylene (bottom) has been subtracted from the middle spectrum.

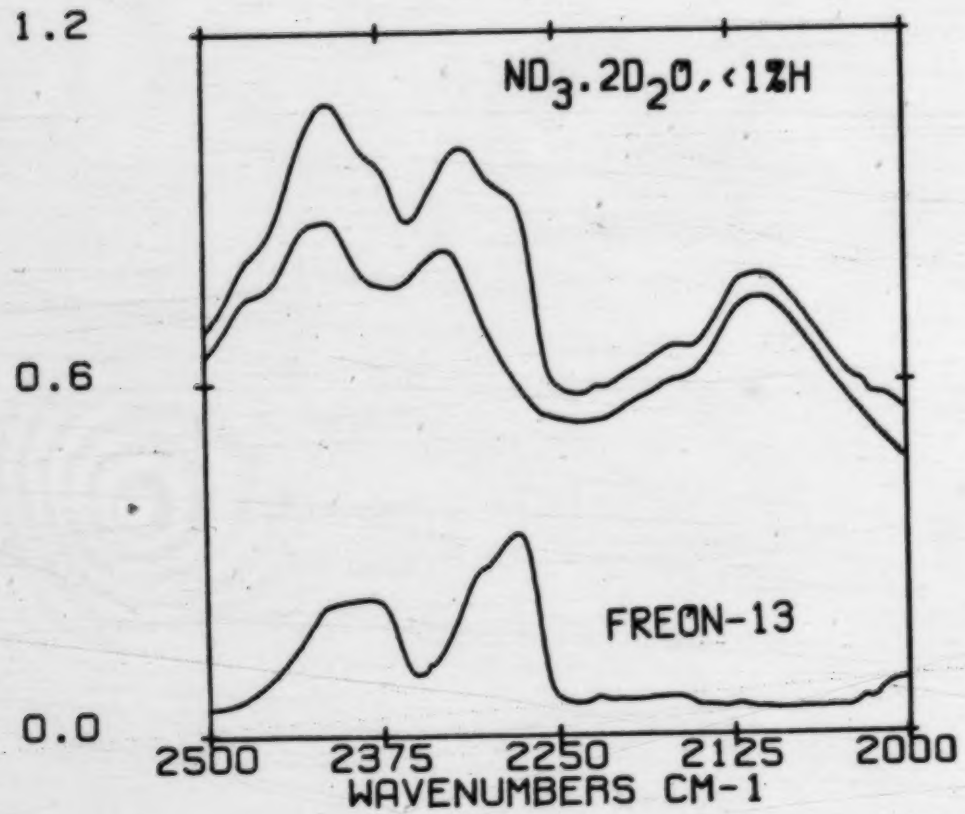

Figure 3.38 O-D stretching absorbance bands of $ND_3 \cdot 2D_2O$ mulled in Freon-13 at 100K. The absorption by Freon-13 (bottom) has been subtracted from the middle spectrum.

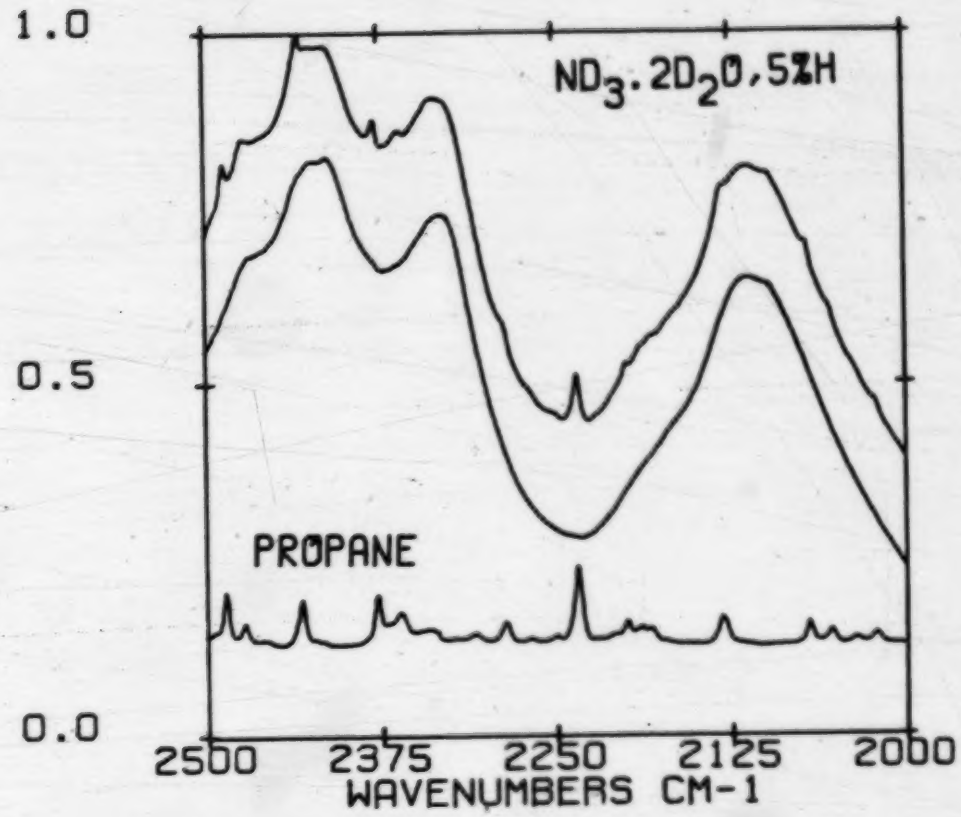

Figure 3.39 O-D stretching absorbance bands of $ND_3 \cdot 2D_2O$, 5% H mulled in propane at 100K. The absorption by propane (bottom) has been subtracted from the middle spectrum.

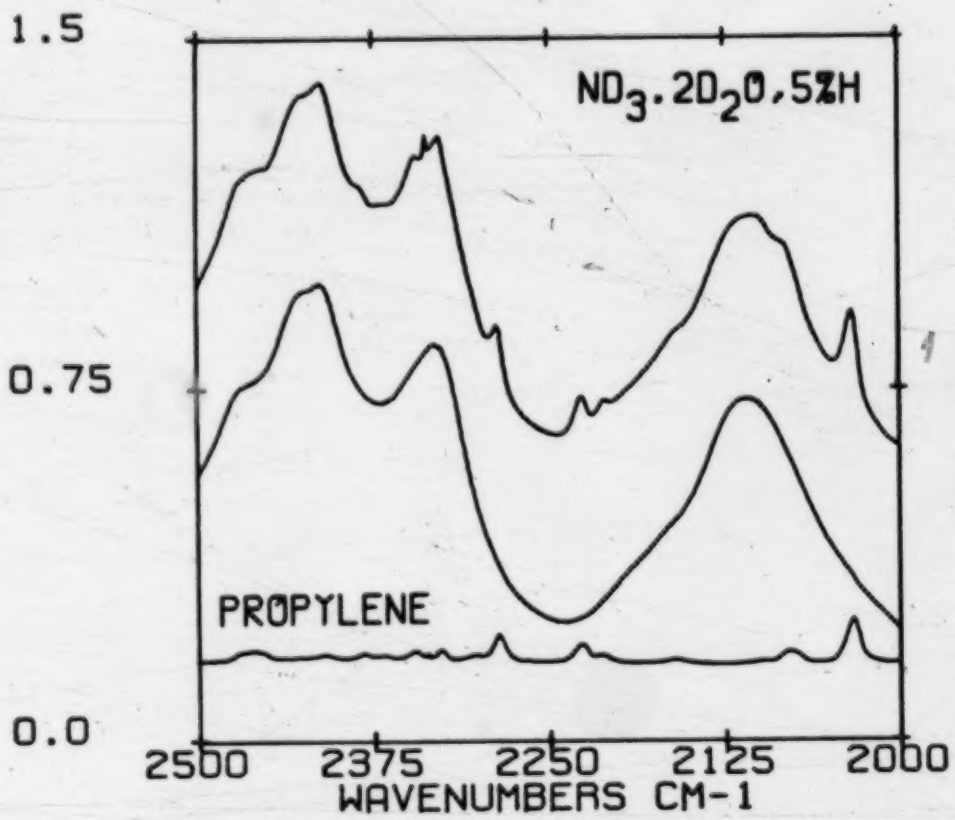

Figure 3.40 O-D stretching absorbance bands of $ND_3 \cdot 2D_2O$, 5% H mulled in propylene at 100K. The absorption by propylene (bottom) has been subtracted from the middle spectrum.

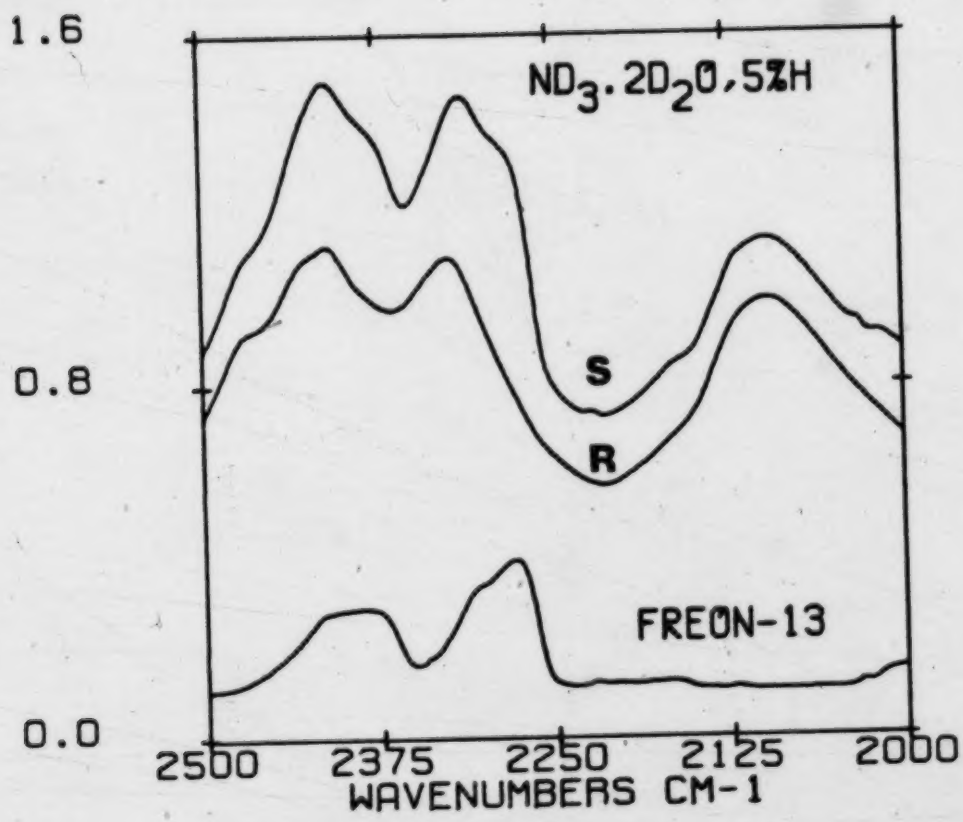

Figure 3.41 O-D stretching absorbance bands of $ND_3 \cdot 2D_2O$, 5% H mulled in Freon-13 at 100K and 1 cm^{-1} resolution. The absorption by Freon-13 (bottom) has been subtracted from the middle spectrum.

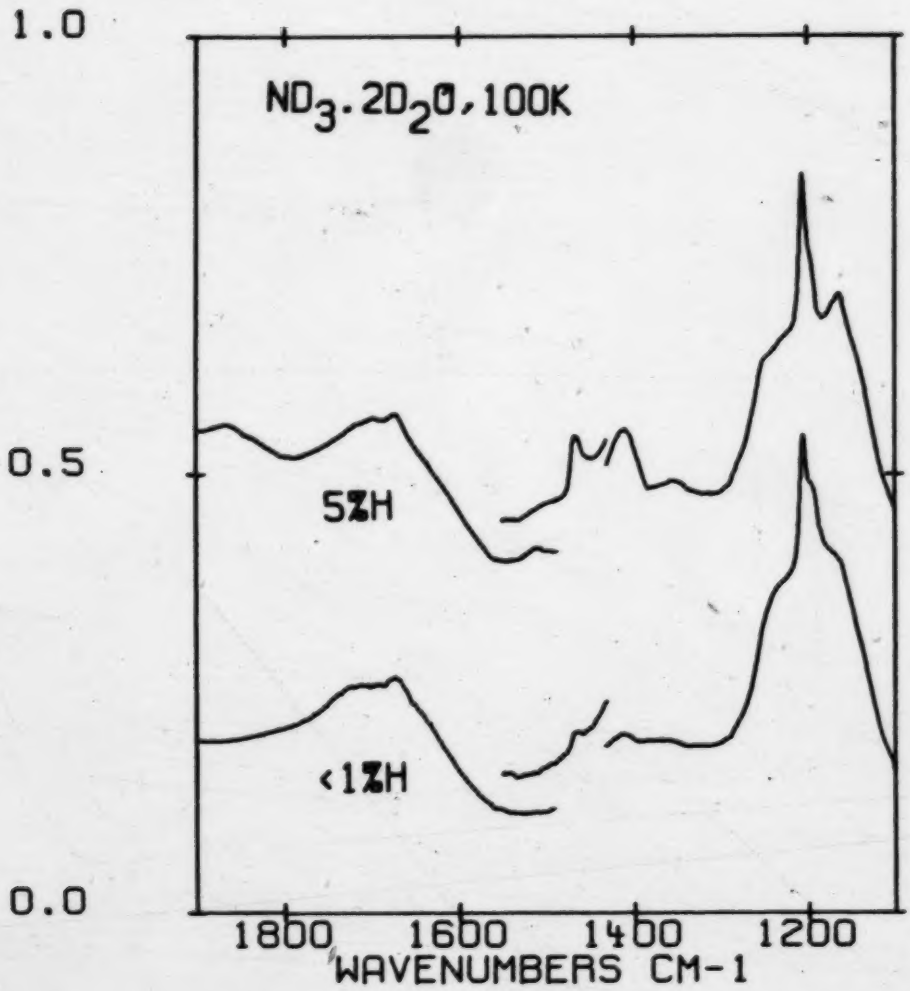

Figure 3.42 Infrared absorbance spectra of $ND_3 \cdot 2D_2O$, containing <1 and 5% H. From mulls in propane. The region of strong propane absorption (1490-1430 cm^{-1}) was replotted in each case from mulls in Freon-13 (1550-1430 cm^{-1}).

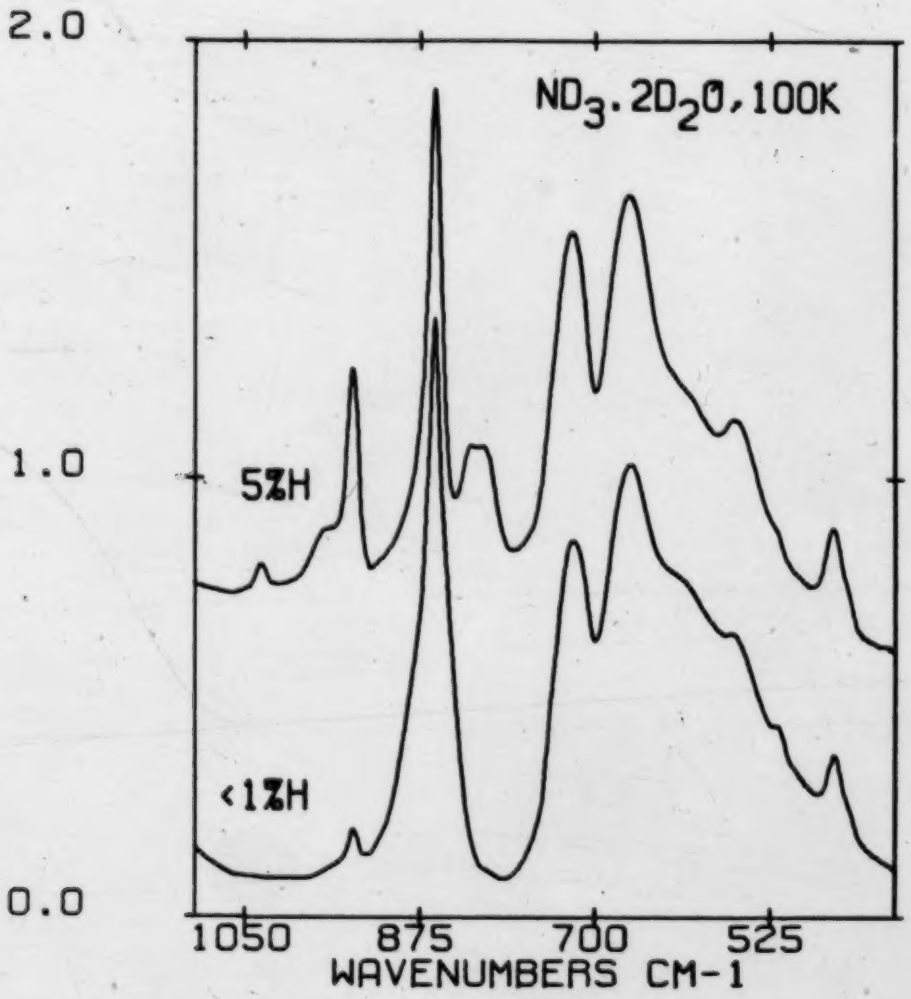

Figure 3.43 Infrared absorbance spectra of $ND_3 \cdot 2D_2O$ containing <1 and 5% H. From mulls in propane.

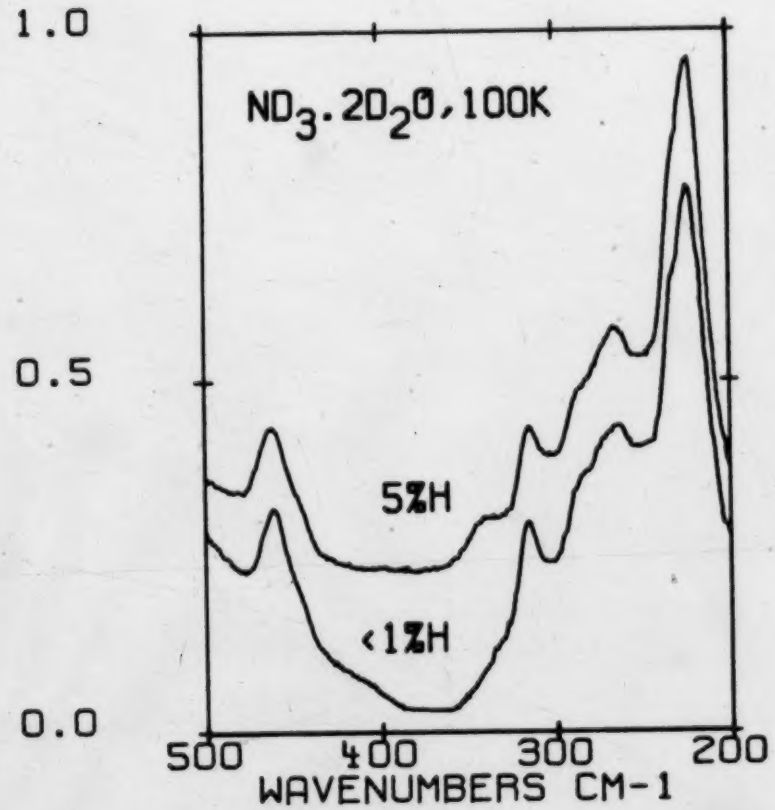

Figure 3.44 Infrared absorbance spectra of $ND_3 \cdot 2D_2O$ containing <1% H (from a mull in propane) and 5% H (from a mull in Freon-13).

Table 3.10 Infrared spectral features of deuterated ammonia dideuterate containing <1 and 5 mole% H at 100K.

$ND_3 \cdot 2D_2O$, <1% H		$ND_3 \cdot 2D_2O$, 5% H		
ν/cm^{-1}[a]	Intensity[b]	ν/cm^{-1}[a]	Intensity[b]	Assignment[c]
~5032	vw	~5040	vw	
~4833	vw	~4838	vw	
~4599	vw	~4601	vw	
3721(1)	w	3721(1)	w	$(\nu_3+\nu_4)ND_3$
~3678	sh	3680	sh	
~3610	vw,br	~3611	vw,br	
~3467	vw	~3466	vw	
3395(2)	w	3394(2)	w	$(\nu_3+\nu_2)ND_3$
~3393[d]	vw	3393[d]	vw	$\nu_{NH}(NH_2D)$
3364(2)	w	3363(2)	w	
3351(2)	w	3352(2)	w	$\nu_{NH}(ND_2H)$
3345(2)	w	3346(2)	w	
3273(2)	m	3275(2.5)	m	$\nu_{(O_{II}-D...O_I(HOD))}$
3242(3)	m	3240(3)	m	$\nu_{(O_I-D...O_{II}(HOD))}$
~3120	w,br	~3110	w,br	
		~3073[d]		
		~3010	vw,br	
~2830	vw,br	~2830	sh	
~2760	w,br	2763	m	$\nu_{(O_{II}-D...N(HOD))}$
2535.5(5)	vs	2535.4(5)	vs	
2529.8(5)	vs	2529.9(5)	vs	$\nu_3(ND_3)$
2525.1(7)	vs	2525.2(5)	vs	
~2466	sh	~2467	sh	
2424(3)	vs	2425(3)	vs	$\nu_{O-D...O(D_2O)}$
2411(2)	vs	2411(2)	vs	
~2350	sh,br			
2330(3)	vs	2329(4)	vs	$\nu_{O-D...O(D_2O)}$
~2182	sh,br	~2178	sh,br	
2113(5)	s	2110(7)	s	$\nu_{(O_{II}-D...N(D_2O))}$
~1867	vw	1864(5)	w,br	
~1700	w,br	1696(8)	w,br	

(Continued)

Table 3.10 (Continued)

$ND_3 \cdot 2D_2O$, <1% H		$ND_3 \cdot 2D_2O$, 5% H		
ν/cm^{-1}[a]	Intensity[b]	ν/cm^{-1}[a]	Intensity[b]	Assignment[c]
1670(3)	w	1669(3)	w	
~1625	sh	~1620	sh	
		~1505	vw	
1468(4)	w	1466(2)	w	
1412(4)	w	1413(3)	w	
~1360	w,br	~1350	w,br	
		~1250	sh	
~1233	sh	~1230	sh	$\nu_2(D_2O)$
1205.3(5)	ms	1205.4(5)	ms	$\nu_4(ND_3)$
~1195	sh	~1196	sh	
~1166	sh	1164	m	
~1136	sh	~1140	sh	
		1035(2)	vw	$\nu_2(NH_2D)$
~ 966	vw,sh	~ 968[d]	w,sh	$\nu_2(ND_2H)$
942(1)	w	942(1)[d]	ms	
~ 890	sh			
859.1(5)	s	859.6	s	$\nu_2(ND_3)$
		824(2)	m	$\nu_R(HOD)$
~ 808	sh	812(3)	m	
722(2)	s	722(2)	s	$\nu_R(D_2O)$
644(2)	s	665(2)	s	
~ 614	sh	~ 607	sh	
562(3)	m	560(3)	m	
~ 518	sh	~ 519	sh	
461(1)	m	462(1)	m	
~ 446	sh	~ 446	sh	
~ 410	sh,br			
~ 343	sh	342(3)	w	
316(1)	m	316(1)	m	
~ 285	sh	~ 286	sh	

(Continued)

Table 3.10 (Continued)

$ND_3 \cdot 2D_2O$, <1% H		$ND_3 \cdot 2D_2O$, 5% H		
ν/cm^{-1}[a]	Intensity[b]	ν/cm^{-1}[a]	Intensity[b]	Assignment[c]
~ 275	sh,br	~ 275	sh,br	
264(2)	m	266(2)	m	
~ 231	sh	~ 232	sh	
223(1)	s	223(1)	s	

[a]The numbers in parentheses are the 95% confidence limits in the last digit.

[b]vs, ms, s, m, w, vw, sh and br mean: very strong, medium strong, strong, medium, weak, very weak, shoulder and broad, respectively.

[c]The complete assignments are listed in Table 5.8.

[d]After the subtraction of the spectrum of $ND_3 \cdot 2D_2O$ containing less hydrogen.

subtractions of the mulling agents in the region 2500 to 2000 cm^{-1}. The mulling agent's spectra are shown for comparison at the bottom of these figures.

The shoulder at ~2100 cm^{-1} was observed in some spectra of mulls in propane and was not observed when other mulling agents were used. It is probably not due to deuterated ammonia dideuterate.

CHAPTER 4

DISCUSSION OF INFRARED SPECTRUM OF AMMONIA MONOHYDRATE

4.1 General

Ammonia monohydrate crystallizes in the orthorhombic space group $P2_12_12_1(D_2^4)$ with four formula units in the unit cell.[5] The equivalent set of four ammonia molecules and the equivalent set of four water molecules each lies on a general position of site symmetry C_1. Thus, the C_{3v} symmetry of the free ammonia and the C_{2v} symmetry of the free water molecules are reduced to C_1. Each nondegenerate internal vibration or intermolecular degree of freedom of either ammonia or water yields one nondegenerate vibration of A symmetry under the site group. The degenerate internal vibrations of free ammonia, ν_3 and ν_4, and the intermolecular displacements of ammonia that are equivalent in the free molecule (R_x, R_y) and (T_x, T_y), each yields two nondegenerate vibrations of A symmetry under the site group. Each nondegenerate site group vibration (all of A symmetry) is further split by dynamic intermolecular coupling under the unit cell group D_2, to give rise to four vibrations of the unit cell of symmetries A, B_1, B_2 and B_3. The activity of these

modes can be determined by selection rules.[62-66] All modes are Raman active but only B_1, B_2 and B_3 modes are infrared active. These relations between the symmetry species of the free molecules, the symmetry about the center of gravity of each molecule in the crystal, i.e. the site symmetry C_1, and the symmetry of the unit cell D_2, have been established by the correlation method[66] and are summarized in Table 4.1.

A consequence of the symmetry analysis is that there is nothing to stop coupling between water and ammonia vibrations since unit cell group vibrations of the same symmetry can couple. If the vibrations are close enough in frequency for the coupling to be large enough to shift the frequencies detectably, the coupling will be seen.

The vibrational frequencies of a crystal, $\nu(\underline{k})$, are related to the wave vector[67] $\underline{k}$, which has the magnitude of the reciprocal wavelength, λ, of the spatial periodicity of the vibrational frequencies. The direction of $\underline{k}$ is the direction of propagation of the vibration-wave. The plots of $\nu(\underline{k})$ versus $\underline{k}$ are called the dispersion curves. At zero wave vector, $\underline{k} = 0$, the molecular displacements during a crystal vibration have the same magnitude and phase in all unit cells in the crystal and so can be visualized by considering the vibrations of one unit cell. In this thesis, the zero-wave-vector approximation

Table 4.1 Correlation table for ammonia monohydrate.

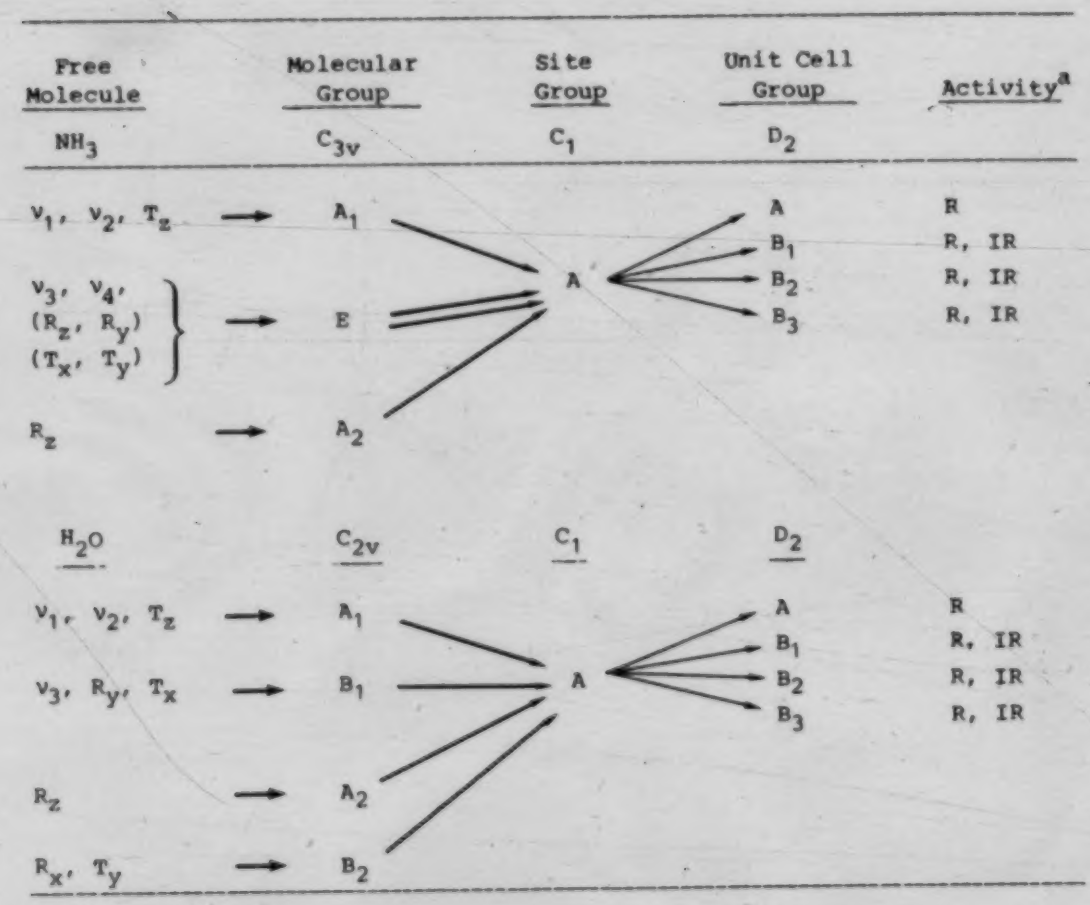

[a]R, Raman active mode; IR, Infrared active mode.

is assumed and so the forms of vibrations are influenced by the symmetry of the unit cell group. Thus, for the vibrations to be active in the infrared they must have a non-zero dipole moment change ($\partial\underline{\mu}/\partial Q$). So they must have the same symmetry under the unit cell group as a component of the dipole moment $\underline{\mu}$.

The assignments of ammonia and water vibrations of ammonia monohydrate, Table 3.6, are made by analogy with spectral assignments for solid ammonia[42,43,46,68-71], ice[72,73] and ammonia hemihydrate[6,7,13]. They are basically those of Bertie and Morrison[6,7] except for those discussed in Section 3.5 and Table 3.6.

4.2 Calculations of the Relative Infrared Intensities of N-H Stretching Modes

The relative infrared intensities can be estimated in the bond moment approximation[74,75] and the assumption that the dipole moment derivative $\partial\underline{\mu}/\partial R$ is the same for all N-H bonds.

In the crystal structure of ammonia monohydrate reported by I. Olovson and D.H. Templeton[5] the nitrogen atoms are above the 100 base of the unit cell by 0.264, 0.236, 0.764 and 0.736 of the a-axis length and the oxygen atoms are at 0.259, 0.241, 0.759 and 0.741 of the a-axis length. This indicates the presence of a pseudo-plane of

symmetry that passes through the heavy atoms in the bc plane and cuts the a-axis at about 0.25 and 0.75 of the unit cell height. For each ammonia molecule in ammonia monohydrate one N-H...O bond lies approximately on the pseudo-plane of symmetry and the other two N-H...O bonds are approximately related to each other by the pseudo-plane of symmetry.

The dipole moment derivative of ν_{3a} of ammonia, $(\partial\underline{\mu}/\partial Q)_{mol}$, which is the sum of the dipole moment changes in the three NH bonds $\sum_{i=1}^{3} (\partial\underline{\mu}/\partial R_i) \cdot (\partial R_i/\partial Q_k)$, lies in a plane perpendicular to the molecular axis (Figures 4.1 and 4.2). The molecular axis approximately bisects the angles between the three O...N distances, so it lies in the bc plane and approximately along the O-H...N bond. The angle between the molecular axis and the c-axis is ~50.4°. If the ammonia molecule had C_3 symmetry one could choose any direction in the plane perpendicular to the molecular axis, and an orthogonal direction in the plane, as the directions of $\partial\underline{\mu}/\partial Q_{3a}$ and of $\partial\underline{\mu}/\partial Q_{3b}$. Thus one could precisely choose the direction in the bc plane orthogonal to the molecular axis for $\partial\underline{\mu}/\partial Q_{3a}$ and the direction parallel to the a-axis for $\partial\underline{\mu}/\partial Q_{3b}$. These choices are made here but, because the molecule does not have exactly C_3 symmetry, they are expected to be only approximately correct.

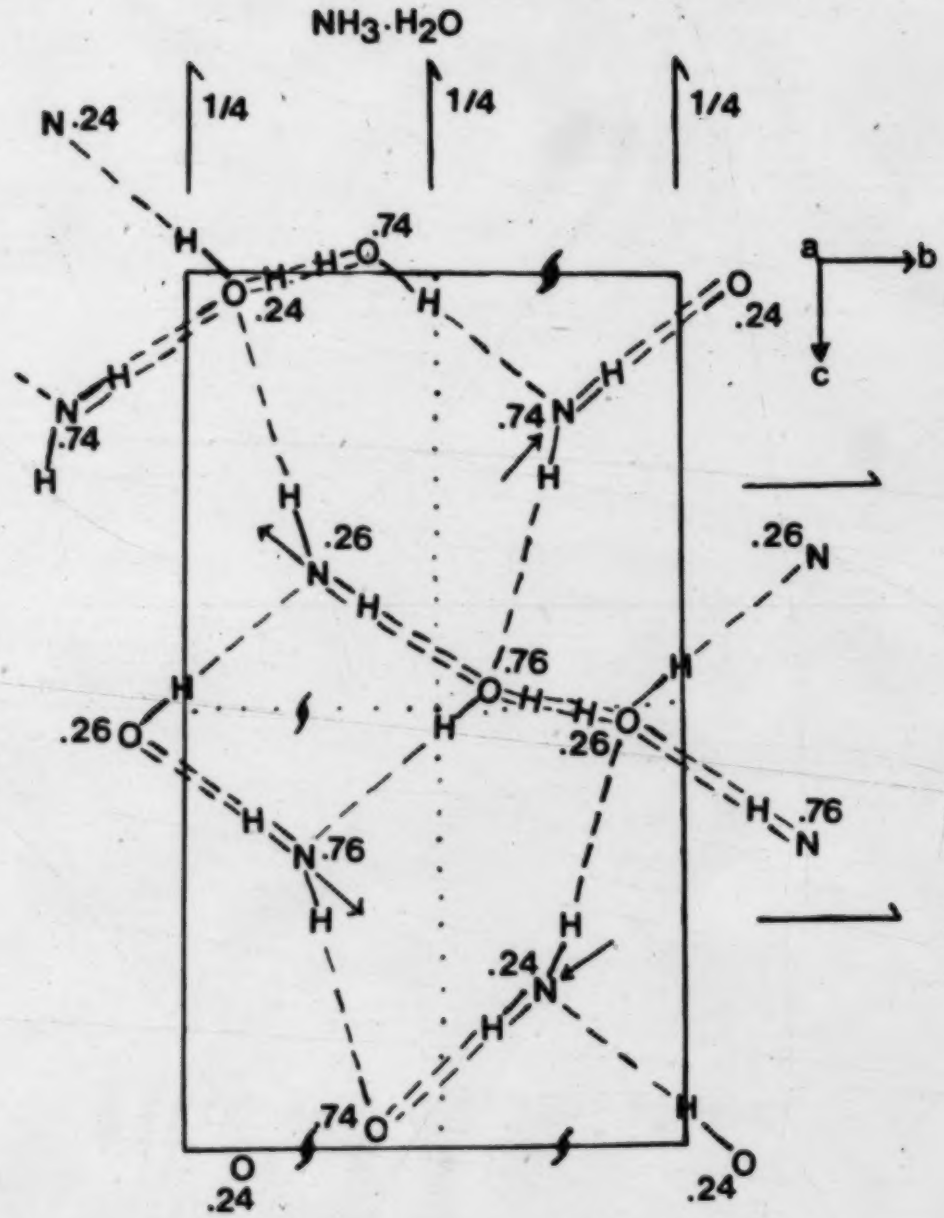

Figure 4.1 The structure of $NH_3 \cdot H_2O$ projected on the 100 plane. The double full or dashed lines in the bc projection represent bonds of two atoms separated by one unit cell along a. The arrows from or to the nitrogen atoms in the unit cell represent the vectorial changes in the molecular dipole moments during the B_3 unit cell group vibration based on ν_{3a}.

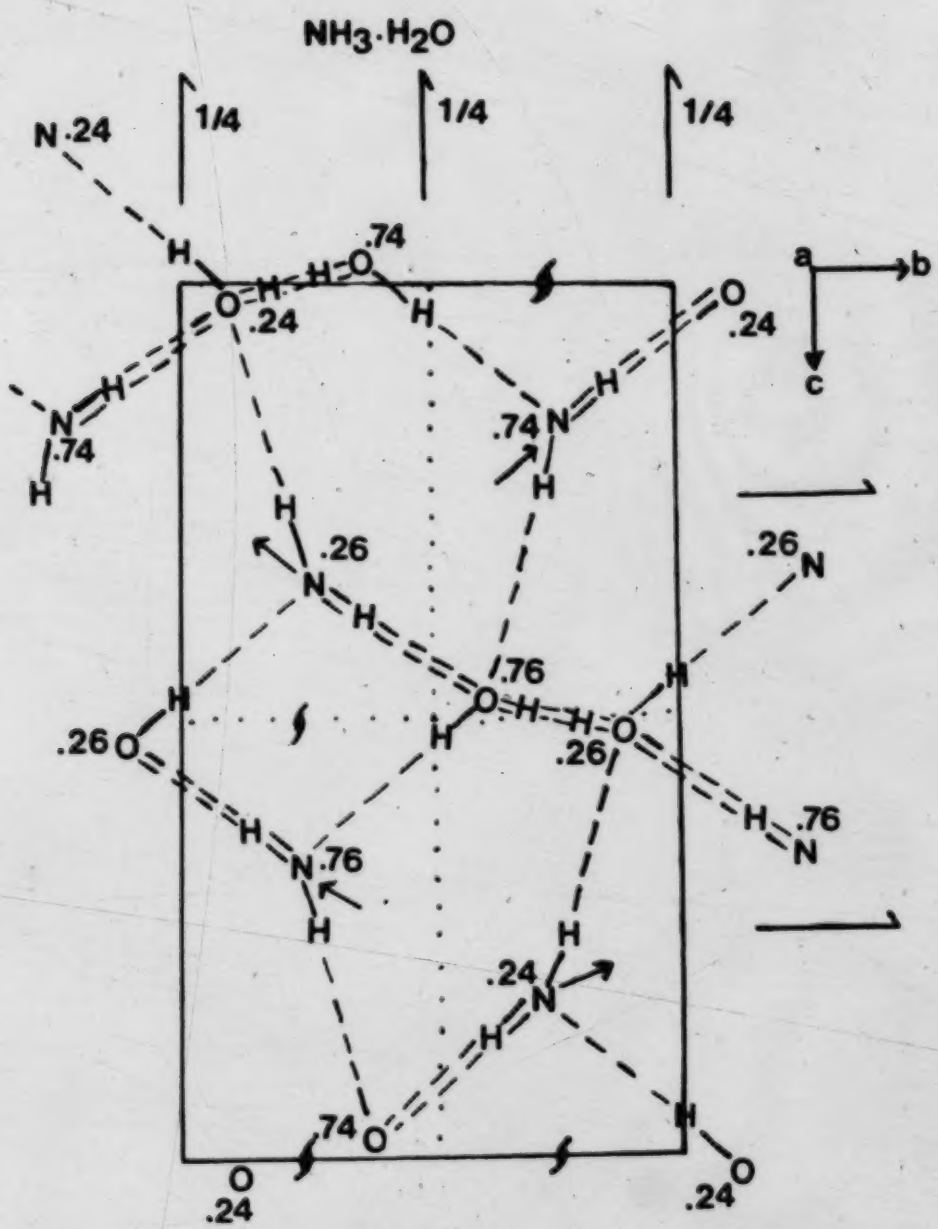

Figure 4.2 The structure of $NH_3 \cdot H_2O$ projected on the 100 plane. The arrows to or from the nitrogen atoms in the unit cell represent the vectorial changes in the dipole moments during the B_1 unit cell group vibration based on ν_{3a}.

Table 4.2 and Figures 4.1 to 4.4 indicate that only two components of $\nu_{3a}(NH_3)$, of symmetry B_1 and B_2, and one component of $\nu_{3b}(NH_3)$, of symmetry B_3, cause a dipole moment change in the unit cell. The relative intensities of $B_1:B_2:B_3$ are approximately 1.5:1:2.5. These relative intensities were calculated by assuming that no mixing occurs between ν_{3a}, ν_{3b} and ν_1 of ammonia.

For $\nu_1(NH_3)$, the dipole moment derivative of each ammonia molecule lies on the molecular axis, which is approximately along the extension of the O-H...N bond at 50.4° to the c-axis. Only two components of $\nu_1(NH_3)$, of symmetry B_1 and B_2, have non-zero intensities (Table 4.2 and Figures 4.5 and 4.6), which are in the ratio 1:1.5.

4.3 The N-H and N-D Stretching Vibrations

The antisymmetric stretching vibration of ammonia, ν_3, is seen as a sharp triplet at 3403.2, 3392.1 and 3387.3 cm^{-1} (Figure 3.10), compared to the doublet observed by Morrison[6] at 3402 and 3387 cm^{-1}. Morrison[7] though, observed a triplet for this vibration of ammonia ^{15}N in $^{15}NH_3 \cdot H_2O$, at 3396, 3384 and 3380 cm^{-1}, where the feature at 3384 cm^{-1} corresponds to that at 3392.1 cm^{-1} in the spectrum of $^{14}NH_3 \cdot H_2O$ (Figure 3.10). The corresponding antisymmetric stretching vibration, ν_3, of deuterated ammonia in $ND_3 \cdot D_2O$ is also a triplet at 2534.3,

Table 4.2 Calculation of the dipole moment derivatives for the stretching vibrations of ammonia in ammonia monohydrate.

O-H...N

	fractional coordinates	actual coordinate
N at	0.264, 0.272, 0.334	1.191, 1.520, 3.245 Å
O at	0.259, -0.111, 0.517	1.168, -0.618, 5.013 Å

The unit vector in the N...H-O direction is:

$$\hat{U}_{N\to O} = -0.008\ \underline{i} - 0.770\ \underline{j} + 0.637\ \underline{k}$$

Therefore, the angle between the molecular axis along O-H...N bond and the c-axis is $\cos^{-1} 0.637 = 50.4°$.

Mode	$(\partial\underline{\mu}/\partial Q)_{u.c.}$	direction of $\underline{\mu}$
ν_{3a}		
A	0	
B_1	$4(\partial\underline{\mu}/\partial Q)_{mol}$ cos 39.6	parallel to 'c'
B_2	$4(\partial\underline{\mu}/\partial Q)_{mol}$ sin 39.6	parallel to 'b'
B_3	0	
ν_{3b}		
A	0	
B_1	0	
B_2	0	
B_3	$4(\partial\underline{\mu}/\partial Q)_{mol}$	parallel to 'a'
Intensities $B_1:B_2:B_3$	1.5:1:2.5	

Mode	$(\partial\underline{\mu}/\partial Q)_{u.c.}$	direction of $\underline{\mu}$
ν_1		
A	0	
B_1	$4(\partial\underline{\mu}/\partial Q)_{mol}$ cos 50.4	parallel to 'c'
B_2	$4(\partial\underline{\mu}/\partial Q)_{mol}$ sin 50.4	parallel to 'b'
B_3	0	
Intensities $B_1:B_2$	1:1.5	

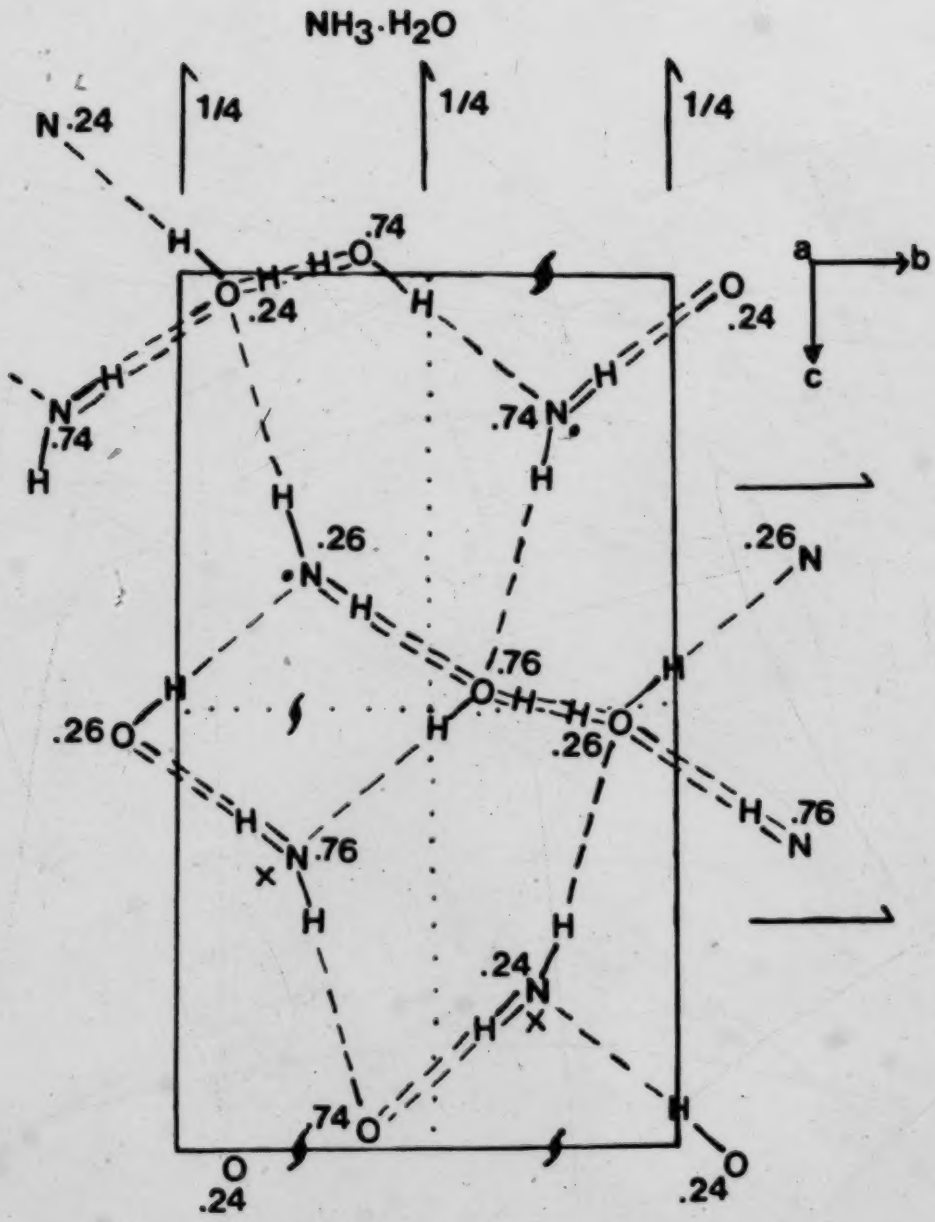

Figure 4.3 The structure of $NH_3 \cdot H_2O$ projected on the 100 plane. The arrows to (X) or from (•) the nitrogen atoms in the unit cell represent the vectorial changes in the molecular dipole moments during the B_1 unit cell group vibration based on ν_{3b}.

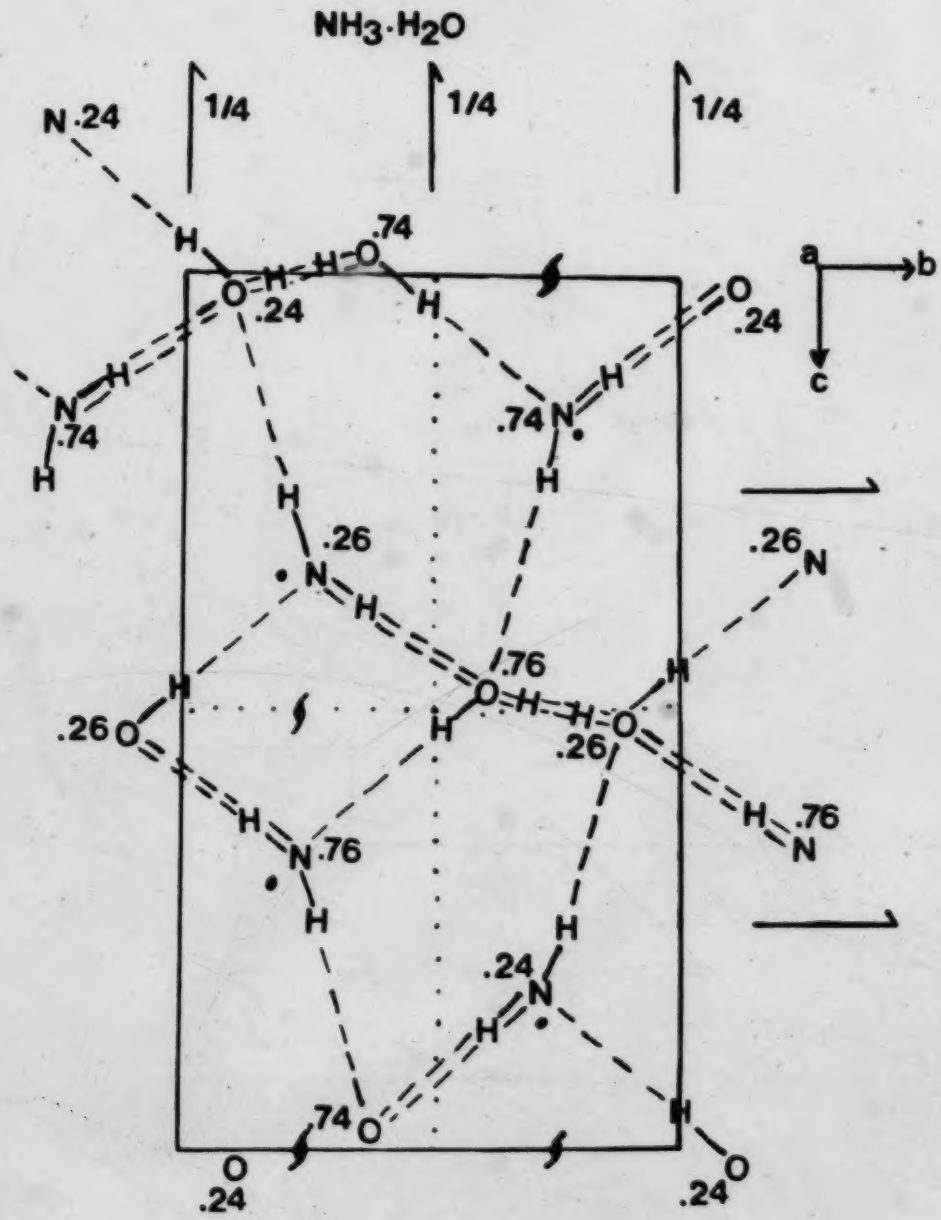

Figure 4.4 The structure of $NH_3 \cdot H_2O$ projected on the 100 plane. The arrows to (X) or from (•) the nitrogen atoms in the unit cell represent the vectorial changes in the molecular dipole moments during the B_3 unit cell group vibration based on ν_{3b}.

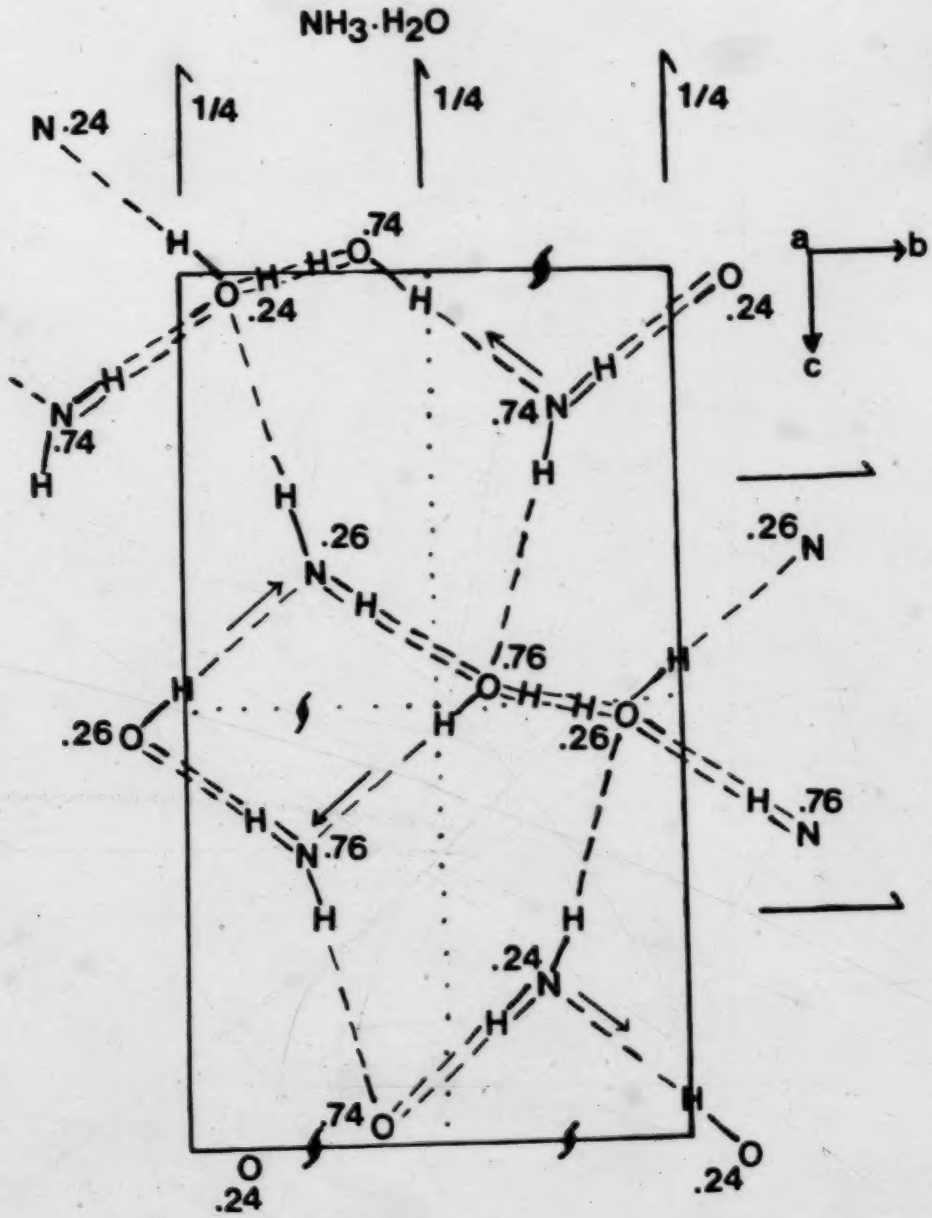

Figure 4.5 The structure of $NH_3 \cdot H_2O$ projected on the 100 plane. The arrows to or from the nitrogen atoms in the unit cell represent the vectorial changes in the molecular dipole moments during the B_3 unit cell group vibration based on ν_1.

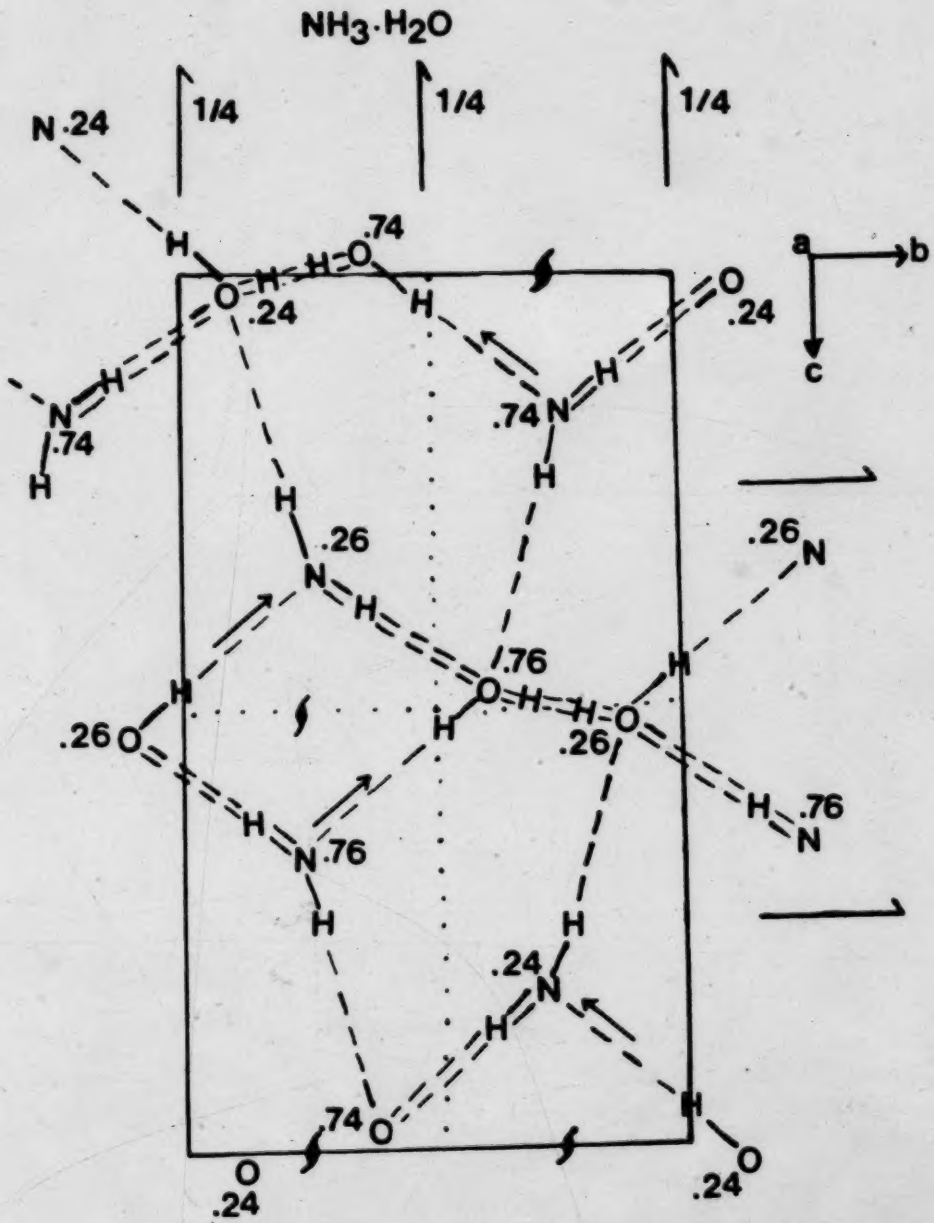

Figure 4.6 The structure of $NH_3 \cdot H_2O$ projected on the 100 plane. The arrows to or from the nitrogen atoms in the unit cell represent the vectorial changes in the molecular dipole moments during the B_1 unit cell group vibration based on ν_1.

2526.1 and 2522.2 cm^{-1} (Figure 3.18). The relative intensities in the ν_3 triplet are slightly different from one mull to the other (Figure 3.18 for $ND_3 \cdot D_2O$, and similar results were observed in spectra of $NH_3 \cdot H_2O$).

The static field which causes site splitting can be investigated in a sample containing isolated ND_2H, i.e. some hydrogen impurities in a deuterated sample. The mass ratio of H to D is enough to ensure that inter- and intramolecuar coupling can be neglected in first approximation. The stretching frequencies of $\nu_{NH}(ND_2H)$ are found at 3362, 3349.2 and 3345 cm^{-1}. The observation of three distinct bands of $\nu_{NH}(ND_2H)$ indicates that the three NH bonds have slightly different force constants and confirms the site symmetry C_1. By neglecting intramolecular coupling in ND_2H, these force constants are calculated to be 6.2606, 6.2130 and 6.1974 mdyne $Å^{-1}$ for the N-H bonds in the N...O distances 3.29, 3.26 and 3.21 Å. These force constants can be used to calculate the N-H stretching frequencies of NH_3. If only intramolecular interactions are considered, normal coordinate calculations of the antisymmetric ν_3, and the symmetric ν_1, stretching vibrations yield two components of ν_3 under the site group at 3391.9 and 3381.2 cm^{-1}, and one for ν_1 at 3282.1 cm^{-1}, if the three inequivalent off diagonal force constants are taken to be zero.

The diagonal force constants were calculated by the diatomic approximation using the stretching frequencies of the isolated NH and ND. The molecular constants used in the calculations are listed in Table 4.3.

The off diagonal force constants were chosen so that the calculated values of $\nu_3(NH_3)$ were near the observed frequencies. This is correct if it is assumed that the effect of intermolecular coupling is small compared to that of intramolecular coupling. For an off diagonal force constant of ~-0.04 mdyne A^{-1} in $NH_3 \cdot H_2O$ the calculated antisymmetric stretching frequencies $\nu_3(NH_3)$ and $\nu_3'(NH_3)$ are at 3402.6 and 3392.1 cm^{-1} (Table 4.4). The observed $\nu_3(NH_3)$ frequencies are at 3403.2, 3392.1 and 3387.3 cm^{-1}. In the case of $\nu_3(ND_3)$ in $ND_3 \cdot D_2O$, the off diagonal force constant is taken to be ~-0.07 mdyne A^{-1}. The diagonal force constants corresponding to $\nu_{ND}(NH_2D)$ frequencies at 2471.3, 2467.0 and 2464.1 cm^{-1} are 6.3353, 6.3133 and 6.2985 mdyne A^{-1}. The calculated antisymmetric stretching frequencies of $\nu_3(ND_3)$ and $\nu_3'(ND_3)$ are at 2530.0 and 2525.7 cm^{-1} (Table 4.4). The observed frequencies for $\nu_3(ND_3)$ are at 2534.3, 2526.1 and 2522.2 cm^{-1}. The off diagonal force constants of ~-0.04 and ~-0.07 mdyne A^{-1} for ammonia molecules in $NH_3 \cdot H_2O$ and deuterated ammonia in $ND_3 \cdot D_2O$, respectively, are comparable to the value -0.0712 mdyne A^{-1} obtained by F.P.

Table 4.3 Molecular constants used in normal coordinate calculations.

m_H = 1.007825[a]

m_D = 2.0140[a]

m_O = 15.99491[a]

m_N = 14.00307[a]

$\hat{HNH}$ = 107.8°[b]

$\hat{DND}$ = 107.6°[b]

[a]Ref. 76, pp. B-256-257.

[b]These are the values for gaseous ammonia from Ref. 77. Neutron diffraction studies showed that about the same value is obtained for $\hat{DND}$ in solid ND_3. At 77K a value of 108.0 ± 0.7° (Ref. 78) and a value of 110.4 ± 2.0° (Ref. 79) were obtained for $\hat{DND}$. Also, at 2K a value of 107.5 ± 0.2° and at 180K a value of 107.8 ± 0.4° were obtained for $\hat{DND}$ (Ref. 78).

Table 4.4 Normal coordinate calculations of ammonia monohydrate stretching frequencies.

a) of NH_3

$\nu_{NH}(ND_2H)$ at 3362, 3349.2, and 3345 cm^{-1}

$f_{11} = 6.2606$, $f_{22} = 6.2130$, $f_{33} = 6.1974$ mdyne $Å^{-1}$
$G_{11} = G_{22} = G_{33} = \mu_N + \mu_H = 1.06365$ amu^{-1}
$G_{12} = G_{13} = G_{23} = \mu_N \cos\phi = -0.02183$ amu^{-1}
$\phi = 107.8°$

$f_{12} = f_{23} = f_{13} =$	0	-0.04	-0.07
ν_{3a}	3391.9	3402.6	3410.7
ν_{3b}	3381.2	3392.1	3400.2
ν_1	3282.1	3261.0	3245.1

The eigenvectors for $f_{12} = -0.04$ mdyne $Å^{-1}$ are:

$$L = \begin{array}{c} \begin{matrix} \nu_{3a} & \nu_{3b} & \nu_1 \end{matrix} \\ \begin{bmatrix} 0.8665 & 0.1021 & -0.5385 \\ -0.4706 & 0.6977 & -0.5917 \\ -0.3127 & -0.7671 & -0.6115 \end{bmatrix} \end{array}$$

One column of L is $(\partial R_i/\partial Q_k)_{\substack{i=1\to3 \\ k=\text{constant}}} = L_{ik}$, $i = 1\to3$

b) of ND_3

$\nu_{ND}(NH_2D)$ at 2471.3, 2467.0, and 2464.1 cm^{-1}

$f_{11} = 6.3353$, $f_{22} = 6.3133$, $f_{33} = 6.2985$ mdyne $Å^{-1}$
$G_{11} = G_{22} = G_{33} = \mu_N + \mu_D = 0.56794$ amu^{-1}
$G_{12} = G_{13} = G_{23} = \mu_N \cos\phi = -0.021593$ amu^{-1}
$\phi = 107.6°$

$f_{12} = f_{23} = f_{13} =$	0	-0.04	-0.07
ν_{3a}	2516.1	2524.0	2530.0
ν_{3b}	2511.8	2519.8	2525.7
ν_1	2371.7	2356.7	2345.3

Reding and D.F. Hornig[42,68] for deuterated solid ammonia at liquid nitrogen temperature. The results of normal coordinate calculations of the stretching frequencies of ammonia in $NH_3 \cdot H_2O$ and of deuterated ammonia in $ND_3 \cdot D_2O$ are listed in Table 4.4.

The appearance of a triplet in the observed spectrum rather than the doublet predicted under the site group for $\nu_3(NH_3)$ indicates that not only intramolecular but also intermolecular coupling has to be considered. The eigen vectors, listed in Table 4.4, indicate that the calculated frequency at 3402.6 cm^{-1} corresponds mainly to $\nu_{3a}(NH_3)$ and that at 3392.1 cm^{-1} mainly to $\nu_{3b}(NH_3)$. This is because the in-plane N...O distance is the longest so that the in-plane $\nu_{NH}(ND_2D)$ is the highest. If the effect of intermolecular coupling is assumed to be small, so that the ~10 cm^{-1} separation between the calculated ν_{3a} and ν_{3b} remained virtually unchanged, one might expect that $\nu_{3a}(NH_3)$ calculated at 3402.6 cm^{-1} yields the one component observed at 3403.2 cm^{-1} and $\nu_{3b}(NH_3)$ calculated at 3392.1 cm^{-1} yields the two components at 3392.1 and 3387.3 cm^{-1}, each mode yielding 3 unit cell group infrared active modes according to the D_2 unit cell group symmetry. But according to the relative intensities calculations, Section 4.2, only one component of ν_{3b} of symmetry B_3 and two components of ν_{3a} of symmetry B_1 and

B_2 have non-zero infrared absorption intensities. This disagreement indicates that the effect of the intermolecular coupling on the antisymmetric stretching frequencies of ammonia molecules in ammonia monohydrate can not be neglected and oauses splitting of more than or equal to ~10 cm^{-1}. Similar considerations and conclusions hold for $\nu_3(ND_3)$ in $ND_3 \cdot D_2O$.

According to the normal coordinate calculations, Table 4.3, the symmetrical N-H stretching vibration, ν_1 is expected around 3261 cm^{-1} in $NH_3 \cdot H_2O$ and around 2345 cm^{-1} in $ND_3 \cdot D_2O$. However, under unit cell group D_2, $\nu_1(NH_3)$ is expected to be a triplet in the infrared, Table 4.1, of symmetries $B_1 + B_2 + B_3$. Only the modes B_1 and B_2 have significant intensities, Table 4.2. Further, $\nu_1(NH_3)$ is expected to be in Fermi resonance with $2\nu_4(NH_3)$. Also, the absorption by the B_1 and B_2 $\nu_{O-H...O}(H_2O)$ modes is expected to be in this region. So, all these transitions can contribute to the bands at 3332, 3294, 3275 and 3235 cm^{-1} in $NH_3 \cdot H_2O$ and 2459 and 2414 cm^{-1} in $ND_3 \cdot D_2O$.

The correspondence between this spectral region of $NH_3 \cdot H_2O$ and the corresponding region of $ND_3 \cdot D_2O$ is not clear. The x-ray powder diffraction of $ND_3 \cdot D_2O$ gives the same relative intensities, and unit cell parameters as for $NH_3 \cdot H_2O$ within the experimental errors. So it is unlikely that structure differences exist between $NH_3 \cdot H_2O$ and

$ND_3 \cdot D_2O$.

4.4 A Useful D_{2h} Pseudo-Symmetry

Intermolecular coupling changes the splitting expected under the site group to that expected under the unit cell group, D_2. Thus (Table 4.1) each site-component of ν_3, ν_{3a} and ν_{3b}, of ammonia is further split into four components, i.e. $\nu_3(NH_3)$ yields a total of eight unit cell group components of symmetries $2A + 2B_1 + 2B_2 + 2B_3$. Of those eight components only six are infrared active, $2B_1 + 2B_2 + 2B_3$, under the unit cell group D_2, and it has been shown in Section 4.2, and used just above, that the near coplanarity of the heavy atoms results in only three having significant intensity.

The existence of these near-symmetry planes at a = 1/4 and 3/4 requires the existence of two more pairs of near-symmetry planes and indicates that the unit cell group is pseudo-D_{2h}, at least for the ammonia molecules. These additional pairs of planes can be seen from the structure to be c-glide planes at b = 0 and 1/2 and diagonal (1/2($\underline{a}$ + $\underline{b}$)) glide (n-glide) planes at c = 1/4 and 3/4. This means that the ammonia molecules in ammonia monohydrate have approximately the symmetry of the orthorhombic space group Pmcn, D_{2h}^{16}, with the pseudo-plane of symmetry m

perpendicular to the a-axis. If the a-, b- and c-axes of the space group Pmcn ($P\frac{2_1}{m}\frac{2_1}{c}\frac{2_1}{n}$) are renamed as b, c and a respectively, one will obtain the standard space group Pnma ($P\frac{2_1}{n}\frac{2_1}{m}\frac{2_1}{a}$), number 62 in the International Tables for X-Ray Crystallography, Vol. I, page 151. The N atoms in $NH_3 \cdot 2H_2O$ sit approximately on the sites m of the space group P_{mcn}.

If the hydrogen atoms in the O-H...O bonds are neglected, the water molecules also are described by this pseudo-D_{2h} space group. Because the O-H...O vibrations are near 3280 cm^{-1}, the O-H...N vibrations are near 2890 cm^{-1} and the antisymmetric N-H stretching vibrations are near 3400 cm^{-1}, interaction between these different types of vibrations is expected to be weak. Consequently it is expected to be a useful approximation to analyze the N-H and O-H...N stretching modes under the pseudo-D_{2h} unit cell group and the O-H...O modes under the D_2 unit cell group which is the correct one if the hydrogen atoms in O-H...O bonds in different chains are related by symmetry.

The correlation between the symmetry species of free ammonia molecules, the site symmetry C_s, and the D_{2h} pseudo-symmetry of the unit cell are listed in Table 4.5. Under the site group, C_s, a doublet is expected for the antisymmetric stretching of ammonia; one due to $\nu_{3a}(NH_3)$ of symmetry A' which is symmetric with respect to

Table 4.5 Correlation table for ammonia molecules in ammonia monohydrate[a].

Free Molecule	Molecular Group	Site Group	Unit Cell Group	Activity[b]
NH_3	C_{3v}	$C_s(bc)$	D_{2h}	
ν_1, ν_2, T_z	A_1	A'	A_g	R
			B_{1g}	R
ν_3, ν_4, (R_x, R_y) (T_2, T_y)	E	A"	B_{2g}	R
			B_{3g}	R
			A_u	-
			B_{1u}	R, IR
R_z	A_2		B_{2u}	R, IR
			B_{3u}	R, IR

[a] If the space group of the ammonia molecule is taken to be pseudo D_{2h}^{16}.

[b] R, Raman active mode; IR, Infrared active mode.

the bc plane and the other due to $\nu_{3b}(NH_3)$ of symmetry A" which is antisymmetric with respect to the bc plane. Under the unit cell group, D_{2h}, $\nu_{3a}(NH_3)$ of symmetry A' is further split into two infrared active components of symmetries B_{1u} and B_{2u} and $\nu_{3b}(NH_3)$ of symmetry A" give rise to only one infrared component of symmetry B_{3u} (Table 4.5). This is the same result that was reached by bond moment approximation using $P2_12_12_1$ space group for ammonia molecules and considering a pseudo-plane of symmetry in the bc plane (Section 4.2).

4.5 Water Stretching Vibrations

X-ray diffraction of ammonia monohydrate[1] reveals two kinds of OH bonds; an O-H...O hydrogen bond with an O...O distance of 2.76 Å and a stronger O-H...N hydrogen bond with an O...N distance of 2.775 Å. The latter is approximately equivalent to an O...O distance of 2.675 Å, since the difference between the ván der Waals radii of nitrogen and oxygen atoms[80] is ~0.1 Å. The isolated HOD frequencies are obtained from spectra of samples of partially hydrogenated $ND_3 \cdot D_2O$ and partially deuterated $NH_3 \cdot H_2O$. The OH and OD frequencies are far apart to prevent any significant coupling. The observation of two OH bands and two OD bands for isolated HOD confirms the presence of two OH bonds or two OD bonds of different

hydrogen bond strength in the unit cell. So, as reported previously[6] and in view of the frequency-bond length correlation[32-37], the bands with higher frequencies at 3259 and 2410 cm^{-1} correspond to the uncoupled stretching frequencies of $\nu_{OH...O}$ and $\nu_{OD...O}$, respectively, and the bands with lower frequencies at 2825 and 2197 cm^{-1} correspond to the uncoupled stretching frequencies of $\nu_{OH...N}$ and $\nu_{OD...N}$.

The $\nu_{OH...O}$ and $\nu_{OH...N}$ uncoupled stretching frequencies are separated by ~430 cm^{-1}, so intramolecular coupling is expected to be negligible. In fact the frequency shift due to intramolecular coupling was calculated to be smaller than the expermental 95% confidence limits of the frequencies, Table 4.6. This was true for $f_{rr'} = 0$ with HOH angle of 109°, the mean value obtained in neutron diffraction of several hydrates,[81] and with HOH angle of 104.5°, which is the value for water vapor[82] (Table 4.6). Similar results of negligible intramolecular coupling were calculated for $\nu_{OD...O}$ and $\nu_{OD...N}$ frequencies (Table 4.7).

Each molecular $\nu_{OH...O}$ and $\nu_{OH...N}$ vibration yields three infrared active components of symmetries B_1, B_2 and B_3, under the D_2 unit cell group. So, if the intermolecular coupling is considered to be significant one would expect a triplet for each kind of OH

Table 4.6 O-H stretching frequencies of ammonia monohydrate.

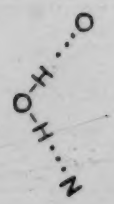

	$\nu_{O-H...O}$		$\nu_{O-H...N}$
Observed for isolated HOD	3259		2825
Observed for coupled H_2O	3275	3182	2887

Calculated for intramolecular coupled H_2O (isolated H_2O)

$f_{rr'} = 0$, $f_{rr} = 5.93247$, $f_{r'r'} = 4.45762$ mdyne A^{-1}

$\alpha = 109°$ (104.5°)*

3261	2823
(3260)	(2824)

*The wavenumbers in parentheses correspond to the calculated frequencies if $\alpha = 104.5°$.

Table 4.7 O-D stretching frequencies of deuterated ammonia monodeuterate

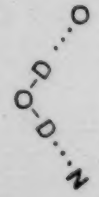

	$\nu_{O-D...O}$		$\nu_{O-D...N}$	
Observed for isolated HOD	2410		2197	
Observed for coupled D_2O	2459	2390	2189	2165

Calculated for intramolecular coupled D_2O (isolated D_2O)

$f_{rr'} = 0$, $f_{rr} = 6.12077$, $f_{r'r'} = 5.08666$ mdyne $Å^{-1}$

$\alpha = 109°$ $(104.5°)$*

2416	2188
(2413)	(2191)

*The wavenumbers in parentheses correspond to the calculated frequencies if $\alpha = 104.5°$.

vibration. The O-H...N bonds lie approximately in the bc pseudo-plane of symmetry (see Section 4.4). Thus, the D_{2h} pseudo-group predicts that $\nu_{OH...N}$ has only two infrared active components, of B_{1u} and B_{2u} symmetry (Table 4.8). The net dipole moment change per unit cell can be calculated using the bond moment approximations. The four OH...N bonds per unit cell would give zero net dipole moment change for the unit cell vibrations of A and B_3 symmetries under D_2. So, the only modes with significant intensity are the ones with the unit cell group symmetries B_1 and B_2 under D_2. The relative intensity of the B_1 mode to that of the B_2 mode is calculated to be about 1:1.5 (Table 4.8). In the spectrum of $NH_3 \cdot H_2O$, Figure 3.8, a broad band is observed at ~2887 cm^{-1} which may either contain both unit cell group components or may be assigned to the higher intensity B_2 mode. The mode of lower intensity, B_1, may yield the shoulder at ~2950 cm^{-1}. In the spectrum of $ND_3 \cdot D_2O$, Figure 3.17, a doublet is observed at 2189 and 2165 cm^{-1} which can be assigned on the basis of relative intensities to $\nu_{OD...N}$ modes of the unit cell symmetries B_1 and B_2, respectively.

In ammonia monohydrate the OH...O bonds form the O...O...O chains. The chains are along the a-axis and their plane is at 11.8° to the ab plane (Figures 4.7 to 4.10, which show only the "O-H...O-H" chains for

Table 4.8 Relative intensities of O-H...N vibrations in $NH_3 \cdot H_2O$.

O-H...N bond makes an angle of 50.4° with the c axis (Table 4.2).

Mode	$(\partial \underline{\mu}/\partial Q)_{u.c.}$	Direction of $\underline{\mu}$
A	0	
B_1	$4(\partial \underline{\mu}/\partial R)$ cos 50.4	parallel to 'c'
B_2	$4(\partial \underline{\mu}/\partial R)$ sin 50.4	parallel to 'b'
B_3	0	

Relative Intensity: $B_1 : B_2$ is 6.49:9.51 ~ 1:1.5

Correlation Table of O-H...N bonds Under the Pseudo-Group D_{2h}

	C_s (bc)	D_{2h}	Activity
O-H...N stretching	A'	B_{1u}	R, IR
		B_{2u}	R, IR

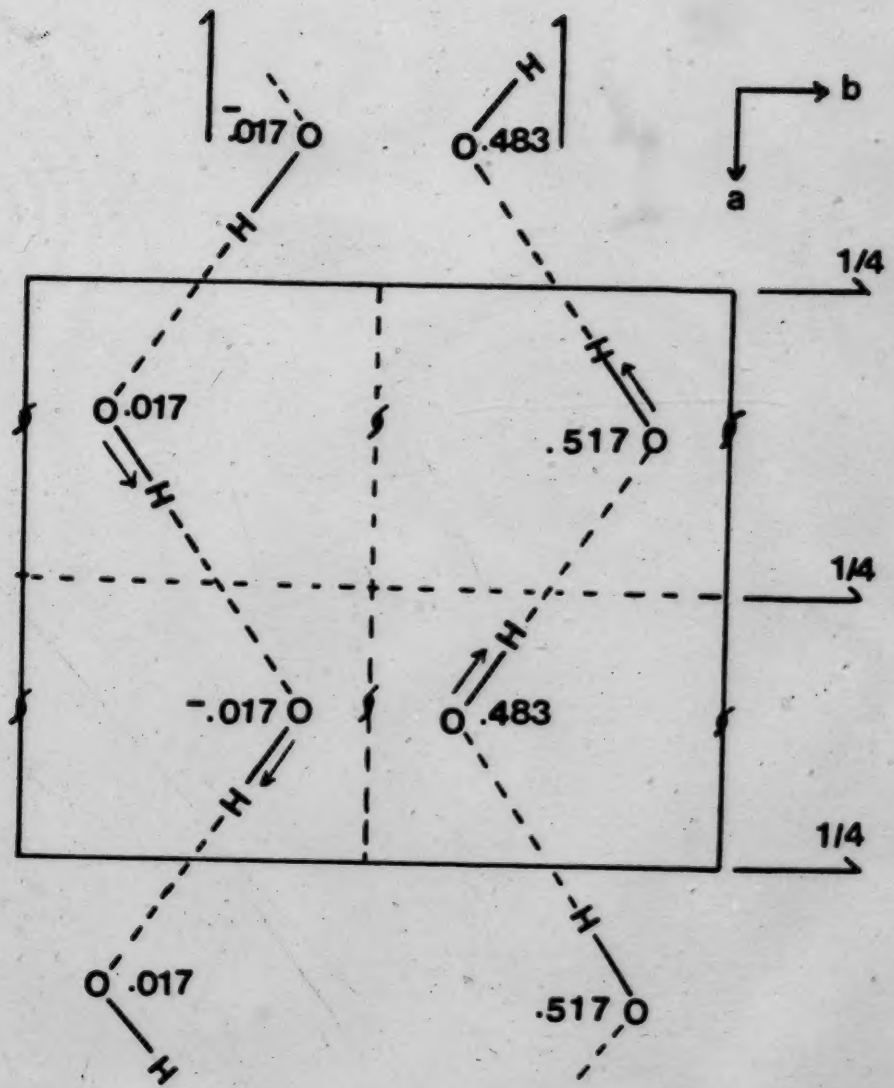

Figure 4.7 Ammonia monohydrate, only the chains of O-H...O are shown. The net dipole moment change per unit cell, $(\partial\mu/\partial Q)_{u.c.} = 0$ for the A unit cell O-H...O stretching vibration.

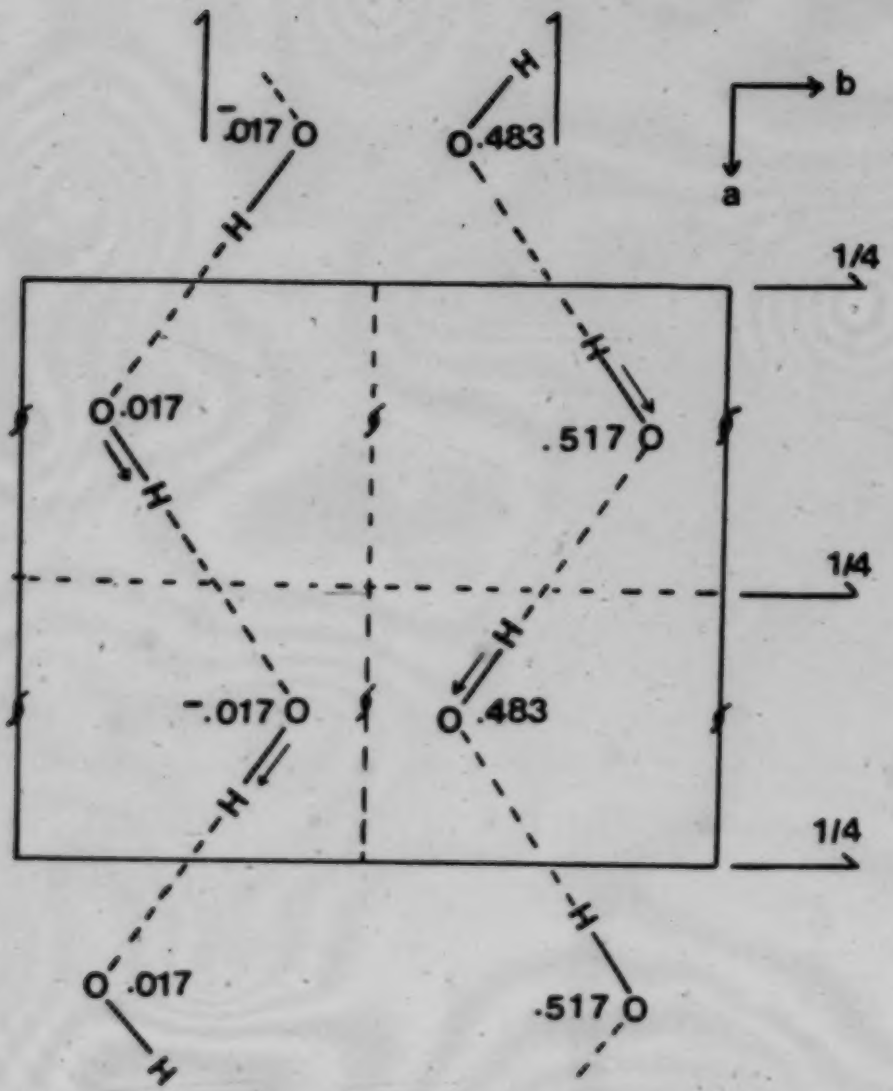

Figure 4.8 Ammonia monohydrate, only the chains of O-H...O are shown. The net dipole moment change per unit cell, $(\delta\mu/\delta Q)_{u.c.} = 4(\delta\mu/\delta R)\cos 35.2 = 3.269\ \delta\mu/\delta R$ in the a direction, for the B_3 unit cell O-H...O stretching vibration.

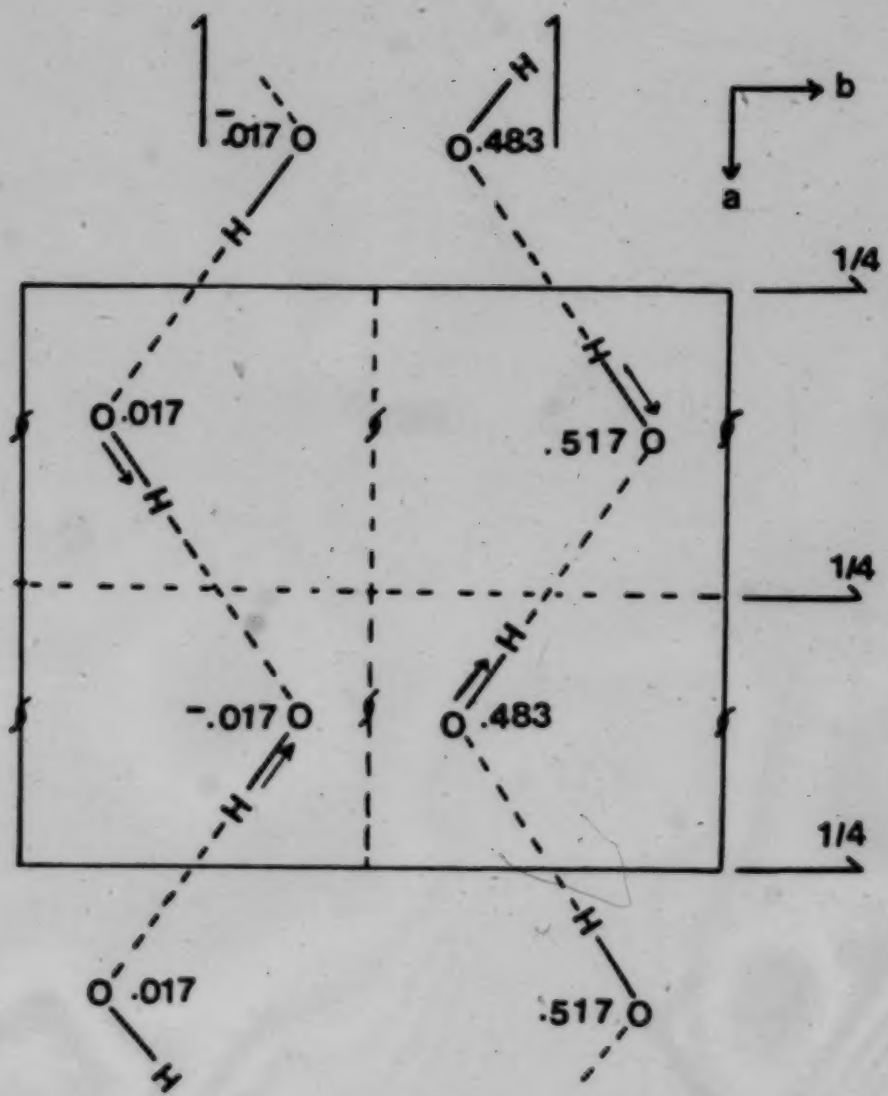

Figure 4.9 Ammonia monohydrate, only the chains of O-H...O are shown. The net dipole moment change per unit cell, $(\partial\mu/\partial Q)_{u.c.} = 4(\partial\mu/\partial R)\cos 54.8 (\cos 11.8) = 2.257\ \partial\mu/\partial R$ in the b direction, for the B_2 unit cell O-H...O stretching vibration.

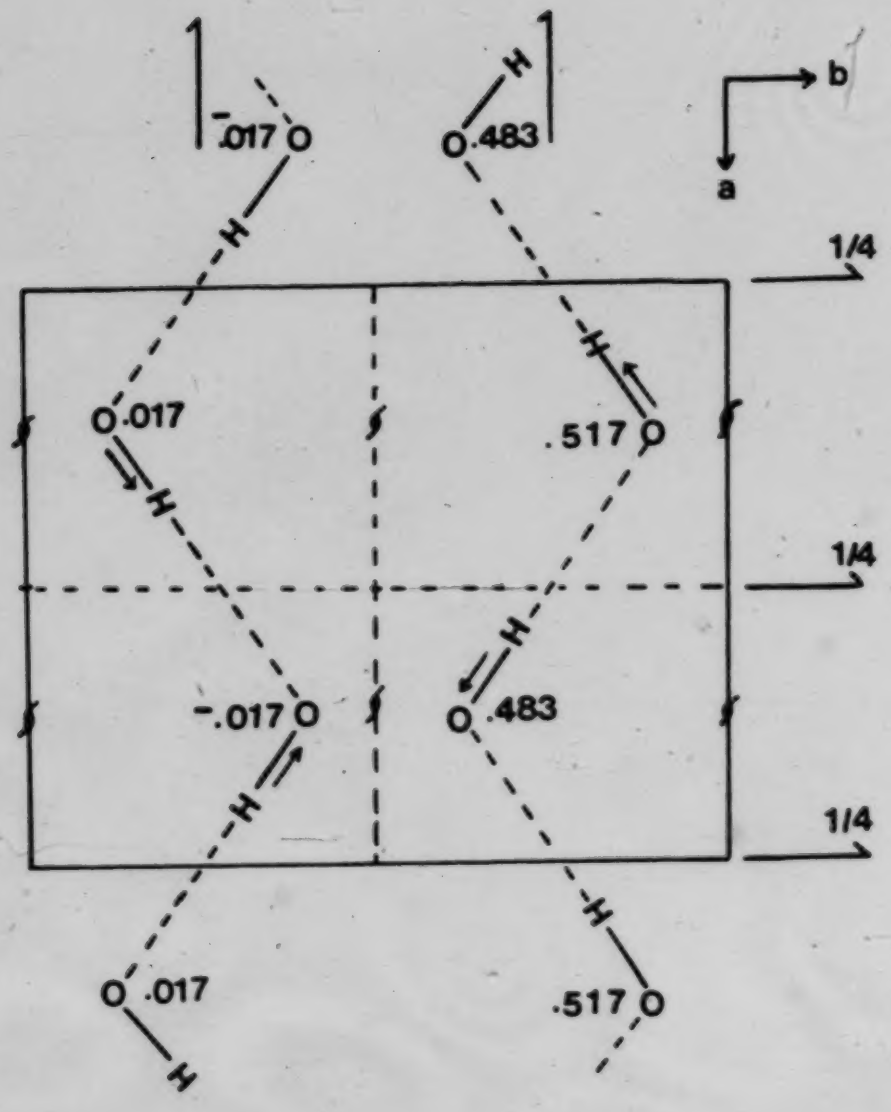

Figure 4.10 Ammonia monohydrate, only the chains of O-H...O are shown. The net dipole moment change per unit cell, $(\partial\mu/\partial Q)_{u.c.} = 0.471\ \partial\mu/\partial R$ in the c direction for the B_1 unit cell O-H...O stretching vibration.

clarity). The O-H...O bonds are not subject to the D_{2h} pseudo-symmetry because they cannot be symmetrical with respect to the pseudo-plane unless the hydrogen atoms are disordered and then they can only be apparently symmetrical. The O-H...O stretching vibrations are expected to yield three infrared active components of symmetries B_1, B_2 and B_3 under D_2.

The neighboring O-H bonds in the chains are coupled intermolecularly to give two different modes in one chain in each unit cell; one when the two OH bonds are stretching in-phase ($O\overrightarrow{-}H...O\overrightarrow{-}H$) and the second when they are out-of-phase ($O\overrightarrow{-}H...O\overleftarrow{-}H$). The net dipole moment change for the in-phase mode, $(\partial\underline{\mu}/\partial Q_1)$ is parallel to the a-axis and perpendicular to the bc plane (Appendix IV). The net dipole moment change for the out-of-phase mode $(\partial\underline{\mu}/\partial Q_2)$, is perpendicular to the a-axis so lies in the bc plane and forms angles of 11.8° and 78.2° with the b- and c-axes, respectively (Appendix IV). There are four O-H...O bonds per unit cell that are related intermolecularly by the unit cell group symmetry, D_2. The in-phase mode of a chain yields two unit cell modes of symmetries A and B_3, Figures 4.7 and 4.8, and the out-of-phase mode yields two unit cell modes of symmetries B_1 and B_2, Figures 4.9 and 4.10. Only B_1, B_2 and B_3 unit cell modes are infrared active and all three have non-zero

dipole moment change per unit cell. The relative intensities of the modes B_1:B_2:B_3 are approximately 1:23:48 (Table 4.9). Practically, one might expect to see only the two intense modes, the in-phase mode B_2 and the out-of-phase mode B_3, with relative intensities of about 1:2, respectively (Table 4.9).

The coupling between O-H bonds in one chain is expected to be much greater than that between chains. The frequency difference between the in-phase and out-of-phase vibrations of a chain can be calculated from the force constants which were calculated from the frequencies of HDO and from the intermolecular O-H, O-H interaction constant which is known to be around -0.1 mdyne A^{-1} in the phases of ice.[38,83,84] Thus the calculated frequencies of out-of-phase and in-phase O-H...O stretching vibrations in $ND_3 \cdot D_2O$ are 2448 and 2369 cm^{-1}, respectively (Appendix V). This corresponds to the bands observed at 2459 and 2390 cm^{-1} in the spectrum of $ND_3 \cdot D_2O$ (Figure 3.17). From this and the relative intensities (Table 4.9), the 2459 and 2390 cm^{-1} bands of $ND_3 \cdot D_2O$ are assigned to the B_1 + B_2, out-of-phase components (mainly B_2 since the B_1 mode is of very low relative intensity) and the B_3 in-phase component of the O-D...O stretching vibrations. In $NH_3 \cdot H_2O$ it is clear that the band at 3182 cm^{-1} corresponds to the B_3, O-H...O, in-phase, vibration but the B_1 and B_2

Table 4.9 Relative intensities of O-H...O stretching vibrations in $NH_3 \cdot H_2O$ (see Appendix IV).

Mode		$(\partial \underline{\mu}/\partial Q)_{u.c.}$	Direction of $\underline{\mu}$
A	in phase	0	
B_1	out of phase	0.472 $\partial \underline{\mu}/\partial R$	c
B_2	out of phase	2.257 $\partial \underline{\mu}/\partial R$	b
B_3	in phase	3.269 $\partial \underline{\mu}/\partial R$	a

Intensities $B_1:B_2:B_3$ is 0.223:5.09:10.68 ~ 1:23:48

Therefore, practically only B_2 and B_3 are expected with relative intensity of ~1:2.

modes are not obvious. They must lie near 3300 cm^{-1}, as do $\nu_1(NH_3)$, calculated near 3250 cm^{-1} (Table 4.4), and $2\nu_4(NH_3)$ and possibly $2\nu_2(H_2O)$. It is probable that these all interact and contribute to the bands at 3332, 3294, 3275 and 3235 cm^{-1}.

4.6 The Intramolecular Angle Deformation Vibrations

The antisymmetric angle deformation of ammonia, ν_4, has six infrared active components under D_2 unit cell group, $2B_1 + 2B_2 + 2B_3$ (Table 4.1). Their predicted relative intensities are the same as for $\nu_3(NH_3)$ so only three unit cell group components have significant infrared intensities. The ratio of the intensities of $B_1:B_2:B_3$ is ~1.5:1:2.5 (Table 4.2). A similar conclusion is reached if one considers the pseudo-D_{2h} selection rules, Table 4.5, where only three infrared active components of $\nu_4(NH_3)$ are expected, $B_{1u} + B_{2u} + B_{3u}$. The sharp features at 1665.5, 1650.1 and 1627.0 cm^{-1} for $NH_3 \cdot H_2O$ (Table 4.10) and 1217, 1209.1 and 1192.6 cm^{-1} for $ND_3 \cdot D_2O$ are assigned to ν_4, and can be assigned on the basis of their relative intensities to the B_2, B_1 and B_3 unit cell group components, respectively.

The symmetric angle deformation of ammonia, ν_2, has three infrared active components, B_1, B_2 and B_3 under the D_2 unit cell group. Their predicted relative infrared

Table 4.10 Infrared spectral assignments of $NH_3 \cdot H_2O$ and $ND_3 \cdot D_2O$.

$NH_3 \cdot H_2O$[a,b] ν/cm^{-1}	$ND_3 \cdot D_2O$[a,c] ν/cm^{-1}	Ratio[a] ν_H/ν_D	Assignment[d]
~5210			
5015(1)	3715(2)	1.350(2)	$(\nu_3 + \nu_4)(a)$
~4953			
~4800	~3610	1.33(1)	
	~3471		
4515(4)	3392(2)	1.331(2)	$(\nu_3 + \nu_2)(a)$
2471*	3362*	1.360	$\nu_{NH}(ND_2H)$ or $\nu_{ND}(NH_2D)$
2467*	3349.2(5)*	1358	
2464*	3345*	1.357	
2410*	3259(2)*	1.352	$\nu_{O-H(D)\ldots O}(HOD)$
~4417			overtone or combination modes
	~3135*		
~4366			
~4320			
~4240 }	~3085		
~4150			
~3771			
	~2954		
~3689			
	~2940		
~3590			
	~2917		
~3531			
2197*	2825(5)*	1.29	$\nu_{O-H(D)\ldots N}(HDO)$
3403.2(5)	2534.3(5)	1.343(1)	$\nu_3(a)$ B, B_2, B_3
3392.1(5)	2526.1(5)	1.343(1)	
3387.3(5)	2522.2(6)	1.343(1)	
3332(2)			$\nu_1(a)$; $2\nu_4(a)$; $2\nu_2(w)$?
~3294			
3275(5)	2459(2)	1.332(4)	$\nu_{O-H(D)\ldots O}(w)$; (B_1 and B_2 out-of-phase)
3235	~2414	1.340	$\nu_1(a)$; $2\nu_4(a)$?
3182(2)	2390	1.331(2)	$\nu_{O-H(D)\ldots O}(w)$, (B_3 in-phase)

(Continued)

Table 4.10 (Continued)

$NH_3 \cdot H_2O$[a,b] ν/cm^{-1}	$ND_3 \cdot D_2O$[a,c] ν/cm^{-1}	Ratio[a] ν_H/ν_D	Assignment[d]
~2950	~2260	1.31(1)	
2887(10)	2819(2)	1.319(6)	$\nu_{O-H(D)\ldots N}$ (B_1)
	2165(2)	1.333(6)	$\nu_{O-H(D)\ldots N}$ (B_2)
	~1929		$3\nu_R(w)$; $\nu_R(w)+\nu_2(w)$;
	~1836		
~2432	1767(3)	1.38(1)	$\nu_4(a)+\nu_R(w)$
2260(3)	~1675	1.35(1)	
2140.8(5)	1666.8(9)	1.284(3)	
2028(4)	1534(2)	1.322(4)	$\nu_2(a) + \nu_R(w)$
1994(5)		1.305(5)	
	1467*		$\nu_2(HOD)$
1834(3)	1319.5(9)	1.390(3)	$2\nu_R(H_2O)$
1773(3)		1.340(3)	
~1696	1243(3)	1.364	$\nu_2(w)$; $\nu_R(w)+\nu_R'(w)$
1665.5(5)	~1217	1.37(1)	$\nu_4(a)$, (B_2)
1650.1(5)	1209.1(5)	1.365(1)	$\nu_4(a)$, (B_1)
1627.0(5)	1192.6(5)	1.364(1)	$\nu_4(a)$, (B_3)
~1594	1169(1)	1.36(1)	$\nu_R(w) + \nu_R'(w)$
1537(2)	1135(3)	1.354(5)	$\nu_R(w) = \nu_R''(w)$
1480(2)			$2\nu_R'(w)$
1439(4)	1060(4)	1.358(8)	$2\nu_R'(w)$
1402(2)	1023(2)**	1.370(5)	$2\nu_R'(w)$; $\nu_2(ND_2H)$
1287.1(5)	943.4(6)	1.364(2)	$2\nu_R''(w)$
1133.4(5)	870.6(9)	1.302(3)	$\nu_2(a)$, (B_1)
1095.9(5)	848.2(8)	1.292(2)	
	~ 806		$\nu_R(HOD)$?
~ 932			
914(2)	682.3(6)	1.340(4)	$\nu_R(w)$
~ 893	661(2)	1.35(1)	
757.6(5)	554(1)	1.368(5)	
~ 750	~ 548	1.37(2)	$\nu_R'(w)$
709.9(5)	516.3(6)	1.375(3)	
644.2(5)	466.7(5)	1.380(3)	$\nu_R''(w)$

(Continued)

Table 4.10 (Continued)

$NH_3 \cdot H_2O$[a,b] ν/cm^{-1}	$ND_3 \cdot D_2O$[a,c] ν/cm^{-1}	Ratio[a] ν_H/ν_D	Assignment[d]
~ 579			
448(3)			B_2
420.4(5)			$\nu_R(a)$ B_1
389(2)			B_3
308(3)			$\nu_R(a)$; ν_T ?
300(2)			
266.6(5)			ν_T
243(2)			

[a] The numbers in parentheses are the 95% confidence limits in the last digit.

[b] The wavenumbers, with asterisk (*) are measured once from a sample of ammonia monohydrate containing ~10% D (mulled in propane).

[c] The wavenumbers with asterisk (*) are the hydrogen impurity in $ND_3 \cdot D_2O$. (**) means it is due to both $ND_3 \cdot D_2O$ and hydrogen impurity.

[d] a ≡ NH_3 or ND_3; w ≡ H_2O or D_2O; B_1, B_2 and B_3 ≡ irreducible representations under unit cell group D_2.

intensities are the same as those of $\nu_1(NH_3)$, Table 4.2. Thus, only two unit cell group components, B_1 and B_2, with significant infrared intensities in the ratio ~1:1.5, respectively, are expected, Table 4.2. This same conclusion is reached, two components of B_{1u} and B_{2u} symmetries, if one considers the pseudo-D_{2h} selection rules, Table 4.5. The B_1 and B_2 components of ν_2 can be readily assigned to 1133.4 and 1095.9 cm^{-1} for $NH_3 \cdot H_2O$ and 870.6 and 848.2 cm^{-1} for $ND_3 \cdot D_2O$, respectively (Figures 3.12 and 3.20 and Table 4.10).

It has been argued[6,7] before that the shift of 37 or 22 cm^{-1} is rather large for intermolecular coupling of the four ammonia molecules in the unit cell since they are separated by water molecules in the crystal. Bertie and Morrison[6,7] attributed this shift and similar shifts in the case of ammonia hemihydrate to Fermi resonance interaction between ν_2 of ammonia and combination bands. Most recently, Bertie and Devlin,[13] confirmed that the splitting in ν_2 of ammonia in ammonia hemihydrate is due to intermolecular coupling of ammonia molecules. In this work, the similarity between the doublets in the spectrum of $NH_3 \cdot H_2O$ and $ND_3 \cdot D_2O$ probably shows that the splitting is mainly due to intermolecular coupling.

The bisectors of the HOH angles of water molecules in ammonia monohydrate make the angles to the crystal axes

listed in Table 4.11. The water bending modes, ν_2, in which the two water molecules in a chain are in-phase yield A and B_3 unit cell group components and those in which the two water molecules in a chain are out-of-phase yield B_1 and B_2 components. The relative intensities of the unit cell components of ν_2 of water are in the approximate ratio $B_1:B_2:B_3 \approx 12:1:14$ (Table 4.11). Thus, one expects a doublet in which one component, B_1, corresponds to out-of-phase coupling in a chain and the other, B_3, is of slightly greater intensity and corresponds to the in-phase coupling within a chain.

The band at 1467 cm^{-1} observed in $ND_3 \cdot D_2O$ spectrum containing less than 1% H is found to increase in intensity with increasing the hydrogen content of the sample and is probably due to $\nu_2(HDO)$. However, a doublet is expected for this vibration because the water molecules are asymmetric in ammonia monohydrate. According to the harmonic approximation, the frequency ratios of ν_2 in H_2O, HDO and D_2O are ~1.36:1.20:1. In practice,[85-87] similar ratios are obtained so if $\nu_2(HDO)$ is at 1467 cm^{-1}, $\nu_2(H_2O)$ is near 1670 and $\nu_2(D_2O)$ is near 1225 cm^{-1}. Accordingly, the features at ~1696 cm^{-1} for $NH_3 \cdot H_2O$ and 1243 cm^{-1} for $ND_3 \cdot D_2O$ may be due to one of the bending modes of water. Due to the complexity of this region of the spectrum, it is not possible to assign the second component of ν_2 of

Table 4.11 Relative intensities of ν_2 bending vibrations of water.

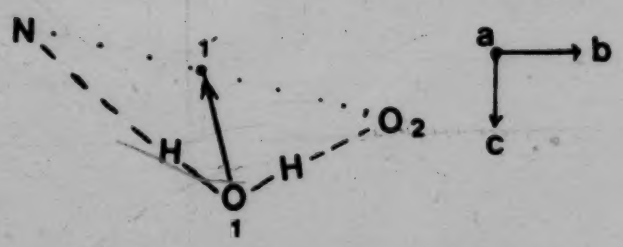

Atom	Fractional coordinates	Actual coordinates
O_1	0.241, 0.111, 0.017	1.087, 0.613, 0.163
O_2	0.741, 0.389, -0.017	3.342, 2.175, -0.163
N	0.236, -0.272, -0.166	1.064, -1.520, -1.605
point 1'	0.489, 0.059, -0.092	2.203, 0.327, -0.888

The unit vector

$$\hat{U}_{O_1-1'} = (1.116\,\underline{i} - 0.291\,\underline{j} - 1.051\,\underline{k})/1.560$$

$$= 0.715\,\underline{i} - 0.186\,\underline{j} - 0.674\,\underline{k}$$

i.e. makes angles of approximately 44, 101 and 132 to a, b and c axes, respectively.

Water molecule	Angles between the bisectors of HOH angle and		
	a	b	c
1	44	101	132
2	44	79	48
3	136	101	48
4	136	79	132

The relation between these angles is required by symmetry.

Mode	$(\partial\underline{\mu}/\partial Q)_{u.c.}$	Direction of $\underline{\mu}$
A	0	
B_1	$4(\partial\underline{\mu}/\partial Q)_{mol}\cdot\cos 132$	c
B_2	$4(\partial\underline{\mu}/\partial Q)_{mol}\cdot\cos 101$	b
B_3	$4(\partial\underline{\mu}/\partial Q)_{mol}\cdot\cos 44$	a

Intensities of $B_1:B_2:B_3$ is $(-2.677)^2:(-0.763)^2:(2.877)^2 \sim 12:1:14$

water. The other bands in this region are assigned to overtones and combinations (Table 4.10).

4.7 Lattice Vibrations

In addition to the internal vibrations of the molecules, motions of the centers of gravity and rotations of the molecules may give rise to infrared absorption. Since the motions are allowed by symmetry to couple, it is not strictly correct to separate the two categories, but it may be anticipated that the higher lattice frequencies are primarily those of rotational vibrations and the lower primarily due to translational vibrations.

The assignments of the rotational and translational vibrations are made by analogy with those of solid ammonia[42,43,46,68-71] and ice,[72,73] and the most recent assignments of ammonia hemihydrate.[13]

The rotational motion of water molecules in ammonia monohydrate is expected to yield nine infrared active modes, $3B_1$, $3B_2$ and $3B_3$ under D_2 unit cell group (Table 4.1). The bands between ~1000 and 600 cm^{-1} in the spectrum of $NH_3 \cdot H_2O$, Figure 3.12, and those between ~780 and 450 cm^{-1} in the spectrum of $ND_3 \cdot D_2O$, Figure 3.20, are assigned, following the evidence provided by the spectra of hemihydrate of ammonia,[13] to rotational vibrations of water (Table 4.10).

The pseudo-D_{2h} selection rules, Table 4.5, apply to the ammonia vibrations. Thus the rotational displacements which re-orient the dipole, R_x and R_y, of ammonia are degenerate in the free molecule and expected to give rise to two kinds of rotational vibrations in the monohydrate crystals; one in which the dipole moment derivative lies in the pseudo-plane, which yields two infrared active modes, B_{1u} and B_{2u} (or B_1 and B_2 under unit cell group D_2), and the other in which the dipole moment derivative is perpendicular to the pseudo-plane, which yields one infrared active mode, B_{3u} (or B_3 under unit cell group D_2). The angle between the molecular axis of ammonia and the c-axis is ~50.4° (Table 4.2), so the expected relative intensity ratio of $B_1:B_2:B_3$ is approximately ~1.5:1:2.5 (Table 4.2). According to these relative intensities and Figure 3.14, the bands at 448, 421 and 389 cm^{-1} are assigned to the B_2, B_1 and B_3 modes, respectively (Table 4.10). The rotation about the z-axis, R_z, yields one active D_{2h} unit cell mode, B_{3u}, Table 4.5 (or B_3 under unit cell group D_2) and probably contributes to the features at 308 and 300 cm^{-1}.

A complete assignment of the translational vibrations cannot be made because the region has not been completely covered. However, the sharp bands at 266.6 and 243 cm^{-1} may be assigned to the hydrogen bond stretching vibrations

of the O...N, and possibly the O...O bonds (Table 4.10).

4.8 Other Features in the Spectrum of Ammonia Monohydrate

All features which have not been discussed in the previous sections are due to overtone and/or combination bands and their assignments are listed in Table 4.10.

The combination bands at 5015 and 4515 cm^{-1} in $NH_3 \cdot H_2O$ and the corresponding bands at 3715 and 3392 cm^{-1} in $ND_3 \cdot D_2O$ are assigned to $\nu_3 + \nu_4$ and $\nu_3 + \nu_2$ of ammonia, respectively. Similar combinations are observed in the spectrum of solid ammonia,[70] $\nu_3 + \nu_4$ = 4923 cm^{-1} and $\nu_3 + \nu_2$ =4397 cm^{-1}, and in the spectra of ammonia hemihydrate, $\nu_3 + \nu_4$ = 5005 cm^{-1} and $\nu_3 + \nu_2$ = 4510 cm^{-1} in the spectrum of $2NH_3 \cdot H_2O$ recorded in this work and the corresponding bands of $2ND_3 \cdot D_2O$[7] $\nu_3 + \nu_4$ = 3710 and 3685 cm^{-1}, and $\nu_3 + \nu_2$ = 3385 cm^{-1}. Similar results are also observed for ammonia dihydrate (Chapter 5).

CHAPTER 5

AMMONIA DIHYDRATE: STRUCTURE AND SPECTRAL ASSIGNMENTS

In this chapter the x-ray diffraction pattern of ammonia dihydrate is indexed, Section 5.1, and the crystal structure is deduced accordingly, Section 5.2, with the help of the observed infrared spectra of ammonia dihydrate and its isotopomers. The infrared spectra of ammonia dihydrate and its isotopomers are assigned in Sections 5.3 to 5.5.

5.1 Indexing of the Powder X-Ray Diffraction Pattern of Ammonia Dihydrate

The powder x-ray diffraction pattern of ammonia dihydrate at ~105K, as determined from photographs with CuK_α and MoK_α radiations, is given in Table 3.2. The x-ray powder diffraction lines were indexed on a cubic unit cell.

For the cubic system,[88-90] the interplanar spacing equation is

$$1/d^2_{hkl} = (h^2 + k^2 + l^2)/a^2 \qquad (5.1.1)$$

where d is the interplanar spacing, h, k, l are the Miller indices, and a is the unit cell dimension. Then the differences between the squares of the reciprocal interplanar distances are given by:

$$(1/d^2_{hkl} - 1/d^2_{h'k'l'}) = ((h^2+k^2+l^2) - (h'^2+k'^2+l'^2))/a^2 = n/a^2 \qquad (5.1.2)$$

where n can only take integer values.

For the cubic system, one expects the differences between the squares of the reciprocal interplanar distances to have the values: $1/a^2$, $2/a^2$, $3/a^2$, $4/a^2$, etc. These differences are shown in Table 5.1 with their frequency of occurrence. If the numbers in column 2 of Table 5.1 are divided by the common factor $1/a^2$, which is ~0.0198, one gets the values in column 4 of Table 5.1, which are close to 1, 2, 3, 4, etc. This and Table 5.2 clearly prove that the dihydrate of ammonia crystallizes in a cubic lattice. This method of finding the crystal class for powder x-ray is the Hesse-Lipson procedure,[90] using the differences between $1/d^2$ values instead of the often used differences between $\sin^2\theta$ values.

A value of 7.10 Å for the unit cell dimension, a, is calculated from equation (5.1.2) and Table 5.1. The estimated unit cell parameters, the Miller indices, and

Table 5.1 The observed differences between the squares of the reciprocal interplanar distances.

n	Observed[a] $(1/d^2_{hkl} - 1/d^2_{h'k'l'})$	No. of Occurrences[b]	Column 2 / 0.0198
1	0.0198(2)	8	1.00
2	0.0395(2)	8	1.99
3	0.0595(4)	8	3.00
4	0.0789(4)	7	3.98
5	0.0985(7)	6	4.98
6	0.1184(4)	6	5.98
7	0.1383(5)	6	6.98
8	0.1580(3)	6	7.98
9	0.1779(3)	8	8.98
10	0.1976(4)	5	9.98
11	0.2176(8)	5	10.99
12	0.2367(8)	3	11.95
13	0.256(2)	3	12.93
14	0.2760(10)	2	13.94
15	0.296(4)	3	14.95
16	0.317(3)	4	16.01
17	0.336	1	16.98
18	0.357(6)	3	18.03
19	0.378(9)	2	19.09
20	0.395	1	19.93
21	0.417(9)	2	21.06
22	0.434	1	21.93
23	0.456(9)	2	23.04
24	0.476(9)	2	24.04
25	0.498	1	25.16
26	0.518	1	26.15
27	0.538	1	27.15

[a] The numbers in parentheses are the 95% confidence limits in the last digit.

[b] The number of times the figure in column 2 appears in the differences between the squares of the reciprocal interplanar distances.

Table 5.2 Indexing of the x-ray powder diffraction lines of ammonia dihydrate in a primitive cubic unit cell.

$h^2+k^2+l^2$ [a]	Miller Indices [b]	$(h^2+k^2+l^2)^{1/2}_{expected}$	$(\frac{d}{7.118})_{observed}$ [c]
1	(100)	1.00	A
2	(110)	0.707	0.708
3	(111)	0.577	0.577
4	(200)	0.500	0.501
5	(210)	0.447	0.448
6	(211)	0.408	0.408
-	-	-	-
8	(220)	0.354	0.354
9	(300),(221)	0.333	A
10	(310)	0.316	0.316
11	(311)	0.302	0.301
12	(222)	0.289	0.289
13	(320)	0.277	0.277
14	(321)	0.267	0.267
-	-	-	-
16	(400)	0.250	A
17	(410),(322)	0.242	A
18	(411),(330)	0.236	0.236
19	(331)	0.229	A
20	(420)	0.224	A
21	(421)	0.218	0.218
22	(332)	0.213	A
-	-	-	-
24	(422)	0.204	0.205
25	(500),(430)	0.200	A
26	(510),(431)	0.196	0.196
27	(511),(333)	0.192	A
-	-	-	-
29	(520),(432)	0.186	0.185

[a] No combination of integers squared gives a value of 7, 15, 23 or 28 for the expression $(h^2+k^2+l^2)$.

[b] From References 88 to 90, Miller indices for cubic systems.

[c] $d/a = (h^2+k^2+l^2)^{1/2}$, where a = 7.118 ± 0.015 Å. A means systematic absences.

the 2θ values (Table 3.2) were input to a program DREFINE,[51] which refines the unit cell parameters by a least-squares fit of $\sin^2\theta$ values. A refined value of a = 7.118 Å with a 95% confidence limit of 0.015 Å was obtained.

5.2 The Crystal Structure of Ammonia Dihydrate

From the previous section the dihydrate of ammonia crystallizes in a cubic lattice. The only systematic absences from Table 5.2, are h00 with h odd, which means that the unit cell is a primitive and there is a 2_1 screw axis along the a-axis.

The volume of the unit cell at ~105K is 360.6 $Å^3$. So, if one assumes four molecules per unit cell, the density of ammonia dihydrate will be 0.977 g cm^{-3}, which is comparable to 0.952 g cm^{-3} for the density of ammonia monohydrate[5] at ~113K, 0.917 g cm^{-3} for the density of ammonia hemihydrate[4] at ~178K and 0.857 g cm^{-3} for the density of ammonia at ~113K.

If one examines the cubic space groups,[27] neglects the hydrogen atoms and considers the presence of 4 nitrogen and 8 oxygen atoms per unit cell, only seven possibilities result: $P23(T^1)$, $P2_13(T^4)$, $Pm3(T_h^1)$, $P\bar{4}3m(T_d^1)$, $P432(O^1)$, $P4_332(O^2)$, and $Pm3m(O_h^1)$. These space groups either have the condition that h00 is absent if h

is odd or no conditions.

The observation of only one OH or OD stretching frequency for the isolated O-H...N or O-D...N bonds, and of a strong singlet for the symmetric bending vibration of ammonia, ν_2, suggests the existence of only one kind of ammonia in ammonia dihydrate. This is also suggested by the observation of one strong absorption band with three sharp features for $\nu_3(NH_3)$, Figure 3.23, instead of two distinct bands observed for $\nu_3(NH_3)$ for the two types of ammonia in ammonia hemihydrate. Further, the presence of two sharp bands for the stretching vibrations of the isolated O-H...O or O-D...O and a third for the stretching vibration of the isolated O-H...N or O-D...N suggests the existence of two kinds of water molecules in ammonia dihydrate. If these suggestions are taken as correct, the 4 nitrogen atoms can only be on sites of multiplicity 4 and the 8 oxygen atoms per unit cell can be on sites of multiplicities 4 and 4 or 6 and 2. These limitations reduce the possibilities for the space group to only four: P23, $P2_13$, $P4_232$ and $P\bar{4}3m$. The space groups P23 and $P\bar{4}3m$ can be rejected because they require all of the heavy atoms to be on the body diagonals, which are too short to permit this. Further, no structure could be found in space group $P4_232$ which would yield bond lengths close to those indicated by the spectroscopic information

(next paragraph and Table 5.3). Thus it was concluded that the space group in the cubic system is $P2_13(T^4)$.

The O...O and O...N distances in ammonia dihydrate were estimated from the spectra-structure correlations for ammonia monohydrate, ammonia hemihydrate,[7,13] and hexamethylenetetramine hexahydrate ($HMT \cdot 6H_2O$),[91] and from the correlation relations[32-37,91] between the OH and OD stretching frequencies and O...O distances which are based on the data for the phases of ice and numerous inorganic hydrates. The isolated stretching frequencies of O_{II}-H...O_I and O_{II}-D...O_I are at 3257 and 2425 cm^{-1}, which are -2 and +15 cm^{-1}, respectively, from those of ammonia monohydrate with O...O distance of 2.76 Å. Thus, the O_{II}-H...O_I and O_{II}-D...O_I are expected to have O_{II}...O_I distances of >2.76 Å (Table 5.3). Similarly, the isolated frequencies of O_I-H...O_{II} and O_I-D...O_{II} at 3240 and 2396 which are -19 and -14 cm^{-1}, respectively, from those of ammonia monohydrate. So, the O_I-H...O_{II} and O_I-D...O_{II} have O_I...O_{II} distances of <2.76 Å. From plots of R(O-H...N) and R(O-D...N) versus ν_{OH} and ν_{OD}, respectively, using the data in Table 5.3, and extrapolating the best straight line that fits the data to 2763 and 2122 cm^{-1}, respectively, an estimated value for R(O-H...N) and R(O-D...N) is obtained to be ~2.74 ± 0.02 Å.

The structure of ammonia dihydrate was found in $P2_13$

Table 5.3 Estimation of R(O...O) and R(O...N) distances in ammonia dihydrate at ~100K.

(A) O-H(D)...O

	ν_{OH}(HOD)/cm^{-1}	ν_{OD}(HOD)/cm^{-1}	R(O...O)/Å expected[a]	found
Ammonia Monohydrate	3259	2410	2.75	2.76
Ammonia Dihydrate	3257	2425	2.76	b
Ammonia Dihydrate	3240	2396	2.75	b

(B) O-H(D)...N

	ν_{OH}(HOD)/cm^{-1}	ν_{OD}(HOD)/cm^{-1}	R(O...N)/Å
Ammonia Hemihydrate			
O-H(D)...N_{II}	3125	2347	2.86
O-H(D)...N_{I}	3050	2275	2.84
HMT[c]	3050	2295	2.81
Ammonia Monohydrate	2825	2197	2.77
Ammonia Dihydrate	2763	2122	(2.74±0.02)[d]

(C)N-H(D)...O

	ν_{NH}(ND_2H)/cm^{-1}[e]	ν_{ND}(NH_2D)/cm^{-1}[e]	R(N...O)/Å
Ammonia Hemihydrate			
N_{II}H(D)...O	~3355	~2473	unbound
N_{I}H(D)...O	~3317	~2440	~3.2
Ammonia Monohydrate	~3352	~2467	~3.25
Ammonia Dihydrate	~3354	~2470	(>3.2)[f]

[a]Calculated from the correlation relation: R(O...O) = 0.1391 (25.56 - ln(2727 - ν_{OD}), the standard deviation of the bond length calculated from an observed frequency using this correlation is 0.03 Å (Refs. 36 and 91).

[b]Estimated R(O...O) for ammonia dihydrate is ~2.76 Å.

[c]HMT, means hexamethylenetetramine hexahydrate.

[d]Estimated from plots of R(O-H(D)...N) versus ν_{OH} or ν_{OD} using the data in this table.

[e]The average frequency.

[f]The estimated value for R(N-H(D)...O) in ammonia dihydrate.

with all of the heavy atoms on the special positions with site symmetry C_3: (x, x, x); (0.5+x, 0.5-x, $\bar{x}$); ($\bar{x}$, 0.5+x, 0.5-x); (0.5-x, $\bar{x}$, 0.5+x).[27] The fractional coordinates x = 0.1410 for O_{II}, x = 0.3635 for N and x = 0.7111 for O_I yield distances that are reasonable compared to those in Table 5.3, $O_I...O_{II}$ = 2.764 Å, O_{II}-H...N = 2.743 Å and N-H...O_I = 3.260 Å. The interatomic distances program, in which the fractional coordinates are adjusted to give the above distances, and the results of this structure are listed in Appendix II.

The crystal structure of ammonia dihydrate in space group $P2_13$ is shown in Figure 5.1, where the hydrogen atoms on the O-H...O bonds are not shown because they can be closer to either O_I or O_{II}. In this structure, the nitrogen atom is hydrogen bonded to three (type I) oxygen atoms through three N-H...O_I bonds and one (type II) oxygen atom through an O_{II}-H...N bond. The type I oxygen atom is hydrogen bonded to three (type II) oxygen atoms, and the remaining lone pair of electrons is shared between three N-H bonds. The type II oxygen is hydrogen bonded to three (type I) oxygen atoms, and one nitrogen atom, O_{II}-H...N. The structure around O_I, O_{II} and N atoms and the bond lengths and angles are shown in Figure 5.2. By comparison with the structures of ammonia hemihydrate[4] and ammonia monohydrate,[5] this is a perfectly reasonable

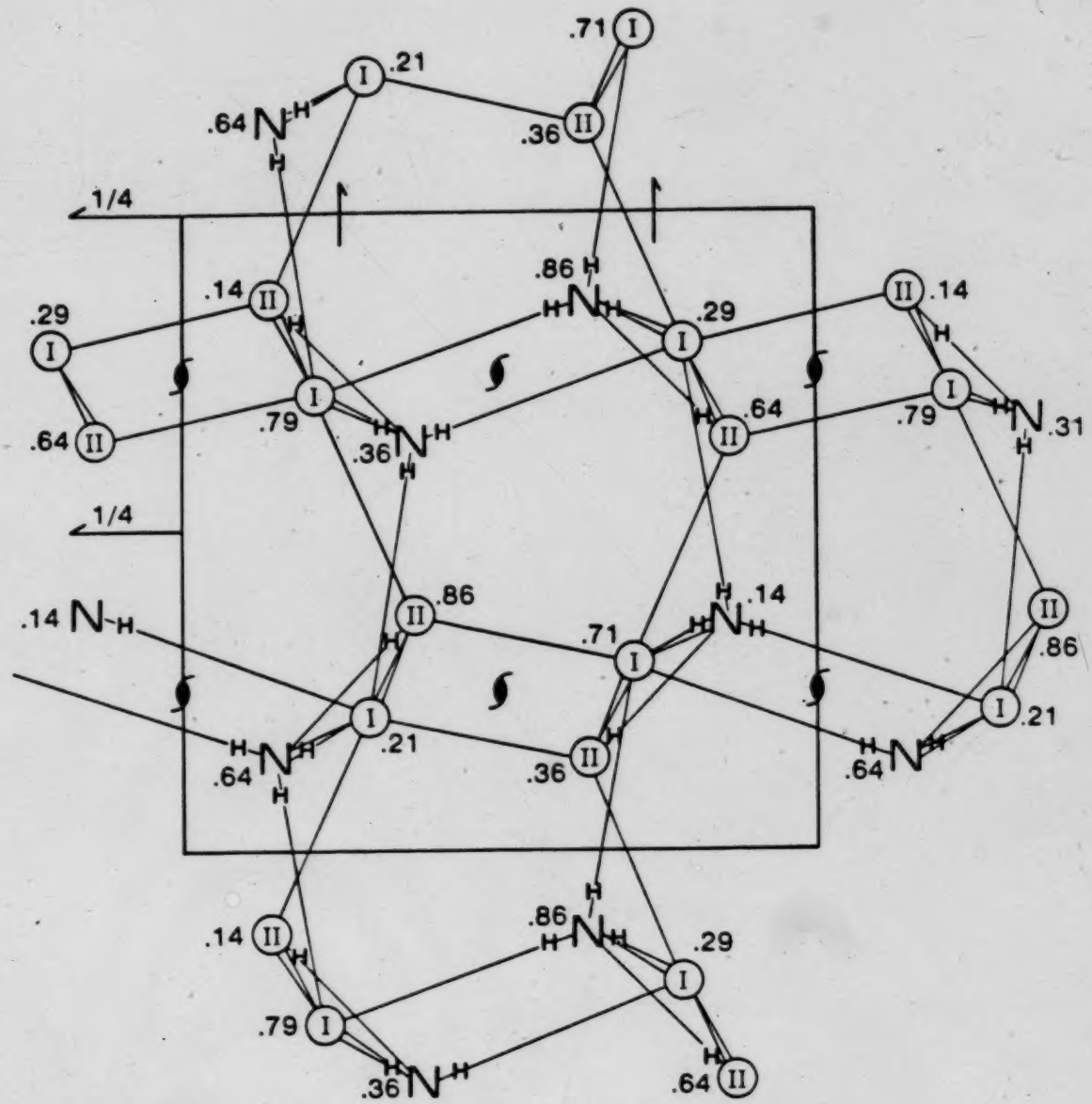

Figure 5.1 The structure of $NH_3 \cdot 2H_2O$ at 100K. Pseudo $P2_13$ space group or probably $P2_12_12_1$; a = b = c = 7.12 Å, z = 4; O_I x = 0.711, O_{II} x = 0.141 and N x = 0.364. The hydrogen atoms in O-H...O bonds are not shown.

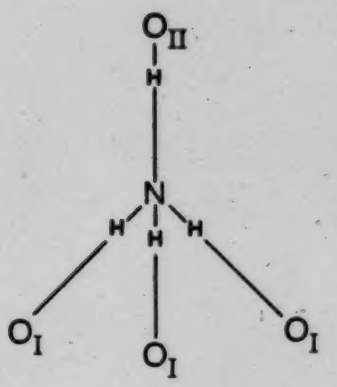

$O_{II}H$ ——— N	2.74A°
NH ——— O_I	3.26A°
O_I — N — O_I	114.0°
O_{II} — N — O_I	104.5°

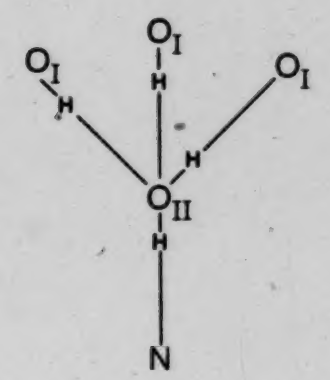

O_I ——— O_{II}	2.76 A°
O_I — O_{II} — N	101.5°
O_I — O_{II} — O_I	116.1°

O_{II} — O_I — O_{II}	104.5
N — O_I — N	84.1
N — O_I — O_{II}	83.9
N — O_I — O_{II}	85.3

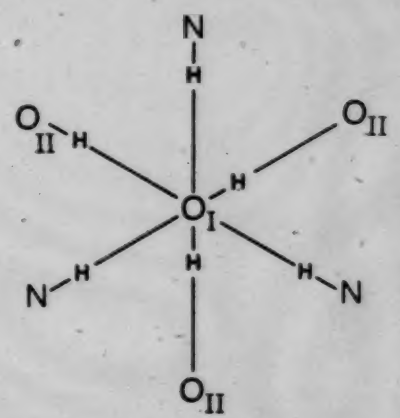

Figure 5.2 The geometry around the atoms O_I, O_{II} and N in the ammonia dihydrate structure.

structure. To test further the validity of this structure, the diffraction intensities expected on a flat-plate powder photograph were calculated, Table 3.2, using equation (3.2.1). The structure factors were calculated from the scattering factors[61] for oxygen and nitrogen atoms, and the isotropic thermal parameters, B_t = 1.42 for oxygen and 1.57 for nitrogen, which were found for ammonia monohydrate.[5] The hydrogen atoms were neglected in the calculation. The calculation of the relative intensities and the computer program used are described in Appendix II. The observed relative intensities, listed in Table 3.2, were measured as peak heights and as areas of peaks on a microdensitometer trace of CuK_α photographs, one of which is shown in Figure 3.2. The observed and the calculated diffraction intensities, Table 3.2, compare very well and support the above structure for the heavy atoms.

The positions of the hydrogen atoms have not been considered, and the eight oxygen atoms per unit cell occupy sites of C_3 symmetry, which is higher than the C_{2v} symmetry of a water molecule. This is only possible if the water molecules are orientationally disordered, such that on the average the hydrogen atoms can also be related by C_3 symmetry. The four ammonia molecules are on C_3 sites, and if this is applicable for the hydrogen atoms,

one expects for $\nu_3(NH_3)$ two infrared active modes, 2F, under unit cell group T^4, Table 5.3. As shown in Figure 3.23 a triplet was observed for $\nu_3(NH_3)$. This means that the cubic structure does not apply to the hydrogen atoms in ammonia dihydrate. Further, the isolated stretching vibrations, $\nu_{NH}(ND_2H)$ or $\nu_{ND}(NH_2D)$, yield a triplet, Figure 3.31, which indicates that the three N-H...O bonds are non-equivalent so the ammonia molecules must occupy sites of symmetry C_1 and the space group cannot be the cubic $P2_13$. If one removes the C_3 symmetry elements from the $P2_13$ space group, one obtains the orthorhombic space group $P2_12_12_1$, in which the oxygen and nitrogen atoms can occupy the general positions (x, y, z); (0.5+x, 0.5-y, $\bar{z}$); $\bar{x}$, 0.5+y, 0.5-z); (0.5-x, $\bar{y}$, 0.5+z),[27] obtained by slight distortion of the $P2_13$ structure. Thus ammonia dihydrate probably crystallizes in the space group $P2_12_12_1$ in the structure obtained by a slight orthorhombic distortion of the $P2_13$ structure with a = 7.12 Å; $x_{O_I} = 0.711$, $x_{O_{II}} = 0.141$, and $x_N = 0.364$. The validity of these structures will be further discussed in the next sections.

5.3 The NH and ND Stretching Vibrations

The isolated NH stretching vibrations appear as a triplet at 3363, 3352 and 3346 cm^{-1}, Figure 3.31, thus indicating the existence of three different NH bonds. The isolated ND stretching vibrations also appear as a triplet at 2476.2, 2470.5 and 2462.7 cm^{-1}, Figure 3.31. So, the ammonia molecules cannot be on sites of symmetry C_3 and the space group $P2_13(T^4)$ is not the correct one at least for the hydrogen atoms in ammonia dihydrate. The cubic space group, $P2_13$, with C_3 removed is the orthorhombic space group $P2_12_12_1(D_2)$, which is probably the correct space group for ammonia dihydrate.

Further, the factor group analysis, Table 5.4, yields one infrared active mode, E, for $\nu_3(NH_3)$ under the cubic site symmetry C_3, or two infrared active modes, 2F, under the cubic unit cell group, T. However, a triplet is observed for $\nu_3(NH_3)$ stretching vibrations at 3404.0, 3396.3 and 3391.2 cm^{-1}, Figure 3.23, and the corresponding absorption by $\nu_3(ND_3)$ is observed at 2535.5, 2529.8 and 2525.1 cm^{-1}, Figure 3.33. This confirms the above conclusion that the vibrations of the ammonia molecules are not according to T selection rules, Table 5.4. However, the infrared D_2 selection rules, Table 4.1, predict six components of $\nu_3(NH_3)$ or $\nu_3(ND_3)$. It is possible that these six components, $2B_1 + 2B_2 + 2B_3$, under

Table 5.4 Correlation table for ammonia molecules in the pseudo-structure of ammonia dihydrate.[a]

Free Molecule	Molecular Group	Site Group	Unit Cell Group	Activity[b]
NH_3	C_{3v}	C_3	T	
ν_1, ν_2, T_z	A_1	A	A	R
ν_3, ν_4, (R_x, R_y) (T_x, T_y)	E	E	E	R
			F	R,IR
R_z	A_2			

[a] The space group $P2_13$ (T^4).

[b] R, Raman active mode; IR, Infrared active mode.

unit cell group D_2 are not resolved and are combined to form a resultant three components or, as in the case of ammonia monohydrate, Section 4.2, that some of these components have very weak infrared intensities for unknown reasons.

As in the case of ammonia monohydrate, Section 4.3, only the intramolecular interactions are considered in the normal coordinate calculations of the antisymmetric, ν_3, and the symmetric, ν_1, stretching vibrations of ammonia (Table 5.5). Again as in the case of ammonia monohydrate, the off-diagonal force constants were chosen to be ~-0.04 and ~-0.07 mdyne A^{-1} in $NH_3 \cdot 2H_2O$ and $ND_3 \cdot 2D_2O$, respectively. The diatomic simple harmonic approximation was used to obtain the diagonal force constants for $\nu_{NH}(ND_2H)$, 6.2643, 6.2234, and 6.2011 mdyne A^{-1}, and those for $\nu_{ND}(NH_2D)$ are calculated at 6.3605, 6.3312 and 6.2913 mdyne A^{-1} (Table 5.5). These calculations indicate that the antisymmetric stretching vibrations ν_{3a} and ν_{3b} are expected at 3402.6 and 3392.1 cm^{-1} for NH_3 and at 2534.2 and 2526.3 cm^{-1} for ND_3, provided only intramolecular interactions are considered. The triplet observed at 3404.0, 3396.3 and 3391.2 cm^{-1} for $\nu_3(NH_3)$ and at 2535.5, 2529.8, and 2525.1 cm^{-1} for $\nu_3(ND_3)$ indicate, as in the case of $\nu_3(NH_3)$ and $\nu_3(ND_3)$ of ammonia monohydrate, that the effect of intermolecular interactions cannot be neglected in ammonia dihydrate.

Table 5.5 Normal coordinate calculations of ammonia dihydrate stretching frequencies of NH_3 and ND_3.

a) $\underline{NH_3}$

$\nu_{NH}(ND_2H)$ 3363, 3352 and 3346 cm^{-1}

$f_{11} = 6.2643$, $f_{22} = 6.2234$ and $f_{33} = 6.2011$ mdyne A^{-1}
$G_{11} = G_{22} = G_{33} = \mu_N + \mu_H = 1.06365$ amu^{-1}
$G_{12} = G_{13} = G_{23} = \mu_N \cos\phi = -0.02183$ amu^{-1}
$\phi = 107.8°$

$f_{12} = f_{23} = f_{13} =$	0	-0.04	-0.07
ν_{3a}	3391.9	3402.6	3410.7
ν_{3b}	3381.2	3392.1	3400.2
ν_1	3282.1	3261.0	3245.1

For $f_{12} = -0.04$ the eigenvectors are:

$$L = \begin{array}{c} \begin{matrix} \nu_{3a} & \nu_{3b} & \nu_1 \end{matrix} \\ \begin{bmatrix} 0.8704 & 0.1087 & -0.5426 \\ -0.4791 & 0.6846 & -0.5883 \\ -0.3137 & -0.7793 & -0.6162 \end{bmatrix} \end{array}$$

One column of L is $(\partial R_i/\partial Q_k)_{\substack{i=1\to3 \\ k=\text{constant}}} = L_{ik}$, $i=1\to3$

b) $\underline{ND_3}$

$\nu_{ND}(NH_2D)$ 2476.2, 2470.5 and 2462.7 cm^{-1}

$f_{11} = 6.3605$, $f_{22} = 6.3312$ and $f_{33} = 6.2913$ mdyne A^{-1}
$G_{11} = G_{22} = G_{33} = \mu_N + \mu_D = 0.56794$ amu^{-1}
$G_{12} = G_{13} = G_{23} = \mu_N \cos\phi = -0.021593$ amu^{-1}
$\phi = 107.6°$

$f_{12} = f_{23} = f_{13} =$	0	-0.04	-0.07
ν_{3a}	2520.4	2528.3	2534.2
ν_{3b}	2512.5	2520.4	2526.3
ν_1	2373.8	2358.8	2347.5

The symmetrical stretching vibration of ammonia, ν_1, is calculated at 3261 cm^{-1} in $NH_3 \cdot 2H_2O$ and at 2347.5 cm^{-1} in $ND_3 \cdot 2D_2O$ (Table 5.5). $\nu_1(NH_3)$ and $\nu_1(ND_3)$ are expected to be in Fermi resonance with $2\nu_4(NH_3)$ and $2\nu_4(ND_3)$, respectively, and the resultant absorptions may contribute to the strong OH and OD stretching vibrations, Figures 3.22 and 3.33, respectively.

5.4 Water Stretching Vibrations

The assignments of water stretching vibrations are made with reference to those of ammonia monohydrate (Chapter 4), ammonia hemihydrate[6,7,13] and the ices.[72,73] The infrared spectra of isolated OH and OD bonds in $ND_3 \cdot 2D_2O$ and $NH_3 \cdot 2H_2O$, respectively, Figure 3.31, reveal two types of water molecules in ammonia dihydrate, as in the proposed structure (Section 5.2). In this structure, there are four O_{II}-H...N bonds, four O_{II}-H...O bonds and two similar sets of four O_I-H...O_{II} bonds per unit cell. Hence the ν_{OH}(HOD) of O_I-H...O_{II} should be more intense than those of O_{II}-H...O_I. The two sets of O_I-H...O_{II} are similar, their lengths in the proposed $P2_13$ parent structure are identical, and they are both assigned to the stronger of the two O-H...O absorptions of HOD, at 3240 cm^{-1} (2396 cm^{-1} for O_I-D...O_{II}), Figure 3.31 and Table 5.6). The bands at 3275 and 2425 cm^{-1} are assigned

Table 5.6 Infrared spectral assignments of $NH_3 \cdot 2H_2O$ and $ND_3 \cdot 2D_2O$.

$NH_3 \cdot 2H_2O$[a,b] ν/cm^{-1}	$ND_3 \cdot 2D_2O$[a,b] ν/cm^{-1}	Ratio[a] ν_H/ν_D	Assignment[c]
	~5032		
	~4833		
	~4599		
5019.7(8)	3721(1)	1.349(2)	$(\nu_3+\nu_4)$(a)
~4950	~3678	1.35(1)	
~4830	~3610	1.34(1)	
	~3467		
4521.1(9)	3395(2)	1.332(2)	$(\nu_3+\nu_2)$(a)
2527(2)*	~3393**	1.343(5)	$\nu_{ND}(ND_2H)$ or
2523(2)*		1.345(5)	$\nu_{NH}(NH_2D)$
~4424			
~4375			
2476.2(5)*	3363(2)*	1.358(2)	$\nu_{ND}(NH_2D)$
2470.5(5)*	3352(2)*	1.357(2)	or
2462.6(6)*	3346(2)*	1.359(2)	$\nu_{NH}(ND_2H)$
2425(2)*	3275(2.5)*	1.351(3)	$\nu_{O_{II}-H(D)\ldots O_I}(HOD)$
2396(2)*	3240(3)*	1.352(3)	$\nu_{O_I-H(D)\ldots O_{II}}(HOD)$
	~3110		overtone or combination modes
	~3073**		
	~3010*		
	~2830		
2122(6)**	2763(5)*	1.302(6)	$\nu_{O_{II}-H(D)\ldots N}(HOD)$
~2010*			
3404.0(5)	2535.5(5)	1.343(1)	
3396.3(4)	2529.8(5)	1.343(1)	ν_3(a)
3391.2(9)	2525.1(7)	1.343(1)	
~3298	~2466	1.34(1)	
3207(5)	2424(3)	1.323(4)	$\nu_{O-H(D)\ldots O}(w)$
	2411(2)	1.330(4)	
	~2350		$2\nu_2(D_2O)$?
3150(4)	2330(3)	1.352(3)	$\nu_{O-H(D)\ldots O}(w)$
	~2182		
2803(6)	2113(5)	1.327(5)	$\nu_{O_{II}-H(D)\ldots N}(w)$

(Continued)

Table 5.6 (Continued)

$NH_3 \cdot 2H_2O$[a,b] ν/cm^{-1}	$ND_3 \cdot 2D_2O$[a,b] ν/cm^{-1}	Ratio[a] ν_H/ν_D	Assignment[c]
	1864(5)*		
2319(5)	~1700	1.36(1)	
	1670(3)		$\nu_2(w) + \nu_R(w)$
~2200	~1625	1.35(1)	
~2150			
~2103			
	~1505*		$\nu_2(HO_{II}D)$
	1466(2)*		$\nu_2(HO_ID)$
1898(4)	1412(4)	1.344(7)	$\nu_2(a) + \nu_R(w)$
	1413(3)**		$\nu_2(HO_ID)$
1840(3)	~1360	1.35(1)	$\nu_2(a) + \nu_R(w)$
~1697	~1233	1.38(1)	$\nu_2(w)$
1649.2(5)	1205.3(5)	1.368(1)	$\nu_4(a)$
~1631	~1195	1.36(1)	$\nu_4(a)$ or $\nu_2(w)$
~1601*	~1250*	1.28(1)	$\nu_4(NH_2D)/\nu_4(ND_2H)$
1577(2)	~1166	1.35(1)	$\nu_2(w)$ or $\nu_R(w)+\nu_R(w)$
1505(4)	~1136	1.32(1)	$\nu_R(w)+\nu_R'(w)$
~1361			$\nu_R(w)+\nu_R'(w)$
~1279	~ 966	1.32(1)	$\nu_R(w)+\nu_R'(w)$
1231(2)	942(1)	1.31(1)	$2\nu_R(w)$
	~ 968*		$\nu_2(ND_2H)$ or O/C
1041*	942(1)*	1.11(1)	$\nu_2(NH_2D)/\nu_2(ND_2H)$
~1150	~ 890	1.29(1)	$\nu_R(w)+\nu_R'(w)$
115.9(7)	859.1(5)	1.299(2)	$\nu_2(a)$
	824(2)*		ν_R(HOD) mainly
	812(3)*		of OH
986(2)	722(2)	1.366(4)	
900(2)	664(2)	1.355(7)	
~ 838	~ 614	1.36(2)	
766(3)	562(3)	1.363(5)	$\nu_R(w)$
~ 684	~ 518	1.32(2)	
633(1)	461(1)	1.373(5)	
~ 614	~ 446	1.38(2)	
~ 560	~ 410	1.37(2)	

(Continued)

Table 5.6 (Continued)

$NH_3 \cdot 2H_2O$[a,b] ν/cm^{-1}	$ND_3 \cdot 2D_2O$[a,b] ν/cm^{-1}	Ratio[a] ν_H/ν_D	Assignment[c]
554(2)*			ν_R(HOD) mainly of O-D
~ 541*			
532(2)*			
~ 342*	342(3)**		$\nu_R(NHD_2)/\nu_R(ND_2H)$
~ 450	~ 343	1.31(3)	ν_R(a)
415.7(6)	316(1)	1.315(6)	
391(2)	~ 285	1.37(1)	
~ 373		1.31(2)	
297	~ 275	1.08(2)	ν_T
283(1)	264(2)	1.072(12)	
~ 239	~ 231	1.03(2)	
235.0(15)	223(1)	1.054(11)	

[a] The numbers in parentheses are the 95% confidence limits in the last digit.

[b] The wavenumbers with asterisk (*) are of H or D impurities in $ND_3 \cdot 2D_2O$ or $NH_3 \cdot 2H_2O$, respectively. (**) means it is due to both the neat compound and H or D impurities.

[c] a ≡ NH_3 or ND_3; w = H_2O or D_2O; O/C = overtone or combination modes. The features that are left unassigned are probably due to overtone or combination modes.

to $\nu(O_{II}\text{-}H\ldots O_I(HO_{II}D))$ and $\nu(O_{II}\text{-}D\ldots O_I(HO_{II}D))$, respectively (Figure 3.31 and Table 5.6). The spectra-structure correlations, Section 5.2 and Table 5.3, predict that the $O_I\ldots O_{II}$ distances for $O_I\text{-}H(D)\ldots O_{II}$ and $O_{II}\text{-}H(D)\ldots O_I$ to be close to 2.76 Å. The isolated stretching vibration of $O_{II}\text{-}H\ldots N$ is assigned, parallel to that of ammonia monohydrate, to the band at 2763 cm^{-1}, Figure 3.35. Similarly, the $O_{II}\text{-}D\ldots N$ stretching vibration is assigned the band at 2122 cm^{-1}, Figure 3.27. The spectra-structure correlation, Section 5.2 and Table 5.3, predicts an $O_{II}\ldots N$ distance of 2.74 ± 0.2 Å. This indicates a very strong hydrogen bond between type II water and the nitrogen atom in ammonia dihydrate.

The full-width at half-height of the isolated $\nu(O_{II}\text{-}H\ldots N(HOD))$ band is ~100 cm^{-1} and is approximately twice that of each isolated $\nu_{O\text{-}H\ldots O}$ band, Figure 3.35. A strong $O_{II}\text{-}H\ldots N$ hydrogen bond means that the $O_{II}\text{-}H$ bond is longer and the $H\ldots N$ bond is shorter than for weaker hydrogen bonds, so the $O_{II}\text{-}H$ vibrations are largely affected by the $H\ldots N$ vibrations. A high degree of anharmonicity that allows the $O\text{-}H\ldots N$ fundamental vibrational level to interact with overtone and combination levels is the probable cause of the broadness. The isolated $\nu(O_{II}\text{-}D\ldots N)$ band is found to be surprisingly broad and weak, Figure 3.27, compared to

$\nu(O_{II}\text{-}H...N)$, Figure 3.35. The band due to $\nu(O_{II}\text{-}D...N(HOD))$ sits on top of the H_2O combination band and near $2\nu_2$ of NH_3. Again anharmonic interaction probably is the cause of the great breadth, specifically interaction with the above named levels which cannot occur for $\nu_{OH}(HOD)$. Usually ν_{OD} is sharper than ν_{OH}. Thus a mechanism that is specific to ν_{OD} must be the cause of the unusual breadth of $\nu(O_{II}\text{-}D...N(HOD))$.

The bands due to the stretching vibrations of the isolated O-H...O and O-H...N bonds in ammonia monohydrate have full-widths at half-heights of 30 and 55 cm^{-1}, respectively, thus sharper than those of ammonia dihydrate. The O-H...O bonds in both compounds have O...O distances of ~2.76 Å. So, the broader bands of $\nu_{O\text{-}H...O}$ in ammonia dihydrate spectra are possibly evidence of disorder in the orientation of the water molecules in the dihydrate.

As in the case of ammonia monohydrate, Tables 4.6 and 4.7, the intramolecular coupling for type II water in ammonia dihydrate is found to be negligible, Tables 5.7 and 5.8, due to the large separation between the $O_{II}\text{-}H(D)...O_I$ and $O_{II}\text{-}H(D)...N$ stretching frequencies. The intramolecular coupling for type I water yields two frequencies symmetrical about the isolated $O_I\text{-}H$ or $O_I\text{-}D$ frequency and are separated by 63 or 87 cm^{-1},

Table 5.7 O-H stretching frequencies of ammonia dihydrate.

	$\nu_{O_{II}-H\ldots O_I}$	$\nu_{O_I-H\ldots O_{II}}$	$\nu_{O_{II}-H\ldots N}$
Observed for isolated HOD	3275	3240	2763
Calculated f_{rr}/mdyne A^{-1}	5.9908	5.8635	4.2641
Observed for coupled H_2O	3298	3207, 3150	2803

Calculated for Intramolecular coupled H_2O, $f_{rr'} = 0$, $\alpha = 109°$ (or 104.5°)*

H_2O_I		
$f_{rr} = f_{r'r'} =$ 5.86350 mdyne A^{-1}	3271 (3264)	3208 (3216)
H_2O_{II}		
$f_{rr} = 5.9909$, $f_{r'r'} = 4.2641$ mdyne A^{-1}	3276 (3276)	2761 (2762)

*The wavenumbers in parentheses correspond to the calculated frequencies if $\alpha = 104.5°$.

Table 5.8 O-D stretching frequencies of deuterated ammonia dideuterate.

	$\nu_{O_{II}-D\cdots O_I}$	$\nu_{O_I-D\cdots O_{II}}$	$\nu_{O_{II}-D\cdots N}$
Observed for isolated HOD	2425	2396	2122
Calculated fr/mdyne $Å^{-1}$	6.1972	6.0499	4.7453
Observed for coupled D_2O	2466 2424	2411 2330	2113

Calculated for intramolecular coupled D_2O, $f_{rr'} = 0$, $\alpha = 109°$ (or 104.5°)*

D_2O_I

$f_{rr} = f_{r'r'} =$ 6.0499 mdyne $Å^{-1}$	2438 (2428)	2351 (2361)

D_2O_{II}

f_{rr} = 6.1972 $f_{r'r'}$ = 4.7453 mdyne $Å^{-1}$	2429 (2427)	2115 (2117)

*The wavenumbers in parentheses correspond to the calculated frequencies if $\alpha = 104.5°$.

respectively, for an HOH angle of 109° (Tables 5.7 and 5.8). The diagonal force constants are the same for the two O_I-H bonds and equal to 5.8635 mdyne A^{-1} for H_2O_I and 6.0499 mdyne A^{-1} for D_2O_I. The off-diagonal force constant, $f_{rr'}$ was taken to be zero, Tables 5.7 and 5.8.

As mentioned in Section 5.2 the water molecules in ammonia dihydrate cannot occupy sites of symmetry C_3, dictated by space group $P2_13$, unless the water molecules are orientationally disordered. If ammonia dihydrate crystallizes in space group $P2_12_12_1$, the water molecules occupy sites of symmetry C_1 and the correlation table for the water vibrations under unit cell group D_2 is the same as in Table 4.1. Accordingly, the antisymmetric and symmetric stretching vibrations are each expected to have three infrared active components, B_1, B_2 and B_3, under unit cell group D_2. The bands at 2803 and 2113 cm^{-1} can be easily assigned to O_{II}-H...N and O_{II}-D...N, stretching vibrations, respectively, all three unit cell group modes presumably overlapping. However, possible disorder may invalidate all selection rules of intermolecularly coupled O-H...O vibrations and even if this is not the case one does not have the evidence to assign the peaks and shoulders observed to specific unit cell group modes.

Thus, the bands at 3298, 3207, 3150 and 2803 cm^{-1} in the spectrum of $NH_3 \cdot 2H_2O$, Figure 3.22, are assigned to

intermolecularly coupled OH stretching frequencies of H_2O_I and H_2O_{II}. Similarly, the bands at 2466, 2424, 2411, 2330 and 2113 cm^{-1} in the spectrum of $ND_3 \cdot 2D_2O$, Figure 3.32, are assigned to coupled OD stretching frequencies of D_2O_I and D_2O_{II}.

5.5 Intramolecular Angle Deformation Vibrations

The antisymmeteric angle deformation vibration of ammonia, ν_4, and the bending modes of water, ν_2, are expected to absorb in the same spectral region. The antisymmetric angle deformation of ammonia, ν_4, has six infrared active components under the D_2 unit cell group, $2B_1 + 2B_2 + 2B_3$ (Table 4.1). However, only two infrared active components of ν_4, 2F, are expected under the $P2_13$ parent structure. The sharp bands at 1649.2 cm^{-1} in the spectrum of $NH_3 \cdot 2H_2O$, Figure 3.24, and at 1205.3 cm^{-1} in the spectrum of $ND_3 \cdot 2D_2O$, Figure 3.42, are assigned to ν_4 of NH_3 and ND_3, respectively (Table 5.6). Also, the shoulder at ~1631 cm^{-1} in the spectrum of $NH_3 \cdot 2H_2O$ and that at ~1195 cm^{-1} in the spectrum of $ND_3 \cdot 2D_2O$ are slightly merged in the spectra of partially deuterated and partially hydrogenated samples with the sharp bands due to ν_4, Figure 3.28. This indicates that the shoulders are intermolecularly coupled with the sharp bands and they might be also due to ν_4. However, it is not possible to

assign the bands to specific unit cell group components other than to speculate that ν_4 might follow $P2_13$ selection rules. So the two bands at 1649.2 and ~1631 cm^{-1} ($NH_3 \cdot 2H_2O$) and those at 1205.3 and ~1195 cm^{-1} ($ND_3 \cdot 2D_2O$) might be the two F modes expected for ν_4 under this group, Table 5.4. The bands at 1601 and 1250 cm^{-1} in the spectra of the partially deuterated and partially hydrogenated compounds, Figure 3.28, can be assigned to $\nu_4(NH_2D)$ and $\nu_4(ND_2H)$, respectively (Table 5.6).

The bands assigned to water bending modes are obtained from the harmonic ratios of ν_2 in H_2O, HOD and D_2O, ~1.36:1.20:1, and the observed HOD bending frequencies. The hydrogen atoms of type II water in ammonia dihydrate form bonds to one oxygen atom and one nitrogen atom, Figure 5.2, as is the case for water in ammonia monohydrate, except that the O-H...N bonds are longer in case of ammonia monohydrate, Table 5.3. So, the sharp band at 1466 cm^{-1} in the spectrum of the partially hydrogenated $ND_3 \cdot 2D_2O$, Figure 3.43, is probably due to $\nu_2(HO_{II}D)$, being close to the 1467 cm^{-1} frequency of $\nu_2(HOD)$ of ammonia monohydrate, Table 4.10. The hydrogen bonds formed by type II water molecules are stronger than those formed by type I water in ammonia dihydrate, which suggests that the band at 1413 cm^{-1} in the spectrum of partially hydrogenated $ND_3 \cdot 2D_2O$, Figure 3.42, is probably

due to $\nu_2(HO_ID)$. The weak feature at ~1505 is too high for ν_2(HOD) which has been found[92] for 40 compounds to absorb in the range 1470 to 1402 cm^{-1}. The $\nu_2(H_2O_{II})$ and $\nu_2(D_2O_{II})$ frequencies are thus expected to be near 1661 and 1222 cm^{-1}, repectively, so these modes probably cause the absorptions at ~1697 and ~1233 cm^{-1}, Figure 3.28. Also, $\nu_2(H_2O_I)$ and $\nu_2(D_2O_I)$ are expected to be near 1601 and 1178 cm^{-1}, respectively. Thus, the absorptions at ~1631 or 1577 cm^{-1} in $NH_3 \cdot 2H_2O$ and ~1195 or 1166 cm^{-1} in $ND_3 \cdot 2D_2O$, Figure 3.28, can be assigned to $\nu_2(H_2O_I)$ and $\nu_2(D_2O_I)$, respectively. These values of $\nu_2(H_2O)$ and $\nu_2(D_2O)$ lie in the range 1582 to 1721 cm^{-1} and 1171 to 1248 cm^{-1}, respectively, found[92] from reported values of $\nu_2(H_2O)$ and $\nu_2(D_2O)$ in a large range of compounds. However, the overtones and combinations of water rotational vibrations are also expected to absorb in this region, Table 5.6, and may be more intense than the water bending mode, so these assignments are necessarily tentative.

The weak bands at ~1505, 1466 and 1413 cm^{-1} in the partially hydrogenated $ND_3 \cdot 2H_2O$ are probably obscured in the spectra of partially deuterated $NH_3 \cdot 2H_2O$ by the bands at 1505 and 1361 cm^{-1} which are broader in the spectra of the partially deuterated compound than in those of the neat compound.

The symmetric angle deformation vibration of ammonia, ν_2, is expected to yield a triplet under the D_2 unit cell group due to the unit cell components of symmetries B_1, B_2 and B_3. However, ν_2 is expected to yield a singlet due to the F component under the $P2_13$ parent structure. Only one major band is observed, at 1115.9 and 859.1 cm^{-1} due to $\nu_2(NH_3)$ and $\nu_2(ND_3)$, respectively (Figures 3.25 and 3.43). However, these bands are unusually broad at the base, which could indicate the presence of more than one component of ν_2, but probably indicates the existence of anharmonic intermolecular interaction with overtones of water rotations. Thus, the shoulder at ~1150 cm^{-1} in the spectrum of $NH_3 \cdot 2H_2O$ at 100K is shifted to lower frequency, to ~1098 cm^{-1} at 150K, Figure 3.25, which is the behavior expected of overtone or combination transitions of water rotational vibrations. The intensity of these overtones or combination modes is probably enhanced by anharmonic interaction with ν_2 fundamental. Thus, ν_2 might follow $P2_13$ selection rules, so that the observed band is the F mode expected under this space group.

The band at 1041 cm^{-1} in the spectra of partially deuterated $NH_3 \cdot 2H_2O$, Figure 3.29, which correspond to the absorption at 1035 cm^{-1} in the spectrum of 5% H in $ND_3 \cdot 2D_2O$, Figure 3.43, is assigned to $\nu_2(NH_2D)$, which

agrees with the 1024 cm^{-1} frequency calculated[7] using data of ammonia hemihydrate. The absorptions at ~968 and 942 cm^{-1} in the spectrum of partially hydrogenated $ND_3 \cdot 2D_2O$, Figure 3.43, are assigned to ND_2H. However, the shoulder at ~968 cm^{-1} is much weaker and might be due to an overtone or combination transition, thus leaving the sharp band at 942 cm^{-1} to be due to $\nu_2(ND_2H)$ agreeing with the frequency near 928 cm^{-1} calculated using data of ammonia hemihydrate. The bands at ~968 and 942 cm^{-1} are obscured in the spectra of partially deuterated compound due to the strong absorption by the water rotational vibrations at 986 and 900 cm^{-1}.

5.6 Lattice Vibrations

The assignments of the rotational and translational vibrations are made by analogy with those of solid ammonia[42,43,46,68-71] and ice,[72,73] and the most recent assignments of ammonia hemihydrate.[13] Each kind of water in ammonia dihydrate is expected to yield nine infrared active rotational modes $3B_1$, $3B_2$ and $3B_3$ under the D_2 unit cell group, Table 4.1. The absorptions between ~1000 cm^{-1} and 560 cm^{-1} in the spectrum of $NH_3 \cdot 2H_2O$, Figure 3.25, and those between ~800 cm^{-1} and ~400 cm^{-1} in the spectrum of $ND_3 \cdot 2D_2O$, Figure 3.43, are assigned to these rotational vibrations of water by analogy with the proven assignments

of hemihydrate's spectrum.[13] These bands due to the rotational vibrations of water in ammonia dihydrate are much broader than those of the monohydrate or hemihydrate. This suggests the influence of the possible disorder in the orientations of the water molecules in ammonia dihydrate. On the other hand, the water molecules in the dihydrate are far more interconnected than are those of the monohydrate and hemihydrate. It is known that the rotational vibrations in ordered lattices of interconnected water molecules (in ices II and IX)[37,38] yield broad absorption with sharp features superimposed, the sharp features broadening when isotopic impurity is present. This broadening when deuterium is present is observed for $NH_3 \cdot 2H_2O$, Figure 3.29. Thus the increasing breadth in the rotational-vibration bands of water as one goes from the hemihydrate to the monohydrate to the dihydrate may well be due to increasing intermolecular coupling between the rotational modes, rather than to disorder. The sharper bands in the hemihydrate spectra are probably because the water molecules in ammonia hemihydrate are not interconnected as those in ammonia monohydrate and dihydrate.

The bands at 824 and 812 cm^{-1} in the partially hydrogenated $ND_3 \cdot 2D_2O$, Figure 3.43, are assigned to the rotational vibrations of HOD which mainly involve movement of the hydrogen atom. These bands are obscured in the

partially deuterated $NH_3 \cdot 2H_2O$ by $\nu_R(H_2O)$. The bands at 554, 541 and 532 cm^{-1} in the spectra of partially deuterated $NH_3 \cdot 2H_2O$, Figure 3.30, can be assigned to the rotational vibrations of HOD which mainly involve movement of the deuterium atom. These weak bands are obscured by bands due to $\nu_R(D_2O)$ in the partially hydrogenated $ND_3 \cdot 2D_2O$.

The rotational vibrations of ammonia in ammonia dihydrate are expected to give rise to nine infrared active modes of symmetries $3B_1$, $3B_2$ and $3B_3$ under the D_2 unit cell group, Table 4.1. Under the $P2_13$ parent structure only three rotational modes, 3F, are expected. The absorptions at ~450, 415.7, 491 and ~373 cm^{-1} in the spectrum of $NH_3 \cdot 2H_2O$, Figure 3.30, and those at ~343, 316 and ~285 cm^{-1} in the spectrum of $ND_3 \cdot 2D_2O$, Figure 3.44, can be assigned to $\nu_R(NH_3)$ and $\nu_R(ND_3)$ modes, respectively (Table 5.6). The absorption at ~342 cm^{-1} in the spectra of partially hydrogenated $ND_3 \cdot 2D_2O$, Figure 3.44, and a very weak absorption near 350 cm^{-1} in the spectra of partially deuterated $NH_3 \cdot 2H_2O$, Figure 3.30, are probably due to rotational vibrations of NHD_2 and NH_2D.

The bands due to translational vibrations are assigned using the isotopic frequency ratios, Table 5.6, which are about 1.08 and 1.05 under the harmonic approximation for $\nu_T(NH_3)/\nu_T(ND_3)$ and $\nu_T(H_2O)/\nu_T(D_2O)$,

respectively. A complete assignment of the translational vibrations cannot be made because the region has not been completely covered. However, the absorptions at 297, 283, ~239 and 235.0 cm^{-1} in the spectrum of $NH_3 \cdot 2H_2O$, Figure 3.30, and those at ~275, 264, ~231 and 223 cm^{-1} in the spectrum of $ND_3 \cdot 2D_2O$, Figure 3.44, are assigned to the hydrogen bond stretching vibrations of the $O_{II}...N$, and possibly the O...O bonds (Table 5.6).

The absorptions due to translational modes are broader for ammonia dihydrate, Figures 3.30 and 3.44, than those for ammonia monohydrate, Figure 3.14, which could be an indication of disorder in the structure of ammonia dihydrate.

All features which have not been discussed in the previous sections are due to overtone and/or combination bands and their tentative assignments are listed in Table 5.6.

CHAPTER 6

CONCLUSION

In this work, the dihydrate of ammonia has been isolated. Its crystal structure is deduced from powder x-ray diffraction pattern and infrared spectra. The heavy atoms of ammonia dihydrate form a cubic primitive unit cell $P2_13$, which is supported by the calculated diffraction intensities.

The spectral assignment of the ammonia dihydrate has been made as far as the spectral evidence and x-ray results allow. Two kinds of water molecules are suggested by the isolated OH and OD stretching vibrations. Water molecules of type I, which have two O-H...O bonds of lengths ~2.76 Å and water molecules of type II, which have one O-H...O bond of length ~2.76 Å and O-H...N bond of length 2.74 ± 0.02 Å.

The observation of three sharp bands for the isolated NH or ND stretching frequencies suggests a C_1 site symmetry for the ammonia molecules. Also, the water molecules cannot occupy sites of symmetry C_3 unless there is a disorder in the crystal. Therefore, the orthorhombic space group $P2_12_12_1$, which is a distortion of $P2_13$ if C_3

symmetries are replaced by C_1, is the possible space group of ammonia dihydrate.

There is no indication of crystal disorder from the mid-infrared spectra of ammonia dihydrate. The broad absorptions at the base of the coupled OH or OD stretching bands and at the base of the rotational vibration bands could be attributed to strong intermolecular coupling of the water network other than to disorder. However, a definitive indication of the disorder can be deduced from the region of translational lattice vibrations of water and ammonia. This region is not completely covered in this work, only to 200 cm^{-1}, and no indication of disorder exists in the spectra above 200 cm^{-1}. Raman spectra can also add more information about the ammonia dihydrate structure. However, a more definitive confirmation of the crystal structure should be obtained from x-ray of a single crystal of ammonia dihydrate.

A D_{2h} pseudo-symmetry in ammonia monohydrate crystal is used to explain the spectral features of ammonia monohydrate and its isotopomers. The mid-infrared spectrum of $NH_3 \cdot H_2O$ is slightly modified from that obtained by Morrison.[6] Observation of a triplet for ν_3 of ammonia instead of six unit cell components predicted under D_2, is explained by a D_{2h} pseudo-symmetry. Oriented gas model calculations gave the approximate relative

intensities of the unit cell components of the molecular vibrations.

The bands in the O-H stretching vibration region are explained to be due to intermolecular coupling, where intramolecular coupling is negligible. The sharp lines in the rotational and translational vibration region 800 to 200 cm^{-1} indicate that the monohydrate crystal is ordered. However, a possible disorder of the hydrogen atoms in the "O-H...O-H" chains, suggested by I. Olovsson and D.H. Templeton,[5] is not ruled out in this work. More definitive evidence of the disorder can be obtained from far-infrared and low-frequency Raman spectra.

The strong intermolecular coupling is evident in the spectra of ammonia monohydrate and dihydrate and is explained by the complicated network of hydrogen bonds in both compounds. Also, the surprising low frequencies of the O-H...N and O-D...N stretching vibrations in the spectra of both compounds indicate a very strong type of hydrogen bonding.

Finally, it is worth noting that a great deal can be learned about hydrogen bonding and the hydrates of ammonia from far-infrared and Raman spectra.

REFERENCES

1. S. Postma, Rec. trav. chim. pays-Bas 39, 515 (1920).
2. A.P. Rollet and G. Vuillard, C.R. Acad. Sci. 243, 383 (1956).
3. G. Vuillard, Ann. de Chim. Series 13 2, 233 (1957).
4. W.J. Siemons and D.H. Templeton, Acta Cryst. 7, 194 (1954).
5. I. Olovsson and D.H. Templeton, Acta Cryst. 12, 827 (1959).
6. J.E. Bertie and M.M. Morrison, J. Chem. Phys. 73, 4832 (1980).
7. J.E. Bertie and M.M. Morrison, J. Chem. Phys. 74, 4361 (1981).
8. G. Sill, U. Fink and J.R. Ferraro, J. Chem. Phys. 74, 997 (1981).
9. C. Thornton, M.S. Khatkale and J.P. Devlin, J. Chem. Phys. 75, 5609 (1981).
10. T. Huston, I.C. Hisatsune and J. Heicklen, Can. J. Chem. 61, 2077 (1982).
11. J.E. Bertie and J.P. Devlin, J. Chem. Phys. 78, 6203 (1983).
12. J.E. Bertie and J.P. Devlin, J. Chem. Phys. 79, 2092 (1983).

13. J.E. Bertie and J.P. Devlin, J. Chem. Phys. 81, 1559 (1984).

14. J.E. Bertie and M.R. Shehata, J. Chem. Phys. 81, 27 (1984).

15. D.L. Hildenbrand and W.F. Giauque, J. Am. Chem. Soc. 75, 2811 (1953).

16. F.F. Rupert, J. Am. Chem. Soc. 31, 866 (1909).

17. F.F. Rupert, J. Am. Chem. Soc. 32, 748 (1910).

18. A. Smits and S. Postma, Wisk en Natk. Afd. 18, 94, thru Chem. Zentr., I, 1217 (1910).

19. A. Smits and S. Postma, Verslag Akad. Wetenschapper 23, 110 (1914).

20. G. Baume and A. Tykociner, J. Chim. Phys. 12, 270 (1914).

21. L.D. Elliott, J. Phys. Chem. 28, 887 (1924).

22. K.E. Mironov, Zhur. Obshchei. Khim. 25, 1081 (1955).

23. M.M. Morrison, M.Sc. Thesis, University of Alberta (1980).

24. F. Freidrichs, Z. anorg. allgem. chem. 127, 228 (1923).

25. P.H.G. Van Kasteren, Bull. Inst. Int. Froid., Annexe. 4, 81 (1973).

26. R.D. Waldron and D.F. Hornig, J. Am. Chem. Soc. 75, 6079 (1953).

27. International Tables for X-Ray Crystallography, 2nd Edition, Vol. I, Edited by F. Henry and K. Lonsdale, T. Kynoch Press: Birmingham, 1965.

28. S. Eletr and C.T. O'Konski, J. of Chem. Phys. 54, 4312 (1971).

29. I. Olovsson and D.H. Templeton, Acta Cryst. 12, 832 (1959).

30. J.E. Bertie and E. Whalley, Spectrochim. Acta 20, 1349 (1964).

31. G.C. Pimentel and A.L. McClellan, "The Hydrogen Bond", Freeman: San Francisco, 1960, p. 87.

32. D. Hadzi and S. Bratos, in "The Hydrogen Bond", Recent Developments in Theory and Experiments, Edited by P. Schuster, G. Zundel and C. Sandorfy, North Holland: Amsterdam, 1976, Vol. 2, p. 575.

33. J.R. Scherer, "Advances in I.R. and Raman Spectroscopy, Edited by R.J.H. Clark and R.E. Hester, Heyden: London, 1979, Vol. 5, p. 149.

34. A. Novak, Struct. Bonding 18, 177 (1974).

35. B. Berglund, J. Lindgren and J. Tegenfeldt, J. Mol. Struct. 43, 179 (1978).

36. M. Falk and O. Knop, in "Water: A Comprehensive Treatise", Edited by F. Franks, Plenum: New York-London, 1973, Vol. 2, Chapter 2, p. 105.

37. F.E. Bates, Ph.D. Thesis, University of Alberta (1978).

38. J.E. Bertie and F.E. Bates, J. Chem. Phys. 67, 1511 (1977).

39. J.E. Bertie, Appl. Spectrosc. 22, 634 (1968).

40. J.E. Bertie, F.E. Bates and D.K. Hendrickson, Can. J. Chem. 53, 71 (1975).

41. P.A. Staats and H.W. Morgan, J. Chem. Phys. 31, 554 (1959).

42. F.P. Reding and D.F. Hornig, J. Chem. Phys. 19, 594 (1951).

43. F.P. Reding and D.F. Hornig, J. Chem. Phys. 22, 1926 (1954).

44. J.E. Bertie, H.J. Labbé and E. Whalley, J. Chem. Phys. 50, 5401 (1969).

45. W.S. Benedict, N. Gailar and E.K. Plyler, J. Chem. Phys. 24, 1139 (1956).

46. H. Wolff, H.-G. Rollar and E. Wolff, J. Chem. Phys. 55, 1373 (1971).

47. "Handbook of Chemistry and Physics", 55 edition, Edited by R.C. Weast, CRC Press, 1974-1975.

48. T.C. Waddington, "Non-Aqueous Solvent Systems", Academic Press: New York, 1965, p. 4.

49. Computer program written by S. Sunder in this laboratory.

50. R. Brill and A. Tippe, Acta Cryst. 23, 343 (1967).

51. K. Simpson, Ph.D. Thesis, University of Alberta, 1973.

52. J.E. Bertie, "Apodization and Phase Correction", in 'Analytical Applications of FT-IR to Molecular and Biological Systems', Edited by J.R. Durig, NATO Advanced Study Institutes Series, Series C, Volume 57, D. Reidel: Dordrecht, 1980.

53. P.R. Griffiths, C.T. Foskett and R. Curbelo, Applied Spectroscopy Reviews 6(1), 31 (1972).

54. R.J. Bell, "Introductory Fourier Transform Spectroscopy", Academic Press: New York, 1972.

55. D.C. Champeney, "Fourier Transforms and their Physical Applications", Academic Press, 1973.

56. P.R. Griffiths, "Chemical Infrared Fourier Transform Spectroscopy", Wiley: New York, 1975.

57. J.E. Bertie, "Energy-Limited Spectra", in 'Analytical Applications of FT-IR to Molecular and Biological Systems', Edited by J.R. Durig, NATO Advanced Study Institutes Series, Series C, Volume 57, D. Reidel: Dordrecht, 1980.

58. C.A. Anderson and D.R. Mattson, Proc. Soc. Photo-Opt. Instrum. Eng. 191, 101 (1979).

59. "IUPAC Tables of Wavenumbers for the Calibration of Infrared Spectroscopy", 2nd edition, compiled by A.R.H. Cole, Pergamon Press: New York, 1977.

60. E.W. Nuffield, "X-ray Diffraction Methods", Wiley and Sons Inc.: New York, 1966, pp. 107-111.

61. Ref. 27, Vol. III, p. 99.

62. E.B. Wilson, Jr., J.C. Decius and P.C. Cross, "Molecular Vibrations", McGraw-Hill: New York, 1955.

63. G. Turrell, "Infrared and Raman Spectra of Crystals", Academic Press: London, 1972.

64. J.C. Decius and R.M. Hexter, "Molecular Vibrations in Crystals", McGraw-Hill: New York, 1977.

65. L.A. Woodward, "Introduction to the Theory of Molecular Vibrations and Vibrational Spectroscopy", Oxford Univ. Press: London, 1972.

66. W.G. Fateley, F.R. Dollish, N.T. McDevitt and F.F. Bentley, "Infrared and Raman Selection Rules for Molecular and Lattice Vibrations: The Correlation Method", Wiley-Interscience: New York, 1972.

67. Ref. 63, Chapter 3.

68. F.P. Reding and D.F. Hornig, J. Chem. Phys. 23, 1053 (1955).

69. O.S. Binbrek and A. Anderson, Chem. Phys. Letters 15, 421 (1972).

70. A. Bromberg, S. Kimel and A. Ron, Chem. Phys. Letters 46, 262 (1977).

71. J.R. Ferraro, G. Sill and U. Fink, Applied Spectroscopy 34, 525 (1980).

72. J.E. Bertie and E. Whalley, J. Chem. Phys. 40, 1637 (1964).

73. M.S. Bergren, D. Schuh, M.G. Sceats and S.A. Rice, J. Chem. Phys. 69, 3477 (1978).

74. D.F. Hornig and D.C. McKean, J. Chem. Phys. 59, 1133 (1955).

75. J. Overend, in "Infrared Spectroscopy and Molecular Structure", Edited by M. Davies, Elsevier: Amsterdam, 1963, Chapter X.

76. Ref. 47, 62nd Edition, 1982-83, pp. B-256-257.

77. W.S. Benedict and E.K. Plyer, Can. J. Phys. 35, 1235 (1957).

78. A.W. Hewat and C. Riekel, Acta Cryst. A35, 569 (1979).

79. J.W. Reed and P.M. Harris, J. Chem. Phys. 35, 1730 (1961).

80. Ref. 47, 62nd Edition, 1982-83, p. D-166.

81. W.C. Hamilton and J.A. Ibers, "Hydrogen Bonding in Solids", W.A. Benjamin Inc.: New York, 1968, p. 212.

82. W.S. Benedict, N. Gailar and E.K. Plyler, J. Chem. Phys. 24, 1139 (1956).

83. J.E. Bertie and B.F. Francis, J Chem. Phys. 72, 2213 (1980).

84. C. Haas and D.F. Hornig, J. Chem. Phys. 32, 1763 (1960).

85. J.E. Bertie and J.P. Devlin, J. Phys. Chem. 88, 380 (1984).

86. J.E. Bertie, A.M. Heyns and O. Oehler, Can. J. Chem. 51, 2275 (1973).

87. M.V. Falk, Spectrochim. Acta 40A, 43 (1984).

88. Ref. 60, pp. 118-121.

89. H. Lipson and H. Steeple, "Interpretation of X-Ray Powder Diffraction Patterns", MacMillan and Co. Ltd.: New york, 1970, pp. 114-115, 120-123, 143-144.

90. L.V. Azaroff and M.J. Buerger, "The Powder Method in X-Ray Crystallography", McGraw-Hill: New York, 1958, pp. 61, 80-82, 84.

91. J.E. Bertie and M. Solinas, Can. J. Chem. 53, 2624 (1975).

92. M. Falk, Spectrochim. Acta 40A, 43 (1984).

93. International Tables for X-Ray Crystallography, 2nd Edition, Vol. I, Edited by F. Henry and K. Lonsdale, T. Kynoch Press: Birmingham, 1965, p. 385.

94. International Tables for X-Ray Crystallography, 2nd Edition, Vol. III, Edited by F. Henry and K. Lonsdale, T. Kynoch Press: Birmingham, 1965, p. 203.

APPENDIX I

DESCRIPTION OF THE OPERATING PARAMETERS USED

TO OBTAIN THE SPECTRA

1. The Nicolet Operating Parameters

Source: Globar coil

Beamsplitter: Germanium on potassium bromide

Detector: Mercury-cadmium Telluride, MCT

Resolution: 1 cm^{-1}

Region: 6000 to 400 cm^{-1}

Parameter	Value	Meaning
AFA	HG	Apodization function: Happ-Genzel
APT	FL	Source aperture: full, 6.35 mm diameter
COR	MD	Medium correlation test to check newly acquired interferograms against the signal averaged interferogram.
FIT	YS	Fit the plot or display curve between discrete data points. The data points are interpolated with a cubic spline algorithm.

Parameter	Value	Meaning
FSZ	22528	File size of data block on removable disk.
GAN	1 to 8	The base gain of the instrument applied before the filters.
HPS	1	Set the high and low pass filters roll-off frequencies to optimize
LPS	5	the signal-to-noise ratio: 3dB.
NPT	1024	Number of transform points used in phase calculation. The truncated interferogram specified by NPD was zero-filled to NPT prior to transformation.
NSB	500	Number of scans, i.e. interfero-
NSS	500	grams averaged before Fourier transformation for background and sample spectrum.
NSK	1200	Number of skipped points between white light and start of data collection.
NTP	32768	Number of transform points, i.e. 16384 zero-points were added to NDP before Fourier transformation.
PHZ	PH	Phase correction algorithm which computes the phase correction based on the real part of the transformation only.

Parameter	Value	Meaning
SGH	8	Switched gain for data beyond the 1024th point. Applied after the filters.
SGL	1	Switched gain for the first 1024 points. Applied after the filters.
SSP	2	Sample spacing determines how many zero-crossings of the laser will be skipped betwen each sampling point.
VEL	37	Velocity of the moving mirror of 0.783 cm s^{-1} ± 10% was used.

2. The Bruker Operating Parameters

6000 - 1200 cm^{-1}, region (1)

4000 - 400 cm^{-1}, region (2)

700 - 200 cm^{-1}, region (3)

Parameter	Value	Meaning
APF	HG	Apodization function: Happ-Genzel.
APT	3	Source aperture: full, 10 mm diameter.
BMS	1 (1) 4 (2) 2 (3)	Beamsplitter: Si on CaF_2, Ge on KBr, 3μ mylar were used for regions (1), (2) and (3), respectively.
COR	HI	high correlation.

Parameter	Value	Meaning
DTC	MI	deuterated triglycine sulphate, DTGS detector.
GSD	1024	Distance of gain switch from the start of the interferogram.
GSG	1	Signal amplifier gain for data beyond the 1024th point. GSG = 1, means no change in the gain.
HFQ	7000 (1) 5000 (2) 1900 (3)	The higher frequency limit of the computed spectrum to be saved in the disk.
HPF	6	High-pass electronic filter, set with 3dB point at 17 Hz.
LFQ	1000 (1) 300 (2) 0 (3)	The lower frequency limit of the computed spectrum to be saved in the disk.
LPF	1 (1) 1 (2) 4 (3)	Low-pass electronic filter, set with 3dB points at 12,500 Hz for regions (1) and (2), and set at 550 Hz for region (3).
NSR NSS	500 500	Number of scans, i.e. interferograms, averaged before Fourier transformation for background and sample spectrum.

Parameter	Value	Meaning
OPF	3 (1) 3 (2) 2 (3)	Optical filter: blank for regions (1) and (2), and black polyethylene filter for region (3).
PIP	512	The number of interferogram points used for phase correction.
PTS	2048	Controls the size of the Fourier transform used in phase correction.
RES	1	Spectral resolution.
SGN	-1	Main amplifier gain control. -1, the default value, the gain is automatically set by the computer. The normal values for this work are 2 to 4.
SMF	0	Smoothing function, SMF=0, means that the plotted spectrum is not smoothed.
SPZ	NO	Stored phase was not used and the phase angles were calculated from each interferogram.
SRC	MI	Globar source.
SSP	-1	sample spacing, controls the distance between sampling points. SSP=-1 means that the value used is

Parameter	Value	Meaning
		determined by the computer from HFQ and LFQ.
VEL	5 (1) 6 (2) 3 (3)	Velocity of moving mirror. Selected according to detector, 0.140, 0.166 and 0.099 cm s^{-1} for VEL=5, 6 and 3, respectively.
ZFF	2	Zero-filling factors. Allows spectral interpolation by adding zeros to the end of the interferogram. For ZFF=2, the effective file size is doubled before computation.

APPENDIX II

CALCULATIONS OF THE INTERATOMIC DISTANCES

The program DISTANCES reads the fractional coordinates of the atoms O_I, N and O_{II} in the structure of ammonia dihydrate and generates the atomic positions in 8 unit cells, i.e. for 8 × 12 = 96 atoms. It then calculates the interatomic distances between the atoms i and j:

$$R_{ij} = \left[(x(i)-x(j))^2 + (y(i)-y(j))^2 + (z(i)-z(j))^2\right]^{1/2}$$

The fractional coordinates were adjusted until a set of distances which agree with those deduced from the spectroscopic results were obtained.

The program DISTANCES is listed below and is applicable to the orthorhombic space group $P2_12_12_1$ (D_2) or the cubic space group $P2_13$ (T^4), if the heavy atoms are on the special position 4 a 3.

```
1     C    THIS IS A PROGRAM TO CALCULATE THE INTER-
2     C    ATOMIC DISTANCES FOR THE ORTHORHOMBIC SPACE
3     C    GROUP D2
4            DIMENSION X(100),Y(100),Z(100)
5            DIMENSION XAT(3),YAT(3),ZAT(3)
6            A=7.118
7            B=A/2.0
```

```
      DO 5 I=1,3
      READ(5,10) XAT(I),YAT(I),ZAT(I)
    5 CONTINUE
   10 FORMAT(3F5.4)
      DO 15 I=1,3
      WRITE(6,17) XAT(I),YAT(I),ZAT(I)
   15 CONTINUE
   17 FORMAT(2(F5.4,','),F5.4)
      DO 20 I=1,3
      XAT(I)=XAT(I)*A
      YAT(I)=YAT(I)*A
      ZAT(I)=ZAT(I)*A
   20 CONTINUE
C     CALCULATION OF THE ATOMIC COORDINATES
C      OF ATOMS 1 TO 12
      L=1
      DO 30 I=1,3
      X(L)=XAT(I)
      Y(L)=YAT(I)
      Z(L)=ZAT(I)
      X(L+1)=XAT(I)+B
      Y(L+1)=B-YAT(I)
      Z(L+1)=A-ZAT(I)
      X(L+2)=A-XAT(I)
      Y(L+2)=B+YAT(I)
      Z(L+2)=B-ZAT(I)
      X(L+3)=B-XAT(I)
      Y(L+3)=A-YAT(I)
      Z(L+3)=B+ZAT(I)
      L=L+4
   30 CONTINUE
C      OF ATOMS 13 TO 24
      DO 40 I=1,12
      X(L)=X(I)+A
      Y(L)=Y(I)
      Z(L)=Z(I)
      L=L+1
   40 CONTINUE
C      OF ATOMS 25 TO 36
      DO 50 I=1,12
      X(L)=X(I)
      Y(L)=Y(I)+A
      Z(L)=Z(I)
      L=L+1
   50 CONTINUE
C      OF ATOMS 37 TO 48
      DO 60 I=1,12
```

```
      X(L)=X(I)+A
      Y(L)=Y(I)+A
      Z(L)=Z(I)
      L=L+1
   60 CONTINUE
C      OF ATOMS 49 TO 96
      DO 70 I=1,48
      X(L)=X(I)
      Y(L)=Y(I)
      Z(L)=Z(I)+A
      L=L+1
   70 CONTINUE
      WRITE(6,31)
   31 FORMAT(6X,'ATOM',9X,'X',11X,'Y',11X,'Z')
      DO 32 I=1,96
      WRITE(6,33) I,X(I),Y(I),Z(I)
   32 CONTINUE
   33 FORMAT(8X,I2,7X,F7.3,2(5X,F7.3))
      WRITE(6,34)
   34 FORMAT(' DISTANCES LESS THAN 3.60A ')
      WRITE(6,35)
   35 FORMAT(6X,'ATOM',6X,'ATOM',6X,'DISTANCE')
C    CALCULATIONS OF INTERATOMIC DISTANCES
C    LESS THAN OR EQUAL TO 3.6 A
      DO 100 I=1,96
      DO 90 J=1,96
      IF(I-J) 80,90,90
   80 RSQUD=(X(I)-X(J))**2+(Y(I)-Y(J))**2
     -+(Z(I)-Z(J))**2
      R=SQRT(RSQUD)
      IF(3.6-R) 90,95,95
   95 WRITE(6,98) I,J,R
   90 CONTINUE
  100 CONTINUE
      STOP
   98 FORMAT(7X,I3,7X,I3,8X,F5.3)
      END
End of file
```

The results of the atomic coordinates and interatomic distances are listed in the following pages.

```
1     .1410,.1410,.1410
2     .3635,.3635,.3635
3     .7111,.7111,.7111
```

4 ATOM	X	Y	Z
5 1	1.004	1.004	1.004
6 2	4.563	2.555	6.114
7 3	6.114	4.563	2.555
8 4	2.555	6.114	4.563
9 5	2.587	2.587	2.587
10 6	6.146	0.972	4.531
11 7	4.531	6.146	0.972
12 8	0.972	4.531	6.146
13 9	5.062	5.062	5.062
14 10	8.621	-1.503	2.056
15 11	2.056	8.621	-1.503
16 12	-1.503	2.056	8.621
17 13	8.122	1.004	1.004
18 14	11.681	2.555	6.114
19 15	13.232	4.563	2.555
20 16	9.673	6.114	4.563
21 17	9.705	2.587	2.587
22 18	13.264	0.972	4.531
23 19	11.649	6.146	0.972
24 20	8.090	4.531	6.146
25 21	12.180	5.062	5.062
26 22	15.739	-1.503	2.056
27 23	9.174	8.621	-1.503
28 24	5.615	2.056	8.621
29 25	1.004	8.122	1.004
30 26	4.563	9.673	6.114
31 27	6.114	11.681	2.555
32 28	2.555	13.232	4.563
33 29	2.587	9.705	2.587
34 30	6.146	8.090	4.531
35 31	4.531	13.264	0.972
36 32	0.972	11.649	6.146
37 33	5.062	12.180	5.062
38 34	8.621	5.615	2.056
39 35	2.056	15.739	-1.503
40 36	-1.503	9.174	8.621
41 37	8.122	8.122	1.004
42 38	11.681	9.673	6.114
43 39	13.232	11.681	2.555
44 40	9.673	13.232	4.563
45 41	9.705	9.705	2.587
46 42	13.264	8.090	4.531
47 43	11.649	13.264	0.972
48 44	8.090	11.649	6.146
49 45	12.180	12.180	5.062

	ATOM	X	Y	Z
50	46	15.739	5.615	2.056
51	47	9.174	15.739	-1.503
52	48	5.615	9.174	8.621
53	49	1.004	-1.004	8.122
54	50	4.563	2.555	13.232
55	51	6.114	4.563	9.673
56	52	2.555	6.114	11.681
57	53	2.587	2.587	9.705
58	54	6.146	0.972	11.649
59	55	4.531	6.146	8.090
60	56	0.972	4.531	13.264
61	57	5.062	5.062	12.180
62	58	8.621	-1.503	9.174
63	59	2.056	8.621	5.615
64	60	-1.503	2.056	15.739
65	61	8.122	1.004	8.122
66	62	11.681	2.555	13.232
67	63	13.232	4.563	9.673
68	64	9.673	6.114	11.681
69	65	9.705	2.587	9.705
70	66	13.264	0.972	11.649
71	67	11.649	6.146	8.090
72	68	8.090	4.531	13.264
73	69	12.180	5.062	12.180
74	70	15.739	-1.503	9.174
75	71	9.174	8.621	5.615
76	72	5.615	2.056	15.739
77	73	1.004	8.122	8.122
78	74	4.563	9.673	13.232
79	75	6.114	11.681	9.673
80	76	2.555	13.232	11.681
81	77	2.587	9.705	9.705
82	78	6.146	8.090	11.649
83	79	4.531	13.264	8.090
84	80	0.972	11.649	13.264
85	81	5.062	12.180	12.180
86	82	8.621	5.615	9.174
87	83	2.056	15.739	5.615
88	84	-1.503	9.174	15.739
89	85	8.122	8.122	8.122
90	86	11.681	9.673	13.232
91	87	13.232	11.681	9.673
92	88	9.673	13.232	11.681
93	89	9.705	9.705	9.705
94	90	13.264	8.090	11.649
95	91	11.649	13.264	8.090

	ATOM	X	Y	Z
96	92	8.090	11.649	13.264
97	93	12.180	12.180	12.180
98	94	15.739	5.615	9.174
99	95	9.174	15.739	5.615
100	96	5.615	9.174	15.739
101	DISTANCES LESS THAN 3.60A			
102	ATOM	ATOM	DISTANCE	
103	1	5	2.743	
104	2	6	2.743	
105	2	9	2.764	
106	2	24	2.764	
107	3	7	2.743	
108	3	9	2.764	
109	3	34	2.764	
110	4	8	2.743	
111	4	9	2.764	
112	4	59	2.764	
113	9	20	3.260	
114	9	30	3.260	
115	9	55	3.260	
116	10	13	2.764	
117	11	25	2.764	
118	12	49	2.764	
119	13	17	2.743	
120	14	18	2.743	
121	14	21	2.764	
122	15	19	2.743	
123	15	21	2.764	
124	15	46	2.764	
125	16	20	2.743	
126	16	21	2.764	
127	16	34	2.764	
128	16	71	2.764	
129	17	34	3.260	
130	19	34	3.260	
131	20	82	3.260	
132	21	42	3.260	
133	21	67	3.260	
134	23	37	2.764	
135	24	51	2.764	
136	24	53	3.260	
137	24	54	3.260	
138	24	61	2.764	
139	25	29	2.743	
140	26	30	2.743	
141	26	33	2.764	

	ATOM	ATOM	DISTANCE
142	26	48	2.764
143	26	59	2.764
144	27	31	2.743
145	27	33	2.764
146	28	32	2.743
147	28	33	2.764
148	28	83	2.764
149	29	59	3.260
150	30	71	3.260
151	32	59	3.260
152	33	44	3.260
153	33	79	3.260
154	34	37	2.764
155	36	73	2.764
156	37	41	2.743
157	38	42	2.743
158	38	45	2.764
159	38	71	2.764
160	39	43	2.743
161	39	45	2.764
162	40	44	2.743
163	40	45	2.764
164	40	95	2.764
165	41	71	3.260
166	44	71	3.260
167	45	91	3.260
168	48	55	3.260
169	48	75	2.764
170	48	77	3.260
171	48	78	3.260
172	48	85	2.764
173	49	53	2.743
174	50	54	2.743
175	50	57	2.764
176	50	72	2.764
177	51	55	2.743
178	51	57	2.764
179	51	82	2.764
180	52	56	2.743
181	52	57	2.764
182	57	68	3.260
183	57	78	3.260
184	58	61	2.764
185	59	73	2.764
186	61	65	2.743
187	62	66	2.743

	ATOM	ATOM	DISTANCE
188	62	69	2.764
189	63	67	2.743
190	63	69	2.764
191	63	94	2.764
192	64	68	2.743
193	64	69	2.764
194	64	82	2.764
195	65	82	3.260
196	67	82	3.260
197	69	90	3.260
198	71	85	2.764
199	73	77	2.743
200	74	78	2.743
201	74	81	2.764
202	74	96	2.764
203	75	79	2.743
204	75	81	2.764
205	76	80	2.743
206	76	81	2.764
207	81	92	3.260
208	82	85	2.764
209	85	89	2.743
210	86	90	2.743
211	86	93	2.764
212	87	91	2.743
213	87	93	2.764
214	88	92	2.743
215	88	93	2.764

End of file

APPENDIX III

DETERMINATION OF THE STRUCTURE FACTORS AND RELATIVE INTENSITIES OF POWDER DIFFRACTION PATTERN OF AMMONIA DIHYDRATE

The structure amplitude $|F|$ is given by

$$|F| = (A^2 + B^2)^{1/2} \tag{1}$$

where

$$A = \sum_n f_n \cos 2\pi(hx_n + ky_n + lz_n) \tag{2}$$

$$B = \sum_n f_n \sin 2\pi(hx_n + ky_n + lz_n) \tag{3}$$

where x_n, y_n and z_n are the fractional coordinates of an atom n. f_n is the atomic scattering factor for that atom for the value of $\sin \theta/\lambda$ associated with the indices hkl.

The expression of the structure factor can be reduced[93] for the space group $P2_12_12_1$ to

$$A = 4\cos 2\pi(hx - \frac{h-k}{4}) \cos 2\pi(ky - \frac{k-l}{4}) \cos 2\pi(lz - \frac{l-h}{4}) \tag{4}$$

$$B = -4\sin 2\pi(hx - \frac{h-k}{4}) \sin 2\pi(ky - \frac{k-l}{4}) \sin 2\pi(lz - \frac{l-z}{4}) \quad (5)$$

This is the same expression for the space group $P2_13$ for atoms in the special position 4 a 3.

The integrated intensities, I, are calculated according to the flat-plate powder equation:[40,60]

$$I \propto [(1+\cos^2 2\theta)/(\sin^2\theta \cos\theta)] \cos 2\theta \; p \cdot |F|^2 \cdot A \quad (6)$$

where θ is the Bragg angle, p is the multiplicity factor (which takes into account the possible number of reflections from a single crystal that are superimposed to form a powder line). $[(1+\cos^2 2\theta)/(\sin^2\theta \cos\theta)] \cos 2\theta$ is the trigonometric factor for a flat-plate.

The integrated intensities, I', which are corrected for the thermal parameter are given by:

$$I' \propto [(1+\cos^2 2\theta)/(\sin^2 \cos\theta)] \cos 2\theta \; p \cdot |F'|^2 \cdot A \quad (7)$$

where $|F'|$ is the structure amplitude corrected for the thermal parameter and is given by:

$$|F'| = |F| \exp(-B_t \sin^2 \theta/\lambda^2) \quad (8)$$

where B_t is the thermal parameter.

A in equations (6) and (7) is the absorption factor which is the same for all lines and therefore does not affect the relative intensities and was neglected in the calculations. The atomic scattering factors for oxygen and nitrogen atoms were obtained from Ref. 94 and are listed in the data below. The thermal parameters were given the values found for ammonia monohydrate by I. Olovsson and D.H. Templeton[5] (1.42 and 1.57 for oxygen and nitrogen atom, respectively).

The computer program "INTENSITIES", listed below, utilizes equations (1), (4), (5) and (8) to obtain the structure amplitudes |F'| and then to calculate the relative intensities using equation (7) above.

In this program the largest intensity, i.e. the value of 301.7 that is proportional to the intensity of I(211) + I(121) + I(112) was first obtained by running the program once without calculating I(HKL)/I(211) %, which actually means I(HKL)/(I(211) + I(121)+I(112)) × 100%.

A listing of the program "INTENSITIES":

```
1       C   THIS IS A PROGRAM TO CALCULATE THE RELATIVE
2       C   INTENSITIES OF THE DIFRACTION LINES ON POWDER
3       C   X-RAY PHOTOGRAPHS OF AMMONIA DIHYDRATE.
4             DIMENSION F(2),X(3),Y(3),Z(3),B(2)
5             DIMENSION A(200),C(200),V(200)
6             DO 10 I=1,3
7             READ(5,11) X(I),Y(I),Z(I)
8          11 FORMAT(3F5.4)
```

```
 9          10   CONTINUE
10              DO 15 I=1,3
11              WRITE(6,17) X(I),Y(I),Z(I)
12          17  FORMAT(2(F5.4,','),F5.4)
13          15  CONTINUE
14              WRITE(6,80)
15          80  FORMAT(3X,'H',4X,'K',4X,'L',5X,'FCAL',
16             -5X,'ICAL/1000',2X,'I(HKL)/I(211)%')
17              DO 95 I=1,132
18              READ(5,40) H,CK,CL
19          40  FORMAT(3F2.0)
20        C     READING OF THE ATOMIC SCATTERING FACTORS OF
21        C     OXYGEN,F(1),AND NITROGEN,F(2),ATOMS.
22        C     V(I) IS THE  MULTIPLICITY FACTORS,
23        C     A(I) IS SINE THETAS;AND C(I) IS THE
24        C     TRIGONOMETRICAL FACTORS.
25              READ(5,50) F(1),F(2),V(I),A(I),C(I)
26          50  FORMAT(2F6.4,F4.0,F7.5,F8.4)
27        C     CALCULATIONS OF THE STRUCTURE AMPLITUDES
28              FCAL=0.0
29              AN=0.0
30              BN=0.0
31              B(1)=EXP(-1.42*A(I)*A(I)/(1.5418**2))
32              B(2)=EXP(-1.57*A(I)*A(I)/(1.5418**2))
33              DO 70 J=1,3
34              IF(J-2) 21,24,21
35          21  M=1
36              GO TO 55
37          24  M=2
38          55  RX=(H*X(J)-(H-CK)/4.0)*6.28319
39              RY=(CK*Y(J)-(CK-CL)/4.0)*6.28319
40              RZ=(CL*Z(J)-(CL-H)/4.0)*6.28319
41              AI=4.0*(COS(RX))*(COS(RY))*(COS(RZ))*F(M)
42              BI=-4.0*(SIN(RX))*(SIN(RY))*(SIN(RZ))*F(M)
43              AN=AN+AI*B(M)
44              BN=BN+BI*B(M)
45          70  CONTINUE
46              FCAL=SQRT(AN**2+BN**2)
47        C     CALCULATIONS OF THE RELATIVE INTENSITIES
48              CALI=FCAL*FCAL*C(I)*V(I)/1000.0
49              R=100.0*CALI/301.70175
50              WRITE(6,90) H,CK,CL,FCAL,CALI,R
51          90  FORMAT(3(3X,F2.0),2(3X,F8.3),3X,F7.3)
52          95  CONTINUE
53              STOP
54              END
End of file
```

The data used are listed below, where the first three lines are the fractional coordinates of atoms O_{II}, N and O_I. The rest of the data are the indices of each reflection followed by the atomic scattering factors of O and N atoms, the multiplicity factor, sine theta and the trigonometrical factor of that reflection.

```
1     .1410.1410.1410
2     .3635.3635.3635
3     .7111.7111.7111
4     0.0.1.
5     7.610 6.573  2. .10830 163.6123
6     1.0.0.
7     7.610 6.573  2. .10830 163.6123
8     0.1.0.
9     7.610 6.573  2. .10830 163.6123
10    1.1.0.
11    7.255 6.195  4. .15316 78.4581
12    0.1.1.
13    7.255 6.195  4. .15316 78.4581
14    1.0.1.
15    7.255 6.195  4. .15316 78.4581
16    1.1.1.
17    6.929 5.854  8. .18759 50.1392
18    0.0.2.
19    6.629 5.547  2. .21661 36.0283
20    2.0.0.
21    6.629 5.547  2. .21661 36.0283
22    0.2.0.
23    6.629 5.547  2. .21661 36.0283
24    2.0.1.
25    6.354 5.270  4. .24217 27.5999
26    1.2.0.
27    6.354 5.270  4. .24217 27.5999
28    0.1.2.
29    6.354 5.270  4. .24217 27.5999
30    1.0.2.
31    6.354 5.270  4. .24217 27.5999
32    2.1.0.
33    6.354 5.270  4. .24217 27.5999
34    0.2.1.
35    6.354 5.270  4. .24217 27.5999
36    1.2.1.
37    6.099 5.018  8. .26529 22.0120
38    2.1.1.
```

```
39      6.099 5.018  8. .26529 22.0120
40      1.1.2.
41      6.099 5.018  8. .26529 22.0120
42      2.0.2.
43      5.645 4.581  4. .30633 15.0950
44      2.2.0.
45      5.645 4.581  4. .30633 15.0950
46      0.2.2.
47      5.645 4.581  4. .30633 15.0950
48      0.0.3.
49      5.442 4.391  2. .32491 12.8187
50      0.3.0.
51      5.442 4.391  2. .32491 12.8187
52      3.0.0.
53      5.442 4.391  2. .32491 12.8187
54      1.2.2.
55      5.442 4.391  8. .32491 12.8187
56      2.2.1.
57      5.442 4.391  8. .32491 12.8187
58      2.1.2.
59      5.442 4.391  8. .32491 12.8187
60      0.1.3.
61      5.253 4.217  4. .34248 11.0146
62      1.3.0.
63      5.253 4.217  4. .34248 11.0146
64      3.0.1.
65      5.253 4.217  4. .34248 11.0146
66      0.3.1.
67      5.253 4.217  4. .34248 11.0146
68      1.0.3.
69      5.253 4.217  4. .34248 11.0146
70      3.1.0.
71      5.253 4.217  4. .34248 11.0146
72      1.1.3.
73      5.077 4.058  8. .35920  9.5536
74      3.1.1.
75      5.077 4.058  8. .35920  9.5536
76      1.3.1.
77      5.077 4.058  8. .35920  9.5536
78      2.2.2.
79      4.912 3.911  8. .37517  8.3496
80      0.3.2.
81      4.758 3.776  4. .39049  7.3429
82      3.2.0.
83      4.758 3.776  4. .39049  7.3429
84      2.0.3.
85      4.758 3.776  4. .39049  7.3429
86      0.2.3.
```

```
 87      4.758 3.776  4. .39049  7.3429
 88      2.3.0.
 89      4.758 3.776  4. .39049  7.3429
 90      3.0.2.
 91      4.758 3.776  4. .39049  7.3429
 92      3.1.2.
 93      4.613 3.652  8. .40523  6.4910
 94      1.2.3.
 95      4.613 3.652  8. .40523  6.4910
 96      2.3.1.
 97      4.613 3.652  8. .40523  6.4910
 98      2.1.3.
 99      4.613 3.652  8. .40523  6.4910
100      3.2.1.
101      4.613 3.652  8. .40523  6.4910
102      1.3.2.
103      4.613 3.652  8. .40523  6.4910
104      4.0.0.
105      4.349 3.430  2. .43321 5.1339
106      0.0.4.
107      4.349 3.430  2. .43321 5.1339
108      0.4.0.
109      4.349 3.430  2. .43321 5.1339
110      4.1.0.
111      4.229 3.331  4. .44654  4.5875
112      0.4.1.
113      4.229 3.331  4. .44654  4.5875
114      1.0.4.
115      4.229 3.331  4. .44654  4.5875
116      4.0.1.
117      4.229 3.331  4. .44654  4.5875
118      0.1.4.
119      4.229 3.331  4. .44654  4.5875
120      1.4.0.
121      4.229 3.331  4. .44654  4.5875
122      3.2.2.
123      4.229 3.331  8. .44654  4.5875
124      2.2.3.
125      4.229 3.331  8. .44654  4.5875
126      2.3.2.
127      4.229 3.331  8. .44654  4.5875
128      1.1.4.
129      4.116 3.239  8. .45949  4.1092
130      4.1.1.
131      4.116 3.239  8. .45949  4.1092
132      1.4.1.
133      4.116 3.239  8. .45949  4.1092
134      0.3.3.
```

```
135     4.116 3.239  4.  .45949  4.1092
136     3.0.3.
137     4.116 3.239  4.  .45949  4.1092
138     3.3.0.
139     4.116 3.239  4.  .45949  4.1092
140     3.3.1.
141     4.009 3.153  8.  .47208  3.6880
142     1.3.3.
143     4.009 3.153  8.  .47208  3.6880
144     3.1.3.
145     4.009 3.153  8.  .47208  3.6880
146     0.4.2.
147     3.907 3.073  4.  .48435  3.3151
148     2.0.4.
149     3.907 3.073  4.  .48435  3.3151
150     4.2.0.
151     3.907 3.073  4.  .48435  3.3151
152     4.0.2.
153     3.907 3.073  4.  .48435  3.3151
154     2.4.0.
155     3.907 3.073  4.  .48435  3.3151
156     0.2.4.
157     3.907 3.073  4.  .48435  3.3151
158     1.2.4.
159     3.812 2.998  8.  .49631  2.9833
160     4.1.2.
161     3.812 2.998  8.  .49631  2.9833
162     2.4.1.
163     3.812 2.998  8.  .49631  2.9833
164     1.4.2.
165     3.812 2.998  8.  .49631  2.9833
166     2.1.4.
167     3.812 2.998  8.  .49631  2.9833
168     4.2.1.
169     3.812 2.998  8.  .49631  2.9833
170     3.3.2.
171     3.721 2.927  8.  .50799  2.5096
172     3.2.3.
173     3.721 2.927  8.  .50799  2.5096
174     2.3.3.
175     3.721 2.927  8.  .50799  2.5096
176     2.2.4.
177     3.553 2.799  8.  .53057  2.1810
178     2.4.2.
179     3.553 2.799  8.  .53057  2.1810
180     4.2.2.
181     3.553 2.799  8.  .53057  2.1810
182     3.0.4.
```

```
183     3.476 2.741  4. .54151  1.9634
184     4.3.0.
185     3.476 2.741  4. .54151  1.9634
186     0.4.3.
187     3.476 2.741  4. .54151  1.9634
188     4.0.3.
189     3.476 2.741  4. .54151  1.9634
190     3.4.0.
191     3.476 2.741  4. .54151  1.9634
192     0.3.4.
193     3.476 2.741  4. .54151  1.9634
194     5.0.0.
195     3.476 2.741  2. .54151  1.9634
196     0.5.0.
197     3.476 2.741  2. .54151  1.9634
198     0.0.5.
199     3.476 2.741  2. .54151  1.9634
200     1.5.0.
201     3.402 2.686  4. .55224  1.7676
202     5.0.1.
203     3.402 2.686  4. .55224  1.7676
204     0.1.5.
205     3.402 2.686  4. .55224  1.7676
206     5.1.0.
207     3.402 2.686  4. .55224  1.7676
208     1.0.5.
209     3.402 2.686  4. .55224  1.7676
210     0.5.1.
211     3.402 2.686  4. .55224  1.7676
212     4.3.1.
213     3.402 2.686  8. .55224  1.7676
214     1.4.3.
215     3.402 2.686  8. .55224  1.7676
216     3.1.4.
217     3.402 2.686  8. .55224  1.7676
218     4.1.3.
219     3.402 2.686  8. .55224  1.7676
220     3.4.1.
221     3.402 2.686  8. .55224  1.7676
222     1.3.4.
223     3.402 2.686  8. .55224  1.7676
224     1.1.5.
225     3.332 2.634  8. .56276  1.5886
226     1.5.1.
227     3.332 2.634  8. .56276  1.5886
228     5.1.1.
229     3.332 2.634  8. .56276  1.5886
230     3.3.3.
```

```
231     3.332 2.634  8. .56276  1.5886
232     2.4.3.
233     3.202 2.539  8. .58323  1.2752
234     4.3.2.
235     3.202 2.539  8. .58323  1.2752
236     3.2.4.
237     3.202 2.539  8. .58323  1.2752
238     4.2.3.
239     3.202 2.539  8. .58323  1.2752
240     3.4.2.
241     3.202 2.539  8. .58323  1.2752
242     2.3.4.
243     3.202 2.539  8. .58323  1.2752
244     5.2.0.
245     3.202 2.539  4. .58323  1.2752
246     0.5.2.
247     3.202 2.539  4. .58323  1.2752
248     2.0.5.
249     3.202 2.539  4. .58323  1.2752
250     5.0.2.
251     3.202 2.539  4. .58323  1.2752
252     2.5.0.
253     3.202 2.539  4. .58323  1.2752
254     0.2.5.
255     3.202 2.539  4. .58323  1.2752
256     5.2.1.
257     3.142 2.495  8. .59320  1.1374
258     1.5.2.
259     3.142 2.495  8. .59320  1.1374
260     2.1.5.
261     3.142 2.495  8. .59320  1.1374
262     2.5.1.
263     3.142 2.495  8. .59320  1.1374
264     5.1.2.
265     3.142 2.495  8. .59320  1.1374
266     1.2.5.
267     3.142 2.495  8. .59320  1.1374
End of file
```

The results of the structure amplitudes and the relative intensities are listed in the following pages:

1 .1410,.1410,.1410
2 .3635,.3635,.3635
3 .7111,.7111,.7111

4	H	K	L	FCAL	ICAL/1000	I(HKL)/I(211)%
5	0.	0.	1.	0.000	0.000	0.000
6	1.	0.	0.	0.000	0.000	0.000
7	0.	1.	0.	0.000	0.000	0.000
8	1.	1.	0.	8.666	23.571	7.813
9	0.	1.	1.	8.666	23.571	7.813
10	1.	0.	1.	8.666	23.571	7.813
11	1.	1.	1.	2.286	2.097	0.695
12	0.	0.	2.	31.010	69.293	22.967
13	2.	0.	0.	31.010	69.293	22.967
14	0.	2.	0.	31.010	69.293	22.967
15	2.	0.	1.	25.551	72.075	23.889
16	1.	2.	0.	25.551	72.075	23.889
17	0.	1.	2.	25.551	72.075	23.889
18	1.	0.	2.	7.735	6.605	2.189
19	2.	1.	0.	7.735	6.605	2.189
20	0.	2.	1.	7.735	6.605	2.189
21	1.	2.	1.	23.898	100.567	33.333
22	2.	1.	1.	23.898	100.567	33.333
23	1.	1.	2.	23.898	100.567	33.333
24	2.	0.	2.	17.850	19.238	6.377
25	2.	2.	0.	17.850	19.238	6.377
26	0.	2.	2.	17.850	19.238	6.377
27	0.	0.	3.	0.000	0.000	0.000
28	0.	3.	0.	0.000	0.000	0.000
29	3.	0.	0.	0.000	0.000	0.000
30	1.	2.	2.	7.176	5.281	1.750
31	2.	2.	1.	7.176	5.281	1.750
32	2.	1.	2.	7.176	5.281	1.750
33	0.	1.	3.	16.204	11.569	3.835
34	1.	3.	0.	16.204	11.569	3.835
35	3.	0.	1.	16.204	11.569	3.835
36	0.	3.	1.	3.257	0.467	0.155
37	1.	0.	3.	3.257	0.467	0.155
38	3.	1.	0.	3.257	0.467	0.155
39	1.	1.	3.	22.996	40.415	13.396
40	3.	1.	1.	22.996	40.415	13.396
41	1.	3.	1.	22.996	40.415	13.396
42	2.	2.	2.	13.591	12.338	4.089
43	0.	3.	2.	20.998	12.951	4.293
44	3.	2.	0.	20.998	12.951	4.293
45	2.	0.	3.	20.998	12.951	4.293
46	0.	2.	3.	6.704	1.320	0.438
47	2.	3.	0.	6.704	1.320	0.438
48	3.	0.	2.	6.704	1.320	0.438

	H	K	L	FCAL	ICAL/1000	I(HKL)/I(211)%
49	3.	1.	2.	24.716	31.721	10.514
50	1.	2.	3.	24.716	31.721	10.514
51	2.	3.	1.	24.715	31.721	10.514
52	2.	1.	3.	13.330	9.228	3.059
53	3.	2.	1.	13.330	9.228	3.059
54	1.	3.	2.	13.330	9.228	3.059
55	4.	0.	0.	17.236	3.050	1.011
56	0.	0.	4.	17.236	3.050	1.011
57	0.	4.	0.	17.236	3.050	1.011
58	4.	1.	0.	10.047	1.852	0.614
59	0.	4.	1.	10.047	1.852	0.614
60	1.	0.	4.	10.047	1.852	0.614
61	4.	0.	1.	2.882	0.152	0.051
62	0.	1.	4.	2.882	0.152	0.051
63	1.	4.	0.	2.882	0.152	0.051
64	3.	2.	2.	5.099	0.954	0.316
65	2.	2.	3.	5.099	0.954	0.316
66	2.	3.	2.	5.099	0.954	0.316
67	1.	1.	4.	7.232	1.719	0.570
68	4.	1.	1.	7.232	1.719	0.570
69	1.	4.	1.	7.232	1.719	0.570
70	0.	3.	3.	6.355	0.664	0.220
71	3.	0.	3.	6.355	0.664	0.220
72	3.	3.	0.	6.355	0.664	0.220
73	3.	3.	1.	2.805	0.232	0.077
74	1.	3.	3.	2.805	0.232	0.077
75	3.	1.	3.	2.805	0.232	0.077
76	0.	4.	2.	2.754	0.101	0.033
77	2.	0.	4.	2.754	0.101	0.033
78	4.	2.	0.	2.754	0.101	0.033
79	4.	0.	2.	2.754	0.101	0.033
80	2.	4.	0.	2.754	0.101	0.033
81	0.	2.	4.	2.754	0.101	0.033
82	1.	2.	4.	17.140	7.012	2.324
83	4.	1.	2.	17.140	7.012	2.324
84	2.	4.	1.	17.140	7.012	2.324
85	1.	4.	2.	5.418	0.701	0.232
86	2.	1.	4.	5.418	0.701	0.232
87	4.	2.	1.	5.418	0.701	0.232
88	3.	3.	2.	8.402	1.417	0.470
89	3.	2.	3.	8.402	1.417	0.470
90	2.	3.	3.	8.402	1.417	0.470
91	2.	2.	4.	6.178	0.666	0.221
92	2.	4.	2.	6.178	0.666	0.221
93	4.	2.	2.	6.178	0.666	0.221

	H	K	L	FCAL	ICAL/1000	I(HKL)/I(211)%
94	3.	0.	4.	7.928	0.494	0.164
95	4.	3.	0.	7.928	0.494	0.164
96	0.	4.	3.	7.928	0.494	0.164
97	4.	0.	3.	0.264	0.001	0.000
98	3.	4.	0.	0.264	0.001	0.000
99	0.	3.	4.	0.264	0.001	0.000
100	5.	0.	0.	0.000	0.000	0.000
101	0.	5.	0.	0.000	0.000	0.000
102	0.	0.	5.	0.000	0.000	0.000
103	1.	5.	0.	10.625	0.798	0.265
104	5.	0.	1.	10.625	0.798	0.265
105	0.	1.	5.	10.625	0.798	0.265
106	5.	1.	0.	0.714	0.004	0.001
107	1.	0.	5.	0.714	0.004	0.001
108	0.	5.	1.	0.714	0.004	0.001
109	4.	3.	1.	10.818	1.655	0.549
110	1.	4.	3.	10.818	1.655	0.549
111	3.	1.	4.	10.818	1.655	0.549
112	4.	1.	3.	2.379	0.080	0.027
113	3.	4.	1.	2.379	0.080	0.027
114	1.	3.	4.	2.379	0.080	0.027
115	1.	1.	5.	14.362	2.622	0.869
116	1.	5.	1.	14.362	2.622	0.869
117	5.	1.	1.	14.362	2.622	0.869
118	3.	3.	3.	7.012	0.625	0.207
119	2.	4.	3.	17.673	3.186	1.056
120	4.	3.	2.	17.673	3.186	1.056
121	3.	2.	4.	17.673	3.186	1.056
122	4.	2.	3.	4.493	0.206	0.068
123	3.	4.	2.	4.493	0.206	0.068
124	2.	3.	4.	4.493	0.206	0.068
125	5.	2.	0.	10.774	0.592	0.196
126	0.	5.	2.	10.774	0.592	0.196
127	2.	0.	5.	10.774	0.592	0.196
128	5.	0.	2.	4.196	0.090	0.030
129	2.	5.	0.	4.196	0.090	0.030
130	0.	2.	5.	4.196	0.090	0.030
131	5.	2.	1.	13.140	1.571	0.521
132	1.	5.	2.	13.140	1.571	0.521
133	2.	1.	5.	13.140	1.571	0.521
134	2.	5.	1.	0.298	0.001	0.000
135	5.	1.	2.	0.298	0.001	0.000
136	1.	2.	5.	0.298	0.001	0.000

End of file

APPENDIX IV

CALCULATIONS OF THE NET DIPOLE MOMENT CHANGE FOR O-H...O BONDS IN THE WATER CHAINS IN $NH_3 \cdot H_2O$

Atom	Fractional Coordinate	Actual Coordinate
O_1	0.241, 0.111, 0.017	1.087, 0.618, 0.163 Å
O_2	0.741, 0.389, -0.017	3.342, 2.175, -0.163 Å
$O_{1'}$	1.241, 0.111, 0.017	5.597, 0.618, 0.163 Å

$O_1\hat{O}_2O_{1'} = 109.6°$

In-Phase Motion

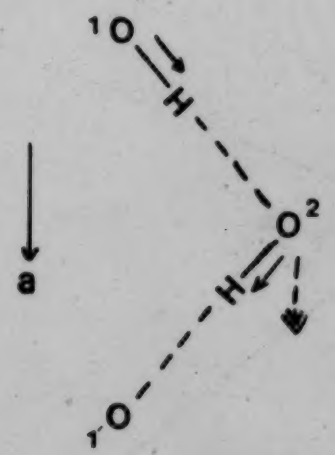

The unit vectors:

$\hat{U}_{O_2-O_1} = 0.817\ \underline{i} + 0.564\ \underline{j} - 0.118\ \underline{k}$

$\hat{U}_{O_1,-O_2} = 0.817\ \underline{i} - 0.564\ \underline{j} + 0.188\ \underline{k}$

Therefore, the angle between the O-H...O bond and the a axis is $\cos^{-1} 0.817 = 35.2°$.

The net dipole moment change is: $\partial\mu/\partial Q_1 = 2(\partial\mu/\partial R)$ cos 35.2 = 1.643 $\partial\mu/\partial R$ along the a axis and perpendicular to the bc plane.

Out-of-Phase Motion

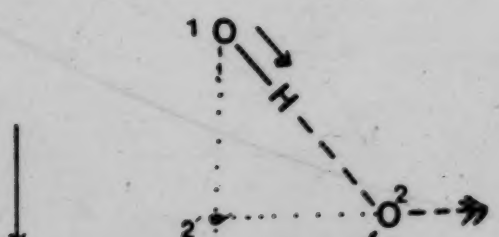

The coordinates of the point 2' are:

3.342, 0.618, 0.163 Å.

The unit vector

$\hat{U}_{O_2-2'} = 0.0\ \underline{i} + 0.979\ \underline{j} - 0.205\ \underline{k}$

Therefore, the net dipole moment change is: $\partial\mu/\partial Q_2 = 2(\partial\mu/\partial R)$ sin 35.2° and is perpendicular to the a axis and lies in the bc plane. It makes angles 11.8 and 78.2° with the b and c axes, respectively.

From Figures 4.7 to 4.10, the modes with non-zero intensities are:

a) B_1 (out-of-phase)

$(\partial\mu/\partial Q)_{u.c.} = 4\ \partial\mu/\partial R$ sin 35.2 (cos 78.2)

$= 0.472\ \partial\mu/\partial R$

In the c direction.

b) B_2 (out-of-phase)

$(\partial\mu/\partial Q)_{u.c.} = 4\ \partial\mu/\partial R$ sin 35.2 (cos 11.8)

$= 2.257\ \partial\mu/\partial R$

In the b direction.

c) B_3 (in-phase)

$(\partial\mu/\partial Q)_{u.c.} = 4\ \partial\mu/\partial R$ cos 35.2

$= 3.269\ \partial\mu/\partial R$

In the a direction.

Intensities: $B_1:B_2:B_3$; 0.223:5.09:10.68; ~1:23:48

APPENDIX V

O-H...O STRETCHING VIBRATIONS AT $\underline{k}=0$ IN ONE CHAIN IN $NH_3 \cdot H_2O$.

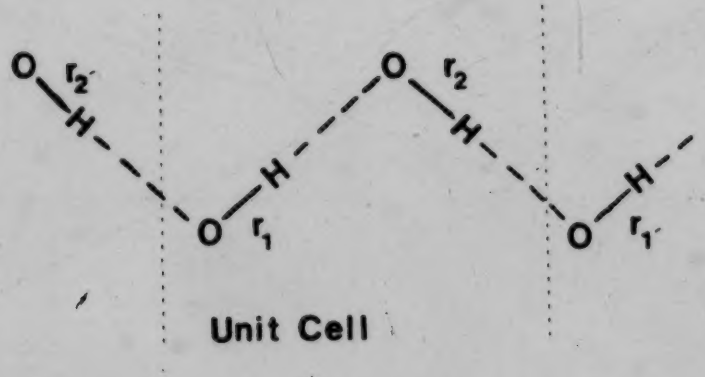

Diagram, of one chain, showing the O-H displacements in one unit cell, r_1 and r_2, and the displacements in the neighboring unit cell, r_1' and r_2'.

During an optically active vibration, the wave-vector $\underline{k}=0$ which means that the displacement $r_1=r_1'$ and $r_2=r_2'$, i.e. equivalent displacements in all unit cells are the same.

Because r_1 is bonded to two equivalent OH groups whose displacements are r_2 and r_2', the potential energy changes by $f_{12}\, r_1 r_2 + f_{12}\, r_1 r_2' = 2\, f_{12}\, r_1 r_2$. Thus the 1,2 element of the $\mathbf{F}_{op}$ matrix is $2\, f_{12}$ and because $\mathbf{F}_{op}$ is symmetrical $(\mathbf{F}_{op})_{21} = 2f_{12}$; $(\mathbf{F}_{op})_{11} = (\mathbf{F}_{op})_{22} = f_1$ and is known from HDO frequencies.

f_{12} can be estimated to be around -0.1 mdyne A^{-1}, from the phases of ice[38,83,84]

$$\mathbf{F}_{op} = \begin{pmatrix} f_1 & 2f_{12} \\ 2f_{12} & f_1 \end{pmatrix}$$

The $\mathbf{G}_{op}$ matrix is also symmetrical and $G_{12} = G_{21} = 0$ because r_1 and r_2 have no common atoms and $G_{11} = G_{22} = 1/m_O + 1/m_H$ or $1/m_O + 1/m_D$.

$$\mathbf{G}_{op} = \begin{pmatrix} G_1 & 0 \\ 0 & G_1 \end{pmatrix}$$

$f_{11} = f_{22} = 5.9325$ mdyne A^{-1} for H_2O or

$= 6.1208$ mdyne A^{-1} for D_2O

The off-diagonal force constant $2f_{12} = 2(-0.1) = -0.2$ mdyne A^{-1}.

$\mathbf{F}_{op}$ and $\mathbf{G}_{op}$ matrices are the **F** and **G** matrices for the entities in one unit cell for $\underline{k}=0$ vibrations.

Diagonalization of $\mathbf{G}_{op}\mathbf{F}_{op}$ yields:

H_2O

In-phase mode at 3203 cm^{-1}.

Out-of-phase mode at 3313 cm^{-1}.

D_2O

In-phase mode at 2369 cm^{-1}

Out-of-phase mode at 2448 cm^{-1}